The Dissertation Committee for Johnathan Nathanael Brantley Certifies that this is the approved version of the following dissertation:

Mechanical Activations of Synthetic and Biological Systems

Committee:

Christopher W. Bielawski, Supervisor

Adrian T. Keatinge-Clay

Dionicio R. Siegel

Dmitrii E. Makarov

Eric V. Anslyn

Jeffrey S. Moore

Mechanical Activations of Synthetic and Biological Systems

by

Johnathan Nathanael Brantley, B.S.

Dissertation

Presented to the Faculty of the Graduate School of

The University of Texas at Austin

in Partial Fulfillment

of the Requirements

for the Degree of

Doctor of Philosophy

The University of Texas at Austin

August 2014

Dedication

For my family, to whom I am indebted for their constant support

In memory of Mike and Reed

Acknowledgements

I am truly honored to have studied under the mentorship of Professor Christopher Bielawski, and I will forever be grateful for the wisdom, encouragement, and support he has so generously imparted during my time in his laboratory. I must also acknowledge those mentors who first inspired my love of the chemical sciences: Mike Watson, and my dear friend, Professor Les Pesterfield. Chris, Les, and Mike not only shaped my intellectual growth as a scientist, but they have also exerted immeasurable influence over my development as a citizen of this ever-evolving world. I count myself fortunate to have known and worked with men such as they, and I will never forget the lessons they have instilled within me.

The friends and colleagues I have come to know over the years are also lovingly acknowledged. I could not have asked for more loyal companions than C.J. Pruitt and Michael Starling, and I thank them for all of the kindness and support they have provided over the years. Garrett Blake, Alex Todd, Aaron Teator, and Dominika Lastovickova have all become beloved friends during my graduate studies, and I will treasure the time we have spent together. I must express special gratitude to Dr. C. Daniel Varnado and Dr. Jonathan Moerdyk, as I consider them both to be cherished friends and mentors whose criticisms and encouragements have impelled me to strive for excellence in all of my endeavors. Penny Kile and Betsy Hamblen are also gratefully acknowledged for their tireless efforts to help me navigate through my doctoral studies. Finally, I would like to thank the following distinguished individuals with whom I have collaborated: Professor Dmitrii E. Makarov, Professor Adrian T. Keatinge-Clay, Professor Jennifer S. Brodbelt, Professor David A. Vanden Bout, Professor Kuppuswamy Arumugam, Dr. Sai S. M.

Konda, Dr. Joeseph R. Cannon, Dr. Vincent M. Lynch, Dr. Amanda J. Hughes, Constance B. Bailey, Bibin T. Varghese, Katie A. Clark, Drew T. Wagner, and Matthew R. Tibby. It has been both a privilege and a pleasure to explore the wonders of the natural world with each of these collaborators, and I humbly offer my gratitude to them for expanding my intellectual horizons.

Most importantly, however, I would like to thank my family for their love and support throughout my life. I am most grateful for the encouragement that my wife, Constance, has given me; her love has uplifted me during my darkest hours, and her endless patience and wisdom serve as wellsprings of inspiration and edification. Finally, I extend my love and gratitude to my mother, father, and two sisters; they are the bedrock of my life, and words cannot express the love and respect I have for each of them.

Mechanical Activations of Synthetic and Biological Systems

Johnathan Nathanael Brantley, Ph.D.

The University of Texas at Austin, 2014

Supervisor: Christopher W. Bielawski

Polymer mechanochemistry, wherein exogenous forces are harnessed to drive chemical processes within polymeric matrices, has afforded access to an astounding array of otherwise kinetically prohibitive reactivity. These multifarious mechanochemical transformations include formally symmetry forbidden electrocyclic processes, thermodynamically disfavored isomerizations, and thermally inaccessible cycloreversions of both carbocyclic and heterocyclic functionalities. The fundamental principles that govern mechanochemistry, however, remain elusive. To address this deficiency, we report a series of experimental and computational efforts that probe chemical reactivity under the action of mechanical force. Specifically, we have explored the formal 1,3-dipolar cycloreversion of 1,2,3-triazole moieties in an effort to understand the interplay between kinetic stability and mechanical perturbation. Briefly, 1,4-disubstituted 1,2,3-triazoles were embedded within high molecular weight poly(methyl acrylate) chains and reverted into their azide and terminal alkyne precursors sonochemically. The liberated azide and alkyne moieties were identified by orthogonal chemical ligation to chromophores, and the reactive azido- and alkynyl-polymer fragments could be recoupled through a copper-mediated cycloaddition.

Inspired by this result, we developed a computational model to rapidly discover qualitative trends in mechanochemical reactivity. Application of this model to the

cycloreversion of 1,2,3-triazoles revealed an intriguing result: the 1,5-disubstitued regioisomer was predicted to exhibit enhanced susceptibility to mechanical cycloreversion in comparison to the 1,4-disubstituted congener. This trend was experimentally verified upon embedding 1,5-disubstituted 1,2,3-triazoles into high molecular weight poly(methyl acrylate) chains and subjecting them to ultrasonication. Specifically, the observed rate constant for chain scission of a poly(methyl acrylate) material containing the 1,5-disubstituted isomer was 20% larger than that of an analogous material containing the 1,4-disubstituted congener. Having established confidence in the predictive capabilities of our model, we undertook an exhaustive evaluation of regiochemical effects on the activation of six previously reported mechanically labile scaffolds. Our theoretical work suggested that all of the evaluated scaffolds could exhibit suppressed reactivity under stress (an underexplored phenomenon), and this result was supported by experimental investigation. Moreover, our theoretical considerations predicted that anti-Hammond effects (*i.e.*, increased structural dissimilarity between reactant and transition state geometries as the two approach energetically) could be predominant in mechanochemical processes.

Finally, we endeavored to expand the scope of polymer mechanochemistry beyond traditional chemical systems to biologically relevant species. We found that the photophysical properties of fluorescent protein variants could be modulated by embedding the proteins within poly(methyl methacrylate) matrices and compressing the resulting composites.

Table of Contents

List of Tables

List of Figures

List of Schemes

Chapter 1: Fundamentals of Polymer Mechanochemistry

INTRODUCTION[1]

When confronted with lethargic chemical transformations, thermal activation is often selected to accelerate the desired reactivity. The application of heat to chemical systems is relatively straightforward, and thermal perturbation often supplies molecules with sufficient kinetic energy to overcome the activation barrier separating the desired products from their starting materials. Heat, however, is not quantized; thus, increasing a reaction's temperature results in a distribution of molecular energies. This familiar Boltzmann relationship[1] has the unfortunate consequence that reagents at elevated temperature often possess sufficient energy to react in undesirable ways (*i.e.*, undergo decomposition). While other stimuli, such as photochemical or electrical, are available, the propensity for decomposition at high energy is a fundamental limitation that is challenging to circumvent. As such, a method through which chemical reactivity can not only be enhanced, but also directed in a controlled manner, is of considerable appeal.

The burgeoning field of polymer mechanochemistry, wherein exogenous forces are harnessed to modulate chemical transformations within polymeric matrices,[2,3] may provide a unique solution to the challenge of selectively activating chemical systems. Here, the term "mechanical" alludes to the fact that classical Newtonian forces are at least partially responsible for the observed phenomena. In principle, polymer mechanochemistry allows chemical reactions to be directed down precise reaction pathways by virtue of the specificity with which forces can be exerted upon covalent bonds. In fact, as early as 1940, Kauzman and Eyring predicted that stretching specific

[1] Portions of this chapter were reproduced from: Brantley, J. N.; Wiggins, K. M.; Bielawski, C. W. *Polym. Int.* **2013**, *62*, 2; Wiggins, K. M.; Brantley, J. N.; Bielawski, C. W. *Chem. Soc. Rev.* **2013**, *42*, 7130. All authors contributed to the writing of the original manuscripts and figure preparation.

bonds within a polymer could selectively alter the potential energy landscapes of reaction coordinates (*e.g.*, by lowering the activation barrier associated with homolytic dissociation).[4] By extension, precise bond activation through the application of mechanical force could also minimize undesirable reactivity and enhance the rates of transformations that are otherwise prohibitive. Current techniques for supplying mechanical force to polymer systems are applicable in both solution and the solid-state, and the various methods that are employed cover a range of strain rates and forces (**Figure 1.1**).[2]

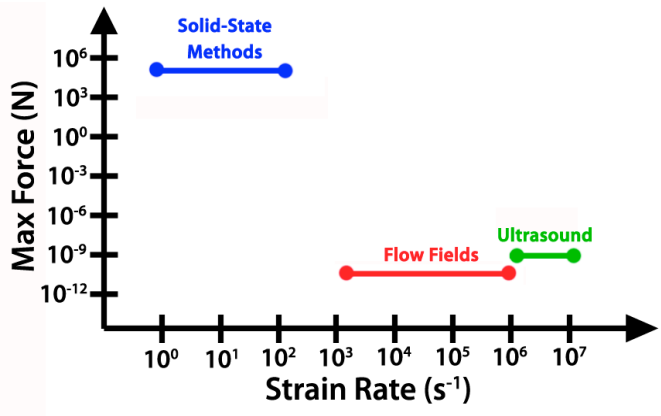

Figure 1.1 Relative strain rates and maximum forces that can be achieved by the different techniques used to apply force to polymers.[2]

In general, solid-state methods can achieve higher maximum forces, whereas solution based approaches typically exhibit larger strain rates. High strain rates in solution are paramount, given that mechanochemical activation of solvated polymers occurs only if the strain rate exceeds ~10^4 s^{-1} (*i.e.*, when polymer deformation is faster than polymer relaxation).[2] The magnitude of the applied force is also critical (both in solution and the solid-state), as the force on a single bond needs to exceed ~10^{-10} N in order for bond scission to occur. As summarized in **Table 1.1**, a variety of methods have

been used to mechanically activate materials, and each approach offers distinct advantages and disadvantages. The remainder of this chapter will discuss the various methods for mechanically activating polymers and provide specific examples of associated mechanochemical processes. Special emphasis will be directed toward ultrasonication and bulk activation, as these approaches were employed in the studies that will be detailed in subsequent chapters.

Table 1.1 Summary of methods for mechanically activating polymers

Method	Typical Conditions	Accessible Strain Rates	Maximum Forces
Flow Fields	dilute solutions (< 0.003 mg/mL); good solvent(s); high flow rates (> 10^4 s^{-1}); high MW polymers (> 5×10^5 Da)	$10^3 – 10^6$ s^{-1}	10^{-10} N
Ultrasound	dilute solutions (< 2.0 mg/mL); polar solvent(s) with low viscosity; applied intensity of 9 – 12 W cm^{-2}; high MW polymers (> 6×10^4 Da)	$10^6 – 10^7$ s^{-1}	10^{-9} N
Manual Elongation	polymer film or mold manually stretched or bent	~ 1 s^{-1}	~ 10^2 N
Tensile Testing Instruments	polymer film or mold; moderate force is used (~ 1 N); low strain rate (< 1 s^{-1})	$0 – 2 \times 10^2$ s^{-1}	10^5 N
Pressure Cells	unprocessed polymer; moderate force (< 8×10^2 N)	$0 – 2 \times 10^2$ s^{-1}	10^5 N
Hydraulic Presses	unprocessed polymer; moderate force (< 2×10^2 N)	$0 – 2 \times 10^2$ s^{-1}	10^5 N

FLOW INDUCED POLYMER SCISSION

Some of the earliest experiments involving the responses of polymers to mechanical stimuli were conducted in flow fields.[5] The majority of these studies focused on mechanically induced polymer chain scission events, which resulted in measurable reductions in the molecular weight (MW) of the polymeric materials.[6-10] Flow fields exert strong hydrodynamic forces on solvated polymer chains, causing the polymers to extend and re-orient in the direction of the flow field. When the elongational forces on the polymer are of sufficient magnitude the rate of chain stretching exceeds the rate of chain relaxation, and the polymer backbone is cleaved.[6] While the precise mechanisms of the aforementioned processes remain debated topics in the literature,[11] experimental evidence shows that chain scission is selective for the polymer midpoint, presumably because this is where the applied forces are maximized.[7,10]

Polymer scission in a flow field depends on the strain rate (or flow rate), initial polymer MW, solvent composition, and polymer concentration.[12] For instance, the selectivity for scission at the chain midpoint decreases when either a theta solvent is employed or the polymer concentration is increased. Similarly, increasing the flow rate increases the extent of polymer degradation. Enhanced chain scission is also observed for polymers with higher MWs, and polymers below a limiting MW threshold ($\sim 1 \times 10^5$ Da) generally do not exhibit significant chain scission in a flow field.

Flow field studies encompass the behavior of polymer solutions in both turbulent (non-uniform) and elongation (uniform) fields. Under turbulent flow conditions, the velocity of the solvent constantly changes; thus, large, non-uniform shear fields are generated. Conversely, the directionality of the fluid motion is regulated and well defined in an elongation flow device *(i.e.*, laminar shear fields are observed). Turbulent flow experiments were the foundation of pioneering efforts in flow field studies[6] and were

typically performed in pressure driven flow devices (**Figure 1.2**). A collection reservoir and steel flow tube were filled with pure solvent, while a dilute polymer solution (~50 ppm) was loaded into a feed reservoir.[7] The system was pressurized (2 – 10 MPa) and a solenoid valve was briefly opened to create a turbulent flow field, which caused the polymer solution to flow through the steel tube and into a sample collection reservoir and holding cylinder.

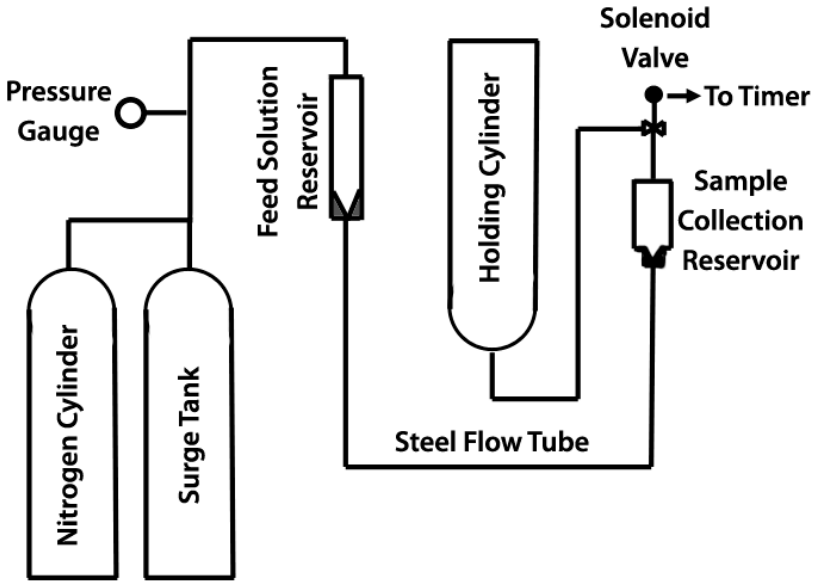

Figure 1.2 Schematic drawing of a turbulent flow device.[7]

Subjecting dilute polymer solutions to the non-uniform flow of a turbulent field was found to cause polymer chain scission, presumably due to the shearing forces generated within the flow field (*vide supra*).[6] For example, early work by Toms showed that solutions of poly(methyl methacrylate) in chlorobenzene underwent chain scission under turbulent flow.[13] Since this seminal work, a number of different polymers have been examined in turbulent fields, including: poly(isobutylene), poly(acrylamide),

poly(acrylic acid), poly(ethylene oxide), and others.[6] Collectively, these studies revealed that turbulent flow is most effective for dilute solutions of high MW polymers (ppm concentrations and $> 5 \times 10^5$ Da, respectively) in solvents where polymer–solvent interactions are favored over polymer–polymer interactions.[6]

While the exact mechanism of polymer activation in turbulent fields remains under investigation, Horn and Merrill modeled extended polystyrene as a chain of hard spheres to describe the associated kinetics of flow-induced scission.[7] Consistent with other studies,[6] Horn and Merrill found that the rates of polymer scission were accurately predicted when they assumed 1) full extension of the polymer chains in the flow field, and 2) tensile stresses were maximized in the center of the polymer chains. Unfortunately, the non-uniform nature of turbulent fields has hindered more detailed studies of the associated mechanism of mechanical activation.

The behavior of polymer solutions under elongation flow has also been explored (**Figure 1.3**).[8-10] Currently, there are two common methods for generating elongation fields: opposed jets[8] and transient elongation.[9] The former involves a cross-slot device with two jet streams that generate flow in opposing directions, which results in a stagnation point, or region of zero velocity (**Figure 1.3a**).[8] When rapidly flowing polymer solutions become trapped in the zero velocity region, elongation of the polymer chains and subsequent chain scission occurs. Conversely, transient elongation utilizes constriction flow cells that generate fleeting elongation fields by decreasing the volume of the reactor while maintaining the flow rate (**Figure 1.3b**).[9] In both methods, the polymer experiences a strong hydrodynamic force that results in polymer extension and, ultimately, selective scission at the chain midpoint. Midpoint selectivity is more pronounced when opposed jets are employed, presumably because the polymers become fully extended with this method.[10]

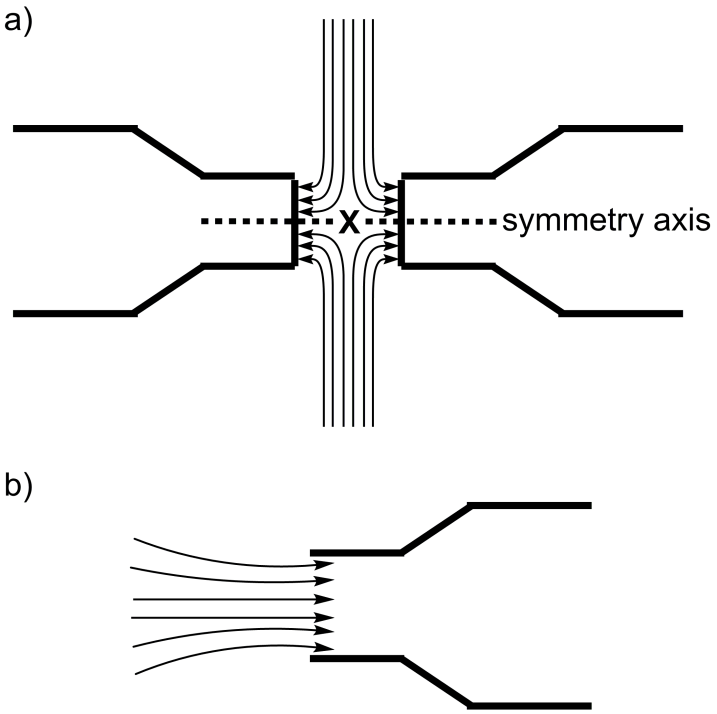

Figure 1.3 Diagrams illustrating the various types of elongation flow, where the arrows illustrate the flow pattern.[12] a) Opposite jet flow cell, with the letter X indicating the stagnation point. b) Constriction flow cell.

Like turbulent fields, activation under elongation flow depends on the polymer molecular weight, concentration, and solvent identity. Typical experiments are performed using dilute solutions (*e.g.*, 0.001 mg/mL) of high MW polymers ($> 5 \times 10^5$ Da) in a good solvent at strain rates of approximately 4.5×10^4 s^{-1}.[11] Interestingly, similar conditions were recently employed to reduce the polydispersity of polymeric materials. Subjecting aqueous solutions of high MW ($2.5 \times 10^6 - 4.3 \times 10^6$ Da) and polydisperse (PDI > 1.4) poly(acrylamide), poly(dimethylacrylamide), or poly(ethylene oxide) to elongation flow resulted in reductions of both the polydispersity (PDI = 1.12 – 1.15) and polymer MW ($3.7 \times 10^5 - 1.7 \times 10^6$ Da) until a limiting threshold (~2×10^5 Da) was achieved.[11]

To summarize, flow fields have been shown to mechanically activate polymers in solution *via* selective scission at the chain midpoint[7,10] and have provided useful insight into the behavior of solvated macromolecules.[6,11,12] Additionally, the controlled flow observed in elongation fields has allowed for kinetic analysis of polymer scission events.[9] However, there are a number of limitations that preclude the broad utility of flow fields. First, the devices used to generate flow fields are highly specialized.[2] Moreover, flow field methods require materials with MWs in excess of 1×10^5 Da in order to achieve the force necessary for activation to occur. Such high MWs can render characterization of the polymer cleavage sites challenging using conventional spectroscopy; however, characterization methods that have recently been developed for other techniques (*vide infra*) may overcome this constraint.

ULTRASONICALLY INDUCED POLYMER SCISSION

Due to high selectivity and technical simplicity, ultrasound has become a popular method for applying mechanical stress to solvated polymers.[2] Moreover, because of the increased strain rates (10^7 s^{-1}) and forces (10^{-9} N) that are generated under ultrasound, a number of novel mechanically facilitated transformations have been realized with this method. Prior to discussing relevant advances in greater detail, however, a discussion of the fundamental behavior of polymers in acoustic fields would be instructive.

Like other solution-based methods, ultrasound generates mechanical stress within solvated polymers through solvodynamic shear.[14] In an acoustic field, propagating pressure waves induce solvent cavitation (*i.e.*, rapid nucleation, expansion, and implosion of solvent microbubbles; **Figure 1.4**). Collapse of these microbubbles causes the surrounding solvent molecules to accelerate toward the resultant void space, thereby creating a solvent velocity gradient. Solvated polymer chains in the vicinity of a

cavitation site are also accelerated toward the void volume. As **Figure 1.4** illustrates, the polymer segments that are distal to the collapse site move more slowly, creating a velocity gradient along the polymer backbone.[14] The velocity gradient, in turn, elongates the polymer and generates tensile forces along the polymer chain. Within the context of polymer mechanochemistry, these tensile stresses are ultimately utilized to elicit a specific chemical response within the polymer chain. Importantly, activation of polymers under ultrasound is a highly selective process, as the tensile forces maximize in a Gaussian manner within ~15% of the center of the polymer chain.[15]

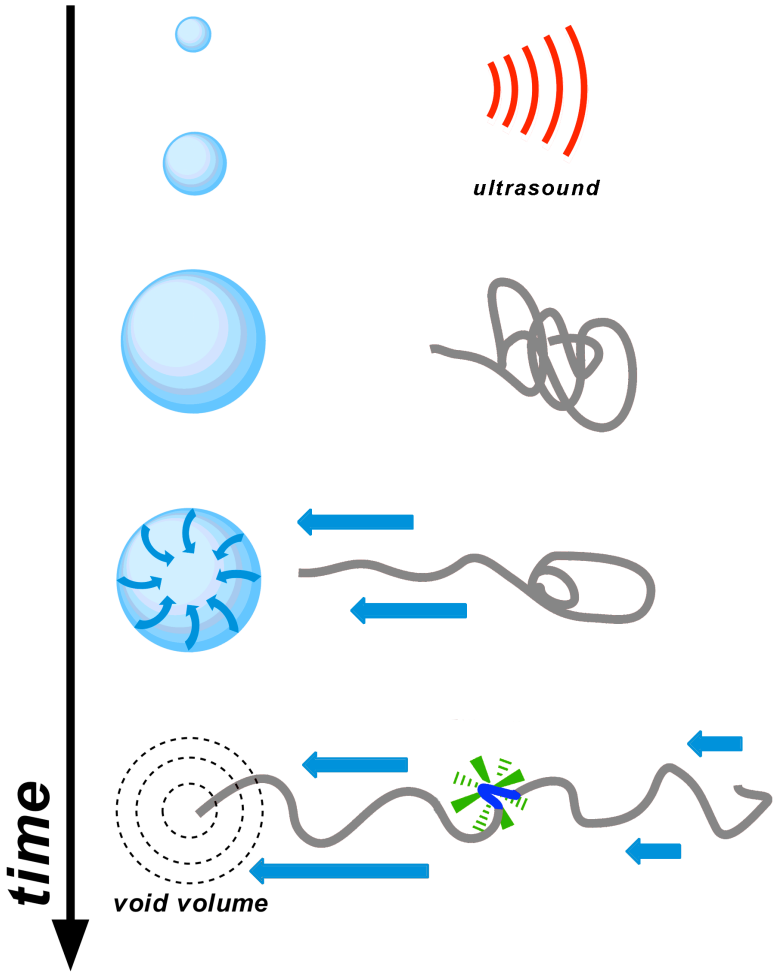

Figure 1.4 Over time, solvent bubble nucleation, growth, and collapse occur under sonication. Polymer chain ends near the resultant void volumes are pulled at faster velocities (represented by the blue arrows) than those distal to the collapsing bubbles, creating tension in the polymer backbone that elicits a response from a centrally positioned mechanophore.[2]

There are a number of factors that influence the behavior of a polymer solution in an acoustic field, including: ultrasound intensity, solvent composition, temperature, and polymer concentration.[14] As **Table 1.2** enumerates, altering any of these conditions can affect the rate of mechanical activation; thus, each factor should be carefully considered when performing ultrasound experiments.[2] Typically, dilute polymer solutions (0.75 – 2.0

mg/mL) in polar solvents with a relatively low vapor pressure (*e.g.*, acetonitrile, methyl isobutyl ketone, etc.) are employed during ultrasonication experiments. Pulsed ultrasound (*e.g.*, 1 s on; 1 s off), moderate ultrasound intensities (9 – 12 W cm^{-2}), and low temperatures are also employed to limit thermal interference.

Table 1.2 Parameters that influence acoustic activations of polymers

Experimental Parameter	Outcome
Increased Ultrasound Intensity	Increased activation (increased cavitation)
Increased Solvent Vapor Pressure	Decreased activation (cavitation reduced by solvent vapor)
Increased Solvent Viscosity	Decreased activation (reduced cavitation)
Increased Temperature	Decreased activation (increased solvent vapor pressure)
Increased Polymer Concentration	Decreased activation (increased solution viscosity)

There are a number of other factors that affect polymer activation under ultrasonication, many of which have been exploited to confirm that the reactivity observed under acoustic activation was due to a mechanical phenomenon.[2] Typical control experiments include independent evaluation of the material's thermal reactivity, the sonication of polymers with varying MWs, and the sonication of either molecules that are not covalently linked to a polymer chain or polymers wherein the desired activation site is located at a chain terminus. Appropriate controls are important, considering that the cavitation events that occur under ultrasound irradiation are known to produce high intensity light and temperatures in excess of 5,000 °C.[14] Accordingly, such control

experiments are frequently used to preclude thermal or photochemical activation.[2] For example, the initial polymer MW significantly influences mechanical reaction kinetics, such that decreasing polymer MW decreases the rate of activation.[14] Ultimately, reactivity ceases when the polymer chain length approaches a lower limit,[16] which is typically $3 \times 10^4 - 6 \times 10^4$ Da. The exact MW threshold, however, is dependent on the polymer structure (*e.g.*, polystyrene's MW threshold for chain scission is $\sim 3 \times 10^4$ Da, whereas poly(methyl acrylate)'s MW threshold is $\sim 9 \times 10^4$ Da).[16] Similarly, when the polymer chains have increasingly high MWs ($> 2 \times 10^5$ Da), activation under ultrasound becomes less selective, and multiple scission events occur per polymer chain.[16] The MW dependence observed under ultrasound provides strong evidence that activation in acoustic fields is mechanical in origin, as the dependence on polymer MW would not be expected for a thermal or photochemical process. Moreover, since tensile forces are maximized in the middle of polymer chains,[15] polymers wherein the desired activation sites are located at either chain terminus would not be expected to undergo mechanical activation during ultrasonication.

Ultrasound has been used to explore the reactivates of a number of mechanically responsive functionalities (termed mechanophores; *vide infra*) within polymers, including many of the systems that are discussed in subsequent chapters. As such, a more detailed discussion of specific examples that highlight the unique chemical reactivity that may be accessed using this technique would be informative.

MECHANOPHORES: DEFINITION AND DESIGN

Prior to any discussion of the known mechanophores, a definition of the term "mechanophore" is required. A mechanophore is any chemical entity that possesses mechanically labile bonds; that is, a chemical functionality that changes under the

influence of exogenous mechanical forces (**Figure 1.5**).[2] Mechanochemical responses can range from isomerizations (either stereochemical or structural) to precise bond scission events. The broad definition of the term "mechanophore" thus presented, however, does not convey what is perhaps the most important element of a mechanophore: its design. Mechanophores are typically selected because they contain a structural element that will respond to force in a predictable manner (*e.g.*, a weakened bond that will undergo scission, a structural motif that could lead to the extrusion of a small molecule, etc.), or they are purposefully synthesized to contain mechanically labile elements (**Figure 1.5**). These caveats preclude chemical entities that simply decompose into indistinguishable products or exhibit random activation under mechanical stress from falling under the umbrella of mechanophores.

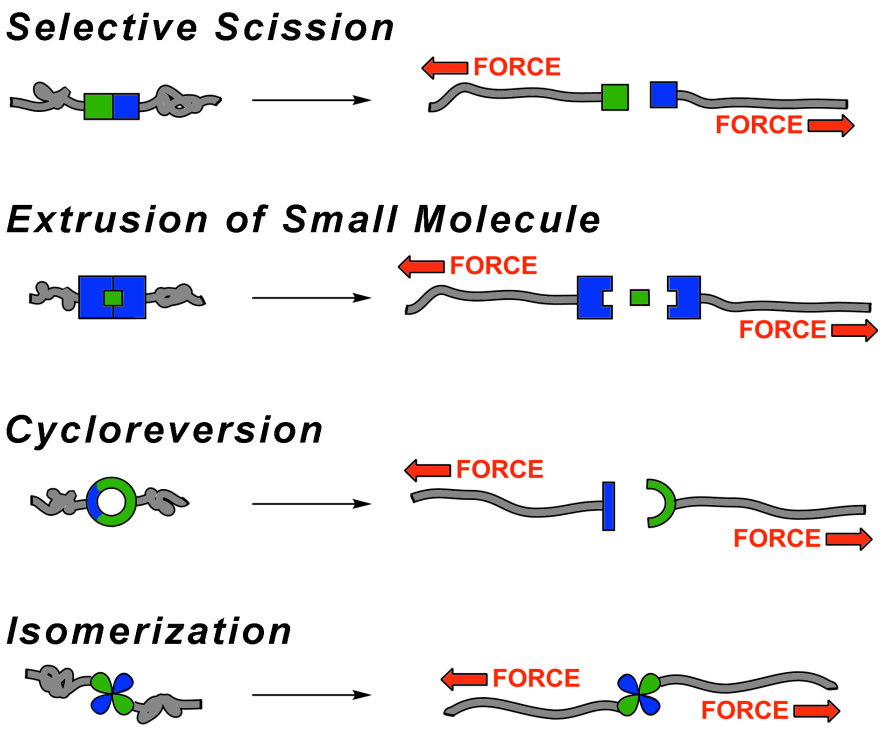

Figure 1.5 Generalized examples of polymer embedded mechanophores and their responses to the applied force.

EARLY STUDIES OF ULTRASONICALLY MEDIATED TRANSFORMATIONS

The use of ultrasound to mechanically activate polymers was first reported in the 1930s, when the degradation of natural polymers (such as starch and agar) under ultrasonication was observed.[17] Following those initial reports, a number of polymers were shown to degrade under ultrasound irradiation, including: polypeptides, polysaccharides, DNA, and various organic polymers.[2,3,18,19] While a variety of polymeric materials may be degraded under ultrasound irradiation, the rate of scission and MW threshold are both dependent upon the structure and composition of the polymer.[2] For example, in 1980, Encina *et al*. found that the rate of degradation of poly(vinylpyrrolidone) under ultrasonication increased tenfold when random peroxide linkages were incorporated into the polymer backbone.[20] While this report demonstrated

that polymer chains could potentially direct mechanical forces to covalent bonds with remarkable selectivity, the field of polymer mechanochemistry remained dormant for several years.

In 2005, Moore and co-workers demonstrated that relatively weak covalent bonds could be selectively targeted using ultrasound.[21] The team prepared a poly(ethylene glycol) (PEG) that contained a single diazo moiety located at the center of the polymer chain. When the material was subjected to ultrasonication, they observed a reduction in the polymer's MW that was consistent with cleavage of the main chain near the midpoint. Nuclear magnetic resonance (NMR) analysis of polymers containing ^{13}C enriched cyano substituents revealed that ultrasound irradiation generated polymers with cyanohydrin end groups, a result that was consistent with homolytic C–N bond cleavage and concomitant extrusion of dinitrogen from the diazo linkage (**Scheme 1.1**). In contrast, thermolysis of the polymer resulted in only a partial reduction in MW, and additional experiments involving ^{13}C labeled substrates provided compelling evidence that thermal activation resulted in the extrusion of dinitrogen with subsequent recombination of the radical-terminated polymer chains (**Scheme 1.1**). The large velocity gradients generated under ultrasonication were posited to prevent this recombination of polymer fragments from occurring by accelerating the radical chain ends away from one another. This seminal contribution suggested that mechanical activation could elicit reactivity that is distinct from that observed under thermal activation, and the work inspired the development of other mechanically responsive materials.

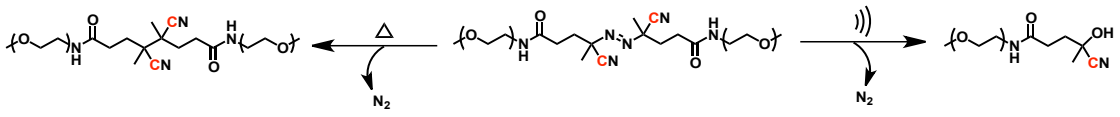

Scheme 1.1 Thermal and sonochemical activation of a diazo-linked poly(ethylene glycol). Isotopically labeled carbons are indicated in red.

ULTRASONICALLY FACILITATED ELECTROCYCLIC PROCESSES

Following their work with diazo-linked polymers, Moore, Sottos, and White began exploring benzocyclobutene mechanophores. Benzocyclobutenes undergo thermally or photochemically induced electrocyclic ring openings (EROs) to afford ortho-quinodimethide products, the stereochemistry of which are governed by the familiar orbital symmetry rules[22] developed by Woodward and Hoffmann (*i.e.*, the products of photochemical activation result from a disrotatory ERO, while thermal activation proceeds by a conrotatory ERO).[23] Surprisingly, mechanical activation of benzocyclobutene was found to break these symmetry rules and facilitate formally disallowed EROs.

This elegant work began with the incorporation of benzocyclobutene moieties into PEG chains such that the relative stereochemistry of the polymer attachment points on the mechanophore was either *cis* or *trans*. The resulting materials were then subjected to ultrasound irradiation, and the putative ortho-quinodimethide products of mechanical activation were selectively trapped with a ^{13}C enriched maleimide derivative through a [4+2] cycloaddition (**Scheme 1.2**). When the isotopically labeled materials were analyzed using ^{13}C NMR spectroscopy, only a single cycloadduct was observed, regardless of the initial benzocyclobutene stereochemistry. These data suggested that the *cis* and *trans* substituted benzocyclobutenes had undergone EROs to afford the same ortho-quinodimethide isomer, a result that could not be reproduced through thermal or photochemical activation (**Scheme 1.2**). As such, the observed stereochemical outcome of ultrasound activation necessitated that a formally disallowed ERO must have occurred. This formal violation of the Woodward-Hoffmann rules demonstrated that mechanical forces are capable of altering reaction coordinates irrespective of orbital symmetry, which

implied that mechanical activation could be used to realize chemical reactions that are inaccessible using other stimuli.

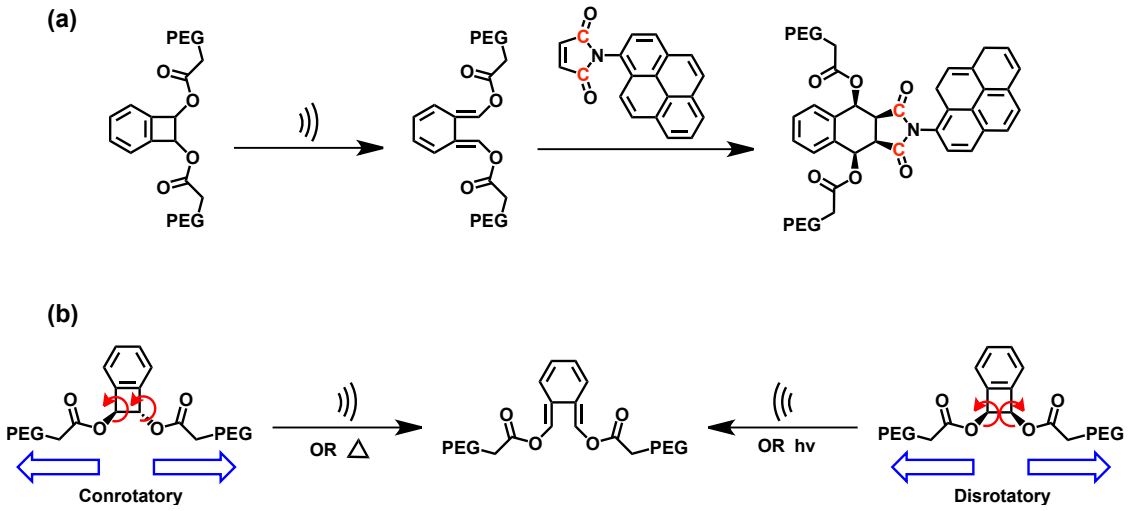

Scheme 1.2 (a) Force induced ERO of benzocyclobutene afforded an ortho-quinodimethide intermediate that was trapped with a ^{13}C-labeled maleimide derivative (red carbons represent isotopically labeled sites). (b) Regardless of the initial stereochemistry, force induced ERO of the benzocyclobutene moiety afforded a single product. The red arrows reflect the ERO process, while the blue arrows indicate the direction of the applied force.

Further efforts by Moore, Sottos, and White revealed that spiropyran mechanophores underwent force induced EROs to afford highly colored merocyanine derivatives.[24] In their investigation, poly(methyl acrylate) (PMA) was polymerized from a bifunctional spiropyran initiator to afford a single, centrally located mechanophore in each polymer chain. As shown in **Scheme 1.3**, irradiating this material with ultrasound resulted in an ERO of the spiropyran to its merocyanine derivative, as evidenced by the characteristic color change from colorless to pink. Moreover, the color change could be

photochemically reversed, which was consistent with photoisomerization of the merocyanine moieties to regenerate the spiropyran starting material.

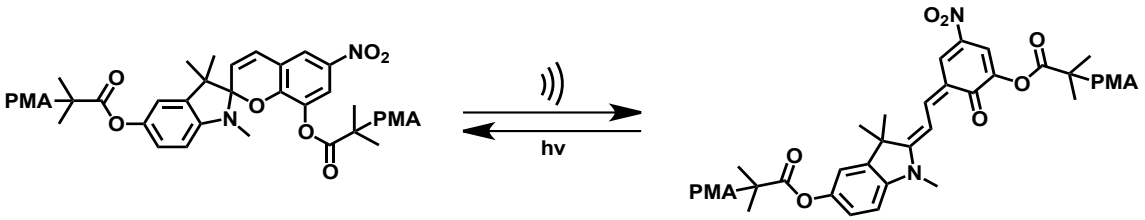

Scheme 1.3 Ultrasound induced ERO of a spiropyran moiety afforded a highly colored merocyanine derivative.

The mechanical activation of spiropyran has also been shown to take place in the solid-state under elongation and compression forces.[25] To probe the mechanical activation under elongation forces, PMA was grown from a difunctional spiropyran moiety and then loaded cyclically under displacement control. A gradual change in color was observed as the bulk material was elongated, and the extent to which mechanophore activation had taken place was quantified using digital image analyses. Similarly, poly(methyl methacrylate) (PMMA) beads containing spiropyran crosslinks were subjected to compression forces using a stepper actuator. As the PMMA beads were compressed, a red color consistent with the activation of the spiropyran mechanophore was observed, and the extent of mechanophore activation was quantified using fluorescence spectroscopy. The ability to monitor stress using colorimetric methods, as shown in these examples, has important implications for the realization of novel force sensors. For example, one application could be the design of load-bearing materials that highlight areas on the verge of failure through a distinct visual cue. Furthermore, the extent to which these materials experience damage could be quantified through optical measurements. The exciting foundation developed by this work, then, could ultimately

enable the development of mechanoresponsive composites that not only qualitatively alert observers to the presence of mechanical damage, but quantify damage as well.[25–28]

Following these seminal reports, other groups began exploring mechanically facilitated ERO processes. In 2009, Craig and co-workers reported that *gem*-dichlorocyclopropanes (gDCCs) could also undergo force induced EROs.[29] To incorporate gDCCs into a polymer backbone, 1,4-poly(butadiene) (PBD) was treated with dichlorocarbene to afford a material with gDCCs randomly dispersed throughout the polymer chain. Ultrasonic irradiation of these gDCC-PBD copolymers resulted in the ERO of some of the gDCCs within the polymer to afford 2,3-dichloroalkenes, which are the known ERO products that result from the thermal rearrangement of gDCCs. Analysis by ^{1}H and ^{13}C NMR spectroscopies revealed that the sonicated material contained a mixture of PBD, gDCCs, and 2,3-dichloroalkene units (**Scheme 1.4**). In addition to demonstrating that multiple mechanophore activations can be induced in a single polymer, this work presented new opportunities for post-polymerization modifications. For instance, Craig and Mahanthappa recently reported the generation of diblock copolymers when gDCC homopolymers were subjected to mechanical stress.[30] Similarly, *gem*-dibromocyclopropanes were found to undergo force induced EROs (even in the solid state) to afford 2,3-dibromoalkenes that were susceptible to nucleophilic substitution chemistry.[31]

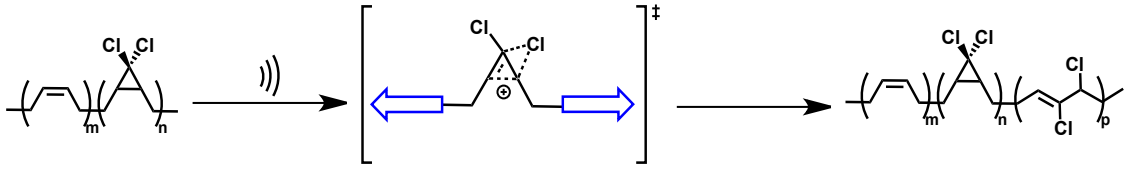

Scheme 1.4 Ultrasound induced ERO of gDCCs afforded 2,3-dichloroalkene units. The blue arrows represent the direction of the applied force.

Further efforts by Craig and Martinez revealed that *gem*-difluorocyclopropane (gDFC) moieties underwent thermodynamically disfavored isomerizations upon mechanical perturbation.[32] A mixture of *cis* and *trans* PBD was reacted with difluorocarbene to afford a cyclopropanated copolymer of *cis*/*trans*-gDFC and PBD. Surprisingly, when these materials were subjected to ultrasound the gDFCs did not undergo EROs to afford 1,2 difluoroalkenes. Instead, irradiation of the gDFCs resulted in their isomerization to predominantly the *cis*-gDFC isomers (*cis*:*trans* = 3.5:1), as shown in **Scheme 1.5**. When the *cis*/*trans*-gDFC-PBD copolymer was heated, however, the thermodynamically preferred *trans*-gDFC isomers were preferentially formed (*cis*:*trans* = 1:2.6). Thermal isomerization of gDFC is known to proceed *via* a disrotatory ERO to afford a diradical transition state that can undergo bond rotation to produce a *trans*-gDFC as the major product. The team hypothesized that mechanical force directed the ERO of both gDFC isomers to the same s-*trans* s-*trans* diradical transition state (*via* a disrotatory ERO of *cis*-gDFCs and a conrotatory ERO of *trans*-gDFCs, respectively). Presumably, bond rotation in the diradical species was minimized due to stabilization of this intermediate from the applied force; however, the diradical could undergo the formally allowed disrotatory ring closure to exclusively form the *cis*-gDFC isomer.

To verify the presence of a stabilized diradical under ultrasonication, the transient intermediate was successfully trapped with a coumarin dye that could be detected using absorbance spectroscopy (**Scheme 1.5**). No trapping was observed when the presonicated polymer was thermally treated, which indicated that the lifetime of the diradical species in the absence of stabilizing forces was sufficiently short to elude detection. The isomerization process was also noted to result in the contraction of the entire polymer (due to the decreased methylene-methylene separation in the *cis* isomer (3.2 Å) compared to the *trans* isomer (4.0 Å)), which was counterintuitive given that elongation forces were

applied to the material. This seminal work elegantly demonstrated that mechanical forces can stabilize reactive intermediates at or near the transition state of a chemical reaction, a phenomenon that could be utilized to gather invaluable mechanistic insights into and/or enable other chemical transformations.

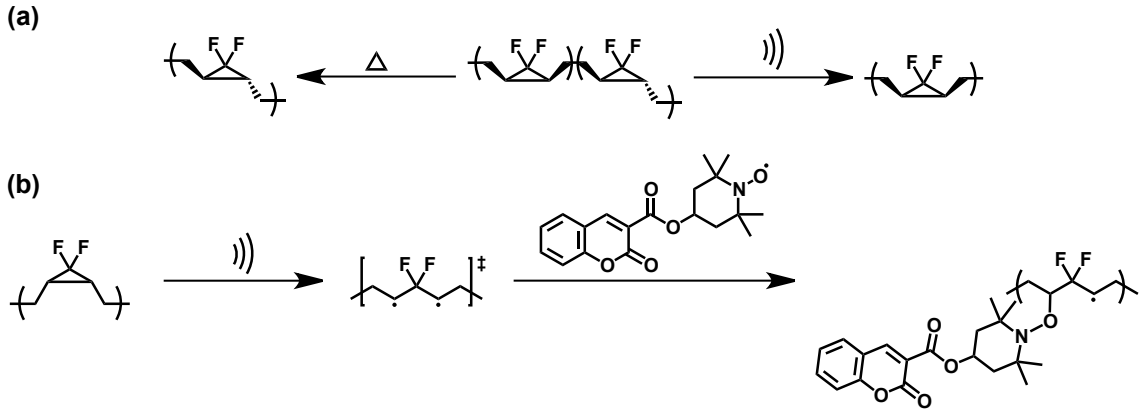

Scheme 1.5 (a) Heating *cis*/*trans* substituted gDFCs resulted in the formation of *trans* isomers; however, mechanical activation resulted in the formation of *cis* isomers. (b) The diradical intermediate of the ERO process was trapped using a coumarin radical scavenger.

Building upon this foundation, Craig and colleagues have recently reported the mechanically assisted ring opening of epoxide mechanophores.[33] The team found that mechanical forces were capable of inducing the opening of epoxide moieties embedded within poly(norbornene) systems, as evidenced by the observed isomerization of *cis* epoxides to the thermodynamically preferred *trans* isomers using ^{1}H NMR spectroscopy. The authors speculated that the ring opening reaction would afford transient carbonyl ylides, and these putative intermediates were confirmed through their selective reaction with a variety of chemical labels (**Scheme 1.6**). While the ring opening could also proceed through a mechanism involving diradicals, the team was unable to trap such species. Importantly, the authors reported that the polymer architecture was crucial for

the observed mechanical reactivity. For example, the ring opening of epoxides embedded within poly(butadiene) was negligible compared to the poly(norbornene) system, most likely a result of reduced chemomechanical coupling. This work, then, provided the first experimental evidence that changing the polymer architecture in which a mechanophore is embedded directly bears upon the observed mechanochemical reactivity.

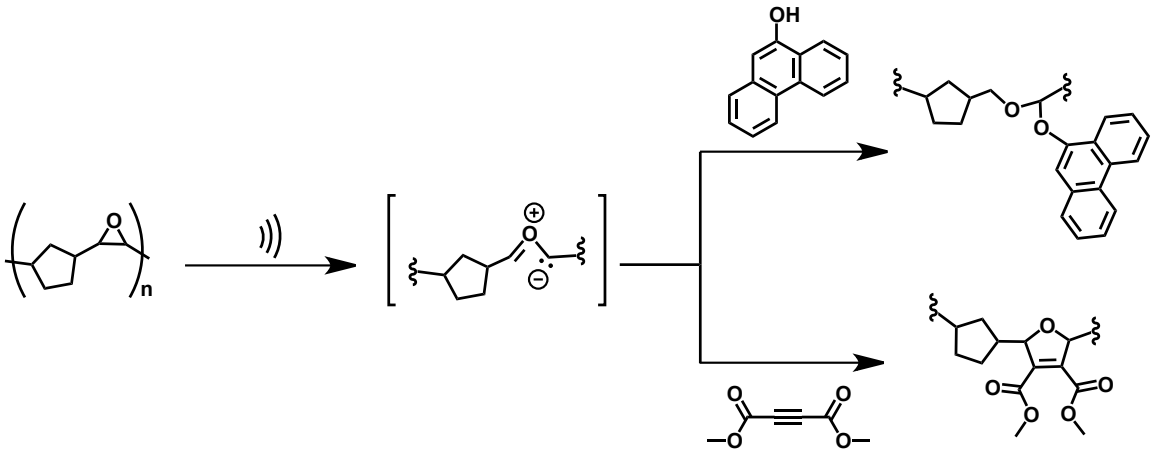

Scheme 1.6 Mechanically facilitated ring opening of epoxide moieties embedded within poly(norbornene) affords reactive carbonyl ylides that can be selectively reacted with chemical labels.

Another interesting report that has recently emerged involved the ring opening of 1,2-dioxetanes (**Scheme 1.7**).[34] These moieties are known to decompose into electronically excited carbonyl products upon chemical or thermal insult, and their electronic relaxation is often accompanied by the emission of blue light. Sijbesma and colleagues found that 1,2-dioxetanes that were incorporated into poly(methyl acrylate) matrices underwent a mechanically facilitated ring opening to the aforementioned carbonyl products upon ultrasound irradiation. The characteristic blue emission of dioxetane activation was observed upon ultrasonication, and the bulk activation of the polymeric materials was found to elicit a similar response. The autoluminescence of these

materials upon mechanical activation holds great promise for the development of novel stress sensors with enhanced temporal resolution.

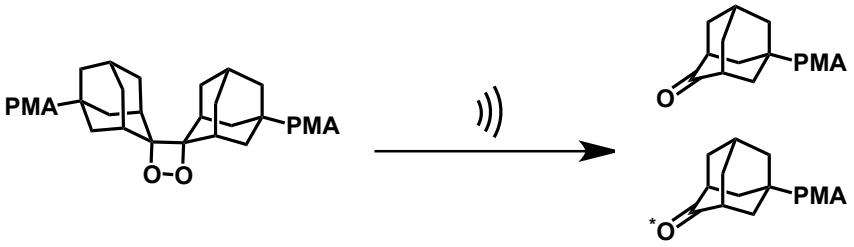

Scheme 1.7 Mechanical activation of 1,2-dioxetane moieties embedded within poly(methyl acrylate) (PMA) chains affords ketone products. The asterisk indicates an electronically excited ketone.

STEREOCHEMICAL RECONFIGURATIONS UNDER ULTRASONICATION

In an effort to expand mechanochemistry beyond bond scission events, the ability to mechanically surmount barriers to non-dissociative transformations became an area of interest. Initial efforts focused on the mechanochemical racemization of 1,1'-bi-2-napthol (binol) atropisomers, which are often utilized as chiral ligands for asymmetric catalysis.[35] Atropisomers exhibit hindered rotation about a sterically congested single bond and, consequently, exist as enantiomers with high thermal barriers to isomerization. Binol derivatives, for example, can possess thermal isomerization barriers in excess of 30 kcal mol^{-1}. Consequently, tedious, low-yielding syntheses or resolutions (which are inherently restricted to maximum yields of 50%) are required to access enantiopure materials. Ideally, this limitation could be circumvented if the stereochemistry of an atropisomer could be selectively (and directly) toggled.

To explore if mechanical approaches could achieve the desired stereochemical reconfiguration, an enantiopure binol moiety was embedded in a PMA chain and irradiated with ultrasound (**Scheme 1.8**). Upon sonication, the gradual formation of a racemic mixture was observed by circular dichroism (CD) spectroscopy. Analysis of the

postsonicated material revealed that the polymer had not degraded and that the binol moiety was still intact. To confirm that the observed racemization was not thermally promoted, an enantiopure binol derivative was heated to 257 °C for 72 h; no change in the material's CD signal was observed, which indicated that the reconfiguration process was not significantly influenced by thermal effects.

Having established that mechanical forces could be used to reconfigure stereoisomers, the next challenge was to employ this methodology in the resolution of a racemic mixture. It was envisioned that the polymer chains could be selectively cleaved from one enantiomer immediately after mechanical isomerization to prevent its further reaction. Removal of the polymer attachments would effectively render the polymer-free enantiomer immune to racemization (because, being of low MW, it would no longer experience the forces generated under ultrasound) and facilitate chiral resolution. Toward this end, the aforementioned mechanical reconfiguration was combined with enzymatic hydrolysis of the polymer chains appended to derivatives of (S)-binol.[36] As illustrated in **Scheme 1.8**, the ultrasonication of PMAs containing centrally located *rac*-binol moieties in the presence of cholesterol esterase resulted in the selective hydrolysis of the polymers attached to (S)-binol. Consequently, the resulting (R)-binol mechanophores, which retained their polymer attachments, remained susceptible to mechanical isomerization. Through this iterative process involving both mechanical isomerization and polymer chain cleavage, a single vessel approach to deracemization of atropisomers was developed. As a testament to the efficacy of this methodology, (S)-binol was isolated in excellent yield (90%) and high enantiopurity (> 99:1 e.r.). Further efforts showed that enantiopure (R)-binol could be converted to (S)-binol using a similar methodology. Combined, these reports demonstrated new approaches for toggling molecular configurations using mechanical force.

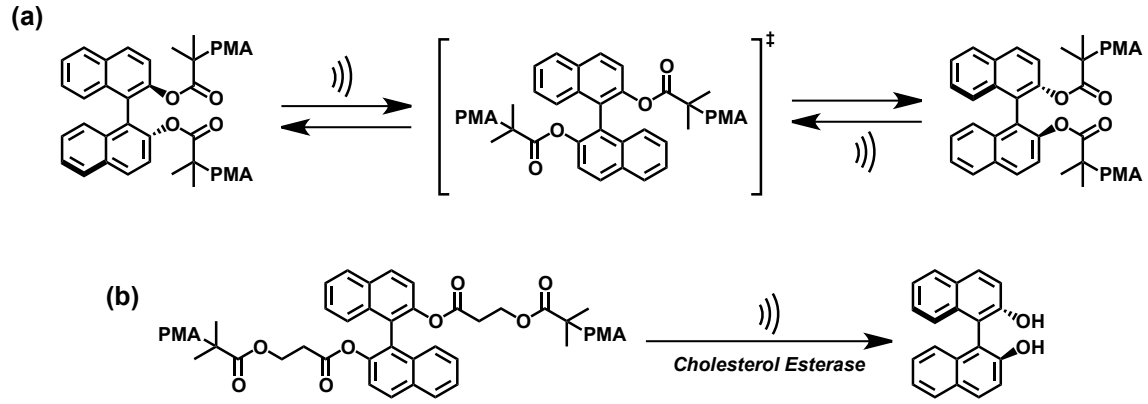

Scheme 1.8 (a) Ultrasound induced reconfiguration of derivatives of (S)-binol and (R)-binol. (b) A racemic binol derivative was selectively converted to the (S)-enantiomer using ultrasound in conjunction with enzymatic resolution.

ULTRASONICALLY FACILITATED CYCLOREVERSIONS

Most recently, the ability to induce cycloreversions through mechanical activation has been of increased interest.[37-41] While cycloaddition and cycloreversion chemistries provide convenient methods for masking and revealing reactive functionalities, respectively, many of these processes require high temperatures that can lead to undesired decomposition processes.[42-45] Mechanically facilitated cycloreversions offer a promising alternative for releasing reactive functionalities with high selectivity. Toward this end, two groups independently reported that cyclobutane mechanophores could undergo formal [2+2] cycloreversions upon mechanical activation.[37,38] Moore and co-workers focused on a dicyanocyclobutane mechanophore centered within a PMA chain.[37] They proposed that mechanical activation of the dicyanocyclobutane would result in a stepwise cycloreversion involving a diradical intermediate that could ultimately generate highly reactive cyanoacrylates. Since cyanoacrylates are known to autopolymerize, the release of these species upon mechanical damage would presumably afford materials

with self-healing properties (*i.e.*, the materials would repair themselves autonomously). Upon ultrasonication of the cyclobutane-linked polymers, a significant enhancement in the rate of chain scission was observed compared to control polymers that lacked the central cyclobutane moiety. Furthermore, the putative cyanoacrylate products of cycloreversion were successfully trapped with a chromophore-bearing amine through standard Michael addition chemistry (**Scheme 1.9**).

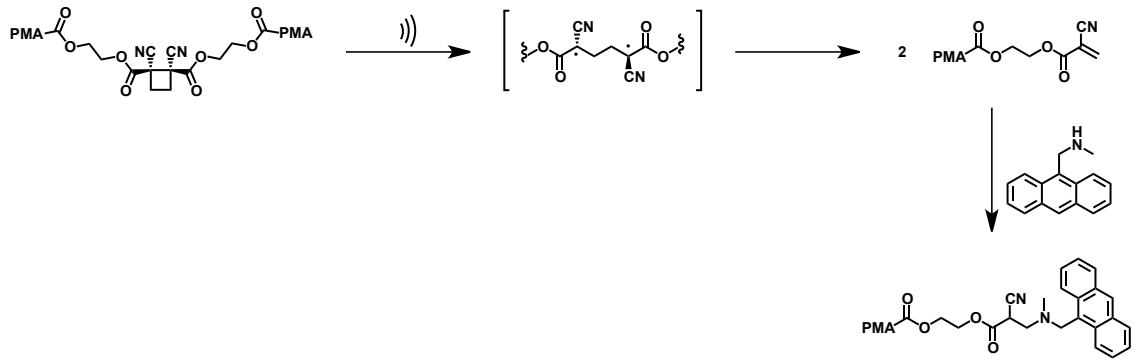

Scheme 1.9 Ultrasound induced cycloreversion of a dicyanocyclobutane mechanophore afforded a cyanoacrylate derivative. A proposed intermediate is shown in brackets.

Similarly, Craig and co-workers reported the formation of trifluorovinyl ethers from the ultrasound induced cycloreversion of perfluorocyclobutane mechanophores.[38] In this system, polymers consisting of perfluorocyclobutane-containing repeat units were prepared such that the mechanophores were dispersed throughout the polymer backbone. Upon irradiation with ultrasound, the formal cycloreversion of the perfluorocyclobutane mechanophores resulted in a significant reduction in the MW of the polymer (**Scheme 1.10**). The trifluorovinyl ether products of mechanical activation were thermally recoupled (presumably through a radical pathway), albeit with limited recovery of the polymer's initial MW (*c.f.* MW of 36 kDa for the recoupled polymer versus 115 kDa for the starting material). The limited thermal recoupling was explained by the fact that

small-scale polymerizations of trifluorovinyl ethers are known to be problematic, with a terminal MW of approximately 30 kDa being common.[38] Moreover, ultrasound induced degradation of a polymer with a MW of 37 kDa, which was near the reported threshold for efficient thermal recoupling, resulted in the formation of fragments that recombined with high fidelity (*c.f.* 13 kDa for the sonicated material versus 36 kDa for the recoupled polymer).

To confirm that the cycloreversion was occurring through a stepwise radical-based mechanism, the putative 1,4-diradical intermediate of the formal cycloreversion process was selectively trapped using coumarin-2,2,6,6-tetramethylpiperidine-1-oxyl. In addition to being consistent with the proposed mechanism of activation, the trapping of this diradical provided additional evidence that mechanical forces can be coupled to reaction coordinates to stabilize reactive intermediates.

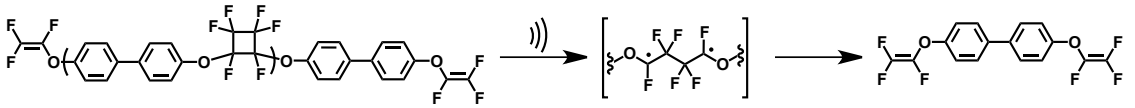

Scheme 1.10 Ultrasound induced cycloreversion of a polymer embedded perfluorocyclobutane. A proposed diradical intermediate of mechanical activation is shown in brackets.

Along the same vein, mechanically facilitated retro-[4+2] cycloadditions have recently been reported.[39] As Diels-Alder adducts (*e.g.*, oxanorbornene derivatives) have been implemented in dynamic covalent materials,[46-48] mechanically facilitated [4+2] cycloreversions are particularly relevant for the development of self-healing systems.[49] To determine the viability of mechanically induced [4+2] cycloreversions, PMA was grown from an oxanorbornene-based bifunctional polymerization initiator and then subjected to ultrasonication. Chain scission near the center of the polymer was observed, and the generation of maleimide-terminated polymer fragments was confirmed by

selectively labeling these moieties using an appropriate chromophore (**Scheme 1.11**). Furthermore, the liberated furan moieties were identified *via* Diels-Alder chemistry with a rhodamine derivative bearing a pendant maleimide. The products obtained from both labeling experiments were characterized using gel permeation chromatography (GPC) visualized with ultraviolet-visible detection, which confirmed the attachment of the chemical labels to the polymeric materials.

In the same report, mechanical activation was shown to promote thermally inaccessible [4+2] cycloreversions (**Scheme 1.11**). Initially, PMA was grown from the Diels-Alder adduct of anthracene and maleimide derivatives, and the resulting material was subjected to ultrasound irradiation. In addition to a reduction in MW consistent with chain scission near the polymer midpoint, the characteristic absorbances of anthracene were observed in the polymeric product upon isolation. Evidence for the mechanical nature of the proposed cycloreversion arose from the observations that neither anthracene absorbances nor a reduction in MW were detected after subjecting the presonicated polymer to forcing thermal conditions. Moreover, the diene and dienophile components liberated upon mechanical cycloreversion could be recoupled through a thermally promoted Diels-Alder cycloadditions for both the anthracene/maleimide and oxanorbornene systems. Collectively, these data demonstrated that the observed degradation of the polymers occurred through a mechanically facilitated [4+2] cycloreversion. Importantly, the ability to cyclorevert thermally robust Diels-Alder adducts under the action of mechanical force could enable new opportunities in the development of force responsive materials, especially for self-healing and sensing applications.[50]

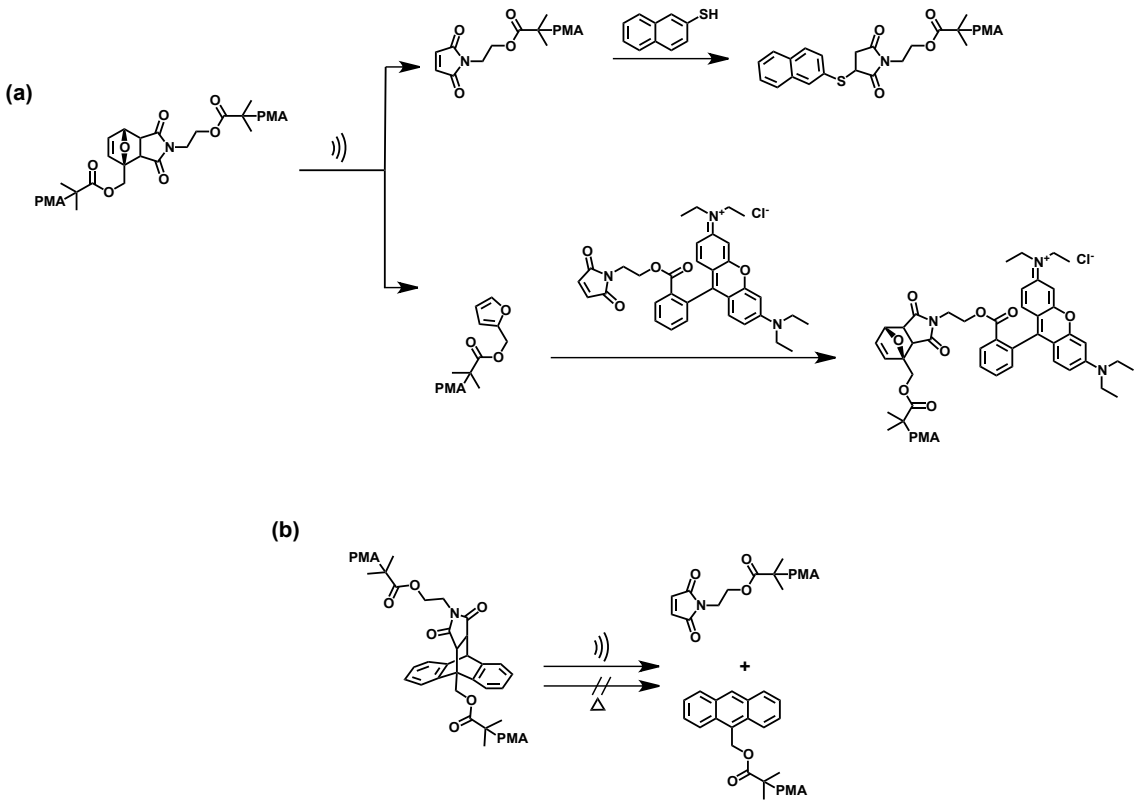

Scheme 1.11 (a) Ultrasound induced cycloreversion of an oxanorbornene-based mechanophore and subsequent trapping of the liberated moieties. (b) Ultrasound induced cycloreversion of a thermally robust maleimide-anthracene cycloadduct.

ULTRASONICALLY ACTIVATED CATALYSTS

Building upon the early work involving site-specific scission within polymer chains, the development of mechanocatalysts (*i.e.*, latent catalysts that could be activated by mechanical forces) became an avenue of exploration. Based on their previous studies involving the behavior of transition metal coordination polymers under ultrasound,[51,52] Sijbesma and co-workers demonstrated that a polymer functionalized silver bis(*N*-heterocyclic carbene) complex could liberate an active *N*-heterocyclic carbene (NHC) organocatalyst that facilitated transesterifications (**Scheme 1.12**).[53] As part of a series of control experiments, they found that the same esterification under ambient conditions

proceeded to less than 3% conversion in the absence of ultrasound irradiation, and heating the silver precursor did not afford the same reactivity that was observed under acoustic activation.

Subsequent efforts by the same group demonstrated that latent olefin metathesis catalysts could also be mechanically activated.[53] When a polymer-functionalized ruthenium alkylidene complex was subjected to ultrasound irradiation, force induced ligand dissociation generated an active catalyst that facilitated the ring closing metathesis (RCM) of diethyl diallylmalonate, as well as the ring opening metathesis polymerization (ROMP) of cyclooctene (**Scheme 1.12**). The metathesis catalyst could be toggled between "on" and "off" states using ultrasound, which validated mechanical approaches to manipulating the catalytic activity of organometallic complexes. Unfortunately, the rate of ROMP reactions decreased with increasing "on-off" cycles, which was determined by NMR spectroscopy to be the result of catalyst decomposition. Regardless, the work provided compelling evidence that organo- and organometallic catalysts could be selectively activated using mechanochemical approaches.

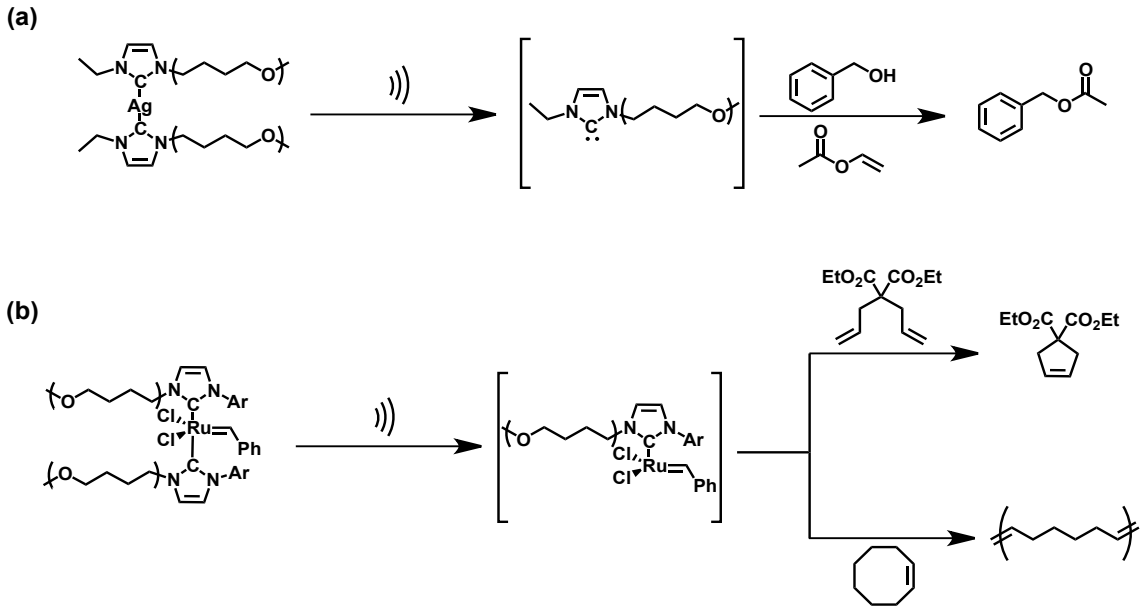

Scheme 1.12 (a) Ultrasound induced activation of a latent transesterification organocatalyst. (b) Ultrasound induced activation of a latent ruthenium metathesis catalyst. The putative catalysts are indicated in brackets.

Other mechanically activated latent catalysts have focused on pincer-type palladium pyridyl complexes.[54] As illustrated in **Scheme 1.13**, ultrasound induced the deligation of one of the pyridine ligands from the putative mechanocatalyst and generated an active species that facilitated the cross coupling of benzylic nitriles and *N*-tosyl imines. Thermal contributions were precluded by the minimal catalyst activity that was observed in the absence of ultrasound. Furthermore, the mechanically liberated pyridine moiety was quantitatively titrated with the HBF_4 adduct of 4-[(4-anilinophenyl)azo]benzenesulfonic acid, which exhibited a colorimetric response to deprotonation by the pyridine released upon ultrasonication. No colorimetric response was observed in the absence of ultrasound irradiation, which provided further evidence that mechanical activation was facilitating the dissociation of the polymer-bound pyridine ligand from the metal center. Moreover, the liberated pyridine moiety facilitated the

polymerization of α-trifluoromethyl-2,2,2-trifluoroethyl acrylate (**Scheme 1.13**). The ability to mechanically activate two latent catalysts, each of which displayed different reactivity, from the same inactive precursor reflected an advance in the design of mechanically responsive catalysts. Expanding on these findings, the activation of a boron-based mechanocatalyst with pyridine-capped PMA ligands was also reported.[55] This system exhibited the same response to colorimetric titrations and polymerization activity as the previously reported palladium-based mechanophore (**Scheme 1.13**).[54]

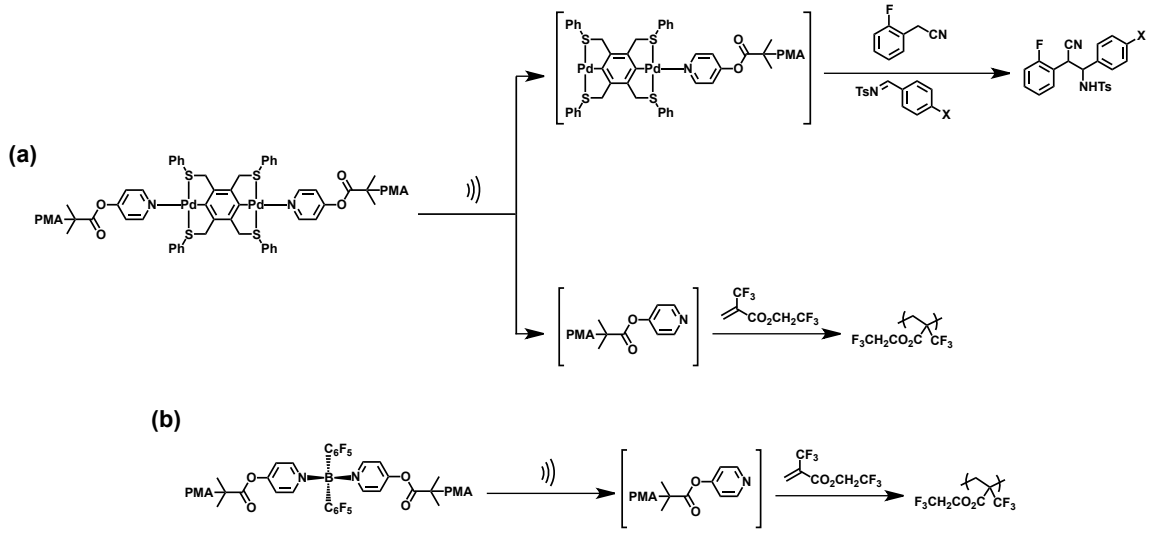

Scheme 1.13 (a) Simultaneous mechanical activation of a pyridine organocatalyst and an organometallic palladium catalyst from the same precursor (X = F or H). (b) Ultrasound induced activation of an organocatalyst from a boron-based precursor. The putative catalysts are indicated in brackets.

Collectively, these examples of mechanocatalysts have opened new opportunities for latent catalysis, and they have provided alternative routes to useful bond forming reactions that could find applications in self-healing materials or as colorimetric indicators of mechanical degradation. Furthermore, the ability to selectively reveal

catalytically active moieties under mechanical perturbation could enable unprecedented control in metal-mediated syntheses and inspire new catalyst designs.

All of the above examples illustrate that ultrasound is not only a straightforward and effective method for the mechanical activation of polymers, but it is also capable of promoting novel chemical reactions with high specificity.[2] Ultrasound is particularly advantageous because numerous control experiments can be used to confirm the mechanical nature of the observed reactivity. Another advantage of ultrasound is that, when combined with other chemistries, it can be used to isolate valuable small molecules.[36] There are, however, some disadvantages to using ultrasound as a means to mechanically activate polymers. Currently, most sonication experiments are performed using dilute polymer solutions and a probe sonicator inserted into a Suslick cell.[56] The size of the apparatus limits the volume of each experiment (~ 10 mL), and many of these experiments require sensitive and/or tedious analyses to properly characterize the products of mechanical activation. While characterization can be challenging, a number of techniques have been employed to overcome this constraint (*vide supra*). Additionally, because of the heat generated in acoustic fields, these experiments must be performed at low temperatures to minimize thermal interference. Nonetheless, ultrasonication has proven valuable for promoting fundamentally new transformations.[2]

MECHANICAL ACTIVATIONS IN BULK POLYMERIC MATERIALS

While mechanical activation of solvated polymers has significantly advanced the field of polymer mechanochemistry, the majority of polymeric materials find applications in the solid-state.[2] Thus, the examination of polymeric materials in the bulk is imperative to the development of mechanoresponisve systems with direct applications beyond the laboratory. As the maximum macroscopic force that can be exerted on bulk materials is

large (up to 10^5 N; see **Fig. 1.1**), a broader range of mechanically induced transformations could potentially be accessed in the solid-state. Indeed, a number of phenomena have been observed during mechanical activation of polymers in the solid-state, including changes in conformation and chain alignment, the disruption of non-covalent interactions (*e.g.*, hydrogen bonding and Coulombic interactions), and the formation or disruption of eximers.[2] In general, force can be applied to polymers in the solid-state through either elongation or compression. A number of techniques, ranging from manual bending to the use of specialized instrumentation (such as the various Instron® apparatuses or rheometers), can enable the application of elongational forces to macromolecules in the solid-state. While manual bending is a relatively simple method for ascertaining whether or not a material is mechanically responsive, the use of specialized instrumentation enables quantification and control of both the strain rate and the applied macroscopic force. In addition, mechanical testing instruments can be coupled to optical spectrometers, thereby facilitating the evaluation of mechanochromic materials. The substantial forces ($0.01 - 6.0 \times 10^5$ N) and strain rates ($0 - 2 \times 10^2$ s^{-1}) that can be generated by specialized instrumentation, however, can potentially degrade the material under investigation. Thus, to avoid undesired material decomposition, elongation experiments are typically performed using moderate forces (~ 1 N) and low strain rates (~ 1 s^{-1}).

In order to apply elongational forces to a polymer, the material must first be processed into a defined shape (*e.g.*, the prototypical "dog bone" sample) either by solution casting, melt processing, or compression molding. Given these constraints, mechanically responsive polymers exhibiting high melting temperatures or limited solubility are particularly challenging to analyze *via* elongation techniques. Moreover, materials that have the same response to thermal and mechanical stimuli should not be

processed in the melt, as this may result in premature thermal activation. Likewise, compression molding can result in mechanical activation of the material prior to elongational testing. Fortunately, most of the polymers that have been analyzed using elongational forces (*e.g.*, poly(methyl acrylate), polyurethane, and low density polyethylene) have relatively low melting temperatures and/or are easily processed.[2]

MANUAL ELONGATION OF POLYMERIC MATERIALS

The simplest way to apply elongational forces to a polymer is to manually stretch the material. While this approach does not allow for quantification of the strain rate, it can permit rapid assessment of a mechanically responsive material. For example, manual elongation has been used to study the cycloreversion of tricinnamate monomers incorporated into polymer films. The fluorescent tricinnamate species were first cross-linked through photochemical [2+2] cycloadditions to prepare polymer films that exhibited minimal fluorescence.[57] Bending the resulting films resulted in crack formation with a concomitant increase in fluorescence, which was consistent with cycloreversion of the tricinnamate dimers (**Figure 1.6**). Moreover, the damage to the materials could be spatially resolved using fluorescence microscopy (which is valuable for the development of novel stress sensors[58]), and additional evidence supporting the proposed mechanical cycloreversion was obtained using infrared (IR) and NMR spectroscopic analyses. As the forces generated by manual elongation cannot be quantified, however, bending is typically only used for preliminary studies or qualitative testing.

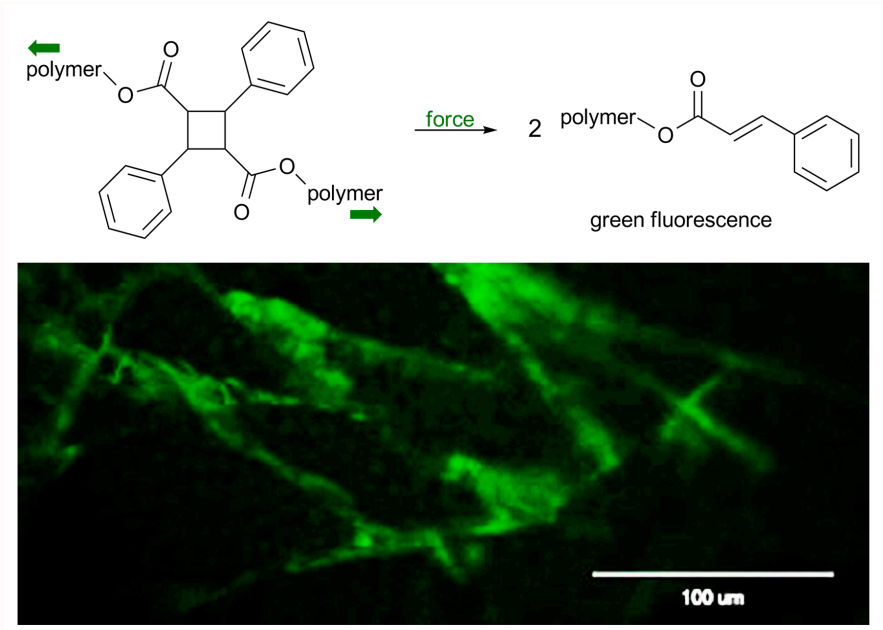

Figure 1.6 Crosslinked-cyclobutane polymers undergo mechanically facilitated cycloreversion to give fluorescent tricinnamates (top), which exhibit green fluorescence allowing for spatially resolved crack-sensing with fluorescence microscopy (bottom). The green arrows indicate the direction of the applied force. Image reprinted with permission from Elsevier, Ref. 57, 2008.

MECHANICAL ACTIVATIONS USING TENSILE TEST INSTRUMENTS

Tensile testing devices and screw-driven load frames have also been used to probe mechanically responsive materials under elongational deformation (**Figure 1.7**).[59] As with rheometers, the advantage of this technique over manual stretching is that the strain rate and applied force can be precisely measured and controlled. Typically, these tests are performed at moderate forces (~ 1 N) and strains (up to 500%), as well as low strain rates (~ 1 s^{-1}) to avoid premature degradation of the material. Thus, despite the fact that tensile testing apparatuses can require large amounts of processed sample for testing, numerous mechanically responsive materials have been studied with these instruments.

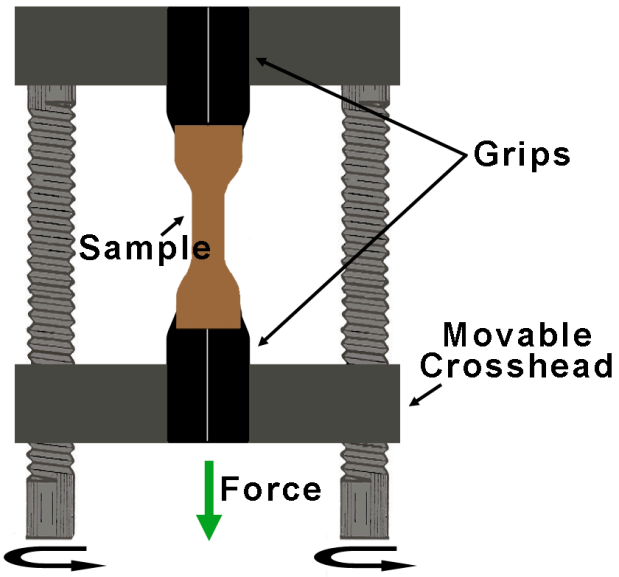

Figure 1.7 Schematic drawing of the components of a typical tensile testing instrument.

For instance, an Instron® tensile testing device was used to study mechanically responsive materials comprised of hydrogen bonded networks.[60] Specifically, azobenzene-containing amide oligomers were locked into their *cis* conformations, incorporated into a polyurethane matrix using condensation chemistry, and cast into films from dimethylformamide. Tensile stress (100 – 300% strain) was found to break the hydrogen bonds, which ultimately led to isomerization of the azobenzene from the *cis*- to the *trans*-isomer (**Scheme 1.14**), as observed by ultraviolet-visible spectroscopy. The reverse reaction (*i.e.*, from *trans*- to *cis*-azobenzene) was not observed due to the relatively high thermodynamic stability of the *trans*-isomer.

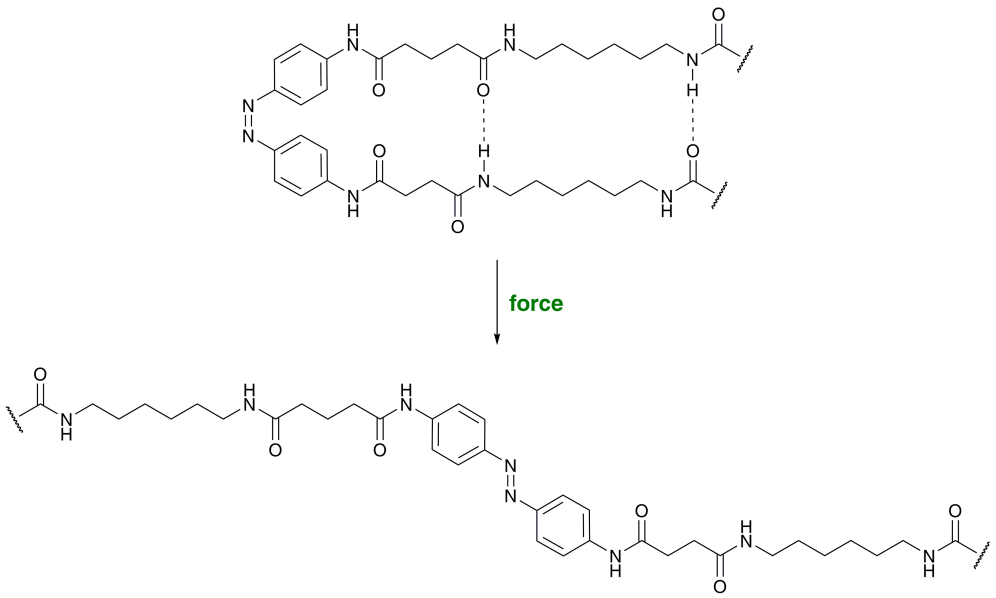

Scheme 1.14 Embedding the shown amide oligomers into a polyurethane matrix and stretching the resultant material caused mechanical rupture of hydrogen bonds with concomitant isomerization of the azobenzene (*cis* to *trans*).[60]

Tensile testing devices can also be coupled with simultaneous optical spectroscopy for the study of mechanochromic materials. For example, tensional stress can result in the mechanical deconstruction of eximers (or excited state complexes) that have been incorporated into a polymeric material. Using a commercial tensile testing device, Weder and colleagues explored how mechanical disruption of dye aggregates in polymer blends modulated the materials' luminescent properties.[61] Specifically, blends of oligo(*p*-phenylene vinylenes) (OPVs) in linear low-density polyethylene (LLDPE) were prepared by solvent diffusion of the OPVs into pre-formed LLDPE films. As illustrated in **Figure 1.8**, blends of LLDPE containing either 1,4-bis(R-cyano-4-methoxystyryl)-2,5-dimethoxybenzene (BCMDB) or 1,4-bis(R-cyano-4-methoxystyryl)benzene (BCMB) exhibited distinct changes in their luminescent properties in response to mechanical

elongation (up to 400% elongation). Similar mechanochromic blends of OPVs with other synthetic polymers have also been studied using tensile testing apparatuses.[58]

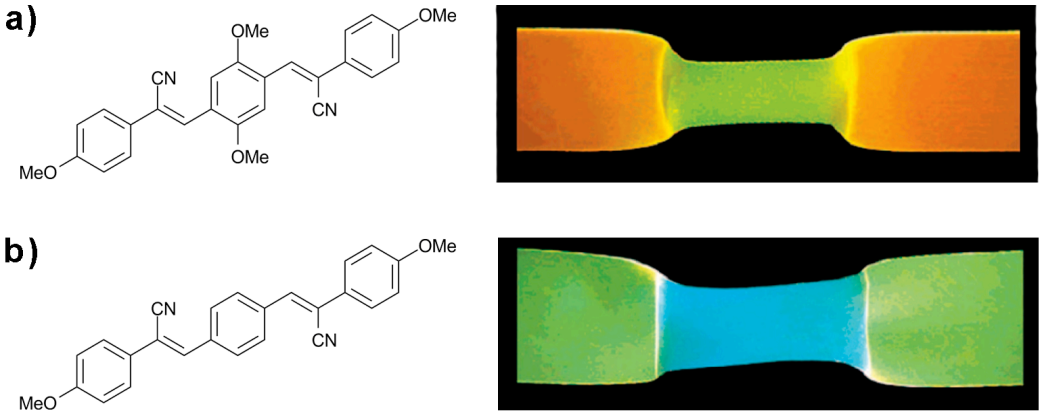

Figure 1.8 LLDPE blends containing a) BCMDB or b) BCMB were elongated by 500% and illuminated at 365 nm. LLDPE = linear low-density polyethylene; BCMDB = 1,4-bis(R-cyano-4-methoxystyryl)-2,5-dimethoxybenzene; BCMB = 1,4-bis(R-cyano-4-methoxystyryl)benzene. Images reprinted with permission from the American Chemical Society, Ref. 61, 2003.

While the above examples detail the mechanical deconstruction of eximers, the mechanically induced formation of excited state complexes can also result in mechanochromic behavior. In one interesting example, Ikara and coworkers examined eximer formation from carbazole units in response to tensile deformation.[62] Blends of poly(*N*-vinyl carbazole) and polystyrene exhibited fluorescence changes consistent with partial overlap of two carbazoles in response to elongation (strain = 0 – 0.8%) in a screw-driven load frame. Analogous research efforts have focused on mechanochromic materials that incorporate Förster resonance energy transfer (FRET) partners[63] or exhibit non-scissile changes in conjugation length upon elongation.[64] One well studied class of conjugated polymers is the poly(alkylthiophenes), which were found to exhibit marked changes in fluorescence decay times and conductivity upon tensile deformation.[64]

As described above, methods for applying tensional force to polymers are particularly advantageous for exploring mechanochromic materials, especially when they can be accompanied by simultaneous optical spectroscopy. Moreover, tensile testing devices allow for the controlled application of stress at a known strain rate ($0 – 2 \times 10^2$ s^{-1}) and macroscopic force ($0.01 – 6.0 \times 10^5$ N). The ability to monitor the stress and strain of mechanoresponsive materials also allows for the quantification of other mechanical properties (*e.g.*, yield strength, elongation at break, Young's modulus, etc.), which is important for identifying potential applications.

The major disadvantage to many of the aforementioned apparatuses (particularly the tensile testing devices) is that they require large quantities of material. Further, the polymers must be processed into well-defined shapes, which can make studying materials with high melting points and/or limited solubility challenging.

MECHANICAL ACTIVATION VIA COMPRESSION

Like tension testing, compressional forces have also been used to activate mechanically responsive materials in the solid-state. However, unlike their elongational counterparts, most compression devices do not require well-defined samples, which can be advantageous when studying materials that are difficult to process. Instead, non-uniform samples can simply be cut or broken into sufficiently sized pieces for the chosen apparatus. There are various systems for testing mechanochemical responses to compression (*e.g.*, pressure cells, diamond anvil cells, and hydraulic presses), and a large range of pressures can be accessed under compression (0.1 MPa – 300 GPa).[2] The force (F) applied under compression can be calculated at a given pressure (P) exerted on a sample of known area (A), since $P = F \times A^{-1}$. Typically, compression is performed on

small samples (< 1 cm^2) and at moderate pressures (0.1 – 8 GPa), which equates to $1.0 \times 10^4 – 8.0 \times 10^5$ N of force.

Because a number of mechanically responsive materials are mechanochromic, it can be important to simultaneously monitor the changes in a material's optical properties as a function of force. As such, a number of compression apparatuses that allow for simultaneous optical spectroscopy have been developed. One such class, the piston-based pressure cells, apply compressional force to polymers using a pressure medium (*e.g.*, an inert gas or Teflon oil; **Figure 1.9**).[65] When the sample chamber is compressed with a steel piston, the pressure in the system increases, and the optical activity of the sample can be simultaneously monitored with an attached spectrometer. Piston-based pressure cells have been used to study compression induced changes in molecular conjugation length, which can result in mechanochromic behavior.[65] For instance, Moses *et al*. found that both *cis*- and *trans*-diacetylene polymers exhibited reversible force induced increases in conjugation length with concomitant broadening of their absorbance peaks under compression in a piston-based cell (up to 5 GPa).[65] At pressures above 5 GPa, irreversible changes were observed in the absorbance spectra, presumably due to force induced cross-linking.

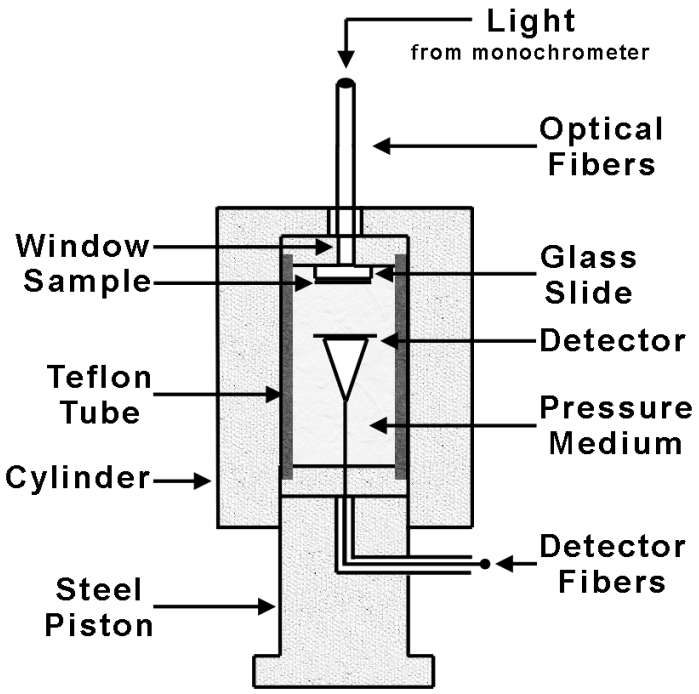

Figure 1.9 Schematic representation of a piston based pressure cell composed of a cylinder, a steel piston, a Teflon tube, and pressure medium. Light enters *via* optical fibers through a window into the sample chamber. The sample sits in the light path on a glass slide, and the transmitted light is detected by a photodetector.[65]

Using a similar mechanism to the piston-based cell, diamond anvil cells have also been used to examine mechanochromic materials under bulk compression. The use of diamond anvils is advantageous because they require smaller amounts of material (< 100 mg) and can achieve pressures in excess of 300 GPa (3.0×10^7 N for a 1 cm^2 sample), which may allow access to an increased number of mechanically induced transformations. Typically, diamond anvil cells employ a ruby reference material to monitor the amount of pressure being applied to the sample (**Figure 1.10**).[66] Like other pressure cells, they employ a pressure medium and can be outfitted with spectrometers to simultaneously measure optical changes under increasing pressure. For example,

Murmatsu *et al*. used a diamond anvil pressure cell to study the mechanochromic response of anthraquinone-containing polymer powders.[67] Under increasing pressure (0.55 – 11 GPa), the color of poly(5,8-dihexadecyloxyanthraquinone-1,4-diyl) changed from yellow to deep red as the effective conjugation length of the material increased (**Figure 1.11**). The observed color change was believed to result from a force induced decrease in the distance between the π-faces of the aromatic rings in the anthraquinones, which resulted in increased arene interactions.

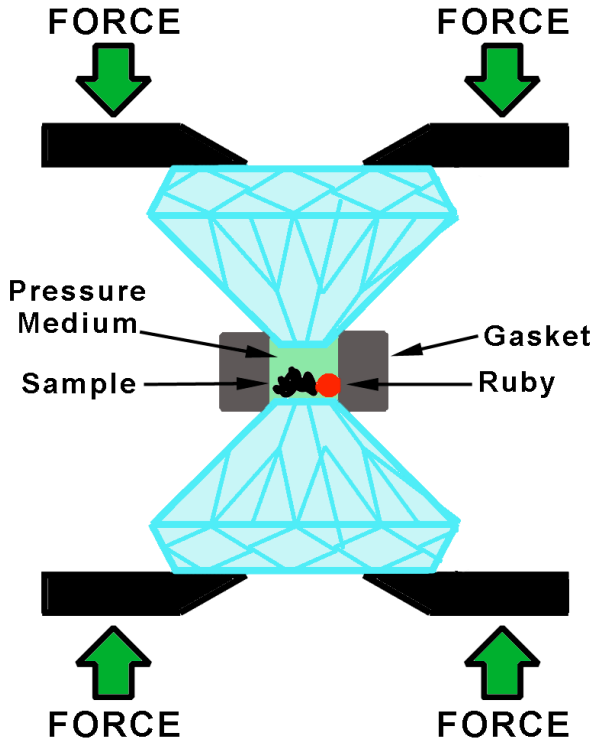

Figure 1.10 Schematic drawing of a diamond anvil press. Two opposing diamonds apply pressure to the sample and a ruby pressure standard that are surrounded by a pressure medium. Slits above and below the sample area allow for simultaneous spectroscopic analysis.

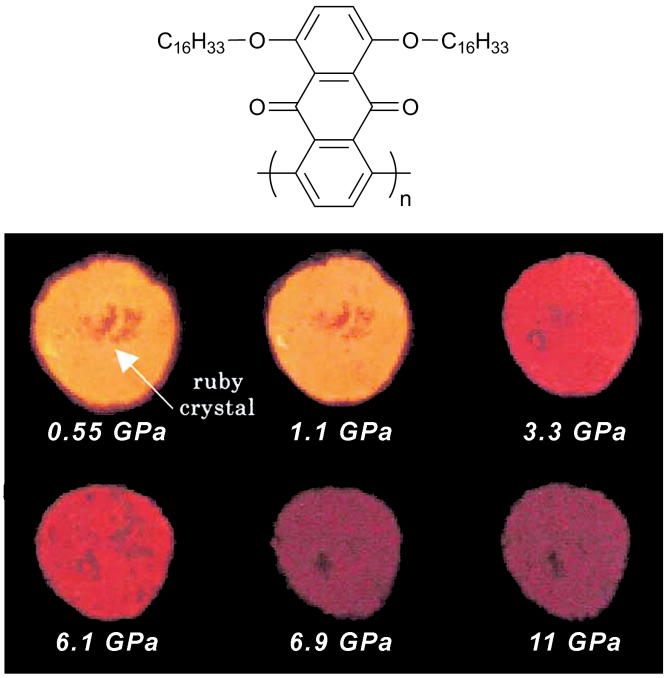

Figure 1.11 Structure and optical images of poly(5,8-dihexadecyloxyanthraquinone-1,4-diyl) under increasing pressures. The shadows resulted from the ruby crystal used to monitor the pressure. Image reprinted with permission from Elsevier, Ref. 67, 2001.

While the compression devices described above are relatively sophisticated, there are comparatively simple methods for applying compressional forces to mechanically responsive materials. One approach is to use a hydraulic press (similar to the ones used to make KBr pellets for IR spectroscopy) and determine the applied stress by measuring the sample area before and after compression.[68,69] Early work by Craig and coworkers used a hydraulic press to examine the reactivity of their previously reported *gem*-dichlorocyclopropanes[29] under compressive forces (36 – 249 MPa).[68] The polycyclopropanated materials underwent mechanically facilitated ring openings to afford 2,3-dichloroalkenes (see **Scheme 1.4**), which eliminated HCl upon thermal treatment.[68] To confirm that the activation was due to mechanical force, different samples

were held at constant pressure (178 MPa) on varying timescales (15 – 600 sec). The number of ring-opened cyclopropanes did not vary with time, which was consistent with a mechanically facilitated process.

Moore and coworkers expanded on this concept by designing a material that was envisioned to spontaneously release mineral acids upon mechanical ring opening.[69] This material contained *gem*-dichlorocyclopropanated indenes, which were selected for two primary reasons: 1) the aromatic system could stabilize the carbocation intermediate associated with the cyclopropane ring opening, and 2) the formation of aromatic products upon mechanical ring opening would provide an additional driving force for the elimination of the acid (**Scheme 1.15**). As such, a poly(methyl acrylate) matrix crosslinked with *gem*-dichlorocyclopropanated indenes was synthesized and subjected to compression (**Scheme 1.15a**). Because the samples were difficult to process, a hydraulic press was used to apply a compressive force. Under mechanical stress (0 – 352 MPa, held for 30 min.), the indene moieties underwent a mechanical rearrangement wherein cyclopropane ring opening resulted in aromatization with concomitant extrusion of HCl (**Scheme 1.15b**). The observed mechanical activation displayed a monotonic response with increasing pressure, with more than 20% activation achieved. Moreover, control experiments showed that the indene moieties had to be covalently bound to the polymer matrix in order for mechanical activation to occur. Both the monotonic response to increasing pressure and the need for covalent attachment of the indene to the polymer matrix suggested that the ring opening was mechanically facilitated. Importantly, the mechanical generation of acids may afford materials that are useful for self-healing applications,[70] wherein the acid could induce cross-linking (or other bond forming) events.

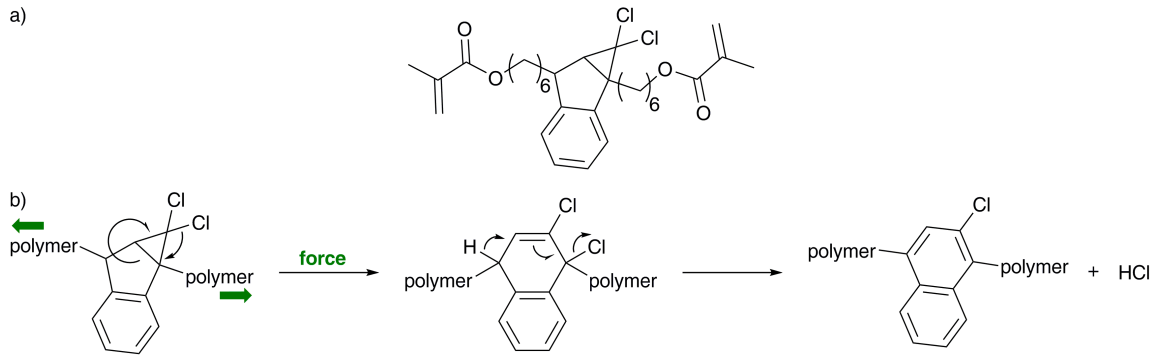

Scheme 1.15 a) A *gem*-dichlorocyclopropanated indene cross-linker. b) Compression of polymer embedded *gem*-dichlorocyclopropanated indenes led to cyclopropane ring opening and subsequent expulsion of HCl. The green arrows indicate the direction of the applied force. polymer = poly(methyl acrylate)[69]

Mechanically responsive ionic polymer brushes have also been studied under compressional forces using a hydraulic press. Azzaroni *et al*. compressed polymer brush films by growing the materials from a glass slide and affixing the slide between two pieces of crosslinked poly(dimethyl siloxane) that were held together in an IR cell. The entire set-up was then subjected to compression with a small laboratory press (**Figure 1.12a**).[71] Compression of the poly([2-methacroyloxy]ethyl trimethyl ammonium chloride) brushes that were intercalated with Bromothymol blue dye resulted in a visible color change from yellow to blue (**Figure 1.12b**). Presumably, when the brushes were pressed together, the dye adopted an anionic form to help shield local areas of high positive charge. The color change associated with the aforementioned process was evaluated using ultraviolet-visible spectroscopy, which revealed an increased absorbance at 625 nm that was consistent with the formation of the deprotonated form of Bromothymol blue.

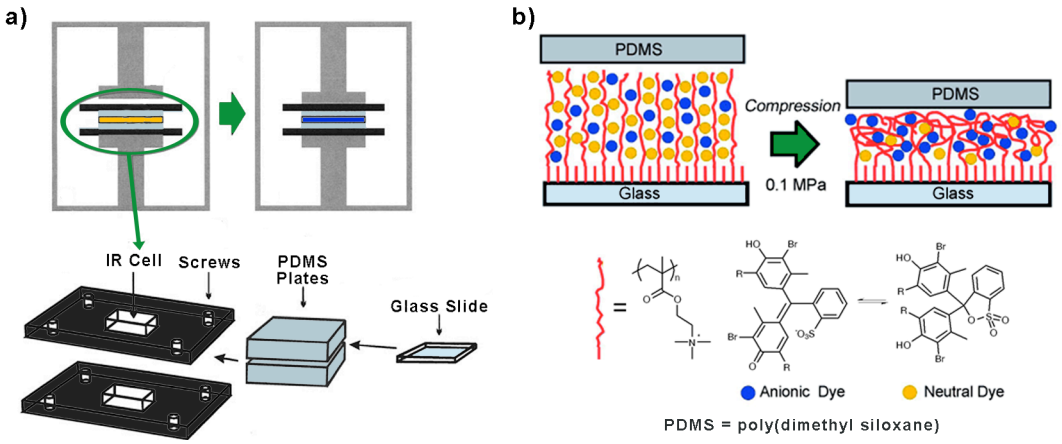

Figure 1.12 a) Schematic drawing of the experimental apparatus used to compress polymer brushes. An IR cell containing a crosslinked poly(dimethyl siloxane) glass slide with polymer brushes grown from the surface was placed into a small laboratory press and compressed. b) Compression of polyelectrolyte brushes caused a color change in the interspersed Bromothymol blue dye molecule as it changed from a neutral (yellow) to an anionic (blue) form. Images reprinted with permission from John Wiley and Sons, Ref. 71, 2006.

Collectively, the compression devices used to apply force to polymers allow for the study of a variety of mechanically responsive materials. Moreover, like their elongational counterparts, many of these methods are ideal for studying mechanochromic materials, as they can be interfaced for simultaneous optical spectroscopy. Unlike the tensile testing devices, however, compression methods do not require large amounts of material and can be performed on unprocessed polymers or powders (*i.e.*, soluble polymers or well-defined films are not necessary), making these techniques more readily accessible. The disadvantages of using compression devices vary depending on the specific method. Pressure cells, for instance, require a pressure medium, which can make isolation of the mechanically activated material challenging. Moreover, pressure cells (particularly diamond anvil cells) can be prohibitively expensive. Alternatively, hydraulic presses do not require a pressure medium and are relatively inexpensive; however, it is

challenging to couple these devices to optical spectrometers to simultaneously mechanically activate and characterize a material.

CONCLUSIONS AND OUTLOOK

In summary, polymer mechanochemistry presents the unique opportunity to selectively direct chemical reactivity in a manner that is often orthogonal to other stimuli. Indeed, exogenous forces can be harnessed by polymeric actuators (and potentially other types of soft matter) in order to drive multifarious transformations involving specially designed functionalities (*i.e.*, mechanophores). While there are a number of methods for activating systems within the purview of polymer mechanochemistry, ultrasonication has proven to be a powerful tool for accessing unprecedented vistas of chemical space. Examples of ultrasonically facilitated mechanochemical phenomena include the selective scission of covalent bonds, electrocyclic ring openings, cycloreversions of carbocycles and heterocycles, thermally inaccessible isomerizations, and the activation of latent organo- and organometallic catalysts. Bulk activation studies are also of increasing importance, given that most synthetic materials find applications in the solid-state. Importantly, many of the mechanically responsive moieties that have been reported in the literature present exciting opportunities for the development of self-healing materials and stress sensors. From a more fundamental perspective, the transduction of mechanical force into chemical potential has been demonstrated to facilitate otherwise prohibitive or inaccessible reactivities, often through counterintuitive or formally disallowed intermediates. Moreover, mechanical forces have been shown to stabilize highly reactive intermediates of chemical transformations, which could be invaluable for garnering mechanistic insight into a variety of reactions.

The anisotropic application of exogenous forces to mechanophores clearly allows for a high degree of selectivity and enhances the rates of a variety of reactions, often with the exclusion of concomitant and detrimental side reactions. Such selectivity is extremely desirable in comparison to thermal or photochemical stimuli, which can result in broad distributions of molecular energies that lead to deleterious reactivity. As such, we expect that the thoughtful design and implementation of new mechanophores will continue to thrive, and the work that will be presented in subsequent chapters details some of our own endeavors in the field of polymer mechanochemistry.

ACKNOWLEDGEMENTS

J.N.B. is grateful to the National Science Foundation for a predoctoral fellowship.

REFERENCES

1 Boltzmann, L. *Lectures on Gas Theory*, Translated by Stephen G. Brush. Univ. of California Press, Berkeley. **1964**.

2 Caruso, M. M.; Davis, D. A.; Shen, Q.; Odom, S. A.; Sottos, N. R.; White, S. R.; Moore, J. S. *Chem. Rev.* **2009**, *109*, 5755.

3 Black, A. L.; Lenhardt, J. M.; Craig, S. L. *J. Mater. Chem.* **2011**, *21*,1655.

4 Kauzmann, W; Eyring H. *J. Am. Chem. Soc.* **1940**, *62*, 3113.

5 Staudinger, H.; Schweitzer, O. *Ber. Dtsch. Chem. Ges.* **1930**, *63*, 3132.

6 Lumley, J. L. *Ann. Rev. Fluid Mech.* **1969**, *1*, 367.

7 Horn, A. F.; Merrill, E. W. *Nature* **1984**, *312*, 140.

8 Carrington, S. P.; Odell, J. A. *J. Non-Newtonian Fluid Mech.* **1996**, *67*, 269 and references cited therein.

9 Merrill, E. W.; Leopairat, P. *Polym. Eng. Sci.* **1980**, *20*, 505.

10 Casale, A.; Porter, R. S. *Polymer Stress Reactions,* Academic Press, New York, **1978**.

11 Buchholz, B. A.; Zahn, J. M.; Kenward, M.; Slater, G. W.; Barron, A. E. *Polymer* **2004**, *45*, 1223.

12 Nguyen, T. Q. *Chimia*, **2001**, *55*, 147.

13 Toms, B. A. *Proc. 1st Int. Congress on Rhelogy*; North Holland, **1948**, pp 135–141.

14 For a review of polymer behavior under ultrasound, see: Mason, T. J.; Lorimer, J. P. in *Applied Sonochemistry: Uses of Power Ultrasound in Chemistry and Processing*, Wiley-VCH Verlag, Weinheim, **2002**.

15 Glynn, P. A. R.; van der Hoff, B. M. E. *J. Macromol. Sci., Part A* **1973**, *A7*, 1695.

16 Florea, M. *J. Appl. Polym. Sci.* **1993**, *50*, 2039 and references cited therein.

17 Flosdorf, E. W.; Chambers, L. A. *J. Am. Chem. Soc.* **1933**, *55*, 3051.

18 Laland, S. G.; Overend, W. G.; Stacey, *M. J. Chem. Soc.* **1952**, 303.

19 Zill, L.; Vanwagtendonk, W. *Biochim. Biophys. Acta* **1950**, *6*, 524.

20 Encina, M. V.; Lissi, E.; Sarasúa, M.; Gargallo, L.; Radic, D. *J. Poly. Sci.: Poly. Lett. Ed.* **1980**, *18*, 757.

21 Berkowski, K. L.; Potisek, S. L.; Hickenboth, C. R.; Moore, J. S. *Macromolecules* **2005**, *38*, 8975.

22 Woodward, R. B.; Hoffmann, R. *Angew. Chem. Int. Ed.* **1969**, *8*, 781.

23 Hickenboth, C. R.; Moore, J. S.; White, S. R.; Sottos, N. R.; Baudry, J.; Wilson, S. R. *Nature* **2007**, *446*, 423.

24 Potisek, S. L.; Davis, D. A.; Sottos, N. R.; White, S. R.; Moore, J. S. *J. Am. Chem. Soc.* **2007**, *129*, 13808.

25 Davis, D. A.; Hamilton, A.; Yang, J.; Cremar, L. D.; Van Gough, D.; Potisek, S. L.; Ong, M. T.; Braun, P. V.; Martínez, T. J.; White, S. R.; Moore, J. S.; Sottos, N. R. *Nature* **2009**, *459*, 68.

26 Lee, C. K.; Davis, D. A.; White, S. R.; Moore, J. S.; Sottos, N. R.; Braun, P. V. *J. Am. Chem. Soc.* **2010**, *132*, 16107.

27 Kingsbury, C. M.; May, P. A.; Davis, D. A.; White S. R.; Moore, J. S.; Sottos, N. R.; *J. Mater. Chem.* **2011**, *21*, 8381.

28 Beiermann, B. A.; Davis, D. A.; Kramer, S. L. B.; Moore, J. S.; Sottos, N. R.; White, S. R. *J. Mater. Chem.* **2011**, *21*, 8443.

29 Lenhardt, J. M.; Black, A. L.; Craig, S. L. *J. Am. Chem. Soc.* **2009**, *131*, 10818.

30 Ramirez, A. L. B.; Ogle, J. W.; Schmitt, A. L.; Lenhardt, J. M.; Cashion, M. P.; Mahanthappa, M. K.; Craig, S. L. *ACS Macro Letters* **2012**, *1*, 23.

31 Black, A. L.; Orlicki, J. A.; Craig, S. L. *J. Mater. Chem.* **2011**, *21*, 8460.

32 Lenhardt, J. M.; Ong, M. T.; Choe, R.; Evenhuis, C. R.; Martinez, T. J.; Craig, S. L. *Science* **2010**, *329*, 1057.

33 Klukovich, H. M.; Kean, Z. S.; Ramirez, A. L. B.; Lenhardt, J. M.; Lin, J.; Hu, X.; Craig, S. L. *J. Am. Chem. Soc.* **2012**, *134*, 9577.

34 Chen, Y.; Spiering, A. J. H.; Karthikeyan, S.; Peters, G. W. M.; Meijer, E. W.; Sijbesma, R. P. *Nat. Chem.* **2012**, *4*, 559.

35 Wiggins, K. M.; Hudnall, T. W.; Shen, Q.; Kryger, M. J.; Moore, J. S.; Bielawski, C. W. *J. Am. Chem. Soc.* **2010**, *132*, 3256.

36 Wiggins, K. M.; Bielawski, C. W. *Angew. Chem. Int. Ed.* **2012**, *51*, 1640.

37 Kryger, M. J.; Ong, M. T.; Odom, S. A.; Sottos, N. R.; White, S. R.; Martinez, T. J.; Moore, J. S. *J. Am. Chem. Soc.* **2010**, *132*, 4558.

38 Klukovich, H. M.; Kean, Z. S.; Iacono, S. T.; Craig, S. L. *J. Am. Chem. Soc.* **2011**, *133*, 17882.

39 Wiggins, K. M.; Syrett, J. A.; Haddleton, D. M.; Bielawski, C. W. *J. Am. Chem. Soc.* **2011**, *133*, 7180.

40 Brantley, J. N.; Wiggins, K. M.; Bielawski, C. W. *Science* **2011**, *333*, 1606.

41 Brantley, J. N.; Konda, S. S. M.; Makarov, D. E.; Bielawski, C. W. *J. Am. Chem. Soc.* **2012**, *134*, 9882.

42 Kwart, H.; King, K. *Chem. Rev.* **1968**, *68*, 415.

43 Herndon, W.; Grayson, C. *J. Org. Chem.* **1967**, *32*, 526.

44 Pool, B.; White, J. *Org. Lett.* **2000**, *2*, 3505.

45 Corbett, P. T.; Leclaire, J.; Vial, L.; West, K. R.; Wietor, J. L.; Sanders, J. K. M.; Otto, S. *Chem. Rev.* **2006**, *106*, 3652.

46 Lehn, J. M. *Chem. Soc. Rev.* **2007**, *36*, 151.

47 Boul, P. J.; Reutenaur, P.; Lehn, J. M.; *Org. Lett.* **2005**, *7*, 15.

48 Masci, B.; Pasquales, S.; Thuery, P. *Org. Lett.* **2008**, *10*, 4835.

49 Chen, X.; Dam, M.; Ono, K.; Mal, A.; Shen, H.; Nutt, S. R.; Sheran, K.; Wudl, F. *Science* **2002**, *295*, 1698.

50 Song, Y. K.; Lee, K. H.; Hong, W. S.; Cho, S. Y.; Yu, H. C.; Chung, C. M. *J. Mater. Chem.* **2012**, *22*, 1380.

51 Paulusse, J. M. J.; Sijbesma, R. P. *Chem. Commun.* **2008**, 4416.

52 Karthikeyan, S.; Potisek, S. L.; Piermattei, A.; Sijbesma, R. P. *J. Am. Chem. Soc.* **2008**, *130*, 14968.

53 Piermattei, A.; Karthikeyan, S.; Sijbesma R. P. *Nat. Chem.* **2009**, *1*, 133.

54 Tennyson, A. G.; Wiggins, K. M.; Bielawski, C. W. *J. Am. Chem. Soc.* **2010**, *132*, 16631.

55 Wiggins, K. M.; Hudnall, T. W.; Tennyson, A. G.; Bielawski, C. W. *J. Mater. Chem.* **2011**, *21*, 8355.

56 Suslick, K. S.; Goodale, J. W.; Schubert, P. F.; Wang, H. H. *J. Am. Chem. Soc.* **1983**, *105*, 5781.

57 Cho, S.- Y.; Kim, J.- G.; Chung, C.- M. *Sens. Actuators B* **2008**, *134*, 822.

58 For advances in force sensors, see: Pucci, A.; Riggeri, G. *J. Mater. Chem.* **2011**, *21*, 8282 and references cited therein.

59 Davis, J. R. *Tensile Testing*, ASM International, Ohio, 2nd ed., **2004**, ch. 1, pp 1–12.

60 Kim, S.- J.; Reneker, D. H. *Polym. Bull.* **1993**, *31*, 367.

61 Crenshaw, B. R.; Weder, C. *Chem. Mater.* **2003**, *15,* 4717 and references cited therein.

62 Ikawa, T.; Shiga, T.; Okada, A. *J. Appl. Polym. Sci.* **1997**, *66,*1569.

63 Bruns, N.; Pustelny, K.; Bergeron, L. M.; Whitehead, T. A.; Clark, D. S. *Angew. Chem. Int. Ed.* **2009**, *48*, 5666.

64 Ikawa, T.; Shiga, T.; Okada, A. *J. Appl. Polym. Sci.* **2002**, *83*, 2600 and references cited therein.

65 Moses, D.; Feldblum, A.; Ehrenfreund, E.; Heeger, A. J.; Chung, T.- C.; MacDiarmid, A. G. *Phys. Rev. B.* **1982**, *26*, 3361 and references cited therein.

66 Spain, I. L.; Dunstan, D. J. *J. Phys. E: Sci. Instrum.* **1989**, *22*, 923.

67 Muramatsu, Y.; Yamamoto, T.; Hasegawa, M.; Yagi, T.; Koinuma, H. *Polymer* **2001**, *42*, 6673.

68 Lenhardt, J. M.; Black, A. L.; Beirmann, B. A.; Steinberg, B. D.; Rahman, F.; Somaborski, T.; Elsakr, J.; Moore, J. S.; Sottos, N. R.; Craig, S. L. *J. Mater. Chem.* **2011**, *21*, 8454.

69 Diesendruck, C. E.; Steinberg, B. D.; Sugai, N.; Silberstein, M. N.; Sottos, N. R.; White, S. R.; Braun, P. V.; Moore, J. S. *J. Am. Chem. Soc.* **2012**, *134*, 12446.

70 For recent developments in self-healing materials, see: White, S. R.; Caruso, M. M.; Moore, J. S. *MRS Bull.* **2008**, *33*, 766 and references cited therein.

71 Azzaroni, O.; Trappmann, B.; van Rijn, P.; Zhou, F.; Kong, B.; Huck, W. T. S. *Angew. Chem. Int. Ed.* **2006**, *45*, 7440.

Chapter 2: Formal (3+2) Cycloreversions of 1,4-Disubstituted 1,2,3-Triazoles under the Action of Mechanical Force

INTRODUCTION[2]

The copper-catalyzed Huisgen cycloaddition,[1,2] which affords access to a variety of 1,4-disubstituted 1,2,3-triazoles, has found broad applicability throughout the chemical and biological sciences over the past decade. The requisite 1,3-dipoles and dipolarophiles (*i.e.*, azide and alkyne moieties, respectively) can be installed within a variety of molecular scaffolds with relative synthetic ease, and the triazole products exhibit high thermal stability and excellent compatibility under a variety of reaction conditions. Moreover, the cycloaddition exhibits rapid kinetics under mild conditions, high functional group and solvent tolerance, and good atom economy. In addition to finding compelling use in molecular and polymer functionalizations, this coupling motif has become ubiquitous within the purview of chemical biology, where triazoles are routinely applied in chemically orthogonal ligations for the study of biological systems.[3-11] However, a consequence of the high kinetic stability of 1,2,3-triazoles is that no simple method capable of cleanly reverting these heterocycles into their constituent azides and alkynes is known. We envisioned that mechanical force could potentially surmount the otherwise formidable barrier to triazole cycloreversion; that is, under the judicious application of mechanical stress, triazoles might not retain their structural integrity. Such a retro-cycloaddition could be of considerable synthetic appeal, given that it would provide a method by which reactive azide or alkyne intermediates could be selectively un-masked to effect desired transformations (**Scheme 2.1**).

---

[2] Portions of this chapter and the corresponding appendix were reproduced from: Brantley, J. N.; Wiggins, K. M.; Bielawski, C. W. *Science* **2011**, *333*, 1606. JNB performed the majority of the experimental work, and KMW contributed to figure preparation and writing of the original text. JNB and CWB evaluated the experimental data and wrote the majority of the original text.

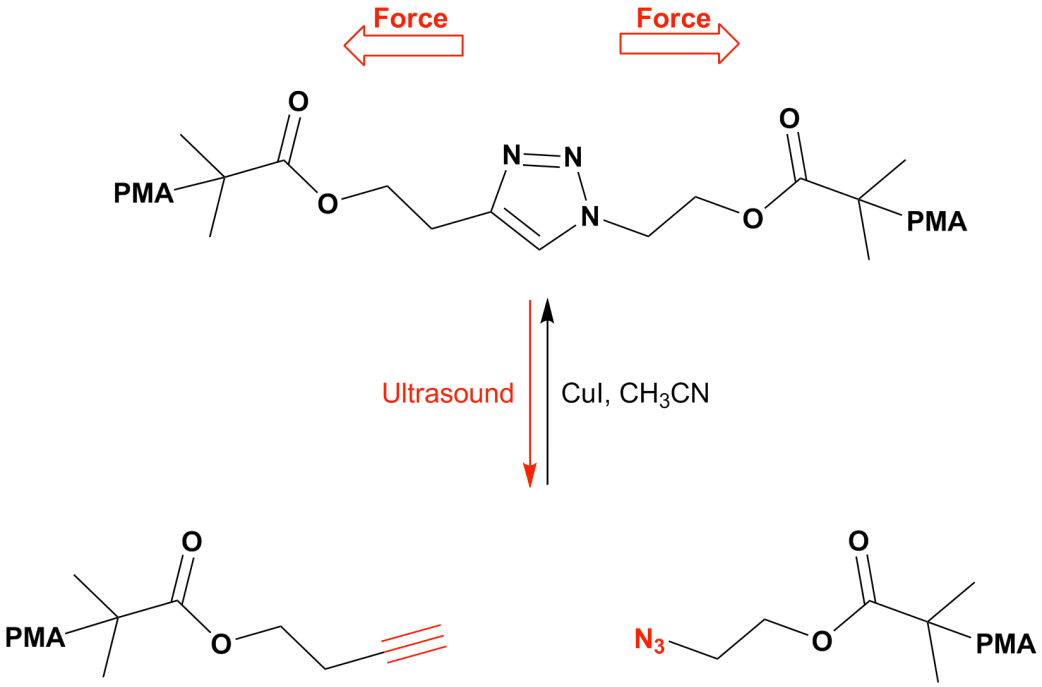

Scheme 2.1 The application of ultrasound to a triazole embedded within a poly(methyl acrylate) (PMA) chain results in a formal retro-(3+2) cycloaddition (red). Subsequent cycloaddition of the liberated azide and alkyne moieties affords the triazole-based starting material (black).

Recent advances in polymer mechanochemistry[12] – wherein exogenous forces are directed to mechanophores (*i.e.*, chemical functionalities possessing mechanically labile bonds) embedded within polymeric matrices – have demonstrated that formally disallowed pericyclic reactions and thermally inaccessible isomerizations can be induced through site-specific mechanical activation.[13-18] Such forces may be generated through the application of ultrasound to polymer solutions, whereby cavitation induces velocity gradients and attendant stress in the solvated polymer chains through solovodynamic shear.[12] Mechanical forces are presumed to promote otherwise prohibited reactions through: 1) ground state destabilization of the reactants (as a result of changes in molecular geometry), or 2) the stabilization of reactive intermediates at or near the

transition state of the reaction coordinate.[19,20] Based upon this foundation, we hypothesized that triazoles, while remarkably inert toward chemical and thermal insult, could be coerced to undergo cycloreversion through the strategic application of mechanical force.

INITIAL EVALUATION OF MECHANICAL ACTIVITY

In order to assess the mechanophoricity of the triazole moiety, diol **2.1** was condensed with 2-bromoisobutyryl bromide to afford bifunctional initiator **2.2** (**Scheme 2**). Subsequent copper-mediated controlled radical polymerization of methyl acrylate from **2.2** afforded a triazole-centered poly(methyl acrylate) (**2.3**$_{\mathbf{Mn}}$, where M_n refers to the number average molecular weight of the polymer). Analysis by gel permeation chromatography (GPC) revealed that the material (**2.3**$_{\mathbf{140}}$) had an M_n of 140 kDa and a polydispersity index (PDI) of 1.4 (**Scheme 2.2**; see Appendix A for additional details).

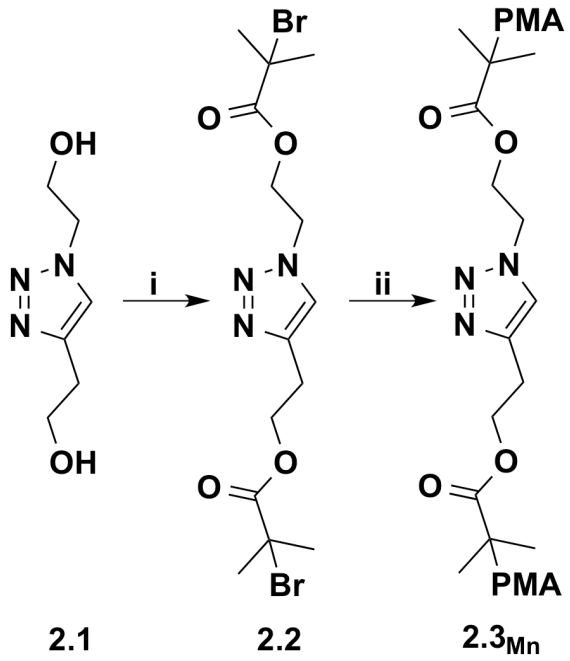

Scheme 2.2 Synthesis of triazole-containing polymers. i: 2-bromo-2-methylpropionyl bromide, triethylamine, ethyl acetate, 0 °C→ 25 °C; ii: methyl acrylate, tris[2-(trimethylamino)ethyl] amine, dimethyl sulfoxide (PMA = poly(methyl acrylate)).

Subjecting an acetonitrile (CH_3CN) solution of $\mathbf{2.3_{140}}$ to sonication for 2 hours in a Suslick cell[21] at 6 °C resulted in a decrease in the polymer's M_n from 140 to 82 kDa (**Figure 2.1A**, black and red lines, respectively). This change was consistent with chain scission near the center of the polymer, which indicated the potential activation (*i.e.*, cycloreversion) of the centrally located mechanophore. Additionally, the infrared (IR) spectrum obtained following ultrasonication of a related polymer (M_n of 96 kDa; $\mathbf{2.3_{96}}$) revealed diagnostic signals consistent with the presence of azide (2133 cm^{-1}) and terminal alkyne (2039 cm^{-1}) functionalities that were not observed in the IR spectrum of the presonicated material (**Figure 2.1B**).

CHEMICAL LABELING OF MECHANICALLY GENERATED ALKYNES AND AZIDES

To further demonstrate that the result of mechanical scission was the expected azide and alkyne products of triazole cycloreversion, we sought to selectively label these moieties with diagnostic chromophores possessing complementary functionalities. Pyrene derivatives exhibit distinct absorbances in the ultraviolet-visible spectrum; thus, 1-azidopyrene was chosen to selectively label the mechanically liberated alkynes with a chromophore through a copper-mediated (3+2) cycloaddition (**Scheme 2.3**). The postsonicated $\mathbf{2.3_{140}}$ was dissolved in CH_3CN, and 1-azidopyrene was cycloadded to the free alkyne moieties using CuI. GPC with concomitant ultraviolet-visible detection revealed that the labeled polymer had an increased absorbance at λ = 240 nm (a λ_{max} associated with pyrene; see Appendix A) relative to the starting material reacted under similar conditions at the same concentration (**Figure 2.1C**).

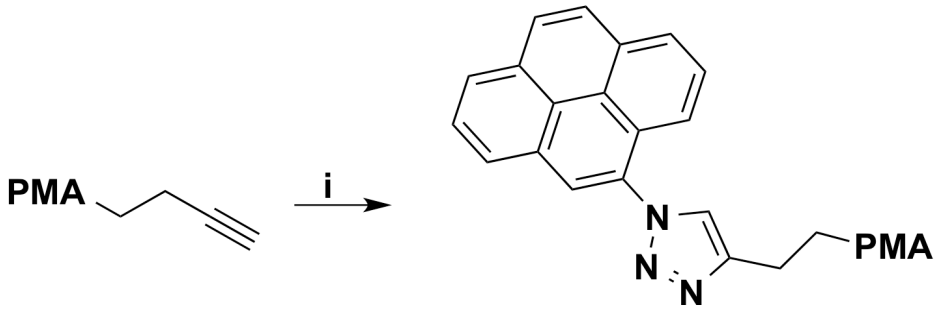

Scheme 2.3 Labeling of alkynes generated under sonication with 1-azidopyrene. i: 1-azidopyrene, CuI, CH_3CN.

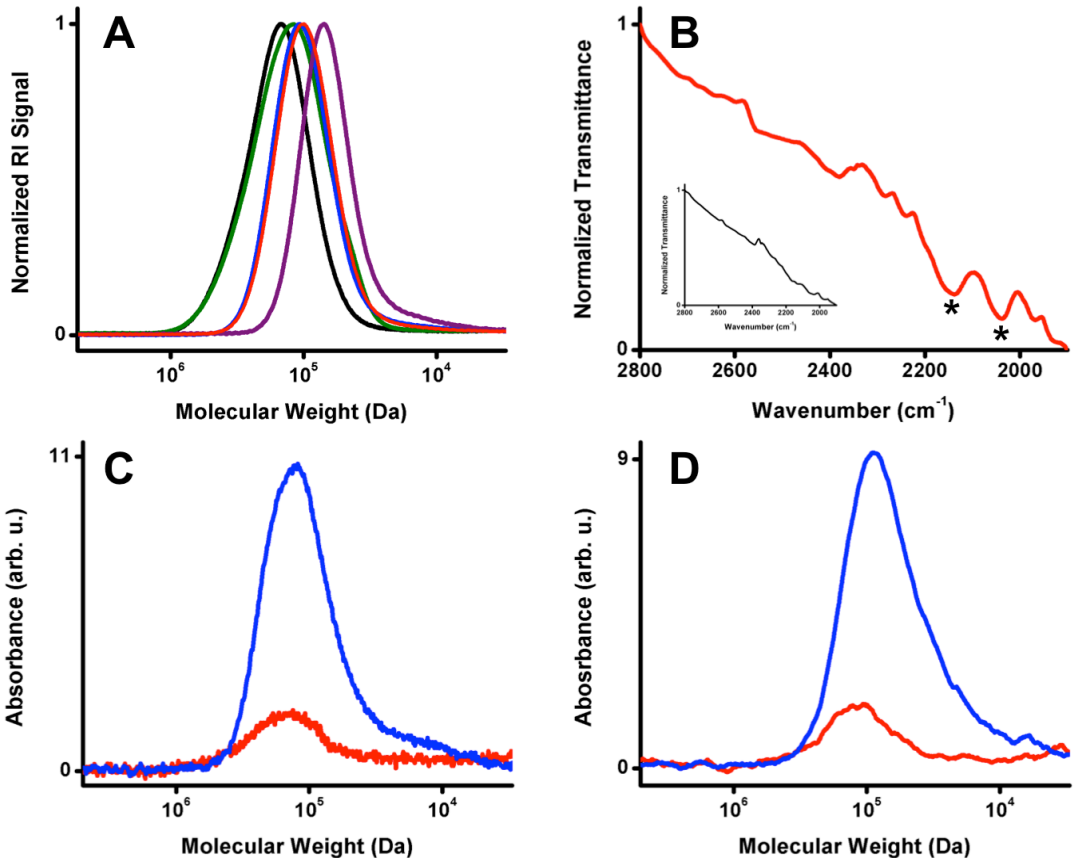

Figure 2.1 (A) GPC traces showing the scission of $\mathbf{2.3}_{140}$ (black) under sonication (red), reformation of the traizole through a CuI-mediated cycloaddition (blue), and subsequent scission of the recoupled material (violet). Heating a thin film of $\mathbf{2.3}_{140}$ (180° C) for 19 hours resulted in only a partial reduction of polymer molecular weight (green). (B) Infrared spectra (in THF) of $\mathbf{2.3}_{96}$ after sonication (red) showing the appearance of the expected azide and alkyne stretching frequencies (*) at 2133 cm^{-1} and 2039 cm^{-1}, respectively. The inset displays the spectrum of the preseonicated $\mathbf{2.3}_{96}$ material in the same region (in THF). (C) GPC traces (visualized using ultraviolet-visible detection at 240 nm) showing an increased absorbance for the postsonicated $\mathbf{2.3}_{140}$ polymer upon reaction with 1-azidopyrene (blue) compared to presonicated $\mathbf{2.3}_{140}$ (red) reacted under similar conditions at the same concentration. (D) GPC traces (visualized using ultraviolet-visible detection at 310 nm) showing an increased absorbance for the postsonicated $\mathbf{2.3}_{140}$ polymer upon reaction with **NQMes** (blue) compared to presonicated $\mathbf{2.3}_{140}$ (red) reacted under similar conditions at the same concentration.

Parallel efforts to selectively label liberated azide moieties focused on *N*-heterocyclic carbenes (NHCs), such as 1,3-dimesitylnapthoquinimidazolylidene (**NQMes**), which are known[22,23] to produce intensely colored, acyclic triazines upon reaction with azides (**Scheme 2.4**). **NQMes** was added to a solution of postsonicated $\mathbf{2.3_{140}}$ in dry tetrahydrofuran (THF) under an inert atmosphere. Within 20 minutes of the **NQMes** addition, the color of the solution changed from green to blue. Upon isolation of the polymer product, ultraviolet-visible spectroscopy revealed the labeled polymer had increased absorbance at λ = 264, 295, and 310 nm relative to the starting material (see Appendix A). Further analysis by GPC with concomitant ultraviolet-visible detection indicated that the labeled polymer displayed an increased absorbance at λ = 310 nm when compared to the starting material reacted under similar conditions at the same concentration (**Figure 2.1D**). Thus, the selective labeling of both azide and alkyne functionalities in postsonicated $\mathbf{2.3_{140}}$, but not presonicated $\mathbf{2.3_{140}}$, provided further support for the proposed mechanically facilitated (3+2) cycloreversion process.

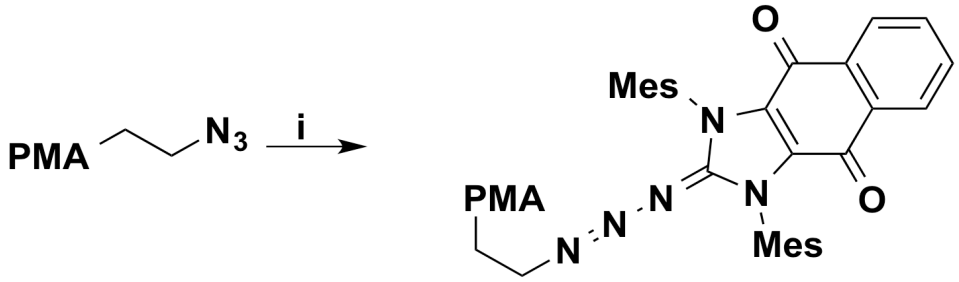

Scheme 2.4 Labeling of azides with 1,3-dimesitylnapthoquinimidazolylidene (**NQMes**). i: **NQMes**, tetrahydrofuran.

EXPERIMENTS DESIGNED TO PRECLUDE THERMAL ACTIVATION

Thermally induced cycloreversion was excluded through a series of control experiments. Previous reports[12-18] have demonstrated that ultrasonically facilitated

transformations are dependent upon the length of the polymer chains attached to the mechanophore (a phenomenon that is not expected if mechanophore activation is a purely thermal process). As such, a series of poly(methyl acrylate) chains of varying M_n were synthesized from **2.2** *via* controlled radical polymerization (M_n = 16 – 140 kDa; **Table 2.1**). The $\mathbf{2.3}_{Mn}$ polymers were then individually subjected to the sonication conditions described above for $\mathbf{2.3}_{140}$. After sonication, GPC analysis of the isolated polymers revealed that chain scission was dependent upon polymer M_n, as only higher molecular weight polymers (> 36 kDa) underwent activation (**Table 2.1**). Moreover, when a thin film of $\mathbf{2.3}_{140}$ was heated at 180 °C for 19 hours there was only partial chain scission detected by GPC (**Figure 2.1A**, green). Together, these data excluded a thermally promoted cycloreversion of the central triazole units as a viable pathway for the chain scission observed under ultrasound.

Table 2.1 Selected Molecular Weight Data for $\mathbf{2.3}_{Mn}$ Polymers†

	Presonication		Postsonication		Sonication Time
	M_n (kDa)	PDI	M_n (kDa)	PDI	(h)
$\mathbf{2.3}_{140}$	140	1.4	82	1.3	2
$\mathbf{2.3}_{96}$	96	1.3	48	1.4	2
$\mathbf{2.3}_{63}$	63	1.3	32	1.4	7
$\mathbf{2.3}_{36}$	36	1.3	33	1.3	7
$\mathbf{2.3}_{16}$	16	1.4	16	1.4	7

†The polydispersity index (PDI) was calculated using the equation PDI = M_w/M_n, where M_w is the weight average molecular weight. M_n and M_w were determined as their polystyrene equivalents by GPC (eluent = THF).

Finally, we reasoned that if the cycloreversion was mechanical in nature then the position of the mechanophore within the polymer chain should effect the activation process.[12] To explore, triazoles bearing a single polymer chain at either the 1- or 4-position were synthesized. The resulting materials were subjected to the sonication and

labeling experiments as described for **2.3**$_{140}$ (*vide supra*); importantly, neither control revealed a positive azide or alkyne labeling result. Collectively, these data suggested that the triazole must be embedded within the polymer chain near the midpoint in order to experience the force necessary to facilitate cycloreversion (see Appendix A).

RECOUPLING OF POLYMER FRAGMENTS

Since the putative 1,3-dipolar cycloreversion generated polymer chains terminated with reactive azide and alkyne moieties, we envisioned recoupling the two polymer chains together using a copper-catalyzed Huisgen cycloaddition. **2.3**$_{140}$ was subjected to the ultrasonication conditions described above and then analyzed by GPC (M_n = 82 kDa). Following dissolution in degassed CH_3CN and the addition of CuI, the resulting mixture was stirred at 90 °C for 72 hours in the absence of light. After isolation of the product, GPC analysis (**Figure 2.1A**, blue) indicated the formation of a polymeric material having a peak molecular weight (M_p, determined by the molecular weight at the peak retention time) approaching that of the presonicated material (*c.f.* M_p = 110 kDa for the coupled material versus M_p = 151 kDa for the presonicated material). De-convolution and integration of the GPC curve for the recoupled polymeric material indicated that approximately 16% of the material had undergone coupling (see Appendix A). The magnitude of the observed conversion to recoupled product suggested that either 1) entropic demands significantly reduced the kinetics of recoupling, 2) lower molecular weight polymer fragments preferentially recoupled under the reported conditions (which would afford a new material having an M_p intermediate to that of the presonicated and postsonicated materials), or 3) every chain scission event did not result from cycloreversion of the central triazole moiety. Importantly, the recoupled material was subsequently subjected to ultrasonication, and the expected reduction in M_n was observed

(**Figure 2.1A**, violet). To demonstrate the reproducibility of these modestly efficient processes, $\mathbf{2.3_{96}}$ was also successfully subjected to mechanically induced cycloreversion and subsequent copper-catalyzed cycloaddition (see Appendix A). Moreover, the enhanced recoupling of postsonicated $\mathbf{2.3_{96}}$ (40% recoupling after 24 h) suggested that the reduced coupling efficiency observed for $\mathbf{2.3_{140}}$ was a reflection of an increased kinetic barrier in the case of the latter (most likely the result of higher entropic demands for coupling larger polymer fragments).

CONCLUSIONS AND OUTLOOK

Collectively, these results demonstrate that directed mechanical forces can effect the previously elusive retro-Huisgen cycloaddition reaction, transforming 1,2,3-triazoles into their azide and alkyne precursors. The ability to selectively deconstruct triazoles with moderate fidelity presents the opportunity to employ these readily accessible moieties in mechanoresponsive materials or as mechanically labile protecting groups. The former could include dye-sensitized force sensors[24] or force responsive fluorescent tags for biological assays. The latter represents an intriguing synthetic strategy whereby highly inert functionalities could be converted into reactive species under conditions that are entirely orthogonal to chemical, thermal, or photochemical approaches. In the specific case of 1,2,3-triazoles, such a strategy would be of particular appeal for preventing undesired side reactivity between azides/alkynes and strong nucleophiles, especially considering that a broad range of substituents covalently bonded to the azide and alkyne coupling partners should tolerate ultrasonication. In a broader perspective, the observed cycloreversion also establishes a method for coaxing other kinetically stable molecules to exhibit uncommon reactivity under the influence of exogenous mechanical forces.

ACKNOWLEDGEMENTS

J.N.B. is grateful to the National Science Foundation for a predoctoral fellowship. Jonathan Moerdyk, Alex Todd, Aaron Teator, and Dominika Lastovickova are gratefully acknowledged for helpful discussions.

REFERENCES

1 Rostovtsev, V. V.; Green, L. G.; Fokin, V. V.; Sharpless, K. B. *Angew. Chem. Int. Ed.* **2002**, *41*, 2596.

2 Tornøe, C. W.; Christensen, C.; Meldal, M. *J. Org. Chem.* **2002**, *67*, 3057.

3 Hein, J. E.; Tripp, J. C.; Krasnova, L. B.; Sharpless, K. B.; Fokin, V. V. *Angew. Chem. Int. Ed.* **2009**, *48*, 8018.

4 Iha, R. K.; Wooley, K. L.; Nyström, A. M.; Burke, D. J.; Kade, M. J.; Hawker, C. J. *Chem Rev.* **2009**, *109*, 5620.

5 Antoni, P.; Robb, M. J.; Campos, L.; Montanez, M.; Hult, A.; Malmström, E.; Malkoch, M.; Hawker, C. J. *Macromolecules* **2010**, *43*, 6625.

6 Agnew, H. D.; Rhode, R. D.; Millward, S. W.; Nag, A.; Yeo, W. S.; Hein, J. E.; Pitram, S. M.; Tariq, A. A.; Burns, V. M.; Krom, R. J.; Fokin, V. V.; Sharpless, K. B.; Heath, J. R. *Angew. Chem. Int. Ed.* **2009**, *48*, 4944.

7 Yamada, T.; Peng, C. G.; Matsuda, S.; Addepalli, H.; Jayaprakash, K. N.; Alam, M. R.; Mills, K.; Maier, M. A.; Charisse, K.; Sekine, M.; Manoharan, M.; Rajeev, K. G. *J. Org. Chem.* **2011**, *76*, 1198.

8 Lietard, J.; Meyer, A.; Vasseur, J.; Morvan, F. *J. Org. Chem.* **2008**, *73*, 191.

9 Pourceau, G.; Meyer, A.; Vasseur, J.; Morvan, F. *J. Org. Chem.* **2009**, *74*, 6837.

10 Seo, T.; Li, Z.; Ruparel, H.; Ju, J. *J. Org. Chem.* **2003**, *68*, 609.

11 Seela, F.; Ingale, S. A. *J. Org. Chem.* **2010**, *75*, 284.

12 Caruso, M. M.; Davis, D. A.; Shen, Q.; Odom, S. A.; Sottos, N. R.; White, S. R.; Moore, J. S. *Chem. Rev.* **2009**, *109*, 5755.

13 Hickenboth, C. R.; Moore, J. S.; White, S. R.; Sottos, N. R.; Baudry, J.; Wilson, S. R. *Nature* **2007**, *446*, 423.

14 Lenhardt, J. M.; Ong, M. T.; Choe, R.; Evenhuis, C. R.; Martinez, T. J.; Craig, S. L. *Science* **2010**, *329*, 1057.

15 Potisek, S. L.; Davis, D. A.; Sottos, N. R.; White, S. R.; Moore, J. S. *J. Am. Chem. Soc.* **2007**, *129*, 13808.

16 Kryger, M. J.; Ong, M. T.; Odom, S. A.; Sottos, N. R.; White, S. R.; Martinez, T. J.; Moore, J. S. *J. Am. Chem. Soc.* **2010**, *132*, 4558.

17 Lenhardt, J. M.; Black, A. L.; Craig, S. L. *J. Am. Chem. Soc.* **2009**, *131*, 10818.

18 Wiggins, K. M.; Hudnall, T. W.; Shen, Q.; Kryger, M. J.; Moore, J. S.; Bielawski, C. W. *J. Am. Chem. Soc.* **2010**, *132*, 3256.

19 Ribas-Arino, J.; Shiga, M.; Marx, D. *Angew. Chem. Int. Ed.* **2009**, *48*, 4190.

20 Kochhar, G. S.; Bailey, A.; Mosey, N. J. *Angew. Chem. Int. Ed.* **2010**, *49*, 7452.

21 Suslick, K. S.; Goodale, J. W.; Schubert, P. F.; Wang, H. H. *J. Am. Chem. Soc.* **1983**, *105*, 5781.

22 Khramov, D. M.; Bielawski, C. W. *Chem. Commun.* **2005**, 4958.

23 Coady, D. J.; Bielawski, C. W. *Macromolecules* **2006**, *39*, 8895.

24 Davis, D. A.; Hamilton, A.; Yang, J.; Cremar, L. D.; Van Gough, D.; Potisek, S. L.; Ong, M. T.; Braun, P. V.; Martínez, T. J.; White, S. R.; Moore, J. S.; Sottos, N. R. *Nature* **2009**, *459*, 68.

Chapter 3: Development of Extended Bell Theory (EBT) as a Computational Model of Mechanochemical Phenomena

INTRODUCTION[3]

Mechanochemistry, an emerging field that explores the coupling between mechanical and chemical phenomena, holds great promise for precisely controlling chemical reactivity. Unlike scalar quantities (such as pressure or temperature), the vectorial character of an applied mechanical force allows one to precisely guide molecular systems along desired reaction pathways. Moreover, mechanical activation has the propensity to access reaction coordinates that are distinct from those associated with thermal or photochemically driven processes.[1,2] Recent developments in mechanochemistry include experimental techniques allowing application of mechanical forces to molecular entities covalently attached to high molecular weight polymers[1,3] and single-molecule methods (AFM and optical tweezers) to stretch individual proteins and RNA.[4] In addition, it is possible to design molecular machines that utilize energy of chemical reactions to exert mechanical forces and perform work.[5,6]

Rational control of chemical reactivity through the application of mechanical stress requires an understanding of the effect of force on 1) the rate of a chemical reaction, and 2) the stability of the respective reactants and/or reactive intermediates. Consider, for example, the reaction shown in **Figure 3.1**: If a stretching force is applied to an arbitrarily selected pair of atoms, will the result be reaction acceleration or suppression? What is the magnitude of the associated effect? Which pair of atoms should be selected in order to achieve the maximum rate enhancement? As electronic structure

[3] Portions of this chapter were reproduced from: Konda, S. S. M.; Brantley, J. N.; Bielawski, C. W.; Makarov, D. E. *J. Chem. Phys.* **2011**, *135*, 164103. All authors contributed to the writing of the original manuscript and figure preparation. SSMK performed the computational experiments with assistance from JNB.

or molecular dynamics calculations are arguably less expensive than the design of an appropriate experimental system, computational predictions are of considerable value for answering these questions.

Mechanical perturbation can be incorporated in electronic structure calculations in a number of ways. Suppose, for example, that one desires to simulate pulling on a pair of atoms, *i* and *j* (as illustrated in **Figure 3.1**). This can be achieved, computationally, by imposing a constraint on the distance R_{ij} between the two atoms.[2,7-9] Alternatively, one can impose a stress on the system *via* an additional energy term of the form $-FR_{ij}$ (where F is the pulling force) that is added to the molecule's potential energy.[9] By computing how stress (or strain) affects the energies of the stable and transition state structures in the reaction of interest, it is possible to estimate the force dependence of the overall reaction rate. This procedure is costly, however, as it requires that multiple transition state searches (and, consequently, multiple energy evaluations) be performed for each value of the force or constraint. If one also desires to know how the pulling depends on the positions *i* and *j* at which the forces are applied, this further increases the computational cost by a factor of $N(N-1)/2$, where N is the total number of atoms in the system.

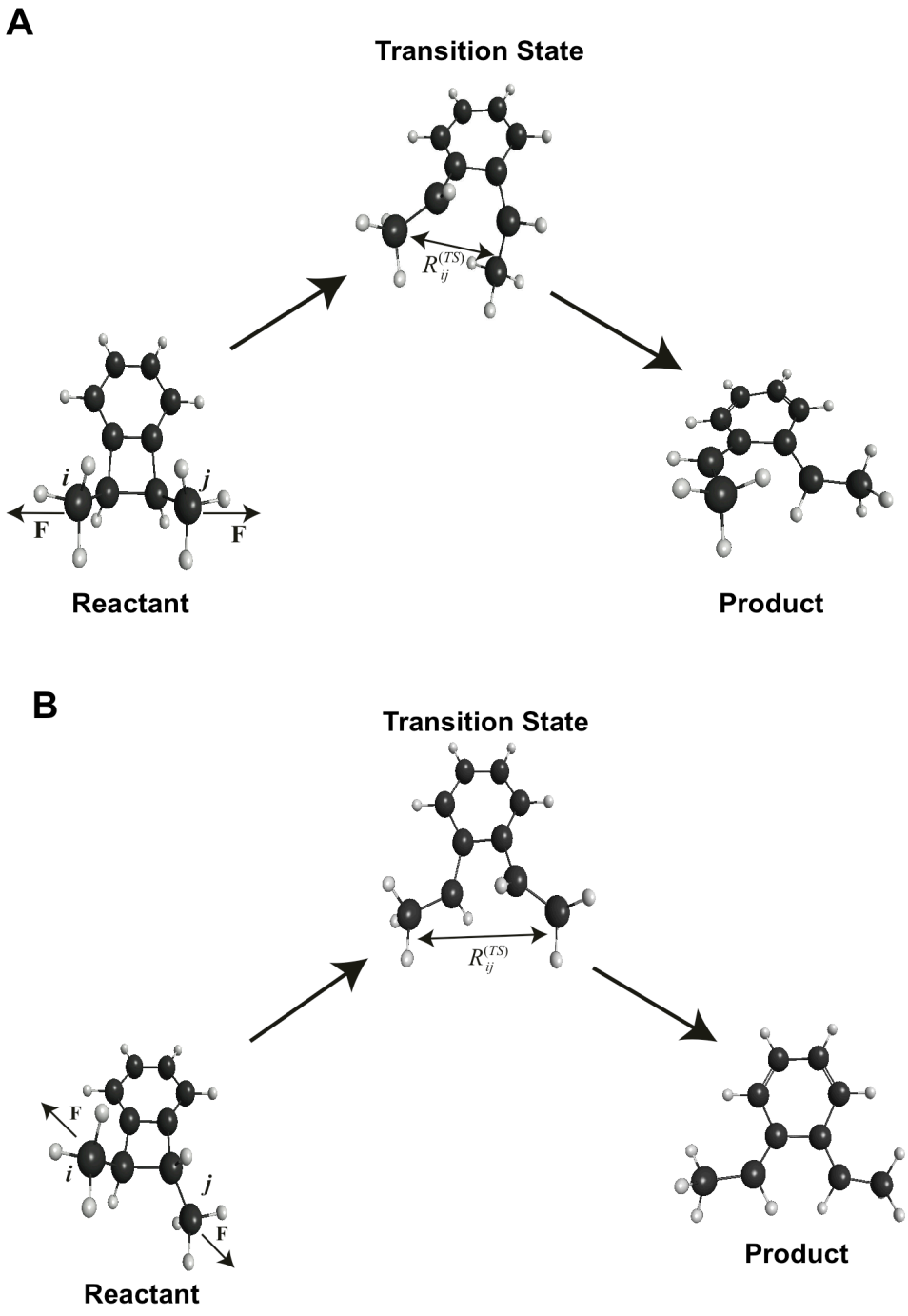

Figure 3.1 Conrotatory pathway for electrocyclic ring opening of (A) *cis* and (B) *trans* 1,2-dimethylbenzocyclobutene. The force applied to two carbons lowers the reaction barrier if the distance Rij between these atoms is longer in the transition state than it is in the reactant state.

To avoid high computational cost, simple, approximate theories have been widely used. Perhaps the most widespread approximation is the one introduced by Bell,[10] which posits that the application of a force F changes the barrier of a chemical reaction by an amount equal to $-F\Delta R_{ij}$. Here, ΔR_{ij} is the change in the distance between the atoms to which the force is applied upon evolving from the stable (reactant) state to the transition state. Thus, Bell's theory predicts a linear relationship between the logarithm of the rate and the applied force. As ΔR_{ij} can be estimated from the stable and transition state geometries at *zero* force, Bell's formula offers tremendous computational savings; indeed, Bell's theory provides the force dependence of the reaction rate (at any force) without having to actually impose any constraint in electronic structure calculations. Unfortunately, the predicted linear relationship is routinely violated because the ΔR_{ij} term is itself force dependent.[2,9,11-15] Other approaches, which approximately account for force induced changes in molecular geometry, have also been proposed.[9] Somewhat surprisingly, however, one straightforward refinement of Bell's formula, although pointed out in the literature,[16,17] has not been commonly used to improve the accuracy of such calculations. Specifically, Bell's formula is simply a Taylor series truncated to first order in the force. The second order term is, however, also readily obtained. Moreover, evaluation of this second order term does not require any additional information other than the Hessian matrices of the molecule in the reactant and the transition states. The latter come at no additional cost, as they are readily evaluated by most electronic structure codes.

Here, we derive such an improved approximation in terms of electronic structure data and evaluate its performance, and we call this approximation extended Bell theory (EBT). In what follows, we show that EBT accounts, rather accurately, for the nonlinearity of the force dependence of a reaction barrier that is observed in more

expensive calculations that explicitly include mechanical forces. We further expose certain mathematical peculiarities of EBT arising from the multidimensional character of the underlying potential energy surface and make connections to other approaches used in the literature. For example, EBT is related to the harmonic transition theory[18] in that both approximations assume quadratic potential energy surfaces in the vicinity of the reactant and transition states. We further show that the same approximation readily yields other useful mechanical properties of the molecule, such as its effective compliance in response to the mechanical stress.

THEORETICAL CONSIDERATIONS

We start with illustrating EBT in a simple one-dimensional model of a reaction governed by a potential $V(s)$, which is a function of a single reaction coordinate s (**Figure 3.2**). The minimum of the potential is located at $s = s^{(0)}$ and the maximum is at $s^{(TS)}$, where the superscripts (0) and (TS) refer to the stable, reactant conformation and to the transition state, respectively.

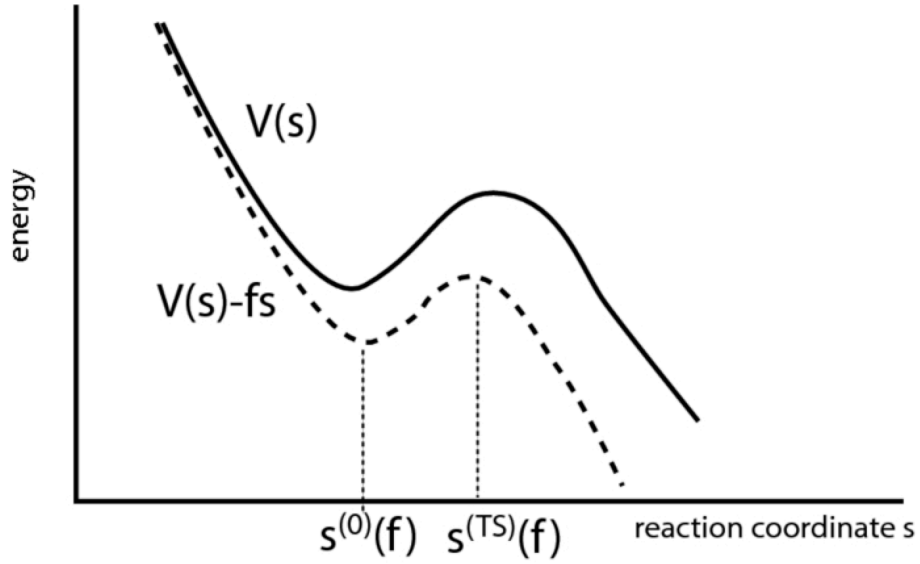

Figure 3.2 Simple one-dimensional model of a chemical reaction modulated by a mechanical force. The force lowers the reaction barrier and shifts the reactant and transition-state conformations toward one another.

When a force f is exerted along the reaction coordinate, the system experiences the potential $V(s) - fs$, with a modified activation energy barrier:[19,20]

$$V^{\neq}(f) = V^{(TS)} - V^{(0)} = V[s^{(TS)}(f)] - V[s^{(0)}(f)] - f[s^{(TS)}(f) - s^{(0)}(f)] \quad (3.1)$$

The force-dependent rate is estimated using transition-state theory as

$$k(f) = \nu(f) \exp\left[-\frac{V^{\neq}(f)}{k_B T}\right] \quad (3.2)$$

where the prefactor ν depends on the vibrational frequency in the stable state. For condensed-phase reactions, the prefactor also contains an appropriate transmission factor that accounts for the recrossings of the transition state.[18] Because $k(f)$ is exponentially dependent on the force, it is reasonable to neglect the much weaker force dependence of the prefactor itself (*i.e.*, $\nu(f) \approx \nu(0)$).

The locations $s^{(0),(TS)}(f)$ of the potential minimum and maximum satisfy the equation

$$V'(s) - f = 0 \tag{3.3}$$

Expanding Equation 3.3 in a Taylor series, we obtain, to first order in f:

$$s^{(TS),(0)}(f) \approx s^{(TS),(0)}(0) + \frac{f}{V''[s^{(TS),(0)}(0)]} \tag{3.4}$$

That is, the potential minimum shifts to the right (since $V'' > 0$) and the transition state is shifted to the left. Substituting this into Equation 3.1, we find, to second order in the force:[16,17]

$$V^{\neq}(f) = V^{\neq}(0) - f\left[s^{(TS)}(0) - s^{(0)}(0)\right] - \frac{f^2}{2}\left\{\frac{1}{V''\left[s^{(TS)}(0)\right]} - \frac{1}{V''\left[s^{(0)}(0)\right]}\right\} \tag{3.5}$$

The first term in Equation 3.5 corresponds to Bell's theory,[10] in which the activation barrier is linearly dependent on the force. The second term describes the "Hammond" effect,[11-13,15] or the force induced shift of the positions of the transition and reactant states. Notice that the second term is always positive since $V''[s^{(0)}(0)] > 0$ and $V''[s^{(TS)}(0)] < 0$.

It should be noted that Equation 3.5 is an approximation that is valid only for a sufficiently low force. As f is increased, there is a critical value $f = f_c$, after which the barrier disappears altogether and Equation 3.5 becomes meaningless. At $f < f_c$, Equation 3.5 is exact for a cusp-shaped parabolic potential,[11,21] provided that one sets $V''\left[s^{(TS)}(0)\right] = \infty$. For more realistic potentials, Equation 3.5 often remains a reasonable approximation as long as the applied force is considerably smaller than f_c. For example, if $V(s)$ is a cubic parabola,[11] the relative error in the barrier introduced by this approximation is less than 3% for $f < 0.5 f_c$. The quadratic approximation of Equation 3.5, however, breaks down in the vicinity of f_c, where the activation barrier vanishes with a power law dependence on $(f\text{-}f_c)$ (see, *e.g.*, references 22-24).

To conclude our discussion of the 1D case, we point out a useful relationship derived by Suzuki and Dudko,[25] which is true for any force (as long as a barrier is still present):

$$dV^{\neq}/df = s^{(0)}(f) - s^{(TS)}(f) \tag{3.6}$$

This follows immediately from Equations 3.1 and 3.3.

We now turn to the general case and describe the configuration of a molecule consisting of *N* atoms by a 3N-dimensional vector: $\mathbf{r} = (x_1, y_1, z_1, ..., x_N, y_N, z_N)$. Conjugate to it is a 3*N*-dimensional force vector $\mathbf{f} = (f_{x1}, f_{y1}, f_{z1}, ..., f_{xN}, f_{yN}, f_{zN})$, where $\mathbf{F}_i = (f_{xi}, f_{yi}, f_{zi})$ is a three-dimensional force vector acting on the *i*-th atom. The energetics of the system is described by the Born-Oppenheimer potential energy surface $V=V(\mathbf{r})$. The generalization of the above equations to many dimensions is rather straightforward. In particular, to first order in the force we find that the stable and the transition state configurations undergo force induced shifts according to an equation analogous to Equation 3.4:

$$\mathbf{r}^{(0),(TS)}(\mathbf{f}) = \mathbf{r}^{(0),(TS)}(0) + \left(\mathbf{h}^{(0),(TS)}\right)^{-1}\mathbf{f} \tag{3.7}$$

where

$$\mathbf{h}^{(0),(TS)} = \left.\frac{\partial^2 V}{\partial r_\alpha \, \partial r_\beta}\right|_{\mathbf{r}=\mathbf{r}^{(0),(TS)}(0)} \tag{3.8}$$

is the Hessian matrix computed for the reactant/transition state at zero force. For the reaction barrier, we obtain an equivalent of Equation 3.5:

$$\begin{aligned} V^{\neq}(\mathbf{f}) &= V^{\neq}(0) - \mathbf{f}\left[\mathbf{r}^{(TS)}(0) - \mathbf{r}^{(0)}(0)\right] - \frac{1}{2}\mathbf{f}^T\left[\left(\mathbf{h}^{(TS)}\right)^{-1} - \left(\mathbf{h}^{(0)}\right)^{-1}\right]\mathbf{f} \\ &\equiv V^{\neq}(0) + \Delta V_1^{\neq}(\mathbf{f}) + \Delta V_2^{\neq}(\mathbf{f}) \end{aligned} \tag{3.9}$$

where $\mathbf{f}^T$ denotes the transposed force vector.

If the molecule is free to rotate and translate in space, its Hessian matrix $\mathbf{h}$ is generally singular (with six zero eigenvalues corresponding to rigid-body motion) and

therefore not invertible. Equations 3.7 and 3.9, then, appear to be ill defined. This predicament is easily circumvented, however, by noting that the only physically meaningful force vectors **f** are those orthogonal to the null space of the Hessian matrix. Indeed, only such vectors can ensure that the system is in mechanical equilibrium such that the total force and the torque acting on the molecule are both zero. As a consequence, all the inverses in Equations 3.7 and 3.9 should be understood as generalized inverses (pseudoinverses), with the six zero eigenmodes suppressed in their spectral expansion.

An important difference between the multidimensional case and the 1D example described above is that, unlike the 1D case, $\Delta V_2^{\neq}$ can be either positive or negative. Indeed, while the compliance matrix in the stable state, $\left(\mathbf{h}^{(0)}\right)^{-1}$, is non-negative definite and so $\mathbf{f}^T\left[\left(\mathbf{h}^{(0)}\right)^{-1}\right]\mathbf{f}$ is nonnegative, nothing can be said in advance about the sign of $\mathbf{f}^T\left[\left(\mathbf{h}^{(TS)}\right)^{-1}\right]\mathbf{f}$. Indeed, the transition-state Hessian has one negative and several non-negative eigenvalues (except in one dimension, where it is negative-definite). Therefore, the second order term can make the force dependence either stronger or weaker.

So far, our theory is general in that it allows forces to be simultaneously applied to several atoms. Most experimental scenarios, however, are limited to pulling on one pair of atoms, i and j (**Figure 3.1**). Let **F** be the three-dimensional vector representing such a force. From here on, we will use upper-case bold symbols for *three-dimensional* vectors representing positions of (and forces on) individual atoms. We will continue to use lower-case boldface symbols to represent *3N-dimensional* vectors and $(3N) \times (3N)$ matrices corresponding to the configuration of the entire molecule. The mechanical equilibrium of the system requires that **F** always act along the line connecting the atoms. Let $\mathbf{E}=\mathbf{F}/|\mathbf{F}|$ be the unit vector along the force direction. Therefore, the following condition must hold at any point of the pulling process:

$$\frac{\mathbf{R}_j - \mathbf{R}_i}{\left|\mathbf{R}_j - \mathbf{R}_i\right|} = \mathbf{E} \tag{3.10}$$

where $\mathbf{R}_i$ is the three-dimensional vector describing the position of atom *i*. To evaluate Equation 3.9, we note that the 3*N*-dimensional force vector has the following components:

$$\begin{aligned} &f_{xi} = -FE_x, f_{yi} = -FE_y, f_{zi} = -FE_z, \\ &f_{xj} = FE_x, f_{yj} = FE_y, f_{zj} = FE_z, \\ &f_{xk} = f_{yk} = f_{zk} = 0, \text{ for } k \neq i, j \end{aligned} \tag{3.11}$$

In particular, the expression for the first order correction to the barrier height can be simplified to give:

$$\begin{aligned} &\Delta V_1^{\neq}(F) = -\mathbf{f}\left[\mathbf{r}^{(TS)}(0) - \mathbf{r}^{(0)}(0)\right] = -F\left\{\mathbf{E}\left[\mathbf{R}_j^{(TS)}(0) - \mathbf{R}_j^{(0)}(0)\right] - \mathbf{E}\left[\mathbf{R}_i^{(TS)}(0) - \mathbf{R}_i^{(0)}(0)\right]\right\} \\ &= -F\left[\left|\mathbf{R}_j^{(TS)}(0) - \mathbf{R}_i^{(TS)}(0)\right| - \left|\mathbf{R}_j^{(0)}(0) - \mathbf{R}_i^{(0)}(0)\right|\right] \equiv -F\left(R_{ij}^{(TS)} - R_{ij}^{(0)}\right) \end{aligned} \tag{3.12}$$

This shows that (weakly) pulling on a pair of atoms will lower the reaction barrier by an amount that is proportional to the difference between the interatomic distances R_{ij} in the transition and the reactant states (at zero force). If the distance R_{ij} between the two atoms is longer in the transition state than it is in the stable configuration then application of a force between these two atoms will accelerate the reaction. Conversely, application of force will slow the reaction down if the atoms move closer together upon evolving to the transition state.

The quadratic correction to the barrier, $\Delta V_2^{\neq}$, is also easily evaluated using Equations 3.9 and 3.11, given the Hessian matrices corresponding to the stable and the transition-state configurations.

Finally, an analog of the Suzuki-Dudko formula[25] can be derived for an arbitrary force (for which the barrier still exists):

$$dV^{\neq} / dF = -\left(R_{ij}^{(TS)} - R_{ij}^{(0)}\right) \tag{3.13}$$

In accord with other predictions,[25] pulling on a pair of atoms that are further apart in the transition state than in the stable conformation will speed up the reaction. In contrast, pulling on the atoms that approach one another when going from the stable state to the transition state will slow the reaction down. In the biophysics literature, the former is referred to as a slip bond, while the latter case is known as catch bond behavior.[26,27] As previously described,[28,29] multidimensionality of the energy landscape is essential for catch bond behavior. More generally, a one-dimensional picture is often insufficient to describe the effect of a mechanical force on many processes involving biomolecules[30-32] or the dependence of the mechanical response on the choice of the atoms to which the force is applied.[33,34]

In sum, the first-order term (Equation 3.12) corresponds to the standard approximation due to Bell.[10] When supplemented with the second-order term, as in Equation 3.9, we call the result extended Bell theory (EBT).

NUMERICAL EVALUATIONS OF EBT

The electrocyclic ring openings of the *cis* and *trans* substituted benzocyclobutenes are pericyclic transformations that are governed by orbital symmetry, as predicted by the Woodward-Hoffman rules.[35,36] For example, as shown in **Scheme 3.1**, the C_1–C_2 σ-bond orbitals open in a conrotatory fashion in order to constructively overlap with the LUMO of the π-system associated with the fused arene. Depending on the stereochemistry of the benzocyclobutene starting material, this process affords either a *cis*, *trans* diene (**3.1**) or a *trans*, *trans* diene (**3.2**) as the product.[35] It should be noted that these are the expected products of thermal activation; photochemical excitation induces disrotatory ring opening and affords the opposite outcomes (*i.e.*, *cis* 1,2-dimethylbenzocyclobutene is converted to **3.2**, and *trans* 1,2-dimethylbenzocyclobutene is converted to **3.1**).[35] The mechanically

facilitated ring opening is unique, however, in that, regardless of the stereochemistry of the benzocyclobutene starting material, application of vectorially opposed forces across the methyl substituents generates only the *trans*, *trans* diene product.[35] Such reactivity necessitates that both formally allowed and disallowed electrocyclic processes take place under the action of stress. As such, the coupling of mechanical forces to chemical systems creates opportunities for accessing otherwise prohibitive transformations. EBT offers a simple, fast, and effective computational method that can provide insight into mechanically induced chemical processes and aid the development of reactions that are altogether new.

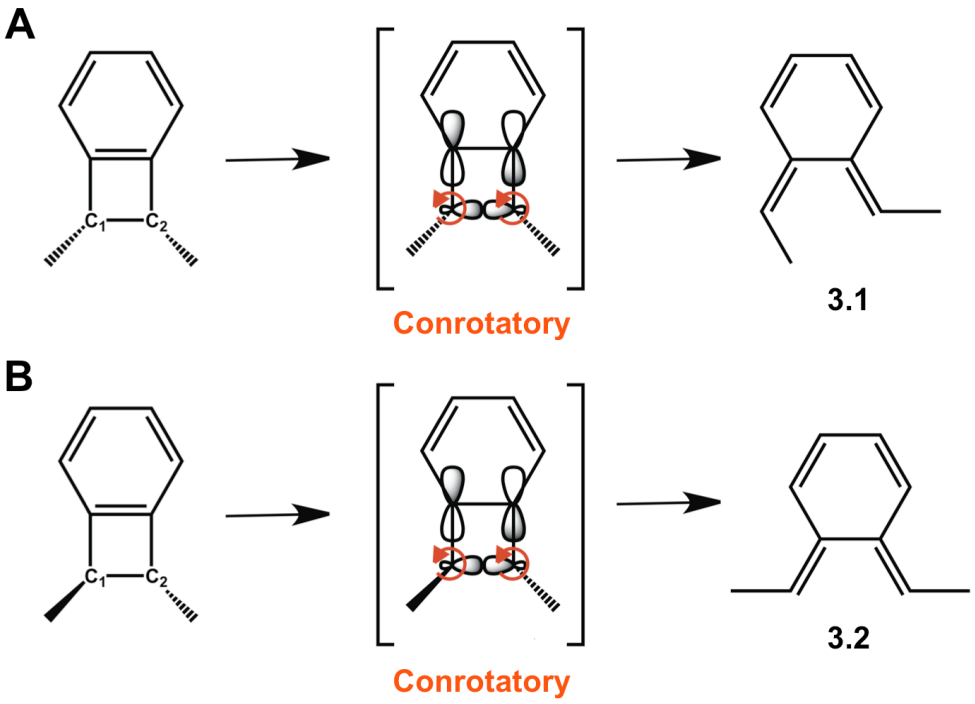

Scheme 3.1 The conrotatory electrocyclic ring-opening of (a) *cis* 1,2-dimethylbenzocyclobutene leads to the *cis*, *trans* diene **3.1** and (b) *trans* 1,2-dimethylbenzocyclobutene leads to the *trans*, *trans* diene **3.2**. The curved arrows indicate the direction in which the orbitals associated with the C_1–C_2 σ-bond open. Hydrogen atoms are implicit in the structures, including at the atoms C_1 and C_1.

To test EBT, we have used it to estimate the force effect on the barrier for the conrotatory electrocyclic ring opening of *cis* and *trans* 1,2-dimethylbenzocyclobutene.[9] As in an earlier study by Ribas-Arino *et al*,[9] the pulling force was assumed to act between the substituent carbon atoms, as shown in **Figure 3.1** (atoms *i* and *j*). In our study, calculations were performed with the NWChem package[37] using density functional theory[38] employing the 6-31G* basis set[39] and the B3LYP exchange-correlation energy functional.[40] EBT involves computing the reactant and transition state structures in the absence of applied force, both of which are shown in **Figure 3.1** (MacMolPlt software[41] was used to generate the structures). The EBT force dependence of the reaction barrier was then computed using Equations 3.9 and 3.11.

To compare EBT with the "exact" (inasmuch as the underlying potential energy surface is deemed exact) result, we have computed the activation barriers for a series of constraints imposed on the distance between the two atoms. It is important, however, to realize that such a "constant extension" calculation does not directly correspond to a constant force scenario assumed above. Indeed, when a constant force is imposed on a pair of atoms, the extension (*i.e.*, the distance between those atoms) is different in the reactant and the transition state. As a result, the barrier encountered by the system is different from that measured under the conditions where the extension is fixed. The observation that controlling stress or strain leads to different mechanical responses underscores the importance of knowing exactly how the pulling process is executed.[19,20]

Assuming one pulls on the atoms *i* and *j*, the correspondence between the constant force and the constant extension scenarios is established by the formula:

$$V^{\neq}(F) = U^{(TS)}[R_{ij}^{(TS)}(F)] - U^{(0)}[R_{ij}^{(0)}(F)] - F\left[R_{ij}^{(TS)}(F) - R_{ij}^{(0)}(F)\right] \qquad (3.14)$$

Here $U^{(0,TS)}(R_{ij})$ is the energy of the molecule in the reactant or transition state computed with the distance between the atoms fixed at R_{ij}, and $R_{ij}^{(0,TS)}(F)$ is the distance between

the atoms (in the reactant or transition state) as a function of the applied force. Thus, to simulate the force through a constraint, one should apply different constraints in the transition and stable states so as to impose the same stretching force in each case. The dependence $R_{ij}^{(0,TS)}(F)$ can be computed by inverting the relationship:

$$F = dU^{(0,TS)}(R_{ij}) / dR_{ij} \tag{3.15}$$

A comparison between Bell's theory, EBT, and "exact" force dependence obtained through Equations 3.14 and 3.15, is shown in **Figure 3.3**. Consistent with earlier observations,[2,9] Bell's formula performs inadequately for the *cis*-isomer (except at very low forces), while EBT reproduces the exact calculations throughout the entire range of forces of ~1 nN and lower (**Figure 3.3A**). Moreover, the force dependence of the barrier found here is nearly identical to that estimated in reference 9. Interestingly, the second-order correction to the activation barrier is negative in this case, rendering the overall force dependence stronger. As previously discussed (*vide supra*), such behavior cannot be predicted by one-dimensional models wherein the second-order correction is always positive.

In the *trans*-case (**Figure 3.3B**) Bell's formula is already nearly exact, and the second-order correction provided by EBT is relatively small. The origins of the difference between the mechanical responses of the *cis*- and *trans*-isomers are further discussed later in this chapter (*vide infra*).

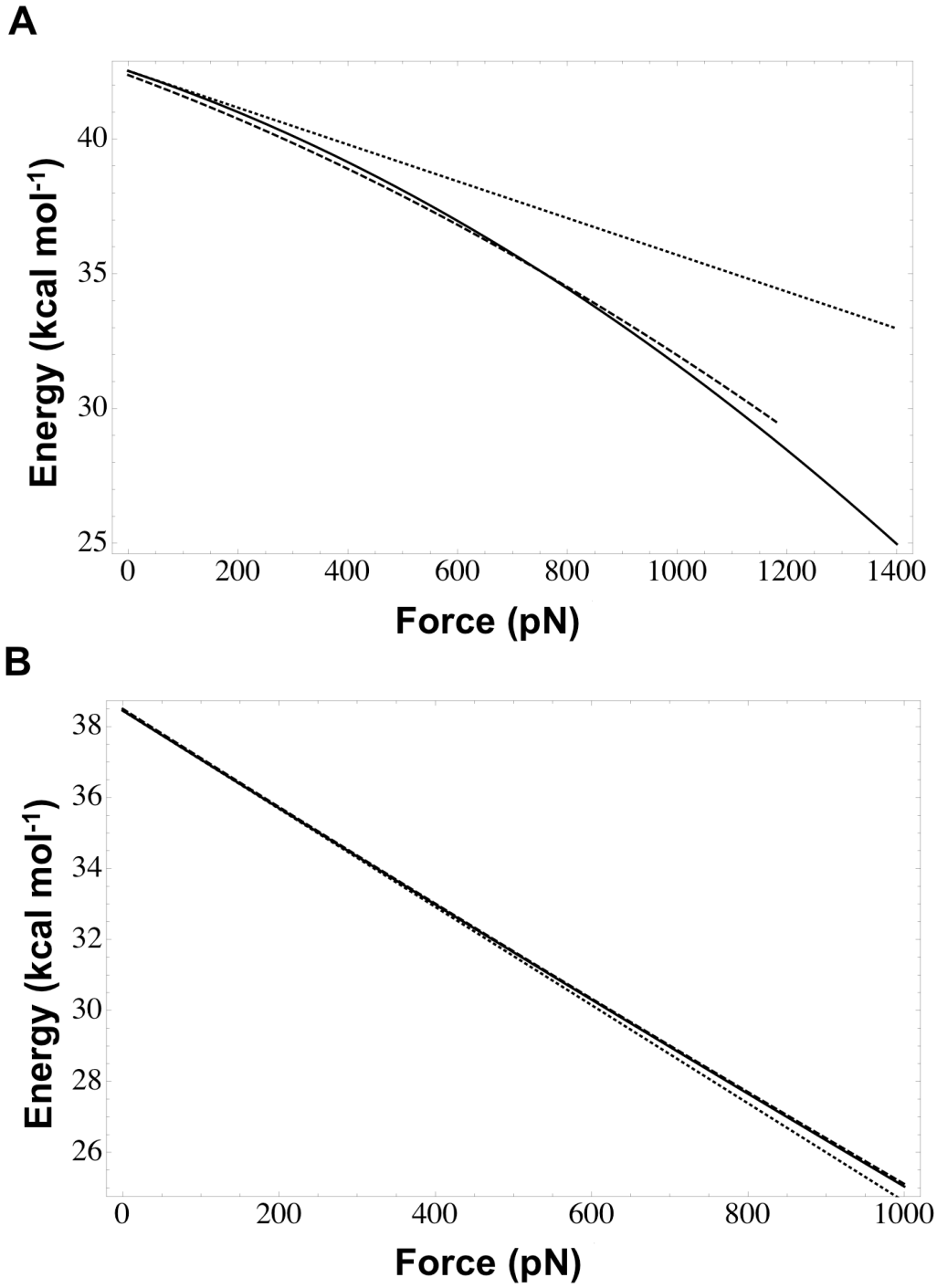

Figure 3.3 Comparison of the force dependence of the reaction barrier obtained by different methods for (A) *cis* and (B) *trans* 1,2-dimethylbenzocyclobutene. Solid line: EBT. Dotted line: Bell's formula. Dashed line: "exact" result obtained from constrained structure optimization.

MECHANICAL COMPLIANCE OF A MOLECULE WITHIN EBT

The harmonic approximation employed in EBT also allows one to readily obtain another important parameter: the effective mechanical compliance of the molecule in the reactant configuration (with respect to pulling on any pair of atoms). That is, EBT allows one to estimate the energy $U^{(0)}(R_{ij})$ as a function of the distance R_{ij} between the atoms one pulls on. Because the underlying potential assumed by EBT is harmonic, one expects that, when stretched between a pair of atoms, the molecule will effectively behave as a Hookean spring with a potential of the form

$$U^{(0)}(R_{ij}) = U^{(0)}[R_{ij}^{(0)}(0)] + k_{ij}^{(0)}[R_{ij} - R_{ij}^{(0)}(0)]^2 / 2 \tag{3.16}$$

where $R_{ij}^{(0)}(0)$ is the equilibrium distance between the atoms. When the distance between a pair of atoms is increased, other atoms must also become displaced. Since no external forces act on those atoms, their positions are determined by the condition that they are in mechanical equilibrium. The finding of $U^{(0)}(R_{ij})$ may be viewed as a coarse-graining procedure in which all of the atomic coordinates, except for the coordinates of the atoms *i* and *j*, are eliminated based on the above mechanical equilibrium condition. As the atoms of the molecule can be arbitrarily relabeled, it is convenient to assume that one always pulls on the first two atoms. We then write the molecule's Hessian matrix in the block-diagonal form:

$$\mathbf{h}^{(0)} = \begin{pmatrix} \mathbf{h}_{11}^{(0)} & \mathbf{h}_{12}^{(0)} \\ \mathbf{h}_{21}^{(0)} & \mathbf{h}_{22}^{(0)} \end{pmatrix} \tag{3.17}$$

Here $\mathbf{h}_{11}^{(0)}$, $\mathbf{h}_{12}^{(0)}$, $\mathbf{h}_{21}^{(0)}$, and $\mathbf{h}_{22}^{(0)}$ are, respectively, 6 × 6, 6 × (3N-6), (3N-6) × 6, and (3N-6) × (3N-6) matrices. The (3N-6) degrees of freedom of the unconstrained atoms are eliminated through the standard coarse graining procedure[42-44] to obtain an effective 6 × 6 Hessian matrix that describes the mechanical response of the pair of atoms one is pulling on. This matrix is given by the Schur complement:

$$\bar{\mathbf{h}}_{11}^{(0)} = \mathbf{h}_{11}^{(0)} - \mathbf{h}_{12}^{(0)} \left(\mathbf{h}_{22}^{(0)} \right)^{-1} \mathbf{h}_{21}^{(0)} \tag{3.18}$$

This matrix should coincide with the Hessian matrix computed from Equation 3.16. This, in particular, means that is has five zero eigenvalues and one nonzero eigenvalue equal to $2k_{ij}^{(0)}$. Starting from the full hessian matrix $\mathbf{h}^{(0)}$, then, one can find the effective spring constant $k_{ij}^{(0)}$ with respect to pulling on any pair of atoms by performing coarse-graining (*via* Equation 3.18) and diagonalizing the resultant 6 × 6 Hessian matrix.

The effective stiffness $k_{ij}^{(TS)}$ of the molecule corresponding to the transition state (or any critical point of the molecule's potential energy surface) can also be defined; however, stretching the molecule while maintaining its transition state configuration does not correspond to any experimental scenario. Regardless, this stiffness can be estimated from Equation 3.18 by using the Hessian matrix corresponding to the transition state. Note that, while $k_{ij}^{(0)}$ is always positive, $k_{ij}^{(TS)}$ may be either positive or negative.

The stiffness k_{ij} (and its inverse, the compliance χ_{ij}) of the molecule in its reactant and transition state configurations determines how these geometries are deformed by the applied force. Using Equations 3.15 and 3.16, we find:

$$R_{ij}^{(0,TS)} = R_{ij}^{(0,TS)}(0) + F / k_{ij}^{(0,TS)} = R_{ij}^{(0,TS)}(0) + \chi_{ij}^{(0,TS)} F \tag{3.19}$$

which is an equivalent of Equations 3.4 and 3.7. Furthermore, the difference between the compliances in the transition and reactant state configurations determines the second-order response of the reaction barrier to the force. Indeed, the EBT formula for the force-dependent rate (Equation 3.9) can be conveniently rewritten in a one-dimensional form similar to Equation 3.5:[16,17]

$$V^{\neq}(F) = V^{\neq}(0) - F\left(R_{ij}^{(TS)} - R_{ij}^{(0)} \right) - (\chi_{ij}^{(TS)} - \chi_{ij}^{(0)}) F^2 / 2 \,, \tag{3.20}$$

which can be derived by substituting Equations 3.16 and 3.19 into Equation 3.14. This result shows that, while the extension or contraction of the distance R_{ij} determines the first-order effect of a force on the barrier, the curvature of the dependence $V^{\neq}(F)$ is

controlled by the difference in the compliances of the transition and reactant states. The latter effect accounts for the change in the elastic energy stored by the molecule when going from the reactant state to the transition state.

The relative importance of the second-order correction depends on the compliance of the molecule in the reactant and the transitions state. More precisely, the second-order term in Equation 3.20 is negligible when $F \ll \left|R_{ij}^{(TS)} - R_{ij}^{(0)}\right| / \left|\chi_{ij}^{(TS)} - \chi_{ij}^{(0)}\right|$. In the same range of forces, therefore, stiffer molecules will be better described by Bell's formula than more compliant ones. For example, the *trans*-isomer of 1,2-dimethylbenzocyclobutene is fairly stiff in both the reactant and transition states ($k^{(0)} \approx 48.5$ N/m, $k^{(TS)} \approx 67.8$ N/m) as compared to the *cis*-isomer ($k^{(0)} \approx 34.0$ N/m, $k^{(TS)} \approx 11.6$ N/m), which exhibits a much softer transition state. This explains the relative success of Bell's theory in the former case, given comparable values of the stretching force. Indeed, a stiffer molecule stretched by a force undergoes a smaller deformation, resulting in a smaller overall elastic energy; this elastic energy can be altogether neglected for sufficiently stiff molecules.

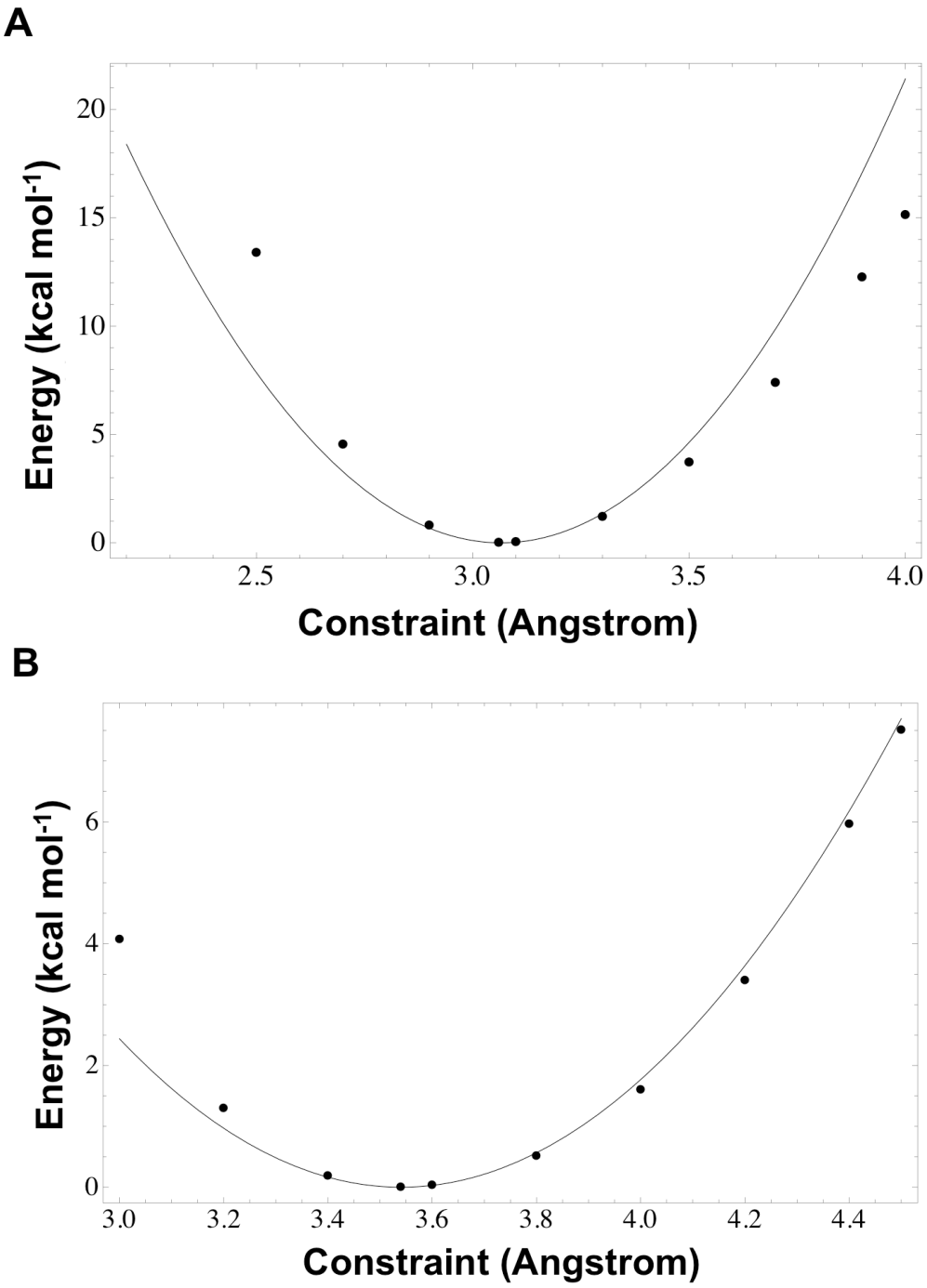

Figure 3.4 The reactant (A) and transition state (B) energies of *cis*-1,2-dimehtylbenzocyclobutene as a function of the extension R_{ij}. The energy in each case is measured relative to its respective minimum value. Solid lines show the harmonic approximation (Equations 3.16 and 3.18) while the solid symbols represent results of constrained optimization.

The quality of the harmonic approximation (Equation 3.18), when applied to the same model systems described above, is examined in **Figure 3.4** and **Figure 3.5**. Using Equations 3.16 and 3.18, we calculate a harmonic estimate of $U^{(0,TS)}(R_{ij})$ and compare it with the "exact" result obtained via constrained optimization of the reactant and transition states. While the harmonic approximation is exact for small extensions, nonlinear effects become significant for larger extensions. In the case of the *cis*-isomer, the harmonic approximation is seen to work better for the transition state than for the reactant. For the *trans*-isomer, we see an opposite trend where significant deviations from the harmonic approximation are observed in the transition state for small deformations (~0.1Å). Nevertheless, the resulting elastic energy of the *trans*-isomer is negligible because the stiffness (*i.e.*, the curvature of the dependence seen in **Figure 3.5B**) of this molecule is much higher than that of the *cis*-congener.

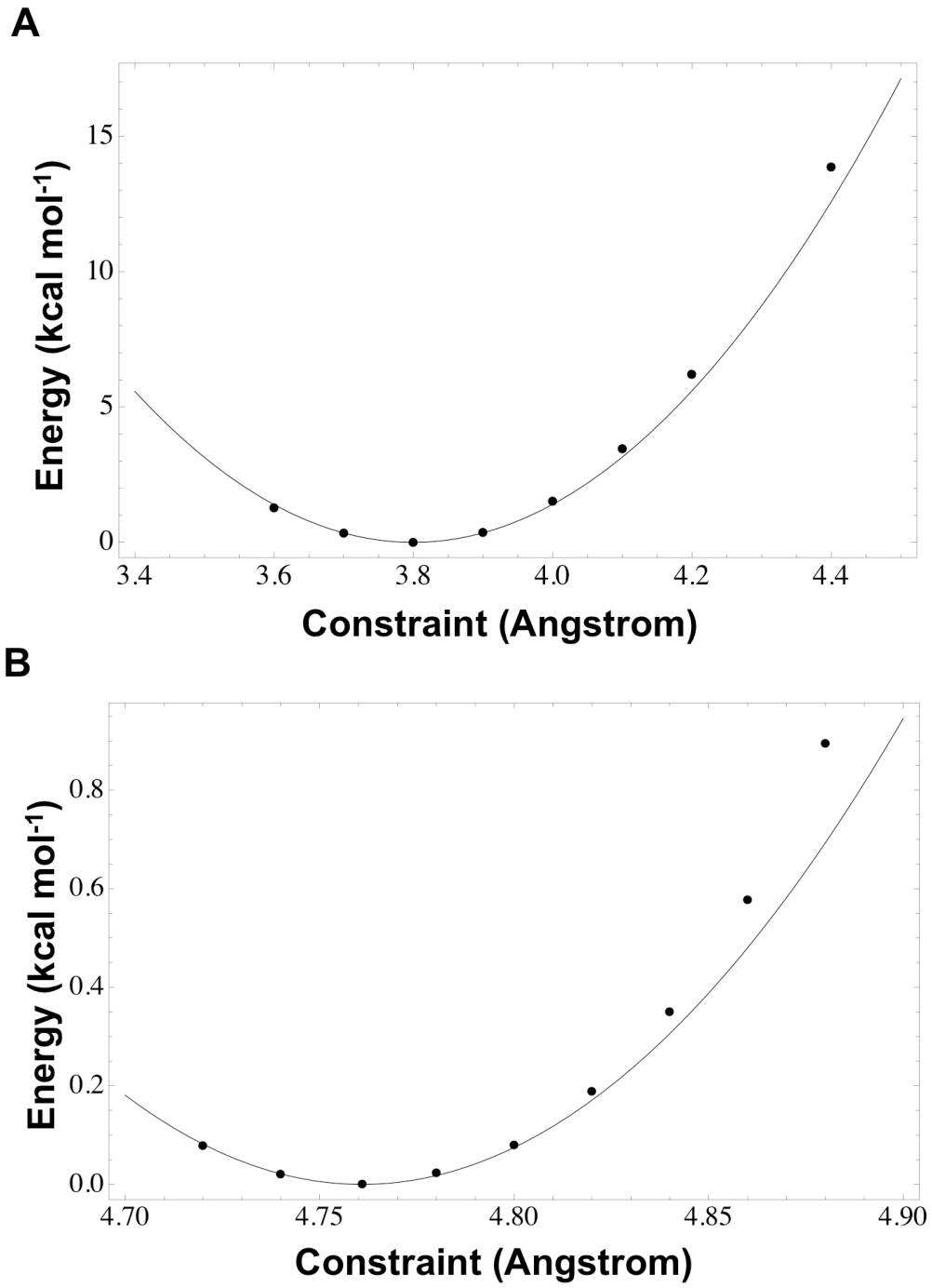

Figure 3.5 The reactant (A) and transition state (B) energies of *trans*-1,2-dimehtylbenzocyclobutene as a function of the extension R_{ij}. The energy in each case is measured relative to its respective minimum value. Solid lines show the harmonic approximation (Equations 3.16 and 3.18) while the solid symbols represent results of constrained optimization.

Finally, it is instructive to compare EBT to the phenomenological cusp-shaped potential model (CSPM),[11,21] which is perhaps the simplest model that can account for experimentally observed deviations from Bell's theory.[12] Similarly to EBT, CSPM considers the effective potential along the pulling coordinate R_{ij} to be a harmonic reactant well. In contrast, the cusp-shaped barrier implies that the location of the CSPM transition state does not depend on the force. Formally, this corresponds to setting $\chi_{ij}^{(TS)} = 0$ in EBT, or, equivalently, to dropping the term that contains the transition state Hessian in Equation 3.9. Both CSPM and EBT predict that the reaction barrier $V^{\neq}(F)$ is a second-degree polynomial of F. However, in the multidimensional case, there is a qualitative difference between the CSPM and EBT predictions regarding the curvature of the $V^{\neq}(F)$ dependence. Specifically, CSPM always predicts the last term in Equation 3.20 to be positive so that the overall force dependence of the reaction barrier $V^{\neq}(F)$ is weaker than in Bell's theory. This, however, is not necessarily the case for EBT: while $\chi_{ij}^{(0)}$ is always positive, the sign of $\chi_{ij}^{(TS)}$ can be variable, and the resulting force dependence of the reaction barrier can be either stronger (*c.f.* **Figure 3.3A**) or weaker than that predicted by Bell's formula.

CONCLUSION AND OUTLOOK

In summary, we have examined an extension of Bell's theory that includes second-order corrections to the dependence of a reaction barrier on an applied mechanical force. Importantly, our approach is exact (inasmuch as the energies predicted by electronic structure calculations are viewed as exact) in the limit of sufficiently weak force. Like the original formulation developed by Bell, the extended Bell theory only requires information about the structures and energies of the transition/reactant states at zero force in order to predict changes in the energy barrier of the associated

transformation under an applied force. Therefore, this approach allows one to predict the effect of applying mechanical force to any of the atoms in a given molecule, without explicitly incorporating stress or strain into electronic structure calculations. Our numerical example shows that EBT is considerably more accurate than the standard formula derived by Bell. Moreover, EBT provides a convenient way of characterizing the sensitivity of any reaction pathway to a mechanical force using two parameters: 1) the change in distance, ΔR, and 2) the change in the compliance, $\Delta\chi$, between the reactant and transition states. The sign and magnitude of these two quantities allow one to quickly predict the overall force dependence of the reaction rate.

The substantial computational gains offered by EBT over explicit calculations involving forces do come at a cost, however. While the second-order correction is sufficient in the examples considered above, there is no guarantee that such is always the case for any value of force that is relevant to experimental studies. Second, our theory assumes that the force continuously transforms the transition state without changing its underlying properties. At sufficiently high forces, however, the topography of the underlying potential surface may change and the saddle point – and the corresponding reaction channel – may, for example, disappear altogether. When this happens, then there is no other choice than to explicitly include force fields in calculations.[9] An example of this behavior is readily seen in the electrocyclic processes described above, where EBT provides no warning that the conrotatory reaction channel disappears[9] for forces higher than ~1nN.

While the above caveats certainly cannot be ignored, we note that the validity of our approach for any given reaction is straightforward to verify. Indeed, one only needs to compare the EBT prediction with a calculation that explicitly includes a force corresponding to the maximum force expected under experimentally relevant conditions.

Such a test is relatively inexpensive because it involves a single transition state search. Moreover, even in the regime where the accuracy of EBT is not satisfactory, using the EBT estimate for the force induced transition state distortion (Equation 3.7) as the initial guess may help speed up the search for the correct transition state.

ACKNOWLEDGEMENTS

J.N.B. is grateful to the National Science Foundation for a predoctoral fellowship. Computational resources were provided by the Texas Advanced Computing Center. Contributions to the content of this chapter from S.S.M.K. and D.E.M. are gratefully acknowledged.

REFERENCES

1 Caruso, M. M.; Davis, D. A.; Shen, Q.; Odom, S. A.; Sottos, N. R.; White, S. R.; Moore, J. S. *Chem. Rev.* **2009**, *109*, 5755.

2 Lenhardt, J. M.; Ong, M. T.; Choe, R.; Evenhuis, C. R.; Martinez, T. J.; Craig, S. L. *Science* **2010,** *329*, 1057.

3 Beyer, M. K.; Clausen-Schaumann, H. *Chem. Rev.* **2005**, *105*, 2921.

4 Bustamante, C.; Chemla, Y.R.; Forde, N. R.; Izhaky, D. *Annu. Rev. Biochem.* **2004**, *73*, 705.

5 Franco, I.; George, C. B.; Solomon, G. C.; Schatz, G. C.; Ratner, M. A. *J. Am. Chem. Soc.* **2011**, *133*, 2242.

6 McCullagh, M.; Franco, I.; Ratner, M. A.; Schatz, G. C. *J. Am. Chem. Soc.* **2011**, *133*, 3452.

7 Beyer, M. K. *J. Chem. Phys.* **2000**, *112*, 7307.

8 Kochhar, G. S.; Bailey, A.; Mosey, N. J. *Angew. Chem. Int. Ed.* **2010**, *49*, 7452.

9 Ribas-Arino, J.; Shiga, M.; Marx, D. *Angew. Chem. Int. Ed.* **2009**, *48*, 4190.

10 Bell, G. I. *Science* **1978,** *200*, 618.

11 Dudko, O. K.; Hummer, G.; Szabo, A. *Phys. Rev. Lett.* **2006**, *96*, 108101.

12 Dudko, O. K.; Mathe, J.; Szabo, A.; Meller, A.; Hummer, G. *Biophys. J.* **2007**, *92*, 4188.

13 Li, P.-C.; Makarov, D. E. *J. Chem. Phys.* **2003**, *119*, 9260.

14 Makarov, D. E. *Biophys. J.* **2007**, *92*, 4135.

15 Hyeon, C.; Thirumalai, D. *Biophys. J.* **2006**, *90*, 3410.

16 Boulatov, R.; Kucharski, T. J. *J. Mater. Chem.* **2011**, *21*, 8237.

17 Huang, Z.; Boulatov, R. *Chem. Soc. Rev.* **2011**, *40*, 2359.

18 Hanggi, P.; Talkner, P.; Borkovec, M. *Rev. Mod. Phys.* **1990**, *62*, 251.

19 Evans, E.; Ritchie, K. *Biophys. J.* **1997**, *72*, 1541.

20 Evans, E.; Ritchie, K. *Biophys. J.* **1999**, *76*, 2439.

21 Hummer, G.; Szabo, A. *Biophys. J.* **2003**, *85*, 5.

22 Dudko, O. K.; Filippov, A. E.; Klafter, J.; Urbakh, M. *Proc. Natl. Acad. Sci. U.S.A.* **2003**, *100*, 11378.

23 Maloney, C. E.; Lacks, D. J. *Phys. Rev. E Stat. Nonlinear Soft Matter Phys.* **2006**, *73*, 061106.

24 Lacks, D. J.; Willis, J.; Robinson, M.-P. *J. Phys. Chem. B* **2010**, *114*, 10821.

25 Suzuki, Y.; Dudko, O. K. *Phys. Rev. Lett.* **2010**, *104*, 048101.

26 Barsegov, V.; Thirumalai, D. *Proc. Natl. Acad. Sci. U.S.A.* **2005**, *102*, 1835.

27 Prezhdo, O. V.; Pereverzev, Y. V. *Acc. Chem. Res.* **2009**, *42*, 693.

28 Dudko, O. K.; Hummer, G.; Szabo, A. *Proc. Natl. Acad. Sci. U.S.A.* **2008**, *105*, 15755.

29 Suzuki, Y.; Dudko, O. K. *J. Chem. Phys.* **2011**, *134*, 065102.

30 Kirmizialtin, S.; Huang, L.; Makarov, D. E. *J. Chem. Phys.* **2005**, *122*, 234915.

31 West, D. K.; Paci, E.; Olmsted, P. D. *Phys. Rev. E Stat. Nonlinear Soft Matter Phys.* **2006**, *74*, 061912.

32 Yew, Z. T.; Schlierf, M.; Rief, M.; Paci, E. *Phys. Rev. E Stat. Nonlinear Soft Matter Phys.* **2010**, *81*, 031923.

33 Brockwell, D. J.; Paci, E.; Zinober, R. C.; Beddard, G. S.; Olmsted, P. D.; Smith, D. A.; Perham, R. N.; Radford, S. E. *Nat. Struct. Biol.* **2003**, *10*, 731.

34 Li, P.-C.; Makarov, D. E. *J. Chem. Phys.* **2004**, *121*, 4826.

35 Hickenboth, C. R.; Moore, J. S.; White, S. R.; Sottos, N. R.; Baudry, J.; Wilson, S. R. *Nature* **2007**, *446*, 423.

36 Woodward, R. B.; Hoffmann, R. *Angew. Chem. Int. Ed.* **1969**, *8*, 781.

37 Valiev, M.; Bylaska, E. J.; Govind, N.; Kowalski, K.; Straatsma, T. P.; Van Dam, H. J. J.; Wang, D.; Nieplocha, J.; Apra, E.; Windus, T. L.; de Jong, W. A. *Comput. Phys. Commun.* **2010**, *181*, 1477.

38 Parr, R. G.; Yang, W. *Density-Functional Theory of Atoms and Molecules*. Oxford Univ. Press, New York, **1989**.

39 Gordon, M. S.; Binkley, J. S.; Pople, J. A.; Pietro, W. J.; Hehre, W. J. *J. Am. Chem. Soc*. **1982**, *104*, 2797.

40 Becke, A. D. *J. Chem. Phys*.**1993**, *98*, 1372.

41 Bode, B. M.; Gordon, M. S. *J. Mol. Graphics Modell*. **1998**, *16*, 133.

42 Eom, K.; Baek, S. C.; Ahn, J. H.; Na, S. *J. Comput. Chem*. **2007**, *28*, 1400.

43 Guyan, R. J. *AIAA J*. **1965**, *3*, 380.

44 Soheilifard, R.; Makarov, D. E.; Rodin, G. J. *J. Chem. Phys*. **2011**, *135*, 054107.

Chapter 4: Regiochemical Effects on the Mechanical Stability of Triazoles

INTRODUCTION[4]

The burgeoning field of polymer mechanochemistry, wherein exogenous forces are directed to chemical functionalities in an anisotropic manner through polymer actuators, offers opportunities to precisely direct chemical reactions down specific pathways.[1,2] As a result, mechanical forces have been shown to facilitate a number of intriguing, and often novel, transformations.[3–9] For example, we recently demonstrated that mechanical forces could effect the formal (3+2) cycloreversion of 1,4-disubstituted 1,2,3-triazoles, a process that currently cannot be accessed through any other stimuli (thermal, photochemical, etc.).[9] We hypothesized that the 1,5-disubstituted isomers[10] of 1,2,3-triazoles might also be susceptible to cycloreversion under mechanical activation (**Scheme 4.1**).

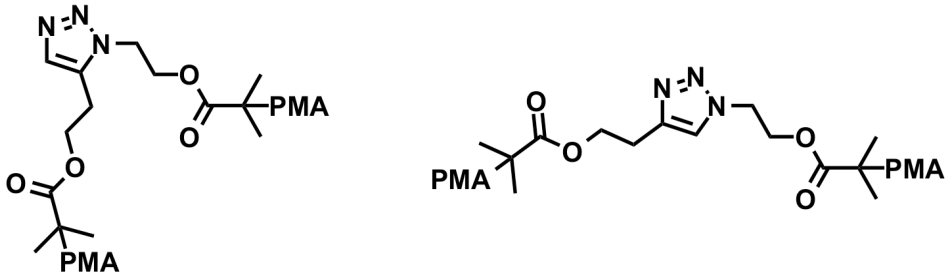

Scheme 4.1 Triazole mechanophores bearing polymer substituents at the 1,5- (left) and 1,4- (right) positions. PMA = poly(methyl acrylate)

Furthermore, we reasoned that 1,4- and 1,5-disubstituted triazole mechanophores could present a unique opportunity to explore regiochemical effects on molecular

[4] Portions of this chapter and the associated appendix were reproduced from: Brantley, J. N.; Konda, S. S. M.; Makarov, D. E.; Bielawski, C. W. *J. Am. Chem. Soc.* **2012**, *134*, 9882. JNB performed the experimental work, and SSMK performed the computational work. All authors contributed to the writing of the original text and figure preparation.

stability through polymer mechanochemistry. Although stereochemistry has been shown to influence mechanochemical transformations,[7,11,12] there have been no reports demonstrating how such processes are influenced by the regiochemistry of the polymer attachments on the mechanophore. Beyond fundamental significance,[13,14] understanding the importance of polymer regiochemistry was envisioned to provide insight that would be beneficial for the rational design of mechanophores[1,2] and force-responsive materials.

INITIAL ULTRASONICATION EXPERIMENTS AND CHEMICAL LABELING STUDIES

Our experimental efforts began with the synthesis of a 1,2,3-triazole bearing polymerization initiators at the 1- and 5-ring positions (**Scheme 4.2**; see Appendix B for additional details). The regioselective cycloaddition of **4.1** and **4.2** was facilitated using [Cp*(PPh_3)$_2$RuCl] as a catalyst in tetrahydrofuran (THF), and the corresponding bifunctional initiator **4.3** was isolated in good yield (79%). Subsequent copper-mediated living radical polymerization of methyl acrylate from **4.3** afforded triazole-centered poly(methyl acrylate) (PMA) materials having number average molecular weights that were dictated by the initial monomer to initiator ratios (**4.4$_{Mn}$**, where M_n indicates number average molecular weight in kDa; see **Table 4.1**).

Table 4.1 Selected Molecular Weight Data for **4.4$_{Mn}$** Polymers†

	Presonication		Postsonication		Sonication Time
	M_n (kDa)	PDI	M_n (kDa)	PDI	(h)
4.4$_{156}$	156	1.4	80	1.5	2
4.4$_{81}$	81	1.4	42	1.3	5
4.4$_{42}$	42	1.3	20	1.4	5
4.4$_{27}$	27	1.4	14	1.6	7
4.4$_{19}$	19	1.4	19	1.3	7

†The polydispersity index (PDI) was calculated using the equation PDI = M_w/M_n, where M_w is the weight average molecular weight. M_n and M_w were determined as their polystyrene equivalents by GPC (eluent = THF).

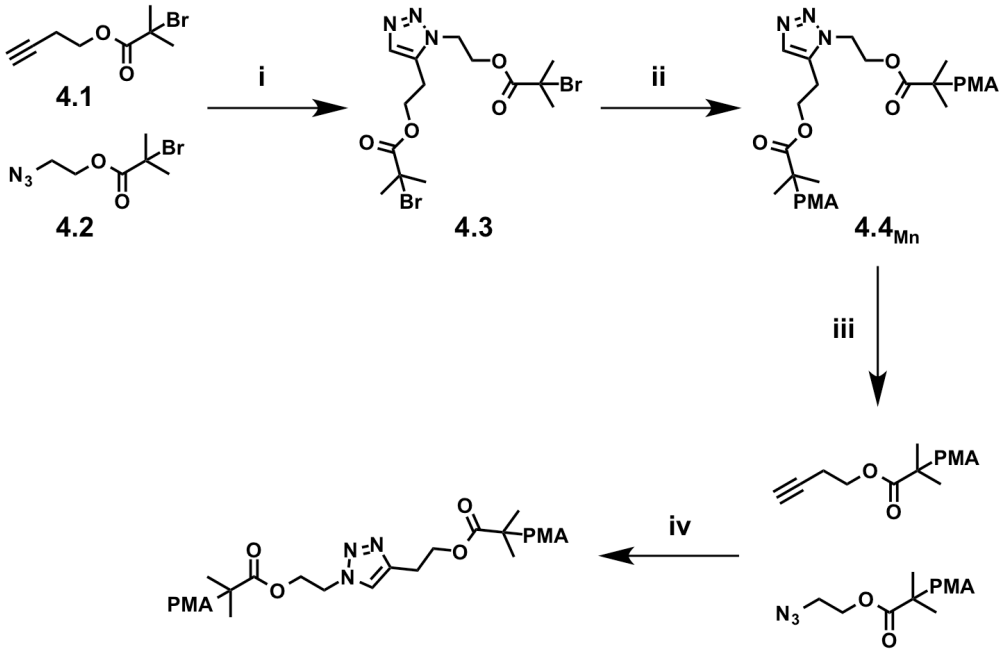

Scheme 4.2 Synthesis and mechanical activation of 1,5-disubstituted triazole mechanophores. i: [Cp*(PPh_3)$_2$RuCl], THF; ii: Methyl acrylate, Me_6TREN, Cu^0, dimethyl sulfoxide; iii: ultrasound; 9.7 W cm^{-2} power intensity; 9 °C). iv: CuI, 85 ºC.

Upon synthesizing the aforementioned polymers, their susceptibility to mechanical activation was explored. Ultrasound irradiation of a 10 mg mL^{-1} solution of **4.4$_{81}$** in acetonitrile (CH_3CN) at 9 °C for 5 h resulted in a reduction of the polymer M_n by approximately half (*c.f.* M_n = 81 kDa presonication versus M_n = 42 kDa postsonication), as determined by gel permeation chromatography (GPC, **Figure 4.1A**). Anticipating that the aforementioned reduction in M_n indicated mechanical activation of the triazole moiety, we sought to characterize the expected azide and terminal alkyne products of the proposed cycloreversion reaction. 1,3-Dimesitylnapthoquinimidazolylidene (**NQMes**), a stabilized carbene known[15–17] to form characteristic acyclic triazene products upon

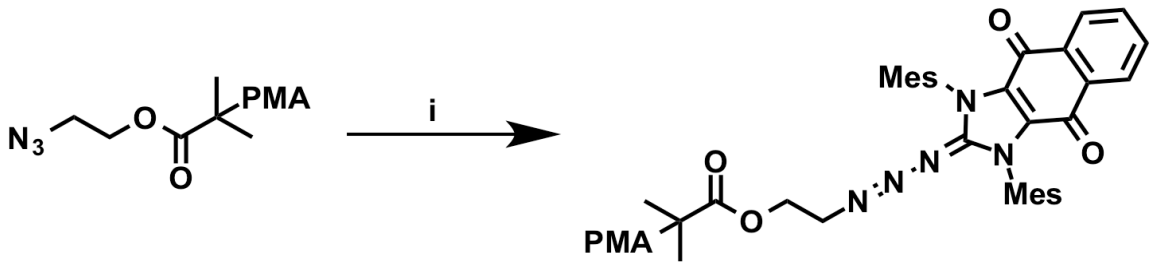

Scheme 4.3 Chemical identification of mechanically liberated azide moieties. i: **NQMes** (10 eq), THF, room temperature (24 h).

reaction with organoazides, was explored as a means to chemically label any mechanically liberated azide functionalities (**Scheme 4.3**).[9] In this experiment, the material obtained following the sonication of $\mathbf{4.4_{81}}$ was dissolved in THF and treated with excess **NQMes** (10 equiv). GPC visualized with ultraviolet-visible detection at 315 nm was consistent[9] with the formation of the expected triazene product. For comparison, minimal change in the material's absorption properties was observed after treating presonicated $\mathbf{4.4_{81}}$ with **NQMes** under otherwise identical conditions (**Figure 4.1B**; see Appendix B for additional details).

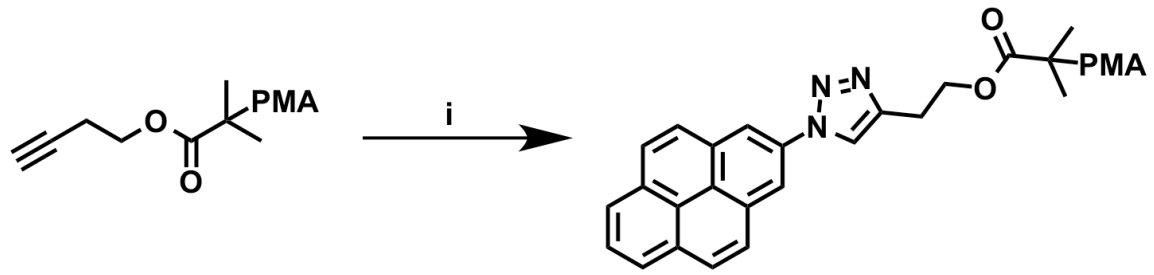

Scheme 4.4 Chemical labeling of mechanically liberated alkynes. i: azidopyrene (10 equiv), CuI (0.1 equiv), MeCN, 85 °C (24 h).

In parallel, efforts were directed toward identifying mechanically liberated terminal alkyne moieties through chemical labeling with 1-azidopyrene (**Scheme 4.4**). After subjecting $\mathbf{4.4_{81}}$ to ultrasonication, the resulting product was treated with excess 1-azidopyrene (10 equiv) in the presence of CuI at 85 °C for 24 h (see Appendix B for

additional details). As shown in **Figure 4.1C**, GPC analysis of the material isolated from this reaction mixture revealed a characteristic pyrene absorbance at 345 nm. In contrast, GPC analysis of the material obtained after treating presonicated $\mathbf{4.4_{81}}$ with 1-azidopyrene under otherwise identical conditions showed a limited increase in absorption at the aforementioned wavelength. Collectively, these results suggested to us that the expected products of the proposed cycloreversion were generated upon ultrasound irradiation of 1,5-disubstituted triazoles embedded within high molecular weight PMAs.

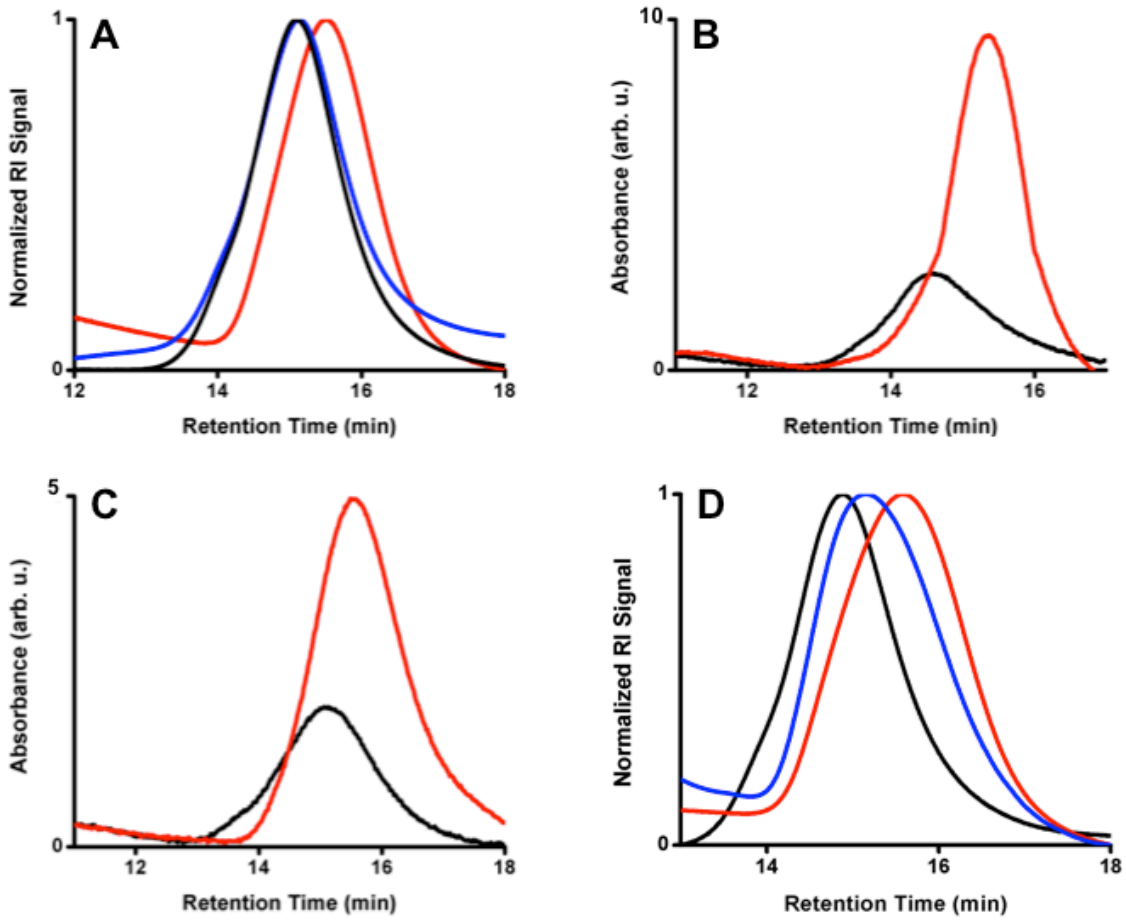

Figure 4.1 (A) GPC traces showing the scission of $\mathbf{4.4}_{81}$ (black) upon sonication (red). No scission was observed when $\mathbf{4.4}_{81}$ was heated in diphenyl ether (220 ˚C) for 24 hours (blue). (B) GPC traces (visualized with ultraviolet-visible detection at 315 nm) showing an increased absorption for the postsonicated $\mathbf{4.4}_{81}$ after treatment with **NQMes** (red) compared to the presonicated $\mathbf{4.4}_{81}$ (black) at the same concentration. (C) GPC traces (visualized with ultraviolet-visible detection at 345 nm) showing an increased absorption for the postsonicated $\mathbf{4.4}_{81}$ upon treatment with 1-azidopyrene (red) compared to the presonicated $\mathbf{4.4}_{81}$ (black) at the same concentration; see text for additional details. (D) GPC traces showing the scission of $\mathbf{4.4}_{81}$ (black) under sonication (red) and reformation of the triazole through a Cu mediated cycloaddition (blue).

RECOUPLING OF POLYMER FRAGMENTS AND THERMAL CONTROL EXPERIMENTS

To further demonstrate that the polymeric products of mechanical activation contained azido- and alkynyl-termini, efforts were directed toward coupling the postsonicated materials using copper-catalyzed catalyzed (3+2) cycloaddition chemistry (**Scheme 4.2**). Upon ultrasound irradiation of a CH_3CN solution of $\mathbf{4.4_{81}}$, the isolated material was first analyzed by GPC (M_n = 42 kDa), dissolved in CH_3CN (10 mg mL^{-1}), and then heated to 85 °C for 24 h in the presence of excess CuI (30 equiv; see Appendix B for additional details). Consistent with a successful coupling reaction, the molecular weight of the polymer product was measured to be nearly twice that of the starting material (M_n = 79 kDa) and nearly identical to that of presonicated $\mathbf{4.4_{81}}$ (**Figure 4.1D**).

The mechanical nature of the observed reactivity was confirmed through a number of control experiments. Importantly, the cycloreversion was found to have a characteristic molecular weight dependence,[1–6,9,11,12,18,19] as only higher molecular weight polymers (*i.e.*, M_n > 19 kDa) underwent activation (**Table 4.1**). Furthermore, cycloreversion was not observed when $\mathbf{4.4_{81}}$ was heated in diphenyl ether at 220 °C for 24 h (**Figure 4.1A**); additional experiments confirmed that thermal effects were negligible (see Appendix B). Collectively, these results demonstrated that cycloreversion was only observed upon mechanical activation of triazole-centered PMAs.

EVALUATION OF CHAIN SCISSION KINETICS

During the course of our studies, we observed activation of 1,5-disbustituted triazoles embedded in polymers of M_n = 27 kDa. This was a surprising result, as we previously found that analogous polymers containing the 1,4-regioisomer did not undergo mechanical activation.[9] To quantify this difference in reactivity, the rate constants for mechanical activation of both isomers embedded within polymers of similar initial molecular weight (M_n = 90 kDa) were measured. The polymers were individually

subjected to ultrasound irradiation as described above, and the change in the M_n of each polymer was monitored using GPC as a function of sonication time.[11] The corresponding rate constants were measured to be: k_{obs} (1,5-triazole) = 3.22×10^{-5} min^{-1}; k_{obs} (1,4-triazole) = 2.76×10^{-5} min^{-1} (**Figure 4.2**; see Appendix B for additional details).[20]

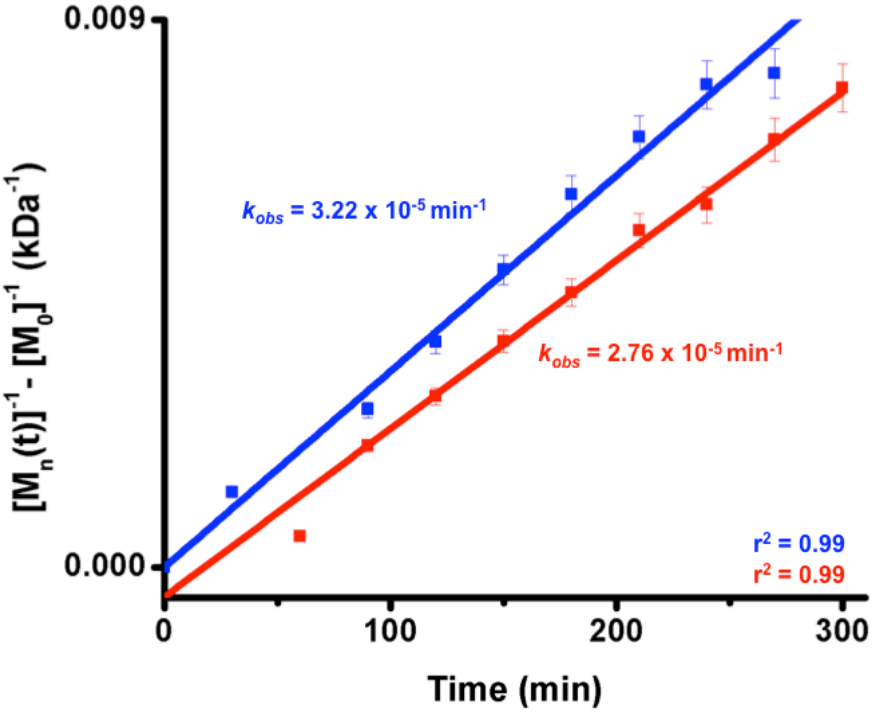

Figure 4.2 Plots of change in M_n versus time used to measure the rate constants for the cycloreversions of 1,5-disubstituted (blue) and 1,4-disubstituted (red) triazoles. Each regioisomer was embedded within a PMA (M_n = 90 kDa) and subjected to ultrasound irradiation.

COMPUTATIONAL MODELING OF 1,2,3-TRIAZOLE CYCLOREVERSIONS

In an effort to explain the differences in the aforementioned rate constants, we first reasoned that the 1,5-triazole was more responsive to mechanical activation (in part, at least) because the vicinal polymer attachments localized mechanical forces at one of the bonds that needed to rupture during cycloreversion (*i.e.*, the N_1–C_5 bond). In contrast,

the polymers attached to the 1,4-regioisomer would translate mechanical energy across the entire heterocyclic scaffold, effectively diminishing the magnitude of the force experienced by the bonds directly involved in the cycloreversion. We also reasoned that (1) the N_1–C_5 bond should exhibit greater flexibility (which could facilitate better alignment with applied forces) than the N_3–C_4 bond due to the rigidity imposed by the π-character in the N_2–N_3 bond, and (2) the N_1–C_5 bond of the 1,5-regioisomer should be slightly weakened as a consequence of steric congestion.

To explore these viewpoints more quantitatively, we employed electronic structure calculations to probe the mechanically induced cycloreversion processes. In particular, we used the recently described extended Bell theory[21] (EBT; see chapter 3), which offers a computationally inexpensive alternative to methods that explicitly determine the effect of mechanical stress[8,22,23] or strain[24] on molecular potential energy surfaces. Regardless, EBT accurately predicts mechanochemical reactivity trends using standard geometry optimizations and saddle point searches performed on mechanically unperturbed molecules.[21] The method also predicts the force dependence of the activation barrier for a given transformation using only two parameters, the first being the change in distance between the two atoms to which force is applied upon evolving from the reactant state to the transition state. If this distance increases, then applying an elongational force across those two atoms should lower the overall reaction barrier.[25] Conversely, if the distance between the nuclei decreases at the transition state then applying an elongational force should retard activation. The second parameter is the difference in the molecular compliance between the transition and reactant states, which determines the curvature of the force dependence of the activation barrier. Thus, EBT generalizes the classic Bell model,[26] where the barrier is assumed to be linearly dependent on the applied force. While accurate EBT predictions require that the applied force is relatively weak, the

amount of information that can be extracted from such a relatively simple set of calculations is highly attractive for the evaluation of mechanochemical phenomena.

EBT calculations for the triazole cycloreversions were performed with the NWCHEM package[27] using density functional theory,[28] employing the 6-31G* basis set[29] and the B3LYP exchange-correlation energy functional (see Appendix B for additional details).[30] Triazoles featuring 1,4- and 1,5-dimethyl substituents (**4.5** and **4.6**, respectively; **Figure 4.3**) were initially chosen for the *in silico* evaluation of the cycloreversion processes. In the case of **4.5**, the N_1 and C_4 atoms were considered to be the points to which the pulling forces were applied, as we reasoned that these nuclei would simulate the direct translation of mechanical force to the triazole moiety. Similarly, the N_1 and C_5 atoms were treated as the pulling points for EBT analysis of **4.6**. To determine which set of pulling points would more readily facilitate the triazole cycloreversion, the internuclear distances between the aforementioned atoms in **4.5** and **4.6** were calculated in the reactant and transition state geometries. As expected, the change in distance between the pulling points in **4.6** was larger than the corresponding change between the pulling points in **4.5** (0.93 Å for **4.6** versus 0.62 Å for **4.5**). Thus, **4.6** was predicted to be more susceptible to mechanical activation than **4.5** (*vide infra*; **Figure 4.4**). By extension, 1,5-disubstituted triazoles should respond to mechanical forces (*i.e.*, undergo mechanical cycloreversion) more readily than their 1,4-disubstituted congeners, which was consistent with the experimental observations previously discussed.

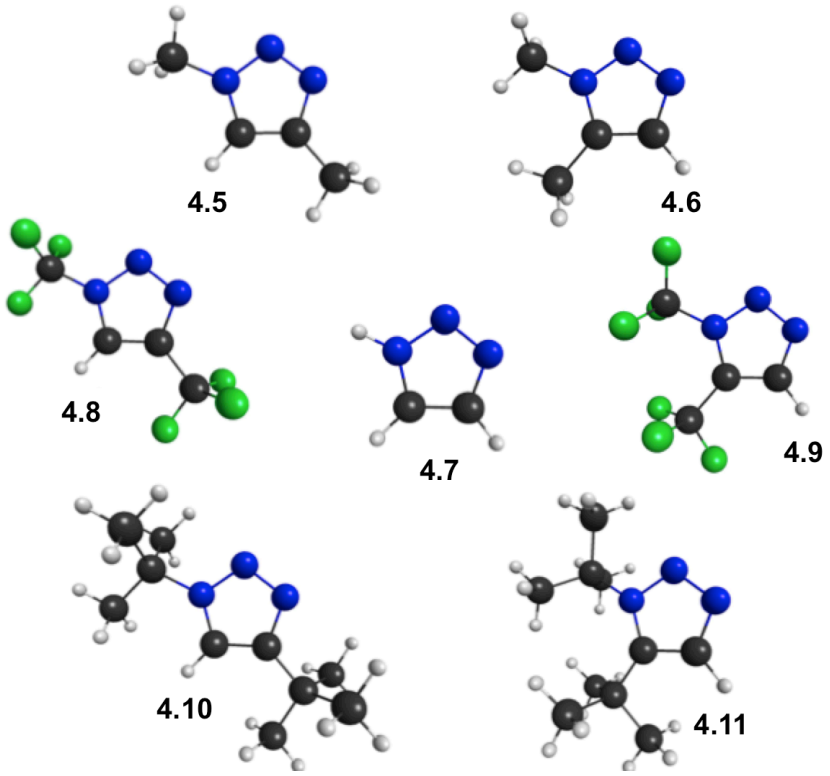

Figure 4.3 Reactant state geometries of **4.5 – 4.11**. Legend: Carbon (Black), Hydrogen (White), Fluorine (Green), Nitrogen (Blue). Figure was prepared using MacMolPlt software.[31]

The intrinsic reactivity of the 1,2,3-triazole was also explored through the evaluation of an analogue bearing only hydrogen substituents, and therefore devoid of steric bulk or highly perturbing electronic effects (**4.7**; **Figure 4.3**). As in the aforementioned calculations, the change in the N_1–C_5 internuclear distance from the reactant state to the transition state was larger than the corresponding change in the N_1–C_4 distance (0.85 Å versus 0.60 Å). This result was consistent with the hypothesis that direct bond activation in the 1,5-regioisomer (in contrast to force dissipation across the 1,4-regioisomer) more readily facilitated the cycloreversion process by efficiently pulling the triazole into a transition state geometry necessary for the retro-(3+2) reaction. Since stereoelectronic effects were negligible in **4.7**, the result also suggested to us that the N_1–

C_5 bond was inherently more susceptible to mechanical deformation than the N_3–C_4 bond, which could result from the rigidity imposed by the N_2–N_3 bond (*vide supra*). Collectively, these data further supported the conclusion that 1,5-disubstituted triazoles were intrinsically more susceptible to mechanical activation than their corresponding 1,4-regioisomers.

Having explored the intrinsic susceptibility of 1,4- and 1,5-disbustituted triazoles to mechanical activation, the response of the cycloreversion energy barrier to exogenous forces was probed using EBT. **Figure 4.4** shows the predicted changes in the reaction barriers for the cycloreversions of **4.5** (black) and **4.6** (blue) as a function of force, hereafter referred to as force curves (FCs). A series of functionalized triazole analogues (**4.8 – 4.11**; **Figure 4.3**; **Figure 4.4**) were also evaluated computationally in the manner previously discussed to elucidate electronic or steric effects on the cycloreversion process. Importantly, barriers corresponding to cycloreversions of the 1,5-regioisomers at zero force were lower than those of the analogous 1,4-regioisomers in all cases. Building on this result, we sought to draw a comparison between predicted trends in cycloreversion and known triazole reactivity. We reasoned that electron deficient triazoles should undergo cycloreversion more readily than electron rich analogues, as electron deficient triazoles are known to participate in the Dimroth rearrangement.[32–34] Toward this end, the barriers to cycloreversion at zero force for bis(trifluoromethyl) substituted triazoles (**4.8** and **4.9**) and dimethyl substituted triazoles (**4.5** and **4.6**) were compared. As expected, the activation energies for the cycloreversions involving the dimethylated isomers (E_a = 90.7 kcal/mol for **4.5**; E_a = 88.9 kcal/mol for **4.6**) were found to be larger than those for the analogous trifluoromethyl congeners (E_a = 85.0 kcal/mol for **4.8**; E_a = 68.7 kcal/mol for **4.9**). Since this result conformed to our prediction, we turned our attention to an evaluation of steric effects on the cycloreversion processes.

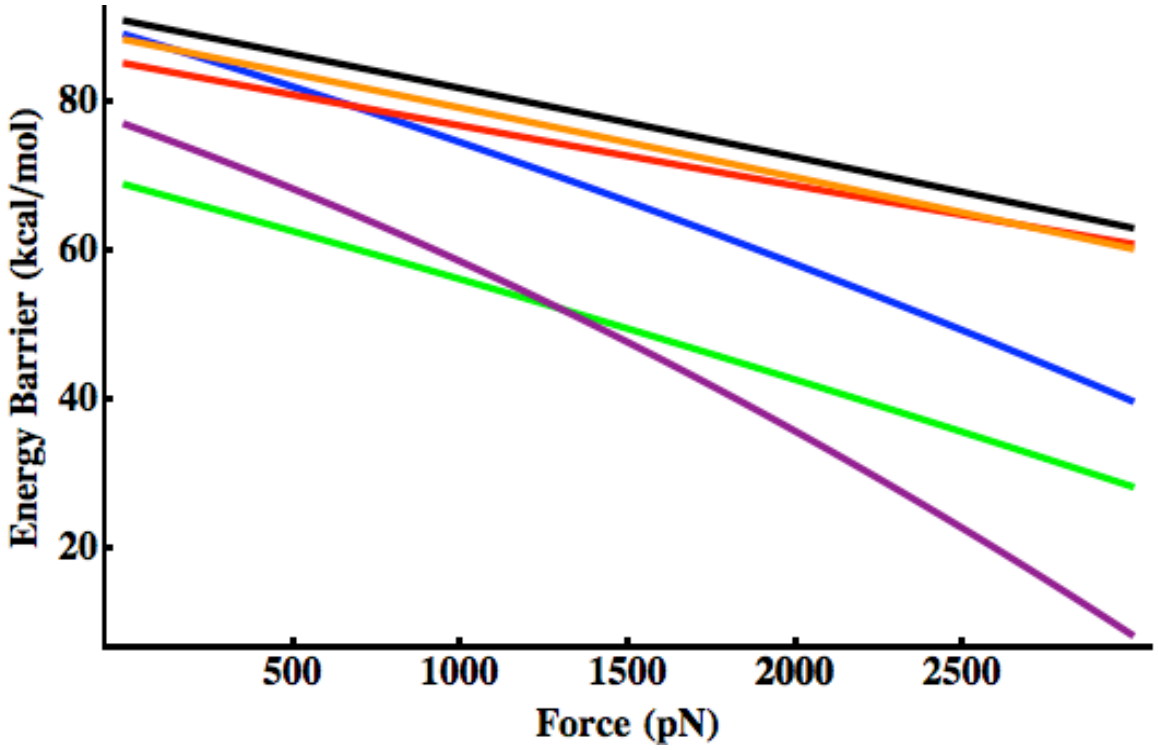

Figure 4.4 Force curves for **4.5** (black), **4.6** (blue), **4.8** (red), **4.9** (green), **4.10** (orange), and **4.11** (violet). Energy barrier refers to the activation energy for triazole cycloreversion.

To explore the role of sterics, the cycloreversions of dimethyl substituted triazoles were compared to bis(t-butyl) analogues (**4.10** and **4.11**). Specifically, we reasoned that the relative differences between the energy barriers at zero force for each set of analogues would reveal the extent to which steric congestion influenced the cycloreversion processes. In accord with this assessment, the difference between the aforementioned barriers for the cycloreversions of **4.5** and **4.6** (ΔE_a= 1.87 kcal/mol) was calculated to be smaller than that between **4.10** and **4.11** (ΔE_a= 11.37 kcal/mol). Moreover, we found that the steric interactions present in 1,5-disubstituted triazoles significantly influenced the compliance of these isomers, a result that is clearly illustrated by the pronounced curvature of the FC calculated for **4.11**. Indeed, the FCs for all of the 1,5-analogues

evaluated exhibited greater curvature than those of the corresponding 1,4-isomers. It should also be noted that **4.11** exhibited the largest force dependence of all the derivatives analyzed using EBT, as evidenced by the precipitous decrease in the associated energy barrier for cycloreversion under increasing force (**Figure 4.4**). Collectively, these results indicated that, in combination with the intrinsic deformability of the N_1–C_5 bond, steric congestion rendered the 1,5-regioisomer of the triazole more susceptible to mechanical activation than the analogous 1,4-regioisomer.

CONCLUSIONS AND OUTLOOK

In summary, we have demonstrated that 1,5-disubstituted triazoles undergo a mechanically facilitated cycloreversion to afford azide and terminal alkyne moieties. The products of the cycloreversion were identified through reaction with chemical labels as well as characterization using spectroscopic and chromatographic techniques. A variety of control experiments ruled out thermal effects and indicated that mechanical forces were responsible for the observed reactivity. The rate of cycloreversion for the 1,5-disubstituted regioisomer was found to be 20% greater than that of its 1,4-congener, which was explained by a combination of increased molecular compliance and direct bond activation in the case of the former. In a broader context, these results show that the relative regiochemistry of the polymer attachments on a mechanophore must be considered when evaluating or designing mechanochemical systems. Moreover, we believe these results demonstrate that EBT could ultimately be used to guide the rational design of mechanically responsive systems.

ACKNOWLEDGEMENTS

J.N.B. is grateful to the National Science Foundation for a predoctoral fellowship. Contributions to the content of this chapter from S.S.M.K. and D.E.M. are gratefully acknowledged. Computational resources were provided by the Texas Advanced Computing Center.

REFERENCES AND NOTES

1 Caruso, M. M.; Davis, D. A.; Shen, Q.; Odom, S. A.; Sottos, N. R.; White, S. R.; Moore, J. S. *Chem. Rev.* **2009**, *109*, 5755.

2 Black, A. L.; Lenhardt, J. M.; Craig, S. L. *J. Mater. Chem.* **2011**, *21*, 1655.

3 Tennyson, A. G.; Wiggins, K. M.; Bielawski, C. W. *J. Am. Chem. Soc.* **2010**, *132*, 16631.

4 Wiggins, K. M.; Hudnall, T. W.; Shen, Q.; Kryger, M. J.; Moore, J. S.; Bielawski, C. W. *J. Am. Chem. Soc.* **2010**, *132*, 3256.

5 Wiggins, K. M.; Hudnall, T. W.; Tennyson, A. G.; Bielawski, C. W. *J. Mater. Chem.* **2011**, *21*, 8355.

6 Wiggins, K. M.; Syrett, J. A.; Haddleton, D. M.; Bielawski, C. W. *J. Am. Chem. Soc.* **2011**, *133*, 7180.

7 Hickenboth, C. R.; Moore, J. S.; White, S. R.; Sottos, N. R.; Baudry, J.; Wilson, S. R. *Nature* **2007**, *446*, 423.

8 Lenhardt, J. M.; Ong, M. T.; Choe, R.; Evenhuis, C. R.; Martinez, T. J.; Craig, S. L. *Science* **2010**, *329*, 1057.

9 Brantley, J. N.; Wiggins, K. M.; Bielawski, C. W. *Science* **2011**, *333*, 1606.

10 Boren, B. C.; Narayan, S.; Rasmussen, L. K.; Zhang, L.; Zhao, H.; Lin, Z.; Jia, G.; Fokin, V. V. *J. Am. Chem. Soc.* **2008**, *130*, 8923.

11 Kryger, M. J.; Munaretto, A. M.; Moore, J. S. *J. Am. Chem. Soc.* **2011**, *133*, 18992.

12 Lenhardt, J. M.; Black, A. L.; Craig, S. L. *J. Am. Chem. Soc.* **2009**, *131*, 10818.

13 Kucharski, T. J.; Boulatov, R. *J. Mater. Chem.* **2011**, *21*, 8237.

14 Hickenboth, C. R.; Rule, J.; Moore, J. S. *Tetrahedron* **2008**, *64*, 8435.

15 Khramov, D. M.; Bielawski, C. W. *J. Org. Chem.* **2007**, *72*, 9407.

16 Khramov, D. M.; Bielawski, C. W. *Chem. Commun.* **2005**, 4958.

17 Coady, D. J.; Khramov, D. M.; Norris, B. C.; Tennyson, A. G.; Bielawski, C. W. *Angew. Chem. Int. Ed.* **2009**, *48*, 5187.

18 Wiggins, K. M.; Bielawski, C. W. *Angew. Chem. Int. Ed.* **2012**, *51*, 1640.

19 Davis, D. A.; Hamilton, A.; Yang, J.; Cremar, L. D.; Van Gough, D.; Potisek, S. L.; Ong, M. T.; Braun, P. V.; Martínez, T. J.; White, S. R.; Moore, J. S.; Sottos, N. R. *Nature* **2009**, *459*, 68.

20 The observed rate constants were taken as those that corresponded to the afrorementioned cycloreversion process.

21 Konda, S. S. M.; Brantley, J. N.; Bielawski, C. W.; Makarov, D. E. *J. Chem. Phys.* **2011**, *135*, 164103. For another study related to the effects of molecular compliance on mechanochemical phenomena, see: Bailey, A.; Mosey, N. J. *J. Chem. Phys.* **2012**, *136*, 044102.

22 Kochhar, G. S.; Bailey, A.; Mosey, N. J. *Angew. Chem. Int. Ed.* **2010**, *49*, 7452.

23 Ribas-Arino, J.; Shiga, M.; Marx, D. *Angew. Chem. Int. Ed.* **2009**, *48*, 4190.

24 Beyer, M. K. *J. Chem. Phys.* **2000**, *112*, 7307.

25 Kauzmann, W.; Eyring, H. *J. Am. Chem. Soc.* **1940**, *62*, 3113.

26 Bell, G. *Science* **1978**, *200*, 618.

27 Valiev, M.; Bylaska, E. J.; Govind, N.; Kowalski, K.; Straatsma, T. P.; Van Dam, H. J. J.; Wang, D.; Nieplocha, J.; Apra, E.; Windus, T. L.; de Jong, W. A. *Comput. Phys. Commun.* **2010**, *181*, 1477.

28 Parr, R. G. and Yang, W. *Density-Functional Theory of Atoms and Molecules*; Oxford University Press: New York, 1989.

29 Gordon, M. S.; Binkley, J. S.; Pople, J. A.; Pietro, I. W. J.; Hehre, W. J. *J. Am. Chem. Soc.* **1982**, *104*, 2797.

30 Becke, A. D. *J. Chem. Phys.* **1993**, *98*, 1372.

31 Bode, B. M.; Gordon, M. S. *J. Mol. Graphics Modell.* **1998**, *16*, 133.

32 Dimroth, O. *Liebigs Ann.* **1909**, *364*, 183.

33 Dimroth, O.; Michaelis, W. *Liebigs Ann.* **1927**, *459*, 39.

34 Horneff, T.; Chuprakov, S.; Chernyak, N.; Gevorgyan, V.; Fokin, V. V. *J. Am. Chem. Soc.* **2008**, *130*, 14972.

Chapter 5: Mechanically Suppressed Reactivity in Polymeric Matrices

INTRODUCTION[5]

The use of mechanical forces to bias chemical reactions, commonly referred to as mechanochemistry,[1] has increasingly found applications in the synthetic and materials science communities. Within this field, polymer mechanochemistry, or the mechanical manipulation of reactive functional groups (termed mechanophores) embedded within polymeric matrices, has attracted considerable attention due to its ability to facilitate a number of otherwise kinetically inaccessible processes.[2] While theoretical models have been shown to successfully account for these experimental observations,[3] such models are typically used as post-experimental rationalizations. Here, we show that theoretical analysis can be used to rationally design mechanophores with unique mechanochemical activity. This analysis further reveals general trends in the mechanical response of polyatomic molecules that have significant implications for the design of new mechanophores and force responsive materials. These trends stem from the inherent multidimensionality of mechanochemical processes and, therefore, cannot be accounted for by one-dimensional models commonly used to explain mechanical activation.[4] Indeed, while one-dimensional approximations necessitate that force acts in the direction of the reaction coordinate (RC), thereby lowering the transition state (TS) barrier and accelerating the associated transformation, we will show that such an alignment between an applied force and a typical RC is extremely improbable in the high-dimensional configuration space of a mechanophore.

---

[5] Portions of this chapter and the associated appendix were reproduced from: Konda, S. S. M.; Brantley, J. N.; Varghese, B. T.; Wiggins, K. M.; Bielawski, C. W.; Makarov, D. E. *J. Am. Chem. Soc.* **2012**, *134*, 9882. JNB and SSMK contributed equally to the original work. BTV and KMW provided assistance with chemical synthesis. JNB, CWB, SSMK, and DEM wrote the original manuscript.

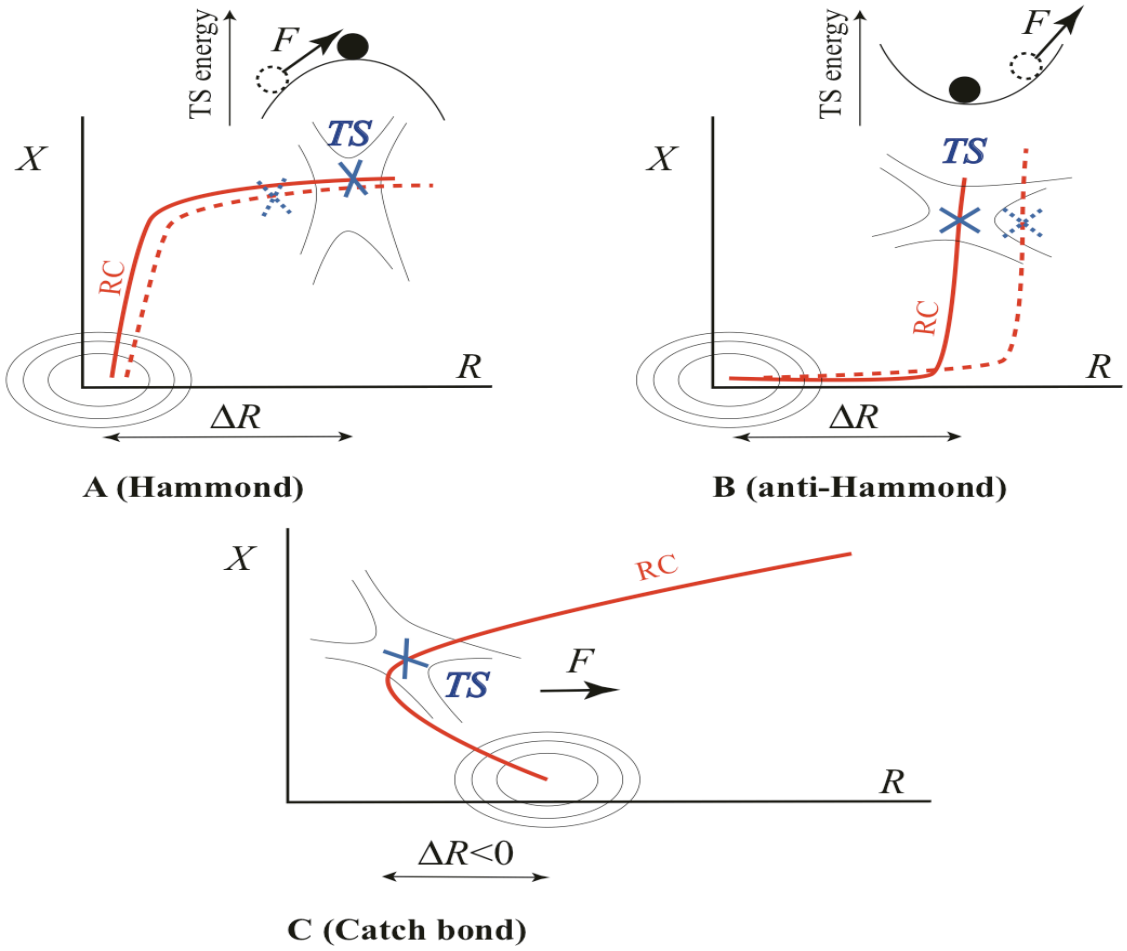

Figure 5.1 Force induced changes on a reaction pathway. (A) The Hammond effect, where the "true" reaction coordinate (RC, red line) is aligned with the mechanical coordinate (*R*). Mechanical equilibrium necessitates that a pulling force (*F*) shifts the TS toward the reactant state minimum (because the TS energy exhibits a maximum along *R*). The shifted RC and the new TS are shown as a dashed red line and a blue "X", respectively. (B) The anti-Hammond effect, where there is misalignment between RC and *R* (so that the TS exhibits a minimum as a function of R) and the TS is more compliant than the reactant. (C) Catch bond behavior, where molecular distortion along *R* initially decreases but later increases along the RC.

THEORETICAL CONSIDERATIONS

The alignment between a mechanical stress and the targeted reaction pathway can result in a number of distinct scenarios. **Figure 5.1** illustrates some of these activation motifs using a model two-dimensional potential energy surface (PES) that exhibits a single minimum (which corresponds to the reactant) and a saddle-point (which corresponds to the TS). Of the two coordinates that specify the molecular configuration, R quantifies the mechanical strain (which corresponds to the distance between a pair of atoms on which the applied force is exerted in many experimental studies), and X represents the remaining molecular degrees of freedom. While similar scenarios to those depicted in **Figure 5.1** have been explored,[5] we emphasize that the reduction to two degrees of freedom is an oversimplification in the present context and is only used for illustrative purposes.

A force F acting along the mechanical coordinate R performs mechanical work ($W = F\Delta R$) as the molecule evolves toward the TS, where ΔR is the change in the mechanical pulling coordinate. The activation energy is accordingly lowered by W, and the transition rate $k(F)$ is enhanced by a factor of $e^{W/k_BT} = e^{F\Delta R/k_BT}$. This result, commonly referred to in the literature as the "Bell formula",[4] however, does not account for the force induced displacement of the reactant and transition states. If the true RC (*i.e.*, the steepest descent path connecting the TS saddle point to the reactant state minimum on the PES) coincides with the mechanical coordinate (**Figure 5.1A**) then a stretching force pushes the TS toward the reactant. This phenomenon is usually referred to as the Hammond effect, which posits that the reactant and TS structures are driven toward each other as the barrier separating them is lowered.[3a,6] As the Hammond effect reduces the overall molecular distortion (*i.e.*, ΔR), it effectively weakens the force dependence of the reaction rate.

A very different scenario is shown in **Figure 5.1B**, where the mechanical coordinate is misaligned with the RC in the vicinity of the TS saddle such that the TS energy exhibits a minimum (rather than a maximum) when R is varied. Consequently, a pulling force F may *increase* the separation between the TS and the reactant. The resulting "anti-Hammond" behavior necessitates that the structural separation between the reactant and the TS increases, despite the fact that the energy barrier between these two states decreases. As the anti-Hammond effect increases the work that must be performed by the applied force, it provides an additional acceleration of the reaction rate.

These considerations are quantified in the recently reported Extended Bell Theory (EBT; see chapter 3),[3c-e] which accounts for the force induced shifts of the TS and reactant state along a given reaction pathway in the $3N$-dimensional configuration space of the molecular system of interest (where N is the total number of atoms). To second order in the applied force, the reaction rate $k(F)$ is given by:[3d]

$$\ln k(F)/k(0) = \left(k_B T\right)^{-1}\left(F\Delta R + F^2\Delta\chi/2\right) \tag{5.1}$$

The $F\Delta R$ term in Equation 5.1 is identical to Bell's formula. The quadratic term results from the interplay between two factors: (1) the elastic energy stored in the molecule as a result of mechanical deformation and (2) the additional work done by the applied force as a result of the Hammond (or anti-Hammond) shift in ΔR. This shift is described by the formula:

$$\Delta\Delta R = \Delta R_{TS} - \Delta R_r = \chi_{TS}F - \chi_r F = \Delta\chi F \tag{5.2}$$

where χ_r and χ_{TS} are the compliances of the reactant state and TS in response to pulling along R, respectively. These compliances can be computed from the molecule's $(3N \times 3N)$ Hessians in the reactant and TS configurations[3d] as described below. A key

departure from one-dimensional theories[4] is that the TS compliance (χ_{TS}) can be either positive or negative;[3d] as a result, both anti-Hammond ($\Delta R > 0; \Delta\chi > 0$) and Hammond ($\Delta R > 0; \Delta\chi < 0$) behavior is possible. We emphasize that the Hammond or anti-Hammond behavior is controlled by $\Delta\Delta R$, which is the shift in the reactant-to-TS distortion in response to force.

COMPUTATIONAL RESULTS AND DISCUSSION

To explore the correlation between mechanical activation and the direction along which the pulling force is exerted, we have performed a comprehensive survey of all possible pulling scenarios within the context of six previously reported mechanochemical transformations: the conrotatory electrocyclic ring opening of *cis* and *trans*-disubstituted benzocyclobutenes,[2a] the formal (3+2) cycloreversion of 1,2,3-triazoles,[2c,e] the formal [4+2] cycloreversions of a furan/maleimide Diels-Alder adduct and a maleimide/anthracene Diels-Alder adduct,[2f] and the isomerization of a spiropyran derivative[2g] (**Scheme 5.1**).

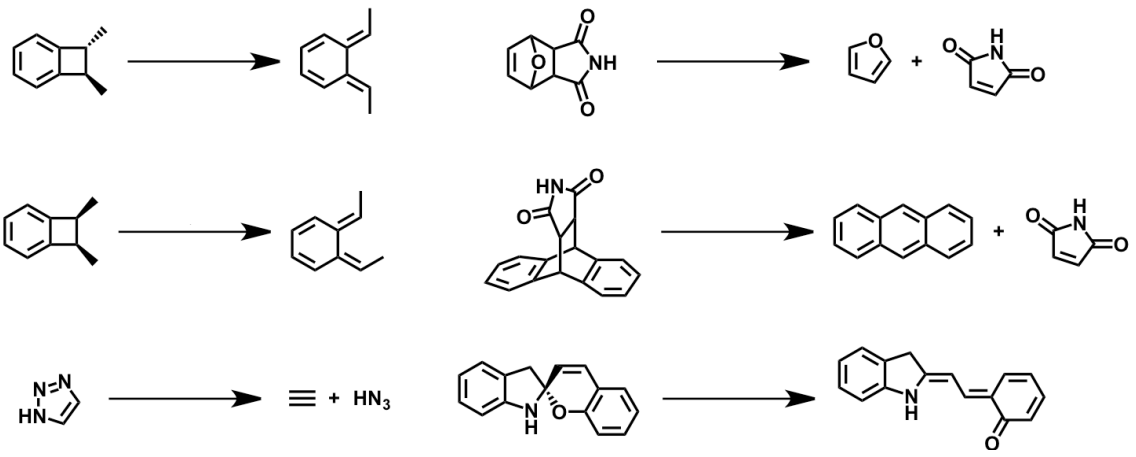

Scheme 5.1 Small molecule analogues of known mechanochemical transformations employed for computational studies

In order to probe the intrinsic reactivity of each mechanophore in the absence of strongly perturbing steric or electronic environments, we employed truncated analogues bearing only hydrogen substituents (although methyl substituents were used to account for stereochemistry when necessary). For the same reason, polymeric handles, while important,[3g,7a] were not included in the calculations. In other words, the force in Equation 5.1 is assumed to be exerted directly on a pair of atoms belonging to the mechanophore. The mechanism through which the force is transmitted to the mechanophore and its dependence on other factors (*e.g.*, experimental design or the structure of the polymer backbone attached to the mechanophore) are not considered here. Instead, we sought to demonstrate that the qualitative trends obtained from our simplified model can aid in the experimental design of new systems (even though some pulling scenarios are strictly gedankenexperiments).

EBT calculations were performed with the NWCHEM package[8] using density functional theory,[9] employing the 6-31G* basis set[10] and the B3LYP exchange-correlation energy functional.[11a] To verify the insensitivity of our results to the choice of the density functional and the basis set, we also repeated calculations using the M05-2X hybrid meta exchange-correlation functional[11b] and the 6-31++G**/6-31G* basis sets (see Appendix C for additional details). The nature of the stationary points was confirmed by a vibrational frequency analysis. In addition, each TS was confirmed by following the reaction coordinate from the TS to the reactant and the product using the intrinsic reaction coordinate (IRC) method.[12,13] The force dependence of the reaction rate was estimated using Equation 5.1, where $\Delta R = R_{TS} - R_r$ was computed from optimized reactant and TS geometries. To compute $\Delta\chi = \chi_{TS} - \chi_r$ we used the identity[3d] $\chi_{r,TS} = 2/\lambda$, where λ is the nonzero eigenvalue of the 6 x 6 matrix

$$\bar{\mathbf{h}}_{11} = \mathbf{h}_{11} - \mathbf{h}_{12}\left(\mathbf{h}_{22}\right)^{-1}\mathbf{h}_{21} \tag{5.3}$$

computed, respectively, from the reactant or TS Hessian matrix

$$\mathbf{h} = \begin{pmatrix} \mathbf{h}_{11} & \mathbf{h}_{12} \\ \mathbf{h}_{21} & \mathbf{h}_{22} \end{pmatrix} \tag{5.4}$$

In Equation 5.4, this matrix is written in block-form in terms of the 6 × 6, 6 × (3N-6), (3N-6) × 6 and (3N-6) × (3N-6) matrices $\mathbf{h}_{11}$, $\mathbf{h}_{12}$, $\mathbf{h}_{21}$, and $\mathbf{h}_{22}$, respectively.[3d] Equation 5.4 further assumes that the atoms are renumbered such that one always pulls on atoms 1 and 2. In contrast to the experimental and earlier computational studies, we evaluated all $N(N-1)/2$ possible pulling points for each mechanophore scaffold containing *N* atoms (which resulted in a total of 1456 simulated pulling experiments). Notably, the use of the EBT approximation allows one to accomplish this seemingly formidable task at modest computational expense.

We systematically determined $\Delta\chi$ (*i.e.*, $\chi_{TS} - \chi_r$) and ΔR (*i.e.*, $R_{TS} - R_r$) for each atom pair associated with the mechanophores in **Scheme 5.1**, and the corresponding results are summarized in **Figure 5.2**. Surprisingly, a comparable number of instances of reaction suppression ($\Delta R < 0$) and enhancement ($\Delta R > 0$) were observed. This finding is counterintuitive, as is apparent from the thought experiment involving the application of forces to the two atoms belonging to a diatomic molecule. Suppressing bond scission would require that the forces push the atoms toward each other; however, such an arrangement of atoms clearly leads to mechanical instability. Direct bond compression, therefore, cannot account for reaction suppression. Instead, reaction suppression must require an indirect mechanism involving the coupled distortions of multiple bonds. An idealized depiction of this suppression mechanism is given in **Figure 5.1C**, where a RC in the multidimensional configuration space diverges from the mechanical coordinate

such that the stretching force pushes the molecule away from its energetically favorable pathway.

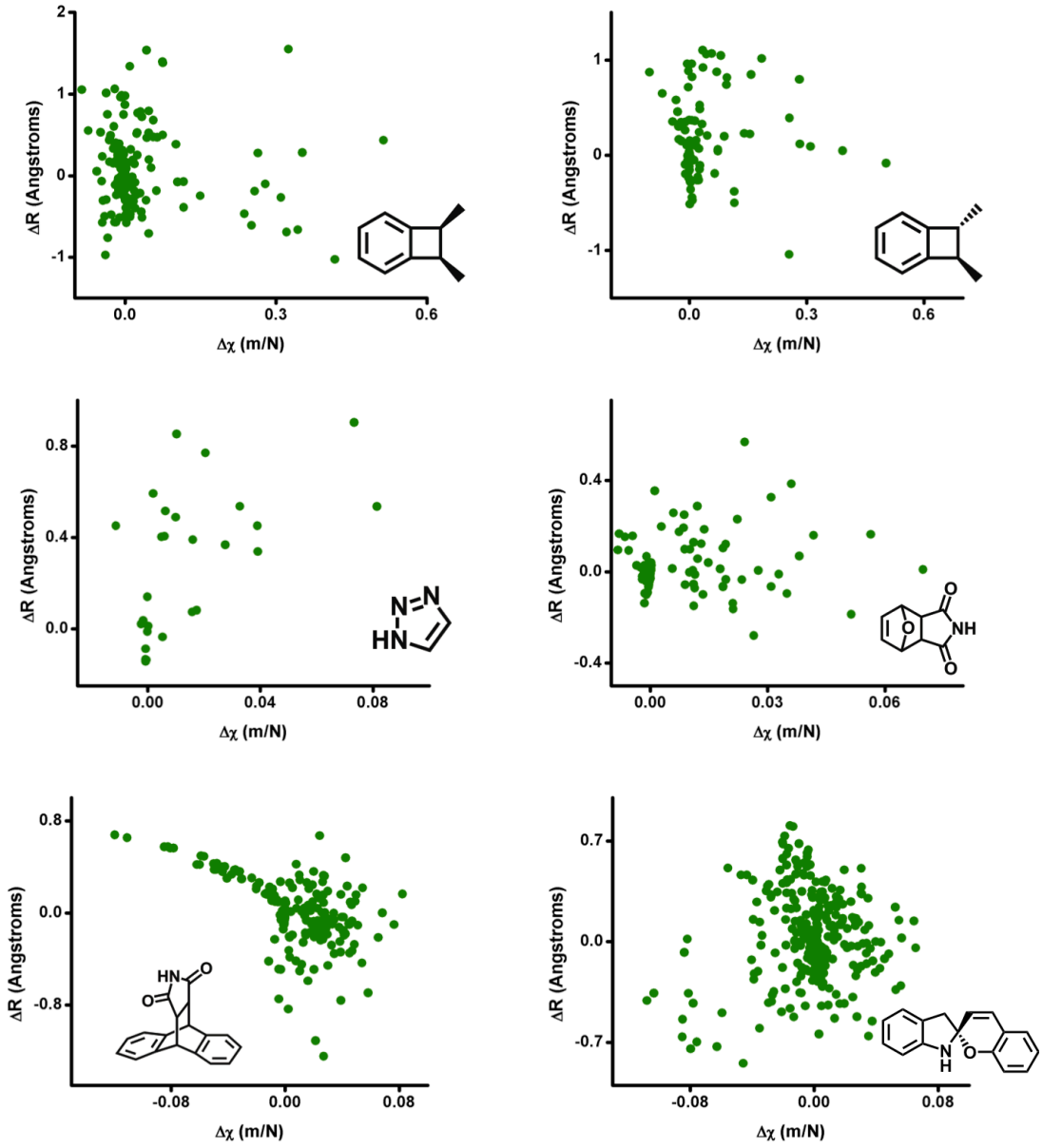

Figure 5.2 Computed values of ΔR and $\Delta\chi$ for all possible combinations of pulling points for the indicated mechanophores. Nearly all combinations result in a positive value of $\Delta\chi$; however, both signs of ΔR are present with almost equal frequency.

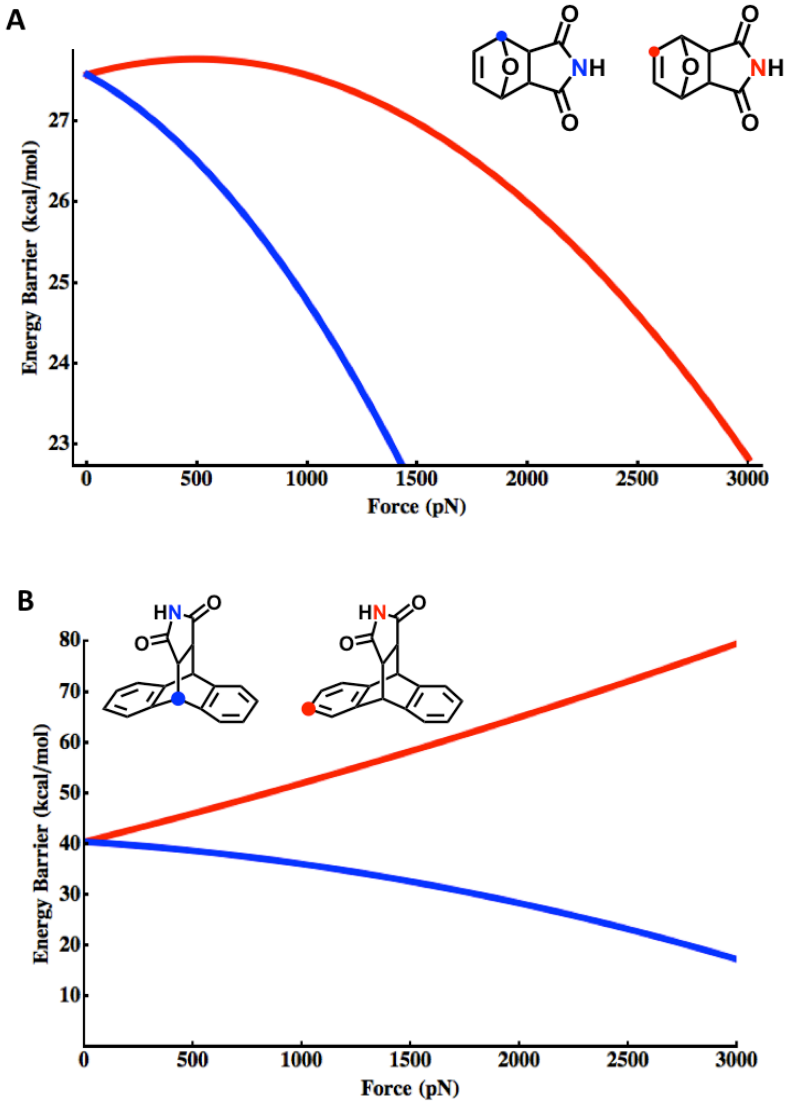

Figure 5.3 Examples of mechanically accelerated and mechanically suppressed reactivity. (A) Computed changes in the activation energy (equal to $U_{TS} - U_R - F\Delta R$, where $U_{r(TS)}$ is the reactant (or TS) energy on the force-modified potential energy surface) for the cycloreversion of a Diels-Alder adduct using pulling points for reaction acceleration (blue) and pulling points for reaction suppression (red). Note the rollover behavior: a catch bond at low forces is superseded by a slip bond at higher forces. (B) Computed changes in the activation energy for the cycloreversion of a Diels-Alder adduct using the pulling points for reaction acceleration (blue) and the pulling points for reaction suppression (red).

A similar phenomenon has been observed for the dissociation of biomolecular adhesion complexes under stress,[14] where mechanical suppression of dissociation is known as the "catch bond" or "molecular jamming" effect.[15] While theoretically predicted,[3c,3f,5] catch bonds are fairly atypical; conversely, "slip bonds", whose dissociation is promoted by force, are more common.[16] Only recently have catch bond effects (*i.e.*, the apparent strengthening of a covalent bond under mechanical stress) been implicated in mechanochemical transformations involving non-biological chemical systems. For example, Boulatov and colleagues reported the kinetic stabilization of esters toward hydrolysis under tension,[17a] and Marx *et al*. showed that certain disulfide bonds are less susceptible to nucleophilic attack under the action of mechanical force.[17b] Our results, however, suggest that catch bonds may be common in a variety of chemical transformations. A few salient examples are presented in **Figure 5.3**, which show that even a subtle change in mechanophore design may result in a switch from slip bond to catch bond behavior. Moreover, a "rollover" phenomenon similar to that predicted for biomolecular catch bonds[3f,5] can be observed (*i.e.*, a catch bond at low forces can become superseded by a slip bond at higher forces; see Appendix C for additional details). The ability to selectively suppress a chemical transformation through the application of mechanical stress could have important design implications, particularly in the context of molecular machines or force responsive materials.[18] For example, mechanical degradation of such systems could be attenuated by directing external loads to mechanically labile bonds in a manner that would suppress bond scission. Furthermore, catch bond effects could potentially be harnessed to access materials that become more mechanically robust under stress.

A separate but equally intriguing trend observed in **Figure 5.2** is the predominantly positive sign of $\Delta\chi$, which suggests the prevalence of anti-Hammond

effects in mechanically facilitated transformations. While puzzling at first glance, this result stems from the multidimensional character of the underlying PES. A negative sign for the TS compliance (χ_{TS}), which would lead to a negative $\Delta\chi$, becomes statistically unlikely for systems of high dimensionality. As shown in **Figure 5.1A**, χ_{TS} is negative only when the RC is sufficiently aligned with the mechanical coordinate *R* such that strain causes the TS energy to decrease. Since the TS configuration corresponds to a first-order saddle, there is only one normal mode along which the energy decreases; conversely, there are 3*N*-1 modes along which the energy increases (or remains constant). Thus, the probability of favorable alignment between *R* and the RC becomes vanishingly small with increasing number of atoms, *N*. If, for example, the pulling direction is a random vector in the 3*N*-dimensional space, then this probability is shown (Appendix C) to decrease exponentially with *N*, thereby rendering a negative value of χ_{TS} highly improbable (even for systems of modest size). Indeed, for all cases displayed in **Figure 5.2**, χ_{TS} was found to have a positive value (Appendix C). Note, however, that symmetry requirements may lead to perfect alignment between *R* and RC in certain pulling arrangements. Such cases would be exceptions to the trend observed here.

Of course, a positive sign for χ_{TS} does not guarantee anti-Hammond behavior, given that $\Delta\chi$ could still be negative if $\chi_{TS} < \chi_r$. This scenario, while explaining the few instances of negative $\Delta\chi$ observed in **Figure 5.2**, should be rare, considering that the TS of a reaction involving bond scission is expected to be more mechanically labile than the reactant state.

Although our findings are based on calculations that employ the EBT approximation (whose limitations have been discussed in the literature[3c,d,7b]), the above general considerations indicate that our conclusions are, in fact, not critically dependent on the underlying EBT assumptions. For example, recent studies[7a,b] highlight the effect of

the statistical-mechanical properties of the polymer backbone attached to the mechanophore on the overall mechanochemical reactivity. Thus, it would appear that multiple polymer conformations would invalidate the EBT assumption of a single TS. This situation is, however, common in condensed-phase rate theory, where the assumption of a single PES saddle is inevitably incorrect. Coarse graining is the standard way of treating this problem, where nonreactive degrees of freedom (such as those of the polymer backbone or a solvent) are integrated out of the problem; as a result, the PES becomes replaced by an effective *free* energy surface (FES).[19a] Within this framework, the EBT formula (Equation 5.1) can be derived from Kramers' type theory or its multidimensional generalization due to Langer (see, *e.g.*, Hanggi et al.[19b]), provided that the extension ΔR is replaced by the *statistically averaged* extension, and the susceptibilities χ_r and χ_{TS} are computed from the Hessian matrices of the FES.[20,5a] While the computation of a FES is a nontrivial task, the above arguments show that the anti-Hammond effect is caused not by some specific properties of the underlying PES, but simply by its inherent multi-dimensionality. As such, this argument equally applies to any multidimensional FES. In support of this coarse-grained view of mechanochemical phenomena, studies of a two-dimensional FES led to the prediction of anti-Hammond behavior in force induced protein unfolding,[5c] a finding that was ultimately supported by kinetic studies.[21]

EXPERIMENTAL METHODS AND DISCUSSION

To test the above computational results and conclusions experimentally, we have focused on a system for which mechanical forces were predicted to suppress chemical reactivity. A Diels-Alder adduct derived from a 2-substituted anthracene moiety (*c.f.* the red pulling points in **Figure 5.3B**) was selected for our study for two reasons. First, this

scaffold represented a very subtle change in mechanophore design (as compared to the originally reported system[2f]) that was predicted by our computational work to manifest drastically altered reactivity. Moreover, the predicted suppression of reactivity appeared at variance with chemical intuition and, thus, provided a genuine example of designing a mechanophore from first-principles. Second, no rollover behavior was predicted in the force dependence of the reaction rate for cycloreversion of this system (**Figure 5.3B**); thus, the predicted change in reactivity was expected to be observable under experimentally relevant conditions.

As shown in **Scheme 5.2**, the difunctional polymerization initiator **5.3** was prepared from the thermally promoted [4+2] cycloaddition between **5.1** (obtained from commercially available 2-anthracenyl methanol) and the known[22a] maleimide derivative **5.2**. Subsequent copper-mediated controlled radical polymerization[22b] of methyl acrylate from **5.3** afforded poly(methyl acrylate) (PMA) materials with varying number average molecular weights (**5.4**$_{\mathbf{Mn}}$; M_n = 16 kDa, 56 kDa, 88 kDa, and 130 kDa; see Appendix C

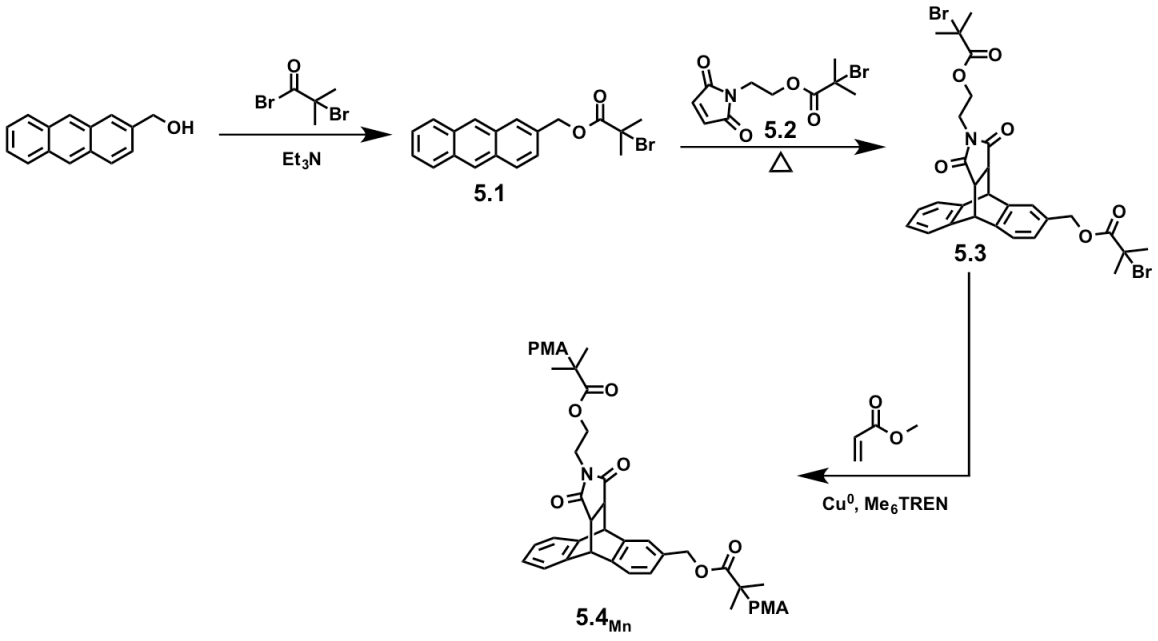

Scheme 5.2 Synthesis of a mechanophore predicted to exhibit mechanical suppression of reactivity. Me6TREN = tris[2-(dimethylamino)ethyl]amine. Et3N = triethylamine. PMA = poly(methyl acrylate).

for additional details), depending on the [methyl acrylate]$_0$/[**5.3**]$_0$. Initially, **5.4$_{88}$** (M_n = 88 kDa; PDI = 1.3) was dissolved in acetonitrile (MeCN; 10 mg ml^{-1}) and subjected to pulsed ultrasound for 5 h. Subsequent gel-permeation chromatography (GPC) revealed negligible changes in the M_n of the material isolated following ultrasonication (*c.f.* M_n = 88 kDa versus M_n = 85 kDa for the presonicated and postsonicated materials, respectively; **Figure 5.4A**). Moreover, ultraviolet-visible spectroscopy revealed no change in the material's absorbance profile following ultrasonication (**Figure 5.4B**). As a mechanically induced cycloreversion would be expected to generate anthracenyl-terminated polymer fragments,[2f] the lack of anthracene absorbances was consistent with the conclusion that mechanical forces were not effecting a formal cycloreversion of the centrally located Diels-Alder adduct within **5.4$_{88}$**.[23]

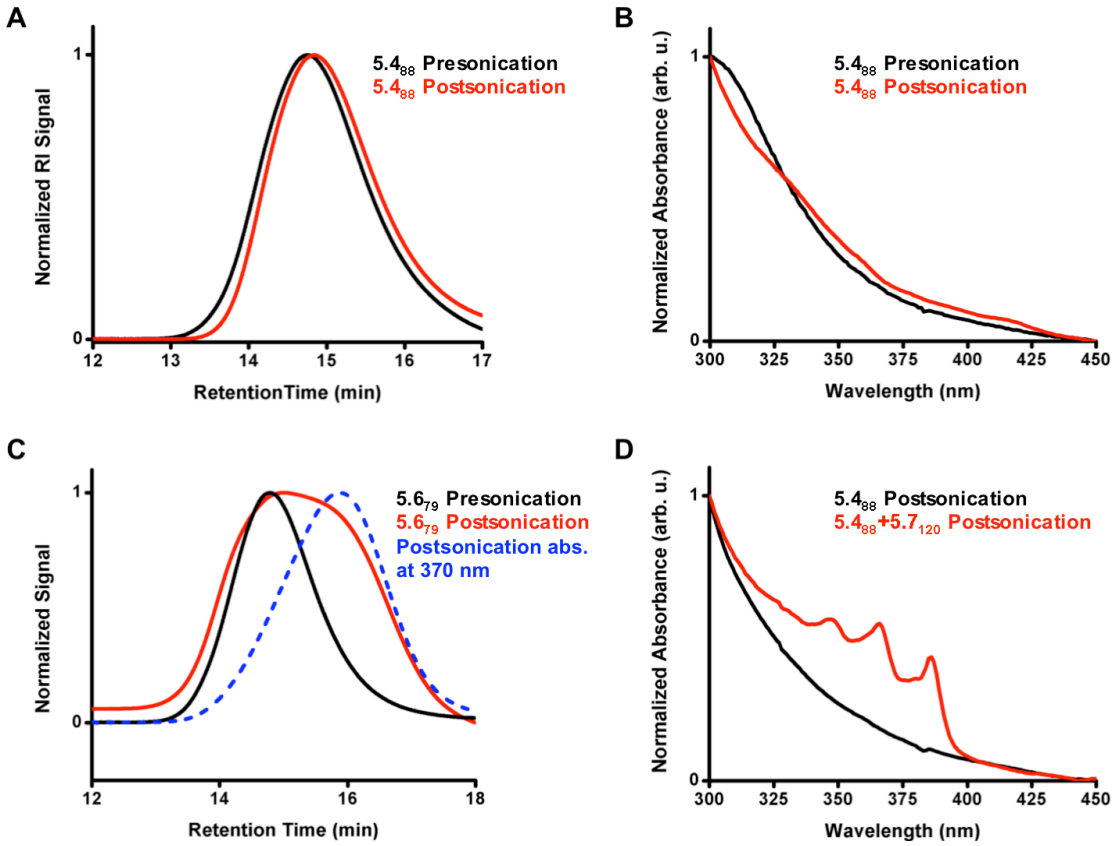

Figure 5.4 Experimental validation of mechanical reactivity suppression. (A) **5.4$_{88}$** (black) exhibited minimal chain scission following ultrasonication (red). (B) Ultraviolet-visible absorption spectrum of **5.4$_{88}$** in THF (10 mg ml-1) prior to ultrasonication (black) and following ultrasonication (red). Absorbances characteristic of anthracene were not observed. (C) **5.6$_{79}$** (*i.e.*, the material prepared *via* polymerization of methyl acrylate from an equimolar mixture of **5.3** and **5.5**; black) exhibited chain scission following ultrasonication (red); however, the bimodal distribution of molecular weights was consistent with only some of the original polymer chains undergoing scission. Ultraviolet-visible detection at 370 nm (a maximal absorbance of anthracene) indicated the generation of anthracenyl-terminated polymers in the low molecular weight region of the bimodal distribution (blue). (D) Ultraviolet-visible spectrum of **5.4$_{88}$** in THF (10 mg ml-1) following ultrasonication (black). Anthracene absorbances were not observed. **5.7$_{120}$** was added to the postsonicated material, and the resulting mixture was re-subjected to ultrasonication. The resulting material was isolated *via* precipitation from MeOH and dissolved in THF (10 mg ml-1-). Ultraviolet-visible absorption spectroscopy revealed the generation of the absorbances characteristic of anthracene (red).

Similarly, ultrasonication of all the aforementioned **5.4$_{Mn}$** polymers did not result in any detectable formation of anthracenyl-terminated polymer fragments (as determined by GPC and ultraviolet-visible spectroscopy; see Appendix C). Moreover, the rate constants associated with chain scission of the **5.4$_{Mn}$** polymers were found to be two orders of magnitude lower than those reported for polymers of similar molecular weight that contained the mechanically labile cycloadduct ($6.39 \times 10^{-5} \pm 3.42 \times 10^{-8}$ min^{-1} for **5.4$_{88}$** versus $5.2 \times 10^{-3} \pm 0.1 \times 10^{-3}$ min^{-1} for the mechanically sensitive congener embedded in a PMA with a M_n of 71 kDa; see Appendix C).[2f] Taken in combination with the lack of anthracene generation following ultrasonication, these data strongly indicated that the **5.4$_{Mn}$** polymers were resistant to mechanical activation and that the low rate constants of chain scission were due to non-specific cleavage along the polymer backbone. Collectively, these results suggested to us that mechanical forces were not inducing the formal [4+2] cycloreversion of the centrally located Diels-Alder adducts present within the **5.4$_{Mn}$** materials.

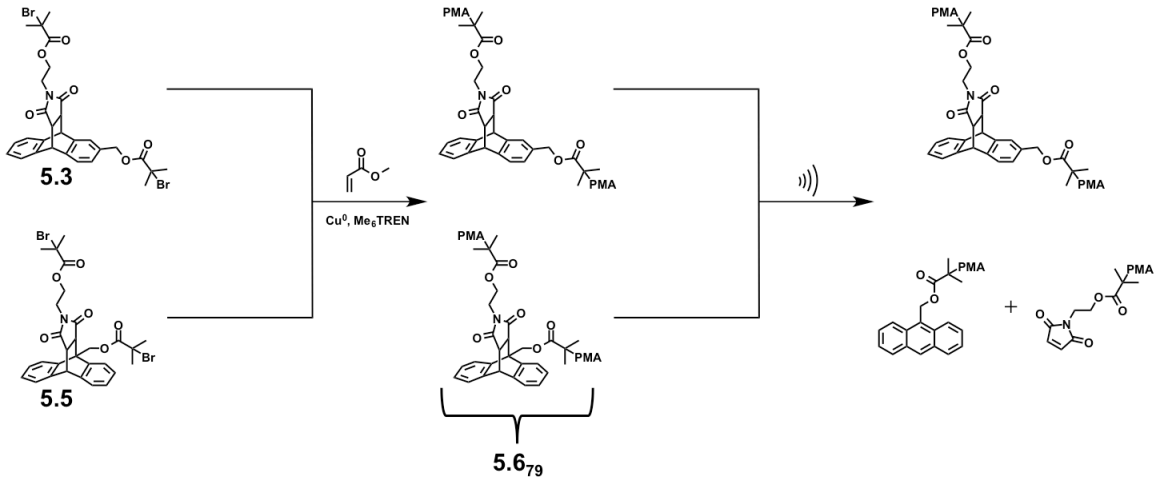

Scheme 5.3 Polymerization of methyl acrylate from an equimolar mixture of **5.3** and regioisomeric **5.5** afforded a mixture of the associated poly(methyl acrylate) materials (*i.e.*, $\mathbf{5.6_{79}}$) . PMA = poly(methyl acrylate). Ultrasonication resulted in selective [4+2] cycloreversions of the centrally located adducts derived from **5.5**.

To further demonstrate that the $\mathbf{5.4_{Mn}}$ materials were not susceptible to mechanically facilitated cycloreversion, we polymerized methyl acrylate from an equimolar mixture of **5.3** and the known[2f] mechanically responsive congener **5.5** (**Scheme 5.3**). Pouring the corresponding reaction mixture into methanol (MeOH) resulted in the precipitation of a PMA material with a M_n = 79 kDa ($\mathbf{5.6_{79}}$; PDI = 1.3). Dissolution of $\mathbf{5.6_{79}}$ in MeCN (10 mg ml^{-1}) and subsequent ultrasonication afforded a new material that was isolated *via* precipitation from MeOH and filtration. GPC analysis of the isolated material revealed a bimodal distribution wherein a low molecular weight material was present (M_n = 38 kDa; **Figure 5.4C**). Moreover, ultraviolet-visible detection at 370 nm (a λ_{max} of anthracene) revealed that only the low molecular weight component exhibited a strong absorbance at this wavelength **(Figure 5.4C**). This result, in combination with the lack of mechanical reactivity that was observed for the $\mathbf{5.4_{Mn}}$ materials, was consistent with the conclusion that polymers containing the previously reported mechanophore[2f]

(*i.e.*, those bearing polymer chains at the former 9-position of the anthracene coupling partner) were undergoing mechanical cycloreversion to afford anthracenyl-terminated polymer fragments.

To gain additional support for these mechanochemical results, we subjected $\mathbf{5.4_{88}}$ to ultrasonication for 3 h as previously described (*vide supra*) and isolated the resulting material *via* precipitation from MeOH. Next, a tetrahydrofuran solution (10 mg ml^{-1}) of the postsonicated $\mathbf{5.4_{88}}$ material was analyzed using ultraviolet-visible spectroscopy (**Figure 5.4D**). As expected, the characteristic absorbances of anthracene were not detected. Upon removal of the residual solvent, an equal mass of a polymer containing the previously reported[2f] mechanophore (M_n = 120 kDa; PDI = 1.4; $\mathbf{5.7_{120}}$) was added, and the polymer mixture was dissolved in MeCN (10 mg ml^{-1}) and subjected to ultrasonication for an additional 3 h. The resulting material was isolated by precipitation from MeOH and dissolved in THF (10 mg ml^{-1}). Ultraviolet-visible spectroscopic analysis revealed characteristic absorbances associated with anthracene (**Figure 5.4D**). As such, we reasoned that while mechanical forces were capable of inducing formal [4+2] cycloreversions in materials comprised of the previously reported[2f] mechanophore, the newly designed "mechanoresist" (*i.e.*, the mechanically inert cycloadduct in $\mathbf{5.4_{Mn}}$) did not undergo significant mechanochemical activation, despite great structural similarity between the two systems. Taken together, these results were consistent with the theoretically predicted trends for the two sets of pulling points (**Figure 5.3B**). We note, however, that a definitive experimental test of our theory would require measurement of the force dependence of the reaction rates in each case, possibly *via* single-molecule pulling studies.

CONCLUSIONS AND OUTLOOK

In sum, the computational data described herein revealed that anti-Hammond behavior should be prevalent in the mechanical perturbations of molecular energy landscapes. In addition, mechanical forces were found to be capable of facilitating or suppressing a given chemical transformation, depending on how they were applied to the chemical systems under investigation. Experimental results supported the computationally predicted reactivity trends and demonstrated that subtle changes in mechanophore design can lead to dramatic (and even counterintuitive) changes in mechanical reactivity. Moreover, the work reported here constitutes the first example of utilizing a theoretical model in the *a priori* design and development of a novel mechanically responsive system. Beyond its fundamental importance, the ability to mechanically suppress chemical reactivity is expected to find applications in materials science (*e.g.*, materials that resist mechanical degradation under stress) and could have implications for mechanically induced biochemical phenomena.[20]

ACKNOWLEDGEMENTS

J.N.B. is grateful to the National Science Foundation for a predoctoral fellowship. Contributions to the content of this chapter from S.S.M.K, B.T.V, and D.E.M. are gratefully acknowledged. Computational resources were provided by the Texas Advanced Computing Center.

REFERENCES AND NOTES

1 (a) Caruso, M. M.; Davis, D. A.; Shen, Q.; Odom, S. A.; Sottos, N. R.; White, S. R.; Moore, J. S. *Chem. Rev.* **2009**, *109*, 5755. (b) Black, A. L.; Lenhardt, J. M.; Craig, S. L. *J. Mater. Chem.* **2011**, *21*, 1655. (c) Brantley, J. N.; Wiggins, K. M.; Bielawski, C. W. *Polym. Int.* **2012**, *62*, 2.

2 (a) Hickenboth, C. R.; Moore, J. S.; White, S. R.; Sottos, N. R.; Baudry, J.; Wilson, S. R. *Nature* **2007**, *446*, 423. (b) Lenhardt, J. M.; Ong, M. T.; Choe, R.; Evenhuis, C. R.; Martinez, T. J.; Craig, S. L. *Science* **2010**, *329*, 1057. (c)

Brantley, J. N.; Wiggins, K. M.; Bielawski, C. W. *Science* **2011**, *333*, 1606. (d) Wiggins, K. M.; Bielawski, C. W. *Angew. Chem. Int. Ed.* **2012**, *51*, 1640. (e) Brantley, J. N.; Konda, S. S. M.; Makarov, D. E.; Bielawski, C. W. *J. Am. Chem. Soc.* **2012**, *134*, 9882. (f) Wiggins, K. M.; Syrett, J. A.; Haddleton, D. M.; Bielawski, C. W. *J. Am. Chem. Soc.* **2011**, *133*, 7180. (g) Davis, D. A.; Hamilton, A.; Yang, J.; Cremar, L. D.; Van, G. D.; Potisek, S. L.; Ong, M. T.; Braun, P. V.; Martinez, T. J.; White, S. R.; Moore, J. S.; Sottos, N. R. *Nature* **2009**, *459*, 68.

3 (a) Boulatov, R.; Kucharski, T. J. *J. Mater. Chem.* **2011**, *21*, 8237. (b) Ribas-Arino, J.; Shiga, M.; Marx, D. *Angew. Chem. Int. Ed.* **2009**, *48*, 4190. (c) Bailey, A.; Mosey, N. J. *J. Chem. Phys.* **2012**, *136*, 044102/1. (d) Konda, S. S. M.; Brantley, J. N.; Bielawski, C. W.; Makarov, D. E. *J. Chem. Phys.* **2011**, *135*, 164101. (e) Huang, Z.; Boulatov, R. *Pure App. Chem.* **2010**, *82*, 931. (f) Dopieralski, P.; Anjukandi, P.; Ruckert, M.; Shiga, M.; Ribas-Arino, J.; Marx, D. *J. Mater. Chem.* **2011**, *21*, 8309. (g) Ribas-Arino, J.; Marx, D. *Chem. Rev.* **2012**, *112*, 5412. (h) Kryger, M. J.; Munaretto, A. M.; Moore, J. S. *J. Am. Chem. Soc.* **2011**, *133*, 18992. (i) Franco, I.; Schatz, G. C.; Ratner, M. A. *J. Chem. Phys.* **2009**, *131*, 124902.

4 (a) Bell, G. I. *Science* **1978**, *200*, 618. (b) Evans, E.; Ritchie, K. *Biophys. J.* **1997**, *72*, 1541. (c) Zhurkov, S. N. *Int. J. Frac. Mec.* **1965**, *1*, 311.

5 (a) Suzuki, Y.; Dudko, O. K. *Phys. Rev. Lett.* **2010**, *104*, 048101. (b) Suzuki, Y.; Dudko, O. K. *J. Chem. Phys.* **2011**, *134*, 065102. (c) Dudko, O. K.; Graham, T. G.; Best, R, B. *Phys. Rev. Lett.* **2011**, *107*, 208301.

6 Hyeon, C.; Thirumalai, D. *Biophys. J.* **2006**, *90*, 3410.

7 (a) Tian, Y.; Boulatov, R. *ChemPhysChem* **2012,** *13*, 2277. (b) Tian, Y.; Boulatov, R. *Chem. Commun.* **2013**, *49*, 4187.

8 Valiev, M.; Bylaska, E. J.; Govind, N.; Kowalski, K.; Straatsma, T. P.; Van Dam, H. J. J.; Wang, D.; Nieplocha, J.; Apra, E.; Windus, T. L.; de Jong, W. A. *Comput. Phys. Commun.* **2010**, *181*, 1477.

9 Parr, R. G. and Yang, W. *Density-Functional Theory of Atoms and Molecules*; Oxford University Press: New York, 1989.

10 Gordon, M. S.; Binkley, J. S.; Pople, J. A.; Pietro, I. W. J.; Hehre, W. J. *J. Am. Chem. Soc.* **1982**, *104*, 2797.

11 (a) Becke, A. D. *J. Chem. Phys.* **1993**, *98*, 1372. (b) Zhao, Y.; Schultz, N.; Truhlar, D. G. *J. Chem. Theory Comput.* **2006**, *2*, 364.

12 Gonzalez, C.; Schlegel, H. B. *J. Chem. Phys.* **1989**, *90*, 2154.

13 Gonzalez, C.; Schlegel, H. B. *J. Phys. Chem.* **1990**, *94*, 5523.

14 Marshall, B. T.; Long, M.; Piper, J. W.; Yago, T.; McEver, R. P.; Zhu, C. *Nature* **2003**, *423*, 190.

15 (a) Barsegov, V.; Thirumalai, D. *Proc. Natl Acad. Sci. USA* **2005**, *102*, 1835. (b) Prezhdo, O. V.; Pereverzev, Y. V. *Acc. Chem. Res.* **2009**, *42*, 693.

16 Li, H.; Cao, Y. *Acc. Chem. Res.* **2010**, *43*, 1331.

17 (a) Akbulatov; S.Tian, Y.; Kapustin, E.; Boulatov, R. *Angew. Chem. Intl. Ed.* **2013**, *52*, 6992. (b) Dopieralski, P.; Ribas-Arino, J.; Anjukandi, P.; Krupicka, M.; Kiss, J.; Marx, D. *Nat. Chem.* **2013**, *5*, 685.

18 Browne, W. R.; Feringa, B. L. *Nat. Nano.* **2006**, *1*, 1748.

19 (a) Voth, G. A.; Hochstrasser, R. M. *J. Phys. Chem.* **1996**, *100*, 13034. (b) Hanggi, P.; Talkner, P.; Borkovec, M. *Rev. Mod. Phys.* **1990**, *62*, 251.

20 Makarov, D. E. In *Single-molecule Studies of Proteins*; Oberhauser, A. F. Ed.; Springer, New York, 2013.

21 Jagannathan, B.; Elms, P. J.; Bustamante, C.; Marqusee, S. *Proc. Natl Acad. Sci. USA* **2012**, *109*, 17820.

22 (a) Mantovani, G.; Lecolley, F.; Tao, L.; Haddleton, D. M.; Clerx, J.; Cornelissen, J. J. L. M.; Velonia, K. *J. Am. Chem. Soc.* **2004**, *127*, 2966. (b) Percec, V.; Guliashvili, T.; Ladislaw, J. S.; Wistrand, A.; Stjerndahl, A.; Sienkowska, M. J.; Monteiro, M. J.; Sahoo, S. *J. Am. Chem. Soc.* **2006**, *128*, 14156-14165.

23 Anthracene was not observed after heating a 10 mg mL-1 solution of $\mathbf{5.4}_{\mathbf{88}}$ to 130 ºC for 19 h.

Chapter 6: Modulating the Photophysical Properties of Fluorescent Proteins Using Mechanical Stimuli

INTRODUCTION[6]

Polymer mechanochemistry[1–4] is a rapidly growing field of study wherein mechanical energy is harnessed to drive useful chemical transformations,[5–11] many of which are otherwise inaccessible. Apart from their fundamental interest, mechanochemical phenomena can be applied toward the development of novel stress-sensing materials with the capacity to quantitatively (or qualitatively) report damage. Salient examples of mechanically facilitated transformations that have been exploited within such materials include the electrocyclic ring opening of spiropyran derivatives,[12–14] formal [4+2] cycloreversions of anthracene derived Diels-Alder adducts,[15,16] and formal [2+2] cycloreversions of 1,2-dioxetanes.[17] Collectively, these systems report stress either through mechanochromism[12–14] or mechanoluminscence,[16,17] which enables quantification of mechanical damage using standard optical spectroscopies. Unfortunately, such stimulus responsive materials typically require tedious chemical syntheses; consequently, tuning their mechanochemical reactivity (*e.g.*, through chemical diversification of mechanically labile scaffolds) can present a significant impediment to the development of new force-responsive sensors.

Recently, attention has been directed toward harnessing the biosynthetic machinery of living organisms to access mechanically sensitive biomolecules (*i.e.*, "biomechanophores").[18] While nature is replete with examples of force-responsive

---

[6] Portions of this chapter and the corresponding appendix were reproduced from: Brantley, J. N.; Bailey, C. B.; Cannon, J. R.; Clark, K. A.; Vanden Bout, D. A.; Brodbelt, J. S.; Keatinge-Clay, A. T.; Bielawski, C. W. *Angew. Chem. Int. Ed.* **2014**, *In Press*. DOI: 10.1002/anie.201306988. JNB and CBB prepared and tested the protein composites. JRC and JSB performed the mass spectrometry studies. KAC and DAVB assisted with fluorescence microscopy. ATKC and CWB helped design and evaluate the experimental results. All authors contributed to the writing of the original text and figure preparation.

systems,[19] there is a relative dearth of reports wherein biomolecules are used for mechanochemical applications. Indeed, although the modulation of enzymatic activity through mechanical stress has been reported,[20–23] few efforts have been directed toward developing biomechanophores that report mechanical stress through optical output. We envisioned that polymeric materials containing fluorescent proteins could serve as useful classes of stress-sensing biocomposites. Fluorescent proteins,[24] which are ubiquitous within the purview of the biochemical sciences, can be modified *via* site-selective mutagenesis[25] to precisely alter their structural and photophysical properties. Additionally, fluorescent proteins have been extensively optimized to achieve high stability and high levels of recombinant overexpression.

The photophysical properties of the canonical fluorescent protein, green fluorescent protein (GFP), stem from a 4-(*p*-hydroxybenzylidene)imidazolidin-5-one chromophore located in the center of the protein's β-barrel structure.[24] Genetic mutations that alter the structure of the chromophore (as in the case of cyan fluorescent protein or blue fluorescent protein) or local residues that impact the stereoelectronic environment surrounding the chromophore (as in the case of yellow fluorescent protein) give rise to a vibrant array of proteins with unique emissive properties.[24] The fluorescence of all photoemissive protein variants is highly dependent on proper folding of the protein;[24,26,27] as such, mechanical perturbation of the β-barrel structure results in modulation of any associated photophysical properties.[28–30] Yellow fluorescent protein (YFP) is particularly attractive for use as a biomechanophore, as the yellow fluorescence results from a weak arene interaction between the chromophore and tyrosine 203 (mutated from threonine in the parent GFP).[26] Gruner and colleagues reported that pressurized crystals of the YFP variant, citrine, exhibited a gradual hypsochromic shift in fluorescence as the pressure was increased from 0 to 360 MPa at low temperatures (77 K).[31,32] The fluorescence was

subsequently found to bathochromically shift upon reducing the pressure and warming the crystals to 180 K. While this work clearly revealed the potential to develop YFP as a mechanosensor, there have been no reports to date wherein an analogous modulation of YFP fluorescence was harnessed for applications in mechanically responsive materials. In addition, surprisingly few efforts have been directed toward developing stress-sensing materials that employ fluorescent proteins. For example, Clark and colleagues utilized Förster resonance energy transfer (FRET) between YFP and cyan fluorescent protein (CFP) to develop stress reporting poly(acrylamide) composites.[33,34] Stretching these materials under uniaxial strain resulted in increased FRET interactions between YFP and CFP near micro-cracks that formed within the material, as determined by fluorescence confocal microscopy and fluorescence lifetime imaging (FLIM).[34] Bruns and colleagues more recently reported that eYFP could serve as a mechanically sensitive link between glass substrates and epoxy resins, where delamination of the resin resulted in denaturation of the protein and subsequent fluorescence quenching.[35] While these examples elegantly demonstrated that fluorescent proteins could be adapted for applications in stress reporting, there have been no reports showcasing diverse and tunable mechanochemical responses from biocomposite materials containing fluorescent proteins, which are features that are expected to be valuable for the design of precisely tailored force-sensing materials. Here, we report the facile preparation of biocomposite materials containing either: 1) an enhanced YFP (eYFP[36]) that exhibits shifts in λ_{em} under mechanical stress, or 2) a genetically modified GFP (GFPuv[37,38]) that exhibits fluorescence quenching under the action of mechanical force.

MECHANICAL ACTIVATION OF POLYMER COMPOSITES CONTAINING EYFP

As eYFP was predicted to exhibit greater mechanical sensitivity than GFPuv,[29] our initial efforts were directed toward the development of eYFP-containing biocomposites. We reasoned that embedding eYFP within a polymeric matrix and subjecting the resulting material to bulk compression would elicit the desired photophysical modulation, as local areas of high pressure generated during material compression could disrupt the arene interaction responsible for yellow fluorescence *via* subtle distortions of the protein's structure (**Scheme 6.1**).

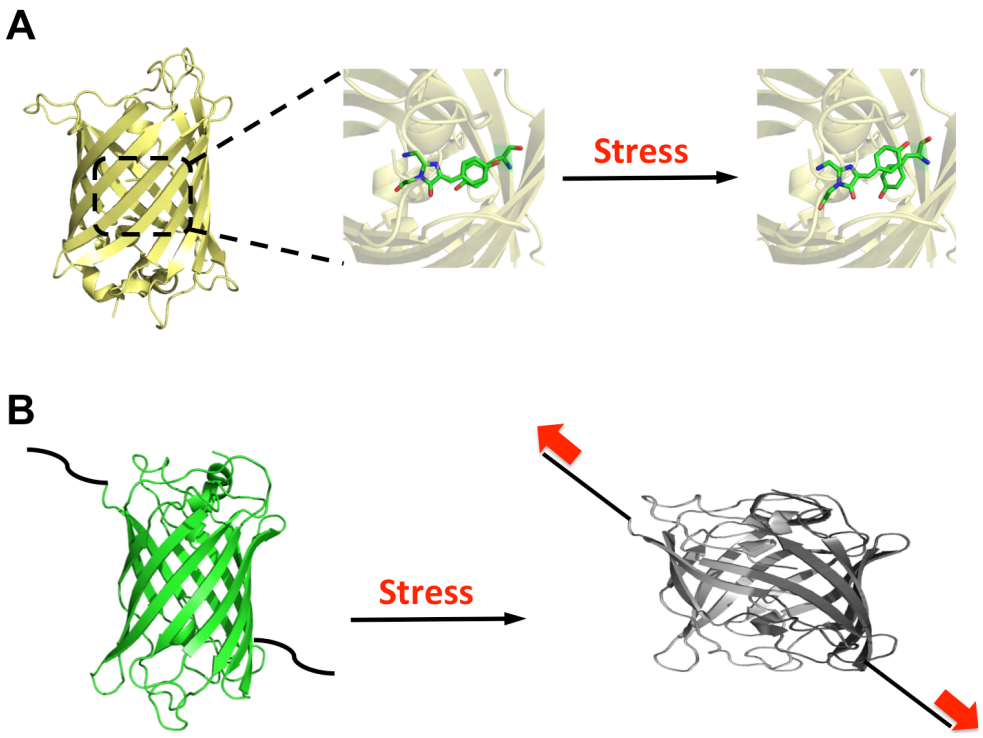

Scheme 6.1 Schematic representations of proposed mechanical activations of fluorescent proteins. (A) Compression of composite materials containing eYFP distorts the arene interaction between the chromophore and tyrosine 203. (B) The incorporation of cysteine residues at strategic sites in GFPuv facilitates the covalent attachment of polymer chains to the protein; subsequent compression of the composite mechanically denatures GFPuv and quenches the protein's fluorescence.

To test the aforementioned hypothesis, we overexpressed hexahistidine-tagged eYFP in *E. coli* BL21 (DE3) and subsequently purified the isolated protein by nickel affinity chromatography. As shown in **Scheme 6.2**, poly(methyl methacrylate) (PMMA) composites were prepared by adding eYFP (**6.1**) directly to a mixture of methyl methacrylate (**6.2**), azobisisobutyronitrile (AIBN, **6.3**), and the plasticizer, 1-butyl-3-methylimidazolium hexafluorophosphate (BMIM-PF_6, **6.4**), at 40 °C (see Appendix D for additional details). The stability of eYFP under these relatively harsh conditions was remarkable, and the composite materials isolated following consumption of the free monomer exhibited strong fluorescence (λ_{ex} = 485 nm; λ_{em} = 540 nm; Φ = 0.64) and relatively uniform protein distribution. Although significant denaturation of eYFP was observed upon dissolution of the isolated biocomposites in tetrahydrofuran (as evidenced by fluorescence quenching), this obstacle to material processing was circumvented by cutting and polishing the composites to afford specimens with defined geometries. The BMIM-PF_6 additive, which is known to serve as a highly effective plasticizer of acrylate derived polymers,[39] allowed precise modulation of the physical properties exhibited by the composites. Specifically, the addition of BMIM-PF_6 enabled the glass transition (T_g) of PMMA to be reduced to approximately 40 °C (as determined by differential scanning calorimetry), which was found to be beneficial for sample processing.

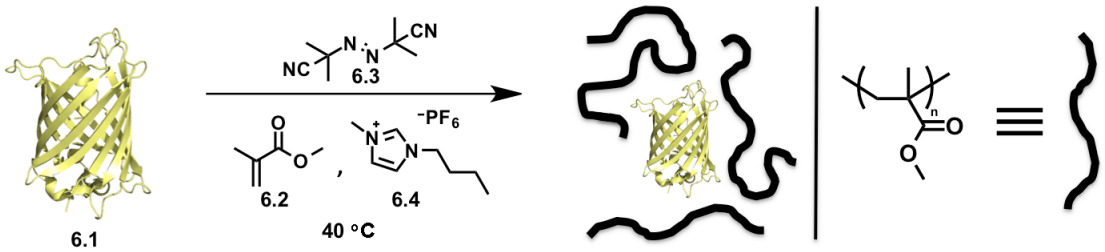

Scheme 6.2 Synthesis of eYFP-containing biocomposites. General conditions: eYFP (**6.1**; 1.0 equiv), MMA (**6.2**; 2.6 x 10^5 equiv), AIBN (**6.3**; 1.3 x 10^3 equiv), and BMIM-PF_6 (**6.4**; 3.1 x 10^4 equiv) were combined in a single vessel under N_2 and heated to 40 °C.

To test the mechanical sensitivity of our composite materials, a 50 mg sample was mounted in a hydraulic press and subjected to compression at incrementally increasing pressures (0 – 360 MPa) for periods of 45 s, after which time the solid-state fluorescence was measured. As shown in **Figure 6.1** (left), the λ_{em} of the sample gradually shifted from 539 nm at 0 MPa to approximately 534 nm at 360 MPa (a hypsochromic shift commensurate with that previously reported by Gruner[32]). Frictional heating during compression appeared to contribute to the overall response of the material through thermal denaturation of the protein (as evidenced by a reduction in fluorescence intensity; see Appendix D for additional details). Importantly, though, the observed change in λ_{em} correlated monotonically with the applied force and was, thus, consistent with a mechanical process.[1-4] Compressing the composites for 1 h did not cause their λ_{em} to shift beyond what was measured after compression for 45 s at the same pressure. Collectively, these data suggested to us that mechanical forces generated upon compressing the composites were inducing subtle distortions of the protein's chromophore.

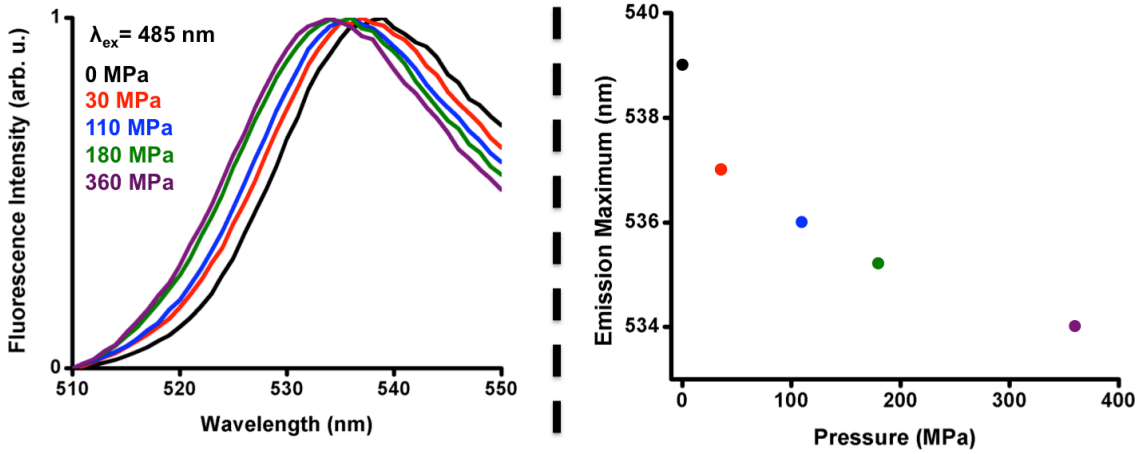

Figure 6.1 (Left) Compression of PMMA composites containing eYFP caused the λ_{em} to gradually undergo a hypsochromic shift. Normalized fluorescence intensities are shown. (Right) The fluorescence maxima of the compressed PMMA composite containing eYFP plotted as a function of applied pressure.

MECHANICAL ACTIVATION OF POLYMER COMPOSITES CONTAINING GFPUV

Having established a straightforward preparation of ratiometric stress sensors, we sought to explore the mechanochromism of another fluorescent protein to realize an intensiometric stress reporter. Such reporters are particularly valuable because, when stressed, they exhibit changes in their optical properties that facilitate rapid assessment of mechanical damage. As mechanical unfolding of GFP has previously been shown to quench the protein's fluorescence,[28] efforts were directed toward expanding the results of these atomic force microscope (AFM) pulling experiments to bulk materials. While the mechanical response of eYFP presumably resulted from the distortion of a weak, local interaction, we reasoned that modulation of GFP's photophysical properties would involve more global phenomena (*i.e.*, complete denaturing of the protein); thus, we surmised that direct translation of force to the ptotien would be required to induce mechanical denaturation. As such, we hypothesized that GFP would need to be

chemically cross-linked to the polymer matrix to sufficiently harness the mechanical forces generated during compression to achieve the desired fluorescence quenching. Guided by the work of Dietz, Rief, and Lorimer,[28] which revealed that the *N*-terminal β-sheet in GFP is mechanically labile, we concluded that polymeric appendages should be introduced on opposing sides of the aforementioned β-sheet in order to direct mechanical forces to this putative "Achilles' heel" (*i.e.*, the most mechanically labile structural element within the protein). The strategic incorporation of cysteine residues within the polypeptide backbone was predicted to facilitate the desired polymer ligation, as Bowman and Cramer have shown that thiyl radicals (which can be generated from thiols under free radical polymerization conditions) react efficiently with propagating acrylate radicals (provided the initial thiol concentration is relatively low).[40]

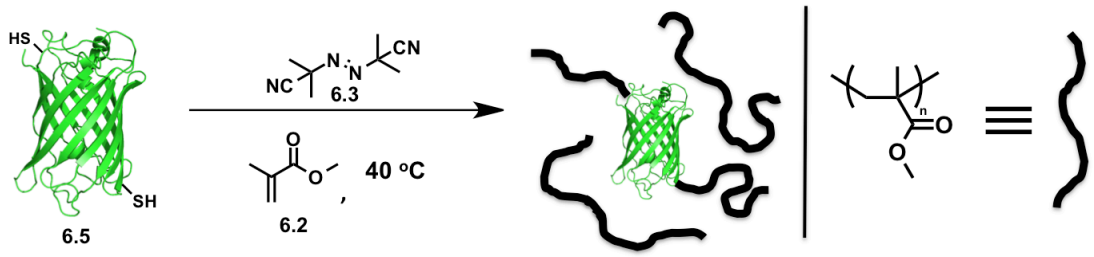

Scheme 6.3 Synthesis of mechanically active GFPuv-containing biocomposites. General conditions: GFPuv(Y39C/D103C) (**6.5**; 1.0 equiv), MMA (**6.2**; 2.6 x 10^5 equiv), and AIBN (**6.3**; 1.3 x 10^3 equiv) were combined in a single vessel under N_2 and heated to 40 °C.

Site-directed mutagenesis was performed to incorporate cysteine residues on opposing sides of the β-barrel (replacing tyrosine 39 and aspartate 103) in GFPuv, as the attachment of polymer chains at these sites could direct mechanical forces to the aforementioned β-sheet and induce mechanical denaturation (and, consequently, fluorescence quenching). GFPuv was selected due to its high stability in bacterial

expression systems and its stronger fluorescence signal than wild-type GFP.[37,38] The resultant hexahistidine-tagged GFPuv(Y39C/D103C) double mutant was overexpressed in *E.* coli BL21 (DE3) and purified by nickel affinity chromatography. As shown in **Scheme 6.3**, PMMA composites were prepared by polymerizing methyl methacrylate (**6.2**) in the presence of GFPuv(Y39C/D103C) (**6.5**; see Appendix D for additional details). Gel-permeation chromatography (GPC) visualized with ultraviolet-visible detection at 280 nm (a λ_{max} of tyrosine) revealed that the resulting polymeric material displayed an increased absorbance at this wavelength relative to a PMMA homopolymer that was prepared in the absence of GFPuv(Y39C/D103C) at the same concentration (see Appendix D for additional details). Moreover, mass spectrometry studies revealed that GFPuv(Y39C/D103C) was coupled to methyl methacrylate under the polymerization conditions, which confirmed that the cysteine residues were solvent exposed. Taken together, these results were consistent with the covalent attachment of GFPuv(Y39C/D103C) to the growing polymer chains during the preparation of the aforementioned composites. As shown in **Figure 6.2**, the solid-state fluorescence of the composites (λ_{em} = 507 nm; λ_{ex} = 420 nm) was in agreement with the successful incorporation of GFPuv(Y39C/D103C) into the polymeric matrix. Compression of these materials in a hydraulic press (41 MPa; 45 s) resulted in a significant reduction in fluorescence intensity (**Figure 6.2A**). Moreover, the fluorescence intensity was found to decrease monotonically with increasing pressure (0 – 41 MPa), which is a hallmark of mechanical phenomena (**Figure 6.2A**).[1-4] Compression of the materials for 1 h did not cause their fluorescence intensity to change beyond what was measured after 45 s at the same pressure. As such, these results suggested to us that mechanical forces were indeed denaturing the GFPuv(Y39C/D103C) upon compression of the composites (**Scheme 6.1**).

To further demonstrate the mechanical origin of the observed activity, we also explored the mechanophoricity of the Y39C and D103C single mutants, wherein only one attachment site was present on the surface of the protein. Presumably, these mutants would function in a manner analogous to semi-telechelic derivatives of chemical mechanophores (*i.e.*, the mutants would not exhibit the same modulation in fluorescence as the Y39C/D103C double mutant).[1–4] Overexpression in *E. coli* and subsequent purification *via* nickel affinity chromatography afforded the desired semi-telechelic biomechanophores, which were subsequently added to the polymerization of poly(methyl methacrylate) as described above. As shown in **Figure 6.2**, compression of the resulting composites did not significantly alter their photophysical properties. Similarly, compression of composites containing unmodified GFPuv did not result in modulation of their associated photophysical properties. Moreover, analysis using mass spectrometry confirmed that unmodified GFPuv was not coupled to methyl methacrylate under the reported polymerization conditions (see Appendix D for additional details). Collectively, these data supported the conclusion that mechanical forces were responsible for the observed fluorescence modulation in the GFPuv(Y39C/D103C)-containing composites.

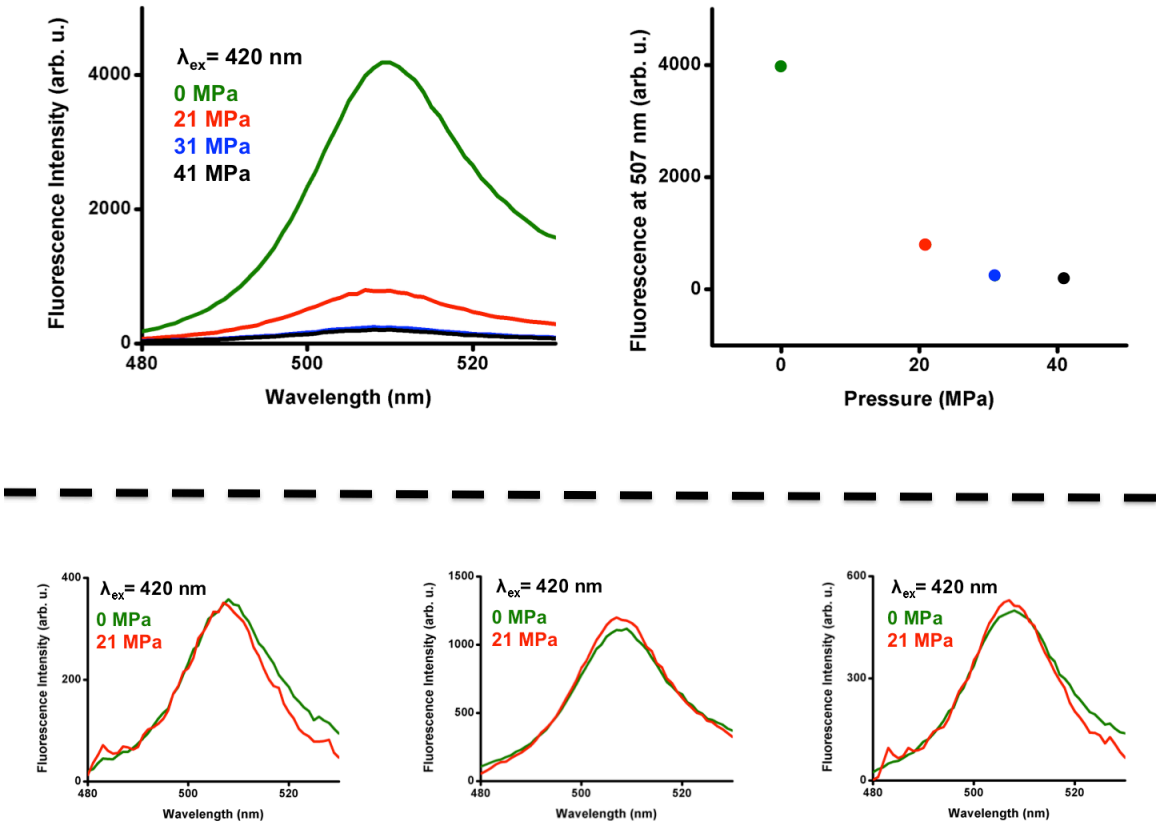

Figure 6.2 (Top) Compressing PMMA composites (0 – 41 MPa) containing double mutant GFPuv(Y39C/D103C) resulted in a monotonic decrease in the fluorescence intensity of the material. The fluorescence intensities at λ_{em} = 507 nm are plotted for clarity. (Bottom) Compression of PMMA composites containing GFPuv (left), GFPuv(Y39C) (center), or GFPuv(D103C) (right) did not significantly alter the fluorescence intensities of the materials.

CONCLUSIONS AND OUTLOOK

In summary, we have demonstrated that mechanical forces may be used to modulate the photophysical properties of fluorescent proteins embedded within polymeric matrices. Our work constitutes the first example of modulating the λ_{em} of eYFP-containing polymer composite materials through the action of mechanical forces, as well as the first example of mechanically modulating the photophysical properties of GFPuv in a bulk material. Moreover, we have shown that mechanical perturbation of

various fluorescent proteins alters their photophysical properties in distinct and tunable manners (*i.e.*, the reported systems exhibited either ratiometric or intensiometric responses to mechanical stress). The ability to precisely manipulate the optical output of composite materials containing biomechanophores through targeted mutations could afford new opportunities for the facile development of stress-responsive materials with tailored sensitivities. Moreover, we have demonstrated that single-molecule experiments can guide the rational design of biomechanophores, and insight garnered from mechanochemical studies involving chemical systems can be translated to those involving force-sensitive biomolecules. Indeed, the technical simplicity associated with preparing the mechanically responsive biocomposites described herein holds promise for their development and utility as new classes of force responsive materials.

ACKNOWLEDGEMENTS

J.N.B. is grateful to the National Science Foundation for a predoctoral fellowship. Contributions to the content of this chapter from C.B.B., J.R.C., K.A.C., D.A.V.B., J.S.B., and A.T.K.-C. are gratefully acknowledged. We thank professors Eric Gouaux and Arthur Glasfeld for generously providing the pNGFP-BC plasmid, and professor Andrew Ellington for providing the EYFP-pET21a expression plasmid.

REFERENCES

1 Brantley, J. N.; Wiggins, K. M.; Bielawski, C. W. *Polym. Int.* **2013**, *62*, 2.

2 Wiggins, K. M.; Brantley, J. N.; Bielawski, C. W. *Chem. Soc. Rev.* **2013**, *42*, 7130.

3 Caruso, M. M.; Davis, D. A.; Shen, Q.; Odom, S. A.; Sottos, N. R.; White, S. R.; Moore, J. S. *Chem. Rev.* **2009**, *109*, 5755.

4 Black, A. L.; Lenhardt, J. M.; Craig, S. L. *J. Mater. Chem.* **2011**, *21*,1655.

5 Brantley, J. N.; Wiggins, K. M.; Bielawski, C. W. *Science* **2011**, *333*, 1606.

6 Hickenboth, C. R.; Moore, J. S.; White, S. R.; Sottos, N. R.; Baudry, J.; Wilson, S. R. *Nature* **2007**, *446*, 423.

7 Lenhardt, J. M.; Ong, M. T.; Choe, R.; Evenhuis, C. R.; Martinez, T. J.; Craig, S. L. *Science* **2010**, *329*, 1057.

8 Baytekin, H. T.; Baytekin, B.; Grzybowski, B. A. *Angew. Chem. Int. Ed.* **2012**, *124*, 3656.

9 Diesendruck, C. E.; Steinberg, B. D.; Sugai, N.; Silberstein, M. N.; Sottos, N. R.; White, S. R.; Braun, P. V.; Moore, J. S. *J. Am. Chem. Soc.* **2012**, *134*, 12446.

10 Groote, R.; van Haandel, L.; Sijbesma, R. P. *J. Polym. Sci. Part A Polym. Chem.* **2012**, *50*, 4929.

11 Kean, Z. S.; Black Ramirez A. L.; Craig, S. L. *J. Polym. Sci. B. Polym. Phys.* **2012**, *50*, 3481.

12 Davis, D. A.; Hamilton, A.; Yang, J.; Cremar, L. D.; Van Gough, D.; Potisek, S. L.; Ong, M. T.; Braun, P. V.; Martínez, T. J.; White, S. R.; Moore, J. S.; Sottos, N. R. *Nature* **2009**, *459*, 68.

13 Kingsbury, C. M.; May, P. A.; Davis, D. A.; White S. R.; Moore, J. S.; Sottos, N. R.; *J. Mater. Chem.* **2011**, *21*, 8381.

14 Beiermann, B. A.; Davis, D. A.; Kramer, S. L. B.; Moore, J. S.; Sottos, N. R.; White, S. R. *J. Mater. Chem.* **2011**, *21*, 8443.

15 Wiggins, K. M.; Syrett, J. A.; Haddleton, D. M.; Bielawski, C. W. *J. Am. Chem. Soc.* **2011**, *133*, 7180.

16 Song, Y. K.; Lee, K. H.; Hong, W. S.; Cho, S. Y.; Yu, H. C.; Chung, C. M. *J. Mater. Chem.* **2012**, *22*, 1380.

17 Chen, Y.; Spiering, A. J. H.; Karthikeyan, S.; Peters, G. W. M.; Meijer, E. W.; Sijbesma, R. P. *Nat. Chem.* **2012**, *4*, 559.

18 Brantley, J. N.; Bailey, C. B.; Wiggins, K. M.; Keatinge-Clay, A. T.; Bielawski, C. W. *Polym. Chem.* **2013**, *4*, 3916.

19 Bustamante, C.; Chemla, Y. R.; Forde, N. R.; Izhaky, D. *Annu. Rev. Biochem.* **2004**, *73*, 705.

20 Klibanov, A.; Samokhin, G.; Martinek, K.; Berezin, I. V. *Biochim. Biophys. Acta* **1976**, *438*, 1.

21 Berezin, I. V.; Klibanov, A. M.; Martinek, K. **1974**, *364*, 193.

22 Choi, B.; Zocchi, G.; Wu, Y.; Chan, S.; Jeanne Perry, L. *Phys. Rev. Lett.* **2005**, *95*, 078102.

23 Saghatelian, A.; Guckian, K. M.; Thayer, D. A.; Ghadiri, M. R. *J. Am. Chem. Soc.* **2003**, *125*, 344.

24 Tsien, R. Y. *Annu. Rev. Biochem.* **1998**, *67*, 509.

25 Sawano, A. *Nucleic Acids Res.* **2000**, *28*, 78e.

26 Niwa, H.; Inouye, S. *Proc. Natl. Acad. Sci. USA* **1996**, *93*, 13617.

27 Ward, W. W.; Cody, C. W.; Hart, R. C.; Cormier, M. J. *Photochem. Photobiol.* **1980**, *31*, 611.

28 Dietz, H.; Rief, M.; Lorimer, G. H. **2004**, *101*, 16192.

29 Perez-Jimenez, R.; Garcia-Manyes, S.; Ainavarapu, S. R. K.; Fernandez, J. M. *J. Biol. Chem.* **2006**, *281*, 40010.

30 Helms, V.; Straatsma, T. P.; McCammon, J. A. *J. Phys. Chem. B* **1999**, *103*, 3263.

31 Barstow, B.; Ando, N.; Kim, C. U.; Gruner, S. M. *Biophys. J.* **2009**, *97*, 1719.

32 Barstow, B.; Ando, N.; Kim, C. U.; Gruner, S. M. *Proc. Natl. Acad. Sci. USA* **2008**, *105*, 13362.

33 Bruns, N.; Clark, D. *Chimia*. **2010**, *65*, 245.

34 Bruns, N.; Pustelny, K.; Bergeron, L. M.; Whitehead, T. A.; Clark, D. S. *Angew. Chem. Int. Ed.* **2009**, *48*, 5666.

35 Makyła, K.; Müller, C.; Lörcher, S.; Winkler, T.; Nussbaumer, M. G.; Eder, M.; Bruns, N. *Adv. Mater.* **2013**, *25*, 2701.

36 Nagai, T.; Ibata, K.; Park, E. S.; Kubota, M.; Mikoshiba, K.; Miyawaki, A. *Nat. Biotechnol.* **2002**, *20*, 87.

37 Kawate, T.; Gouaux, E. *Structure* **2006**, *14*, 673.

38 Crameri, A.; Whitehorn, E. A.; Tate, E.; Stemmer, W. P. *Nat. Biotechnol.* **1996**, *14*, 315.

39 Zhao, L.; Li, Y.; Cao, X.; You, J.; Dong, W. *Nanotechnology* **2012**, *23*, 255702.

40 Cramer, N. B.; Bowman, C. N. *J. Polym. Sci. Part A Polym. Chem.* **2001**, *39*, 3311.

Appendix A

General Experimental Considerations

The following compounds were prepared according to literature procedures: 2-azidoethanol,[1] 3-butynyl-2,2-dimethylpropanoate,[2] 2-azidoethyl-2-bromo-2-methylpropanoate,[3] 1-azidopyrene,[4] 1,3-dimesitylnapthoquinimidazolylidene (**NQMes**),[5] and 3-azido-propane-1,2-diol.[6] All other reagents and solvents were obtained from commercial sources and used without further purification. Unless otherwise noted, solvents were dried over 3 Å molecular sieves or Al_2O_3 and deoxygenated (via a Q5 catalyst) using a Vacuum Atmospheres Company solvent purification system, and then subsequently stored over molecular sieves (3 Å). ^{1}H and ^{13}C NMR data were collected on Varian Unity INOVA 400 MHz spectrometer. Chemical shifts (δ) are reported in ppm and referenced downfield from $(CH_3)_4Si$ using the residual solvent peak as an internal standard ($CDCl_3$: 7.26 ppm for ^{1}H and 77.16 ppm for ^{13}C NMR; DMSO-d_6: 2.50 ppm for ^{1}H NMR; C_6D_6: 7.16 ppm for ^{1}H and 128.06 ppm for ^{13}C NMR). ^{31}P NMR data were acquired on Varian Oxford 600 MHz spectrometer and externally referenced to phosphoric acid (δ = 0 ppm). UV-vis spectra were recorded using a Perkin Elmer Instruments Lambda 35 spectrometer. High-resolution mass spectra (HRMS) were obtained by electrospray ionization (ESI) with a VG analytical ZAB2-E instrument. IR spectra were recorded using either a Perkin-Elmer Spectrum BX FT-IR system (in KBr matrices or in solutions of tetrahydrofuran) or a Thermo Scientific Nicolet iS5 spectrometer equipped with an iD3 attenuated total reflectance (ATR; Ge crystal). Elemental analyses were performed at Midwest Microlab, LLC (Indianapolis, IN). Melting points were obtained on a Melt-temp apparatus and are uncorrected.

MACROMOLECULAR CHARACTERIZATION

Gel permeation chromatography (GPC) was performed using tetrahydrofuran as the eluent on either a Viscotek system equipped with a VE 1122 pump, a VE 7510 degasser, two fluorinated polystyrene columns (I-MBHW-3078 and I-MBLMW-3078) thermostated to 30 °C (using a ELDEX CH 150 column heater) and arranged in series, a Viscotek 270 Dual Detector (light scattering detector and differential viscometer), and a VE 3580 refractive index detector or at room temperature on a home-built gel permeation chromatograph equipped with a Waters Model 510 HPLC pump, two fluorinated polystyrene columns (IMBHW-3078 and I-MBLMW-3078) arranged in series, and a Waters 486 Tunable Absorbance Detector. Molecular weight and polydispersity data are reported relative to polystyrene standards.

GENERAL SONICATION CONSIDERATIONS

The sonication experiments were performed under an atmosphere of argon using a Sonics & Materials VC-505 Liquid Cell Ultrasonic processor operating at 20 kHz equipped with a 12.8 mm replaceable tip titanium probe. Custom Suslick cells[7] were fabricated in house. An argon line was threaded through a septum attached to a cell's side arm and placed in solution, ensuring no contact with the probe. Argon was then bubbled through the solution for 30 min prior to and continuously during each experiment performed. The cell was placed in an ice bath, which was sufficient to maintain a temperature of 6–9 °C, as determined by using a thermocouple placed directly into the solution. Pulsed ultrasound was applied (1.0 s on and 1.0 s off) at 23% power (power intensity = 9.7 W cm^{-2}) for each experiment performed.

SYNTHESES AND CHARACTERIZATION DATA

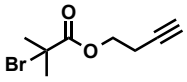

3-butynyl-2-bromo-2-methylpropanoate. A 50 mL flask was charged with 3-butyn-1-ol (0.35 mL, 4.6 mmol) and methylene chloride (10 mL, dried over molecular sieves), and then placed in an ice bath. The resulting solution was degassed by sparging with nitrogen, and the reaction vessel was sealed under an atmosphere of nitrogen. Triethylamine (0.77 mL, 5.5 mmol) was added via syringe, and the reaction mixture was stirred for 10 min. Following the slow addition of 2-bromoisobutryl bromide (0.63 mL, 5.0 mmol) via syringe, the resulting mixture was allowed to warm to room temperature with stirring. After 19 h, the reaction mixture was washed with a saturated sodium bicarbonate solution (3 × 10 mL) and water (2 × 10 mL). The organic fraction was separated, dried over anhydrous sodium sulfate, and evaporated under reduced pressure to afford 0.76 g (76% yield) of the desired product as a pale yellow liquid. ^{1}H NMR ($CDCl_3$, 400.27 MHz): 4.28-4.24 (t, ^{3}J = 6.8 Hz, 2H), 2.59-2.55 (td, ^{3}J = 3.3 Hz, 2H), 2.00-1.99 (t, ^{3}J = 2.8, 1H), 1.93 (s, 6H). ^{13}C NMR ($CDCl_3$, 75.47 MHz): 171.52, 79.55, 70.20, 63.47, 55.59, 30.79, 18.77. IR (ATR): 3295.23, 2975.19, 1735.92, 1463.96, 1390.62, 1971.52, 1273.45, 1160.65, 1109.56, 1012.04. HRMS: $[MNa]^+$ calcd. for $C_8H_{12}BrO_2Na$: 248.0899. Found: 248.0894. Anal. Calcd. for $C_8H_{11}BrO_2$: C, 43.86; H, 5.06. Found: C, 43.89; H, 5.11.

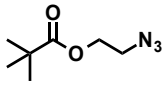

2-azidoethyl-2,2-dimethylpropanoate. A 50 mL flask was charged with 2-azidoethanol (0.40 g, 4.59 mmol) and ethyl acetate (25 mL, dried over molecular sieves), and then placed in an ice bath. The resulting solution was degassed by sparging with nitrogen, and the reaction vessel was sealed under an atmosphere of nitrogen. Triethylamine (0.80 mL, 5.73 mmol) was added via syringe, and the reaction

mixture was stirred for 10 min. Following the slow addition of 2,2-dimethylpropionyl chloride (0.63 mL, 5.12 mmol) via syringe, the resulting mixture was allowed to warm to room temperature. After 19 h, the reaction mixture was filtered over neutral alumina. The filter cake was washed with ethyl acetate (3 × 10 mL), and the filtrate was concentrated under reduced pressure to afford 0.60 g (76% yield) of the desired product as a pale yellow liquid. ^{1}H NMR ($CDCl_3$, 400.27 MHz): 4.22-4.19 (t, ^{3}J = 5.2, 2H), 3.41-3.44 (t, ^{3}J = 4.8, 2H), 1.20 (s, 9H). ^{13}C NMR ($CDCl_3$, 75.47 MHz): 178.18, 63.18, 49.84, 38.70, 26.99. IR (KBr pellet): 3448.24, 2979.65, 2107.92, 1810.34, 1732.99, 1481.81, 1284.33, 1152.31, 1044.36, 1007.88. HRMS: $[M]^+$ calcd. for $C_7H_{14}N_3O_2$: 172.1086. Found: 172.1085. Anal. Calcd. for $C_7H_{13}N_3O_2$: C, 49.11; H, 7.65; N, 24.54. Found: C, 49.15; H, 7.68; N, 24.19.

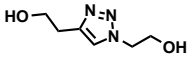

2,2'-(1H-1,2,3-triazole-1,4-diyl)diethanol (2.1). A 25 mL flask was charged with 2-azidoethanol (0.10 g, 1.15 mmol), 3-butyn-1-ol (0.10 g, 1.43 mmol), and CH_3CN (10 mL). After degassing the resulting solution by sparging with nitrogen, copper (I) iodide (0.01 g, 0.05 mmol) was added under a cone of nitrogen. The reaction vessel was then sealed under an atmosphere of nitrogen, and the reaction mixture was allowed to stir at room temperature for 19 h. After filtering the solution over Celite, the filter cake was washed with ethyl acetate (3 × 10 mL) and the filtrate was concentrated under reduced pressure to afford 0.13 g (72% yield) of the desired product as a colorless oil. Spectroscopic data were in accord with literature values.[8]

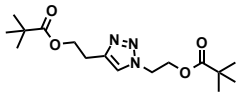

2,2'-(1H-1,2,3-triazole-1,4-diyl)diethyl pivalate (2.4). A 25 mL flask was charged with 2-azidoethyl-2,2-dimethylpropanoate (0.10 g, 0.58 mmol), 3-

butynyl-2,2-dimethyl-propanoate (0.10 g, 0.65 mmol), and CH_3CN (10 mL). After degassing the resulting solution by sparging with nitrogen, copper (I) iodide (0.01 g, 0.05 mmol) was added under a cone of nitrogen. The reaction vessel was then sealed under nitrogen and the reaction mixture was stirred for 19 h at room temperature. After filtering the resulting mixture over Celite, the filter cake was washed with ethyl acetate (3 × 10 mL), and the filtrate was concentrated under reduced pressure to afford 0.12 g (65% yield) of the desired product as a yellow oil. ^{1}H NMR ($CDCl_3$, 400MHz): 7.44 (s, 1H), 4.62-4.67 (m, 2H), 4.42-4.46 (m, 2H), 4.31-4.34 (m, 2H), 3.12-3.1.6 (m, 2H), 1.16 (s, 18 H). ^{13}C NMR ($CDCl_3$, 75.47 MHz): 178.32, 177.90, 144.48, 121.79, 63.08, 62.37, 49.03, 38.67, 27.13, 27.04, 26.48, 25.51. IR (ATR): 2972.10, 1724.97, 1479.93, 1398.75, 1366.33, 1284.74, 1229.15, 1146.69, 1058.13, 1035.85. HRMS $[M]^+$ calcd. for $C_{16}H_{28}N_3O_4$: 326.2080. Found: 326.2082. Anal. Calcd. for $C_{16}H_{27}N_3O_4$: C, 59.06; H, 8.36; N, 12.91. Found: C, 58.97; H, 8.25; N, 12.65.

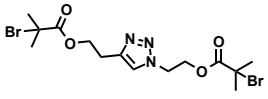

2,2'-(1H-1,2,3-triazole-1,4-diyl)diethyl-2-bromo-2-methylpropanoate (2.2). A 25 mL flask was charged with **2.1** (0.20 g, 1.3 mmol) and ethyl acetate (10 mL, dried over molecular sieves), and then placed in an ice bath. The resulting solution was degassed by sparging with nitrogen, and the reaction vessel was sealed under an atmosphere of nitrogen. Triethylamine (0.39 mL, 2.8 mmol) was added via syringe, and the reaction mixture was stirred for 10 min. Following the slow addition of 2-bromoisobutryl bromide (0.33 mL, 2.7 mmol) via syringe, the resulting mixture was allowed to warm to room temperature. After stirring for 19 h, the reaction mixture was filtered over neutral alumina. The filter cake was washed with ethyl acetate (3 × 10 mL), and the filtrate was concentrated under reduced pressure to afford 0.29 g (50% yield) of

the desired product as a yellow oil. ^{1}H NMR ($CDCl_3$, 400.27 MHz): 7.62 (s, 1H), 4.66-4.64 (t, ^{3}J = 5.0 Hz, 2H), 4.56-4.53 (t, ^{3}J = 5.2 Hz, 2H), 4.44-4.34 (t, ^{3}J = 6.6 Hz, 2H), 3.14-3.11 (t, ^{3}J = 6.6 Hz, 2H). 1.90 (s, 6H), 1.89 (s, 6H). ^{13}C NMR ($CDCl_3$, 75.47 MHz): 171.47, 171.13, 144.17, 122.65, 64.75, 63.93, 55.97, 55.21, 58.79, 30.77, 30.64, 25.27. IR (ATR): 2974.50, 1721.96, 1479.98, 1399.87, 1368.63, 1278.03, 1150.89, 1060.43, 1038.08. HRMS: $[M]^+$ calcd. for $C_{14}H_{22}Br_2N_3O_4$: 453.9977. Found: 453.9979. Anal. Calcd. for $C_{14}H_{21}Br_2N_3O_4$: C, 36.94; H, 4.65; N, 9.23. Found: C, 37.13; H, 4.58; N, 9.00

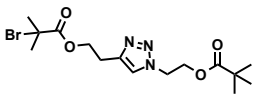

2-(4-(2-(2-bromo-2-methylpropanoyloxy)ethyl)-1H-1,2,3-triazol-1-yl)ethyl pivalate (2.5). A 25 mL flask was charged with 2-azidoethyl-2,2-dimethylpropanoate (0.07 g, 0.41 mmol), 3-butynyl-2-bromo-2-methylpropanoate (0.10 g, 0.46 mmol), and CH_3CN (10 mL). The resulting solution was degassed by sparging with nitrogen, and copper (I) iodide (0.01 g, 0.05 mmol) was added under a cone of nitrogen. After sealing the reaction vessel under nitrogen, the reaction mixture was allowed to stir for 19 h at room temperature. The resulting solution was filtered over Celite and the filter cake was washed with ethyl acetate (3 × 10 mL). The filtrate was subsequently concentrated under reduced pressure to afford 0.10 g (63% yield) of the desired product as a yellow oil. ^{1}H NMR ($CDCl_3$, 400.27 MHz): 7.51 (s, 1H), 4.61 – 4.59 (t, ^{3}J = 3.6, 2H), 4.45- 4.42 (t, ^{3}J = 6.4, 4H), 3.14 – 3.12 (t, ^{3}J = 6.4, 2H), 1.91 (s, 6H), 1.15 (s, 9H). ^{13}C NMR ($CDCl_3$, 400.27 MHz): 178.06, 171.57, 144.21, 122.36, 64.88, 62.50, 55.99, 49.21, 38.85, 30.86, 27.21, 25.38. IR (KBr Pellet): 2973.06, 1732.90, 1463.42, 1282.48, 1225.03, 1161.71, 1110.67, 1047.909, 1012.86. HRMS: $[MH]^+$ calcd. for $C_{15}H_{25}BrN_3O_4$: 390.1026. Found: 390.1026. Anal. Calcd. for $C_{15}H_{24}BrN_3O_4$: C, 46.16; H, 6.20; N, 10.70. Found: C, 46.16; H, 5.94; N, 10.31.

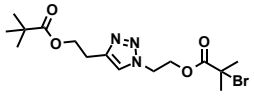

2-(1-(2-(2-bromo-2-methylpropanoyloxy)ethyl)-1H-1,2,3-triazol-4-yl)ethyl pivalate (2.6). A 25 mL flask was charged with 2-azidoethyl-2-bromo-2-methylpropanoate (0.13 g, 0.83 mmol), 3-butynyl-2,2-dimethylpropanoate (0.08 g, 0.91 mmol), and CH_3CN (10 mL). The resulting solution was degassed by sparging with nitrogen, and copper (I) iodide (0.01 g, 0.05 mmol) was added under a cone of nitrogen. After sealing the reaction vessel under at atmosphere of nitrogen, the reaction mixture was allowed to stir for 19 h at room temperature. The resulting solution was filtered over Celite and the filter cake was washed with ethyl acetate (3 × 10 mL). The filtrate was subsequently concentrated under reduced pressure to afford 0.12 g (58% yield) of the desired product as a yellow oil. ^{1}H NMR ($CDCl_3$, 400.27 MHz): 7.53 (s, 1H), 4.67-4.64 (t, ^3J = 5.2 Hz, 2H), 4.57-4.55 (t, ^3J = 4.8 Hz, 2H), 4.35-4.31 (t, ^3J = 6.8 Hz, 2H), 3.10-3.07 (t, ^3J = 6.8 Hz, 2H), 1.90 (s, 6H), 1.17 (s, 9H).). ^{13}C NMR ($CDCl_3$, 75.47 MHz): 178.36, 171.14, 122.53, 63.52, 63.10, 55.22, 48.92, 38.74, 30.64, 27.23, 25.60. IR (ATR): 2980.14, 1719.70, 1457.15, 1368.90, 1284.15, 1228.97, 1148.29, 1057.82, 1035.76. HRMS: $[M]^+$ calcd. for $C_{15}H_{25}BrN_3O_4$: 390.1026. Found: 390.1025. Anal. Calcd. for $C_{15}H_{24}BrN_3O_4$: C, 46.16; H, 6.20; N, 10.70. Found: C, 46.14; H, 5.94; N, 10.31.

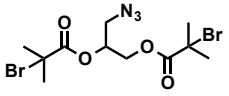

3-azidopropane-1,2-diylbis(2-bromo-2-methyl propanoate) (2.7). A 25 mL flask was charged with 3-azido-propane-1,2-diol (0.10 g, 0.85 mmol) and ethyl acetate (10 mL, dried over molecular sieves), and then placed in an ice bath. The resulting solution was degassed by sparging with nitrogen, and the reaction vessel was sealed under an atmosphere of nitrogen. Triethylamine (0.24 mL, 1.7 mmol)

was added via syringe, and the reaction mixture was stirred for 10 min. Following the slow addition of 2-bromoisobutryl bromide (0.33 mL, 2.7 mmol) via syringe, the resulting mixture was allowed to warm to room temperature. After stirring for 19 h, the reaction mixture was filtered over neutral alumina. The filter cake was washed with ethyl acetate (3 × 10 mL), and the filtrate was concentrated under reduced pressure to afford 0.30 g (86% yield) of the desired product as a colorless liquid. ^{1}H NMR ($CDCl_3$, 400.27 MHz): 5.21-5.17 (m, 1H), 4.42-4.40 (dd, *J* = 7.9, 1H), 4.31-4.22 (m, 1H), 4.19-4.18 (d, *J* = 3.9, 1H), 3.44-3.34 (m, 1H), 1.90-1.87 (m, 12H). ^{13}C NMR ($CDCl_3$, 400.27 MHz): 170.82, 71.27, 63.24, 55.02, 50.29, 30.39. IR (ATR): 2979.64, 2253.87, 2106.61, 1740.05, 1463.42, 1389.64, 1372.74, 1267.96, 1153.81, 1108.21, 1015.34, 906.33. HRMS: $[MNa]^+$ calcd. for $C_{11}H_{17}Br_2N_3O_4Na$: 435.94780. Found: 435.9480. Anal. Calcd. for $C_{11}H_{17}Br_2N_3O_4$: C, 31.83; H, 4.13; N, 10.12. Found: C, 32.02; H, 4.27; N, 10.24.

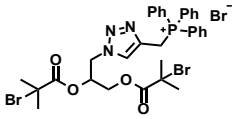

((1-(2,2-bis(2-bromo-2-methylpropanoyloxy)ethyl)-1H-1,2,3-triazol-4-yl)methyl) triphenylphosphonium bromide (2.8). A 25 mL flask was charged with **2.7** (0.10 g, 0.87 mmol), propargyl triphenylphosphonium bromide (0.33 g, 0.87 mmol), and CH_3CN (10 mL). The resulting solution was degassed by sparging with nitrogen, and copper (I) iodide (0.01 g, 0.05 mmol) was added under a cone of nitrogen. After sealing the reaction vessel under nitrogen, the reaction mixture was allowed to stir for 19 h at 70 °C. The resulting solution was diluted with $CHCl_3$ (20 mL) to precipitate excess propargyl triphenylphosphonium bromide. The resulting mixture was filtered over Celite and the filter cake was washed with $CHCl_3$ (3 × 10 mL). The filtrate was subsequently concentrated under reduced pressure to afford 0.42 g (62% yield) of the desired product as a brown oil. ^{1}H NMR ($CDCl_3$, 400.27 MHz): 7.69-7.54 (m, 15H),

6.81-6.76 (m, 1H), 5.37-5.28 (q, J = 11.9, 1H), 5.15-5.09 (m, 1H), 4.41-4.37 (dd, J = 7.94, 1H), 4.28-4.20 (m, 1H), 4.17-4.10 (m, 1H), 3.40-3.28 (m, 1H), 1.83-1.80 (m, 12H). ^{13}C NMR ($CDCl_3$, 400.27 MHz): 170.68, 135.32, 133.58, 130.54, 117.80, 116.89, 80.98, 71.15, 63.10, 55.04, 50.22, 30.29. IR (ATR): 3853.58, 3744.26, 2105.85, 1959.80, 1738.41, 1463.23, 1439.07, 1389.76, 1373.04, 1269.47, 1155.99, 1111.43, 1045.35, 997.88, 907.04, 853.83, 830.99, 796.11, 767.10. HRMS: $[MCH_2]^+$ calcd. for $C_{32}H_{35}Br_2N_3O_4P$: 714.07264. Found: 714.0729. Anal. Calcd. for $C_{32}H_{35}Br_3N_3O_4P{\cdot}9H_2O$: C, 40.10; H, 4.19; N, 4.38. Found: C, 39.98; H, 3.80; N, 4.65.

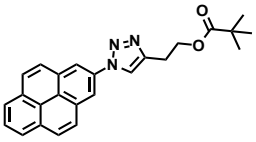

2-(1-(pyren-1-yl)-1H-1,2,3-triazol-4-yl)ethyl pivalate (2.9). A 25 mL flask was charged with 3-butynyl-2,2-dimethylpropanoate (0.06 g, 0.38 mmol), 1-azidopyrene (0.10 g, 0.41 mmol), and CH_3CN (10 mL). The resulting solution was degassed by sparging with nitrogen, and copper (I) iodide (0.01 g, 0.05 mmol) was added under a cone of nitrogen. After sealing the reaction vessel under nitrogen, the reaction mixture was allowed to stir for 19 h at room temperature. The resulting solution was filtered over Celite and the filter cake was washed with ethyl acetate (3 × 10 mL). The filtrate was subsequently concentrated under reduced pressure to afford 0.10 g (67% yield) of the desired product as a purple solid (m.p. 113-116 °C). ^{1}H NMR ($CDCl_3$, 400.27 MHz): 8.29-7.97 (m, 9H), 7.87 (s, 1H), 4.52-4.49 (t, ^3J = 6.6 Hz, 2H), 3.31-3.28 (t, ^3J = 6.4, 2H), 1.20 (s, 9H). ^{13}C NMR ($CDCl_3$, 75.47 MHz): 180.01, 145.54, 136.54, 131.86, 131.76, 130.97, 128.94, 128. 23, 127.65, 126.43, 126.12, 125.23, 125.32, 124.45, 122.32, 120.43, 119.5, 115.67, 63.18, 63.54, 35.67, 26.89, 25.23, 24.56. IR (ATR): 2970.23, 2917.69, 1726.15, 1599.28, 1459.94, 1435.50, 1397.30, 1324.67, 1286.01,

1153.75, 1041.18, 842.78, 830.48, 713.55. HRMS: $[M]^+$ calcd. for $C_{25}H_{24}N_3O_2$: 397.4690. Found: 397.4688. Anal. Calcd. for $C_{25}H_{23}N_3O_2$: C, 75.54; H, 5.83; N, 10.57. Found: C, 75.67; H, 5.91; N, 10.67.

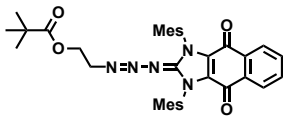

2-((1,3-dimesityl-4,9-dioxo-1H-naphtho[2,3-d]imidazol-2(3H,4H,9H)-ylidene)triaz-1-enyl)ethyl-2-bromo-2-methylpropanoate (2.10). In a glovebox, a 20 mL vial was charged with 2-azidoethyl-2-bromo-2-methylpropanoate (5.0 mg, 0.02 mmol) and tetrahydrofuran (5 mL). Afterward, **NQMes** (6.0 mg, 0.015 mmol) was added and the vial sealed with a Teflon lined cap. After stirring the reaction mixture at room temperature for 20 min, the solvent was removed under reduced pressure to obtain a purple solid. The crude product was found to decompose over time and characterized without further purification. ^{1}H NMR (C_6D_6, 400.27 MHz): 7.83 – 7.80 (m, 2H), 6.93 – 6.90 (m, 2H), 6.79 (s, 4H), 4.00 – 3.97 (t, ^3J = 8.0, 2H), 3.31 – 3.27 (t, ^3J = 8.0, 2H), 2.17 (s, 6H), 2.15 (s, 12H), 1.65 (s, 6H). ^{13}C NMR (C_6D_6, 400.27 MHz): 171.09, 138.93, 135.49, 133.57, 132.06, 129.34, 126.19, 64.50, 64.08, 60.07, 56.17, 55.49, 49.35, 30.73, 30.68, 30.53, 27.50, 21.20, 18.18. IR (tetrahydrofuran): 2359.16, 2103.42, 1739.49, 1666.11, 1597.63, 1573.29, 1428.00, 1418.69, 1266.69, 1229.53, 1163.78. HRMS: $[M+H]^+$ calcd. for $C_{35}H_{37}BrN_5O_4$: 670.2023. Found: 670.2023.

Representative Procedure for Preparation of 2.3_{Mn} (M_n = 140, 96, 63, 36): Synthesis of 2.3_{96}. A 10 mL Schlenk flask was charged with a stir bar wrapped with copper wire, **2.2** (8.4 mg, 0.02 mmol), methyl acrylate (2.0 mL, 22.2 mmol), tris[2-(dimethylamino)ethyl]amine (1 mL, 0.1 M solution in DMSO), and DMSO (2 mL) under an atmosphere of nitrogen. The reaction mixture was stirred for 3 h at room temperature, after which time the resulting polymer was collected by precipitation from methanol

followed by filtration (1.85 g, 93% yield). GPC: M_n = 96 kDa; PDI = 1.3. See also **Table A1**.

2.11$_{122}$. A 10 mL Schlenk flask was charged with a stir bar wrapped with copper wire, **2.5** (8.4 mg, 0.02 mmol), methyl acrylate (2.0 mL, 22.2 mmol), tris[2-(dimethylamino)ethyl]amine (1 mL, 0.1 M solution in DMSO), and DMSO (2 mL) under an atmosphere of nitrogen. The reaction mixture was stirred for 3 h at room temperature, after which time the resulting polymer was collected by precipitation from methanol followed by filtration (1.65 g, 83% yield). GPC: M_n = 122 kDa; PDI = 1.4.

2.12$_{118}$. A 10 mL Schlenk flask was charged with a stir bar wrapped with copper wire, **2.6** (8.4 mg, 0.02 mmol), methyl acrylate (2.0 mL, 22.2 mmol), tris[2-(dimethylamino)ethyl]amine (1 mL, 0.1 M solution in DMSO), and DMSO (2 mL) under an atmosphere of nitrogen. The reaction mixture was stirred for 3 h at room temperature, after which time the resulting polymer was collected by precipitation from methanol followed by filtration (1.40 g, 72% yield). GPC: M_n = 118 kDa; PDI = 1.4.

2.13$_{80}$. A 10 mL Schlenk flask was charged with a stir bar wrapped with copper wire, 3-butynyl-2-bromo-2-methylpropanoate (4.3 mg, 11.1 mmol), methyl acrylate (1.1 mL, 11.6 mmol), tris[2-(dimethylamino)ethyl]amine (1 mL, 0.1 M solution in DMSO), and DMSO (2 mL) under an atmosphere of nitrogen. The reaction mixture was stirred for 3 h at room temperature, after which time the resulting polymer was collected by precipitation from methanol followed by filtration (0.85 g, 82% yield). GPC: M_n = 80 kDa; PDI = 1.3.

2.14$_{39}$. A 10 mL Schlenk flask was charged with a stir bar wrapped with copper wire, 2-azidoethyl-2-bromo-2-methylpropanoate (3.0 mg, 0.01 mmol), methyl acrylate (2.0 mL, 22.2 mmol), tris[2-(dimethylamino)ethyl]amine (1 mL, 0.1 M solution in DMSO), and DMSO (2 mL) under an atmosphere of nitrogen. The reaction mixture was

stirred for 3 h at room temperature, after which time the resulting polymer was collected by precipitation from methanol followed by filtration (0.35 g, 89% yield). GPC = 39 kDa; PDI = 1.3.

2.15_{52}. A 10 mL Schlenk flask was charged with a stir bar wrapped with copper wire, **2.8** (29.1 mg, 0.03 mmol), methyl acrylate (2.0 mL, 22.2 mmol), tris[2-(dimethylamino)ethyl]amine (1 mL, 0.1 M solution in DMSO), and DMSO (2 mL) under an atmosphere of nitrogen. The reaction mixture was stirred for 3 h at room temperature, after which time the resulting polymer was collected by precipitation from methanol followed by filtration (1.53 g, 84% yield). GPC: M_n = 52 kDa; PDI = 1.3. **2.15_{52}** was then dissolved in $CDCl_3$ and analyzed by ^{31}P NMR (**Figure A17**, Top).

Table A1 Selected Yield and Molecular Weight Data†

Polymer	Presonication			Postsonication		Sonication Time
	Yield	M_n (kDa)	PDI	M_n (kDa)	PDI	(h)
2.3_{140}	88%	140	1.4	82	1.4	2
2.3_{96}	93%	96	1.3	48	1.4	2
2.3_{63}	85%	63	1.3	32	1.4	7
2.3_{36}	92%	36	1.3	33	1.3	7
2.3_{16}	73%	16	1.4	16	1.4	7
2.13_{80}	82%	80	1.3	--	--	--
2.14_{39}	89%	39	1.3	--	--	--
2.11_{122}	83%	122	1.4	78	1.2	5
2.12_{118}	72%	118	1.3	60	1.4	5
2.15_{52}	84%	52	1.3	23	1.4	7

†The M_n refers to the number average molecular weight. The polydispersity index (PDI) was calculated using the equation PDI = M_w/M_n, where M_w is the weight average molecular weight. M_n and M_w were determined as their polystyrene equivalents by GPC (eluent = THF).

General Procedure Used For Sonochemical Activation

A Suslick cell was charged with 10 mL of a 10 mg mL^{-1} solution of $\mathbf{2.3}_{Mn}$ in CH_3CN and sonicated using the general procedure described above. After sonication for the time given in **Table A1**, the solvent was removed under reduced pressure. The residual polymer was dissolved in tetrahydrofuran and the polymer was characterized by GPC (**Table A1** and **Figure A1**).

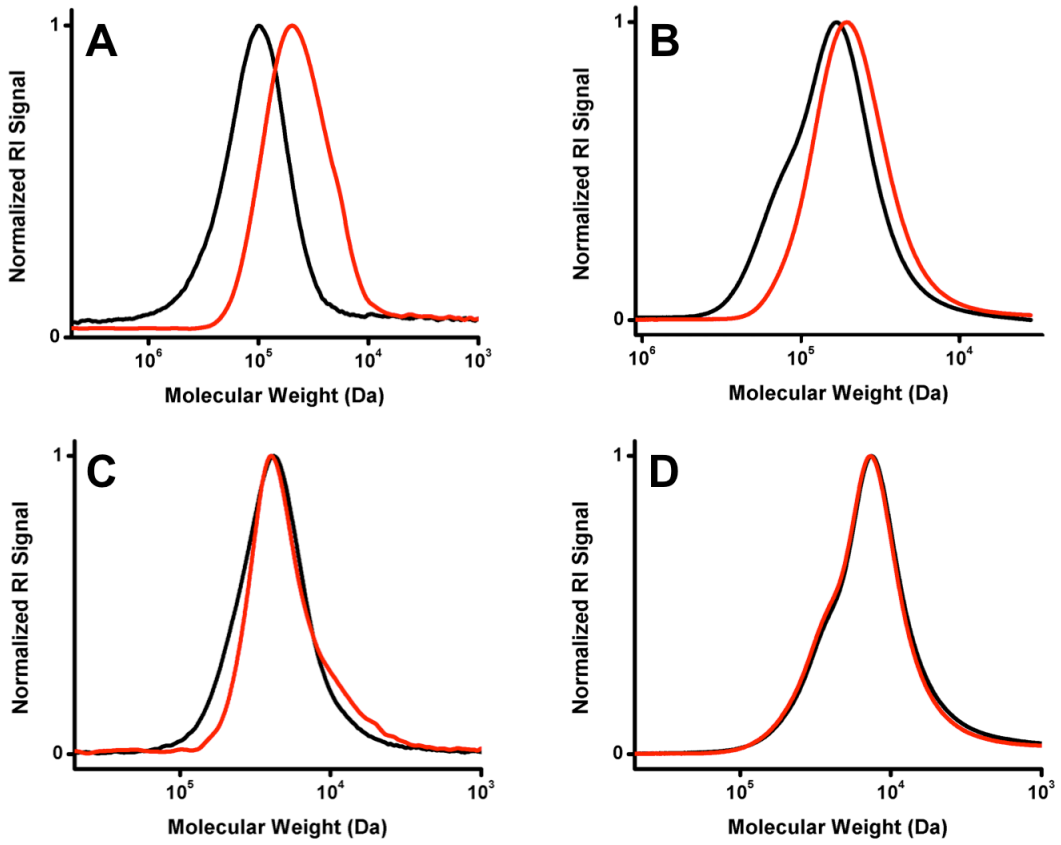

Figure A1 GPC traces of (A) $\mathbf{2.3}_{96}$, (B) $\mathbf{2.3}_{63}$, (C) $\mathbf{2.3}_{36}$, and (D) $\mathbf{2.3}_{16}$ before (black) and after sonochemical activation (red).

DETERMINATION OF THE EXTENT OF CYCLOREVERSION

A Suslick cell was charged with 10 mL of a 10 mg mL^{-1} solution of **2.3**$_{96}$ and subjected to the sonication conditions described above. After 1 h, the solvent was removed under reduced pressure. The residual polymer was dissolved in tetrahydrofuran and analyzed by GPC (**Figure A2**). Deconvolution and integration of the GPC data using PeakFit v4.12 and referencing the data to the peak molecular weight, M_p, values for the pre- and postsonicated material (**Figure A3**) revealed that approximately 52% of the starting material had undergone activation. In a similar manner, deconvolution and integration of the GPC data obtained for the residual material isolated after subjecting **2.3**$_{140}$ (10 mg mL^{-1} solution in CH_3CN) to sonication for 1 h revealed that approximately 57% of the starting material had undergone activation (**Figure A4** and **Figure A5**). Complete cycloreversion of both **2.3**$_{96}$ and **2.3**$_{140}$ was observed after 2 h.

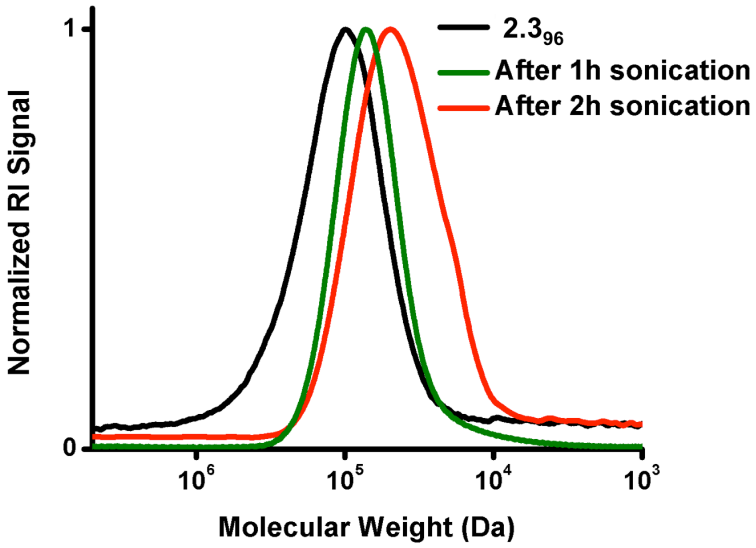

Figure A2 GPC traces of **2.3**$_{96}$ before sonication (black), after sonication for 1 h (green), and after sonication for 2 h (red).

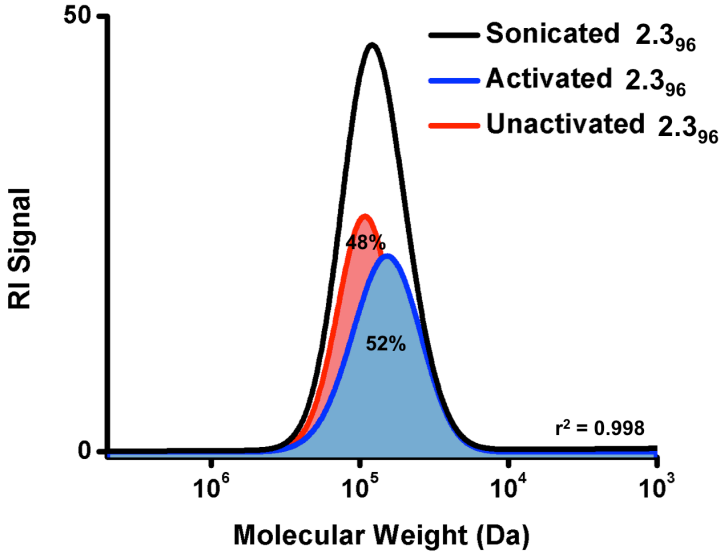

Figure A3 Deconvolution of GPC trace obtained for **2.3$_{96}$** after 1 h sonication.

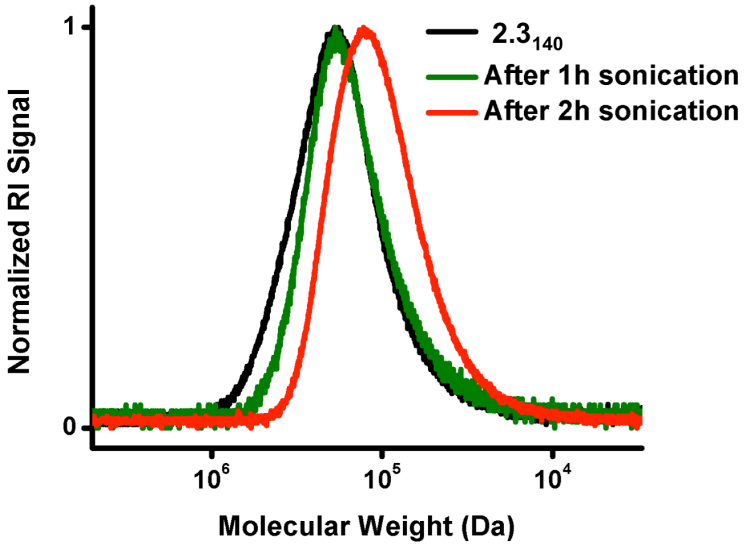

Figure A4 GPC traces of **2.3$_{140}$** before sonication (black), after sonication for 1 h (green), and after sonication for 2 h (red).

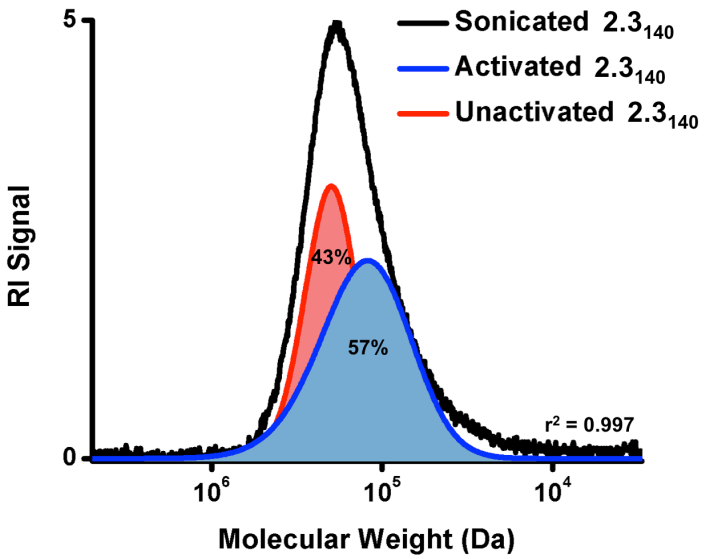

Figure A5 Deconvolution of GPC trace obtained for **2.3**$_{140}$ after 1 h sonication.

2.1.3 General Procedure for the Sonochemical Activation of **2.11**$_{122}$, **2.12**$_{118}$ and **2.4**

For each experiment, a Suslick cell was charged with 10 mL of a 10 mg/mL solution of **2.11**$_{122}$, **2.12**$_{118}$ or **2.4** in CH_3CN. After sonication for 5 h, the solvent was removed under reduced pressure. For the end-functionalized derivatives, **2.11**$_{122}$ and **2.12**$_{118}$, the residue was dissolved in tetrahydrofuran and characterized by GPC (**Table A1** and **Figure A6**). For the small molecule control **2.4,** the corresponding residue was dried under high vacuum and then analyzed by ^{1}H NMR spectroscopy ($CDCl_3$, **Figure A7**).

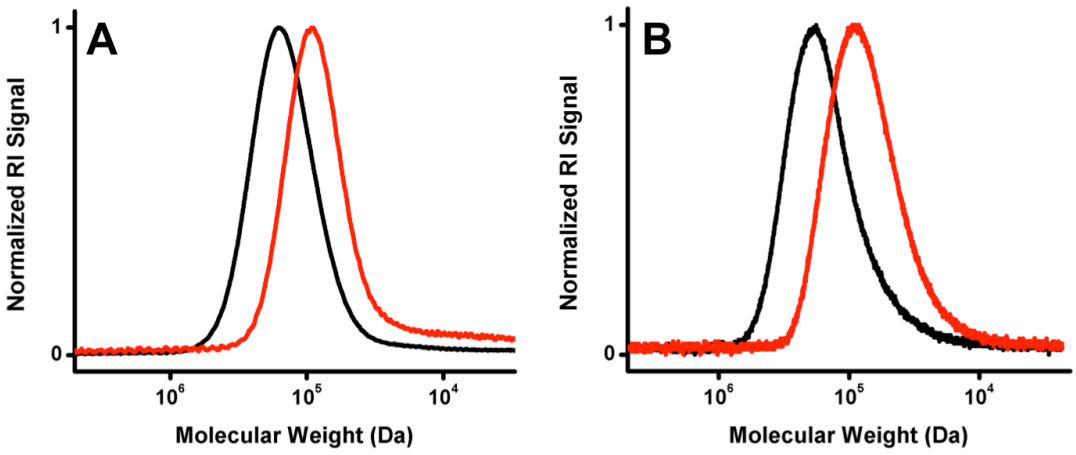

Figure A6 GPC traces of (A) $\mathbf{2.11}_{122}$ and (B) $\mathbf{2.12}_{118}$ before (black) and after (red) ultrasonication.

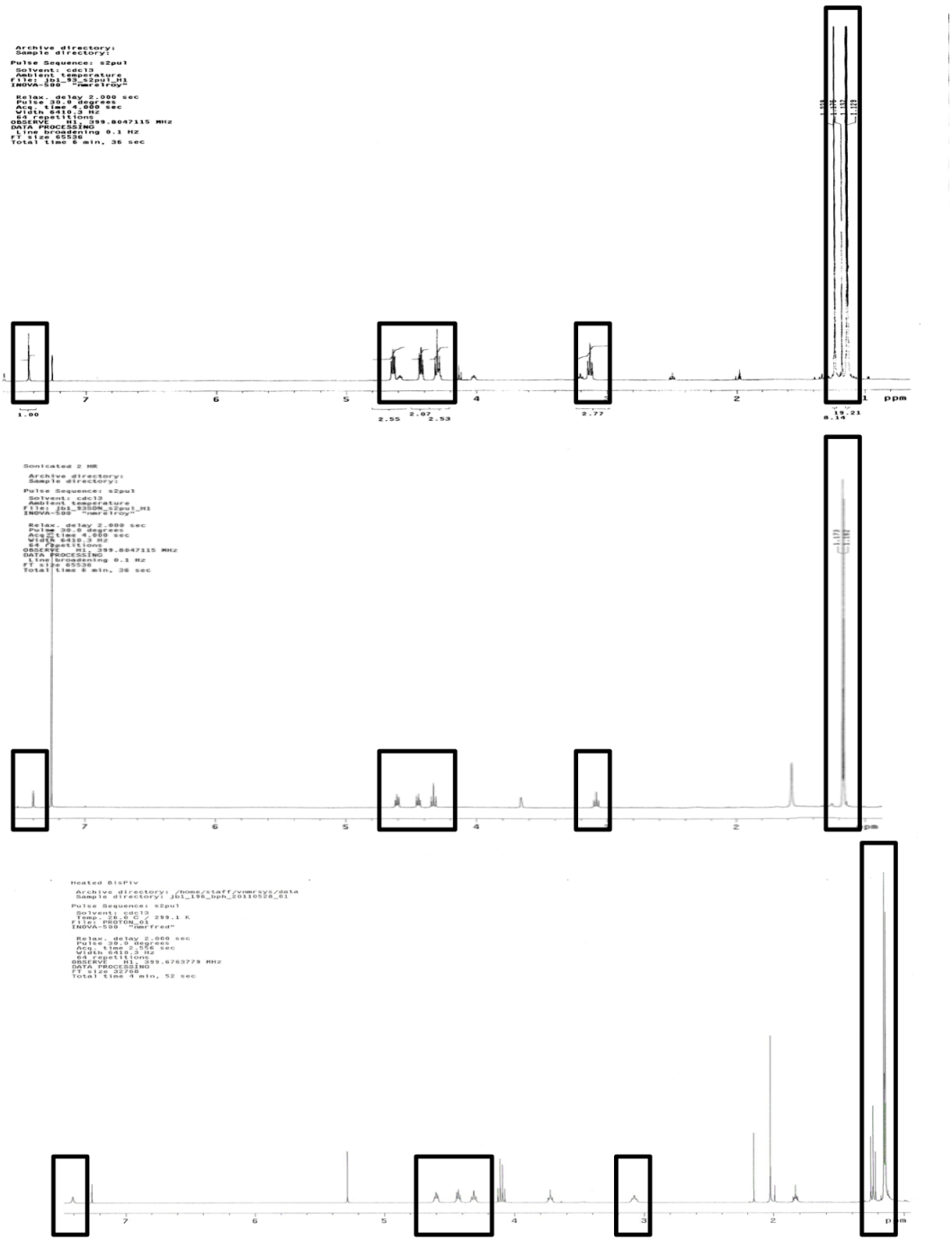

Figure A7 ^{1}H NMR spectra ($CDCl_3$) of **2.4** before (top) and after sonication (middle) or thermal treatment (bottom). The resonances assigned to the triazole moiety have been highlighted in each spectrum with a black square.

PROCEDURE FOR THE THERMAL ACTIVATION OF $\mathbf{2.3_{140}}$

An 8 mL Teflon capped vial was charged with 1 mL of a 10 mg mL^{-1} solution of $\mathbf{2.3_{140}}$ in acetonitrile. The solvent was removed under reduced pressure, and the resulting thin film was heated under nitrogen for 24 h at 180 °C in a sand bath. The resulting material was dissolved in tetrahydrofuran and then characterized by GPC (**Figure 2.1A**).

PROCEDURE FOR THE THERMAL ACTIVATION OF 2.4

An 8 mL Teflon capped vial was charged with 0.10 g of **2.4** under a cone of nitrogen and sealed. The sample was then heated in the bulk for 24 h at 258 °C in a sand bath. After cooling, the residue was analyzed by ^{1}H NMR spectroscopy ($CDCl_3$, **Figure A7**).

ADDITIONAL IR CONTROL EXPERIMENTS

In a 20 mL Teflon capped vial, $\mathbf{2.3_{96}}$ (0.10 g) was dissolved in CH_3CN (10 mL) and stirred for 1 h at room temperature. After removal of the solvent under reduced pressure, the residue was dissolved in tetrahydrofuran and analyzed by IR spectroscopy (**Figure A8**, top).

A 50 mL round bottom was charged 10 mL of a 10 mg mL^{-1} $\mathbf{2.3_{96}}$ in degassed diphenyl ether. The resulting solution was heated under nitrogen for 24 h at 258 °C in a sand bath. After pouring the resulting reaction mixture into excess methanol, the precipitated material was collected by filtration, dissolved in tetrahydrofuran and analyzed by IR spectroscopy (**Figure A8**, middle).

An 8 mL Teflon capped vial was charged with 0.10 g of **2.4** under a cone of nitrogen and sealed. The sample was then heated in the bulk for 24 h at 258 °C in a sand bath. After cooling, the residue was dissolved in tetrahydrofuran and analyzed by IR spectroscopy (**Figure A8**, bottom).

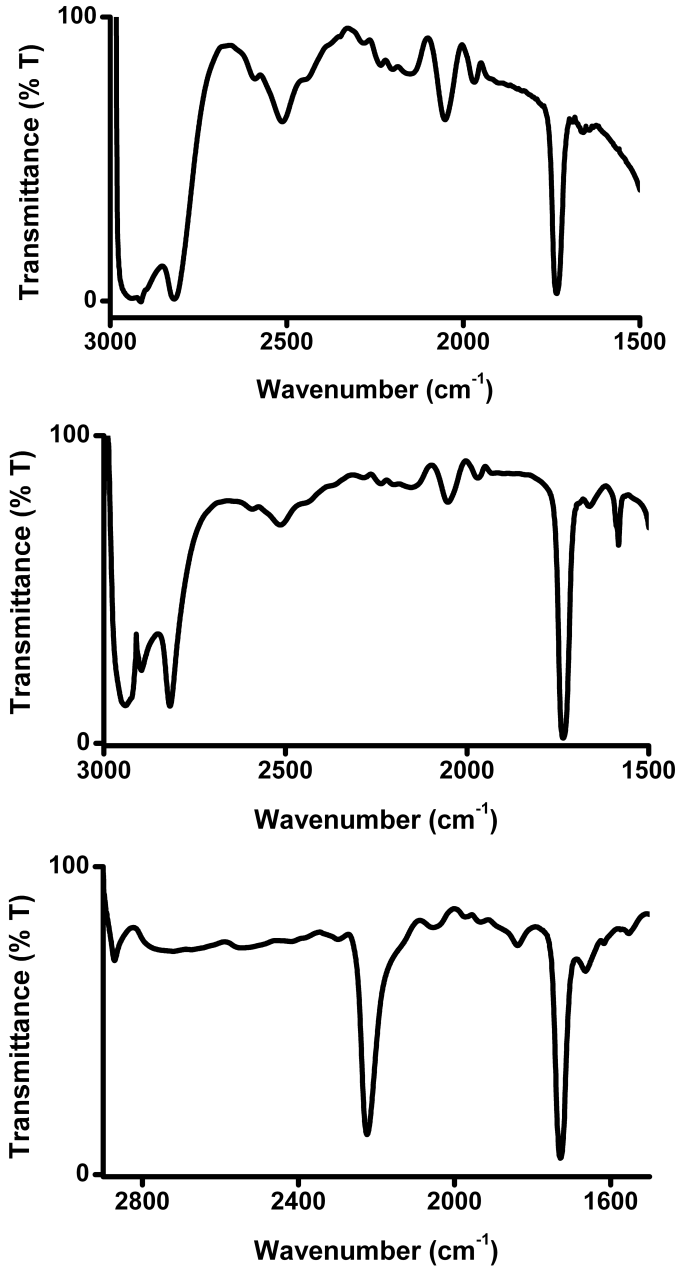

Figure A8 IR spectra (in tetrahydrofuran) of $\mathbf{2.3_{96}}$ after dissolution in CH_3CN and subsequent removal of solvent (top), $\mathbf{2.3_{96}}$ after heating in a solution of diphenyl ether at 258 °C for 24 h (middle), and **2.4** upon heating neat at 258 °C for 24 h (bottom). The spectra do not show signals assigned to azide or alkyne moieties (*i.e.*, at 2133 or 2039 cm^{-1}).

PROCEDURE FOR ALKYNE LABELING EXPERIMENTS PERFORMED AFTER THE SONICATION OF $\mathbf{2.3_{140}}$

A Suslick cell was charged with 10 mL of a 10 mg mL^{-1} solution of $\mathbf{2.3_{140}}$ and subjected to the sonication conditions described above. The polymer was isolated by precipitation into excess methanol followed by filtration. An 8 mL Teflon capped vial was charged with the isolated polymer (10 mg, 0.0001 mmol), 1-azidopyrene (5.0 mg, 0.02 mmol), and CH_3CN (3 mL). The resulting solution was degassed by sparging with nitrogen, and copper (I) iodide (5 mg, 0.025 mmol) was added in a glovebox. After sealing the reaction vessel, the reaction mixture was allowed to stir for 19 h at room temperature. The solvent was removed under reduced pressure, and the resulting residue was washed with a saturated aqueous solution of ethylenediaminetetraacetic acid (EDTA; 3 × 5 mL), water (3 × 5 mL), and methanol (3 × 5 mL). The resulting residue was dissolved in minimal THF, filtered through a 0.2 μm PTFE filter, and diluted with excess methanol. The resulting suspension was centrifuged, and the precipitated material was washed with excess methanol, dissolved in minimal THF, transferred to an 8 mL Teflon capped vial, and dried under reduced pressure. GPC analysis with concomitant ultraviolet-visible detection revealed the polymer had increased absorbance at λ = 240 nm (a λ_{max} associated with pyrene) relative to the starting polymer, which showed negligible absorbance at this wavelength following treatment under identical conditions (**Figure 2.1**).

SYNTHESIS OF $\mathbf{2.16_{80}}$

An 8 mL Teflon capped vial was charged with $\mathbf{2.13_{80}}$ (10 mg, 0.0001 mmol), 1-azidopyrene (5.0 mg, 0.02 mmol), and CH_3CN (3 mL). The resulting solution was then degassed by sparging with nitrogen, and copper (I) iodide (5 mg, 0.025 mmol) was added in a glovebox. After sealing the reaction vessel, the reaction mixture was allowed to stir

for 19 h at room temperature. The solvent was removed under reduced pressure, and the resulting residue was washed with a saturated aqueous solution of ethylenediaminetetraacetic acid (EDTA; 3 × 5 mL), water (3 × 5 mL), and methanol (3 × 5 mL). The resulting residue was dissolved in minimal THF, filtered through a 0.2 μm PTFE filter, and diluted with excess methanol. The resulting suspension was centrifuged, and the precipitated material was washed with excess methanol, dissolved in minimal THF, transferred to an 8 mL Teflon capped vial, and dried under reduced pressure. Ultraviolet-visible spectroscopy revealed increased absorbances compared to the starting material that were consistent with the incorporation of pyrene onto the polymeric scaffold (**Figure A9**).

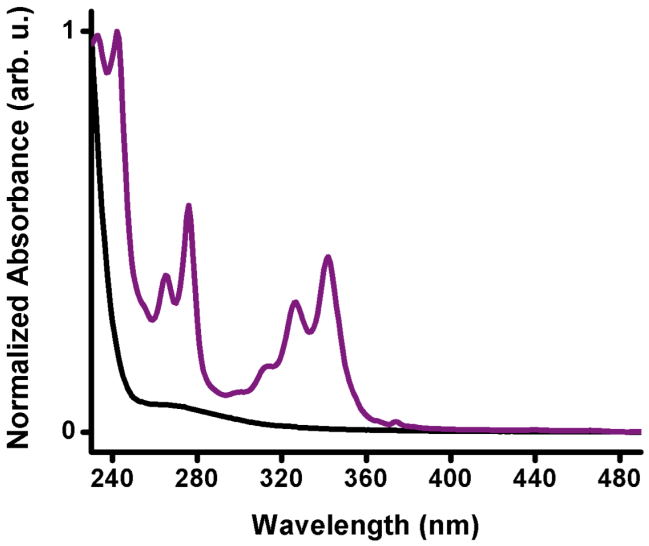

Figure A9 Ultraviolet-visible spectra of **2.13**$_{80}$ before (black) and after (violet) treatment with 1-azidopyrene. The spectra were acquired using [**2.13**$_{80}$] = [**2.16**$_{80}$] = 1 mg mL^{-1} in CH_3CN.

PROCEDURE FOR ALKYNE LABELING EXPERIMENTS PERFORMED AFTER THE SONICATION OF $\mathbf{2.11_{122}}$

A Suslick cell was charged with 10 mL of a 10 mg mL^{-1} solution of $\mathbf{2.11_{122}}$ and subjected to the sonication conditions described above. The polymer was isolated by precipitation into excess methanol followed by filtration. An 8 mL Teflon capped vial was charged with the isolated polymer (10 mg, 0.0001 mmol), 1-azidopyrene (5.0 mg, 0.02 mmol), and CH_3CN (3 mL). The resulting solution was degassed by sparging with nitrogen, and copper (I) iodide (5 mg, 0.025 mmol) was added in a glovebox. After sealing the reaction vessel, the reaction mixture was allowed to stir for 19 h at room temperature. The solvent was removed under reduced pressure, and the resulting residue was washed with a saturated aqueous solution of ethylenediaminetetraacetic acid (EDTA; 3 × 5 mL), water (3 × 5 mL), and methanol (3 × 5 mL). The resulting residue was dissolved in minimal THF, filtered through a 0.2 μm PTFE filter, and diluted with excess methanol. The resulting suspension was centrifuged, and the precipitated material was washed with excess methanol, dissolved in minimal THF, transferred to an 8 mL Teflon capped vial, and dried under reduced pressure. Ultraviolet-visible spectroscopic characterization of the polymer revealed minimal change in absorbance compared to the starting material (**Figure A10**).

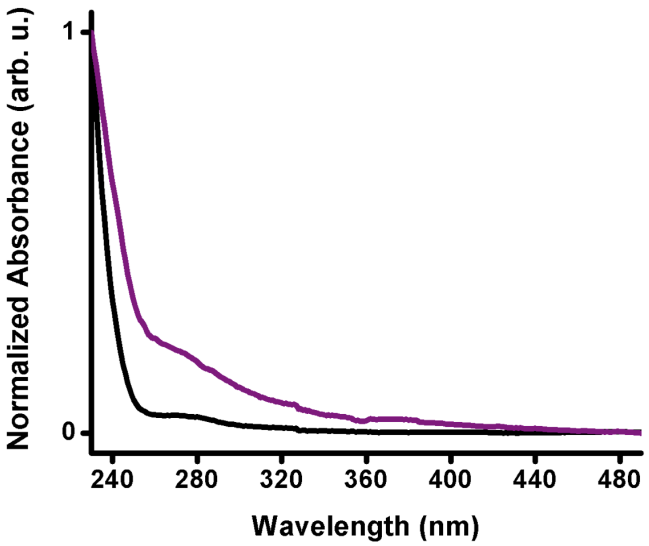

Figure A10 Ultraviolet-visible spectra of $\mathbf{2.11}_{122}$ following ultrasonication (black) and subsequent treatment with 1-azidopyrene (violet). The spectra were acquired using $[\mathbf{2.11}_{122}]$ = 1 mg mL^{-1} in CH_3CN.

Procedure for Alkyne Labeling Experiments Performed After the Sonication of $\mathbf{2.12}_{118}$

A Suslick cell was charged with 10 mL of a 10 mg mL^{-1} solution of $\mathbf{2.12}_{118}$ and subjected to the sonication conditions described above. The polymer was isolated by precipitation into excess methanol followed by filtration. An 8 mL Teflon capped vial was charged with the isolated polymer (10 mg, 0.0001 mmol), 1-azidopyrene (5.0 mg, 0.02 mmol), and CH3CN (3 mL). The resulting solution was degassed by sparging with nitrogen, and copper (I) iodide (5 mg, 0.025 mmol) was added in a glovebox. After sealing the reaction vessel, the reaction mixture was allowed to stir for 19 h at room temperature. The solvent was removed under reduced pressure, and the resulting residue was washed with a saturated aqueous solution of ethylenediaminetetraacetic acid (EDTA; 3 × 5 mL), water (3 × 5 mL), and methanol (3 × 5 mL). The resulting residue was dissolved in minimal THF, filtered through a 0.2 μm PTFE filter, and diluted with excess

methanol. The resulting suspension was centrifuged, and the precipitated material was washed with excess methanol, dissolved in minimal THF, transferred to an 8 mL Teflon capped vial, and dried under reduced pressure. Ultraviolet-visible spectroscopic characterization of the polymer revealed minimal change in absorbance compared to the starting material (**Figure A11**).

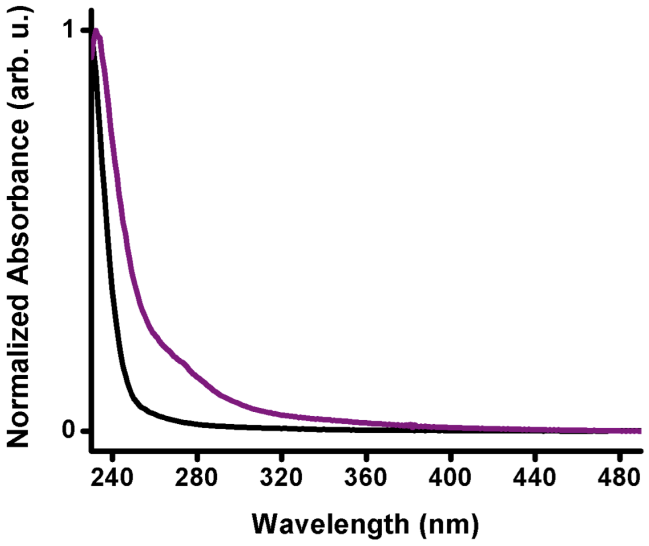

Figure A11 Ultraviolet-visible spectra of $\mathbf{2.12}_{118}$ following ultrasonication (black) and subsequent treatment with 1-azidopyrene (violet). The spectra were acquired using [$\mathbf{2.12}_{118}$] = 1 mg mL^{-1} in THF.

PROCEDURE FOR AZIDE LABELING EXPERIMENTS PERFORMED AFTER THE SONICATION OF $\mathbf{2.3}_{140}$

A Suslick cell was charged with 10 mL of a 10 mg mL^{-1} solution of $\mathbf{2.3}_{140}$ and subjected to the sonication conditions described above. The polymer was isolated by precipitation into excess methanol followed by filtration. In a glovebox, an 8 mL vial was charged with the isolated polymer (10 mg, 0.0001 mmol) and tetrahydrofuran (3 mL). **NQMes** (10 mg, 0.023 mmol) was added, the vial was sealed, and the reaction mixture

was stirred at room temperature. After 20 min, the reaction mixture had changed from a dark green to a dark blue color. At this time, the solvent was removed under reduced pressure, and the resulting residue was washed with excess methanol, dissolved in minimal THF, and diluted with excess methanol. The suspension was centrifuged, and the resulting residue was washed with excess methanol, dissolved in minimal THF, and dried under reduced pressure. Ultraviolet-visible spectroscopic characterization revealed an increased absorbance at λ = 250, 273, 300, 311, and 586 nm compared to the starting polymer (**Figure A12**). GPC analysis with concomitant ultraviolet-visible detection revealed that the treated polymer had an increased absorbance at λ = 310 nm relative to the starting polymer reacted under identical conditions, which showed negligible absorbance at this wavelength (**Figure 2.1**).

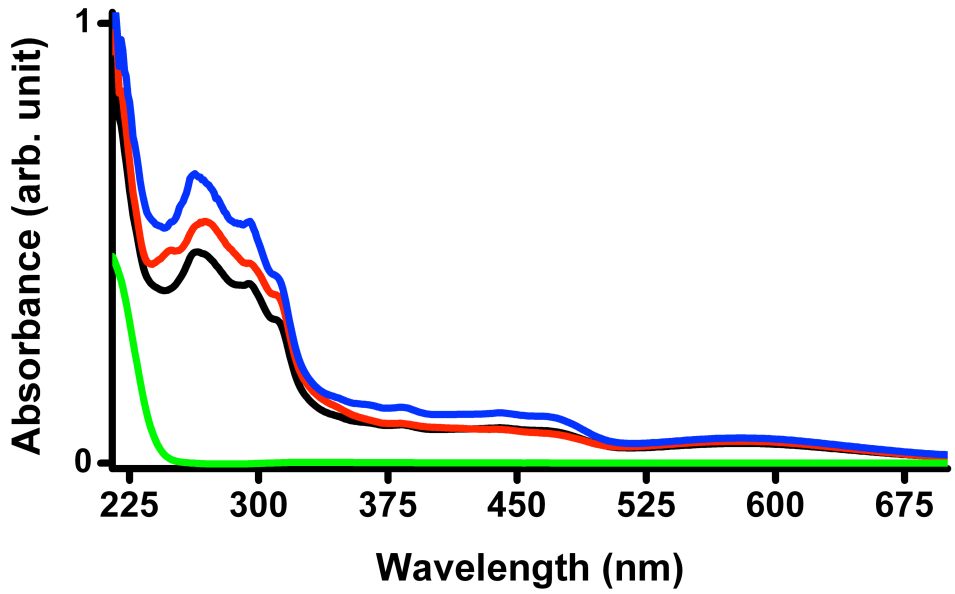

Figure A12 Ultraviolet-visible spectra of **2.3**$_{96}$ treated with **NQMes** after sonication (black), **2.14**$_{39}$ treated with **NQMes** (blue), presonicated **2.3**$_{96}$ (green) and presonicated **2.3**$_{96}$ treated with **NQMes** (red). The spectra were acquired using [**2.3**$_{96}$] = 1 mg mL^{-1} in THF.

SYNTHESIS OF 2.17

In a glovebox, a 20 mL vial was charged $\mathbf{2.14_{39}}$ (0.10 g, 0.002 mmol) and tetrahydrofuran (5 mL). After the polymer was dissolved, **NQMes** (0.10 g, 0.21 mmol) was added. The vial was then sealed with a Teflon lined cap and the reaction mixture was stirred at room temperature. After 20 min, the reaction mixture had changed from a dark green to a dark blue color. At this time, the reaction mixture was diluted with methanol, and the precipitated polymer material was collected by filtration after centrifugation. The isolated polymer was washed with methanol and dried under reduced pressure. Ultraviolet-visible spectroscopy revealed the isolated polymer had increased absorbance at λ = 250, 273, 300, 311, and 586 nm relative to the starting polymer which showed negligible absorbance at these wavelengths (**Figure A12**).

POSTSONICATION COUPLING EXPERIMENTS

A Suslick cell was charged with 10 mL of a 10 mg mL^{-1} solution of $\mathbf{2.3_{140}}$ and subjected to the sonication conditions described above. The resulting polymer product was isolated by precipitation into excess methanol followed by filtration. An 8 mL Teflon capped vial was charged with the isolated material (10 mg, 0.0001 mmol) and CH_3CN (3 mL). The resulting solution was degassed by sparging with nitrogen, and copper (I) iodide (10 mg, 0.05 mmol) was added in a glovebox. After sealing the reaction vessel, the reaction mixture was allowed to stir for 72 h at 90 °C in the absence of light. The solvent was removed under reduced pressure, and the resulting residue was washed with a saturated aqueous solution of ethylenediaminetetraacetic acid (EDTA; 3 × 5 mL), water (3 × 5 mL), and methanol (3 × 5 mL). The resulting residue was dissolved in minimal THF, filtered through a 0.2 μm PTFE filter, and diluted with excess methanol. The resulting suspension was centrifuged, and the precipitated material was washed with excess methanol, dissolved in minimal THF, transferred to an 8 mL Teflon capped vial,

and dried under reduced pressure. GPC: M_n = 95 kDa; PDI = 1.2 (**Table A2**). **2.3$_{96}$** was subjected to the above ultrasonication and recoupling procedures (with the exception that recoupling was performed at 80 ºC) with similar results (**Table A2**).

Table A2 Selected Molecular Weight Data†

Coupled Polymer	Postsonication		Post-Coupling	
	M_n [kDa][b]	PDI	M_n [kDa]	PDI
2.3$_{140}$	82	1.4	95	1.2
2.3$_{96}$	48	1.4	70	1.3

† The M_n refers to the number average molecular weight of the polymer. The polydispersity index (PDI) was calculated using the equation PDI = M_w/M_n, where M_w is the weight average molecular weight and M_n is the number average molecular weight. The M_n and M_w values were determined by GPC (eluent = tetrahydrofuran). Molecular weights are reported as their polystyrene equivalents.

PROCEDURE FOR DETERMINING COUPLING EFFICIENCY

Deconvolution and integration of the GPC data for the **2.3$_{140}$** polymer isolated after sonication and coupling at 90 °C using PeakFit v4.12 and referencing the data to the peak molecular weight, M_p, values for the pre- and postsonicated material (**Figure A13**) revealed that approximately 16% of the cycloreverted **2.3$_{140}$** had undergone coupling. In a similar manner, **2.3$_{96}$** was subjected to sonication followed by coupling at 80 °C for 24 h. Deconvolution and integration of the GPC data (**Figure A14**) revealed that approximately 40% of the material re-coupled.

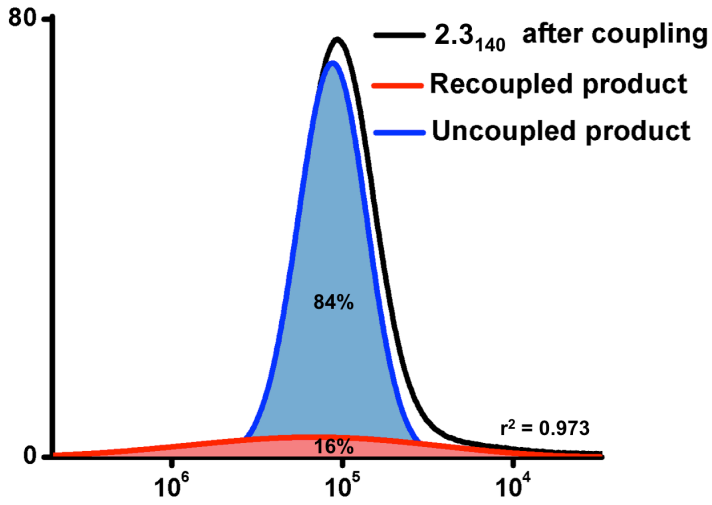

Figure A13 Deconvolution of GPC traces obtained following ultrasonication and recoupling of $\mathbf{2.3}_{140}$.

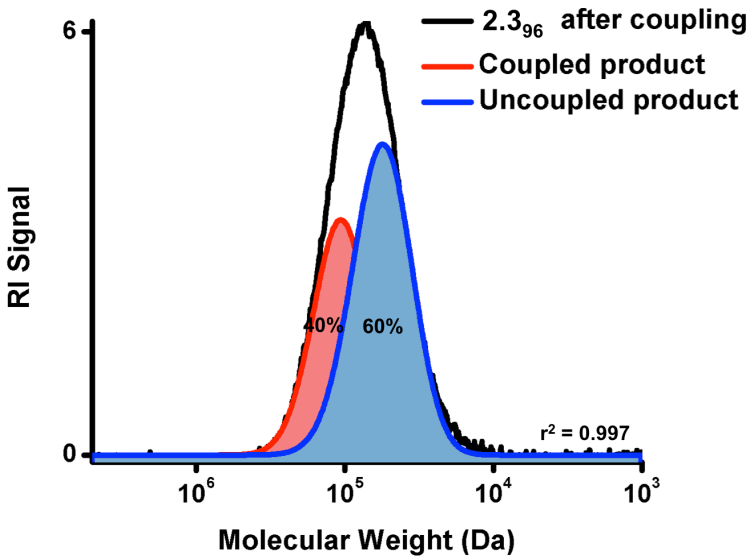

Figure A14 Deconvolution of GPC traces obtained following ultrasonication and recoupling of $\mathbf{2.3}_{96}$.

PROCEDURE FOR ASSESSING THE ABILITY TO SONICATE AND RE-COUPLE MULTIPLE $\mathbf{2.3_{MN}}$ POLYMERS

A Suslick cell was charged with 10 mL of a 10 mg mL^{-1} solution of $\mathbf{2.3_{140}}$ and subjected to the sonication conditions described above. The polymer was isolated by precipitation into excess methanol followed by filtration, and then analyzed by GPC (M_n = 82 kDa; PDI = 1.3). An 8 mL Teflon capped vial was charged with the isolated polymer (10 mg, 0.0001 mmol) and CH_3CN (3 mL). The resulting solution was degassed by sparging with nitrogen, and copper (I) iodide (10 mg, 0.05 mmol) was added in a glovebox. After sealing the reaction vessel, the reaction mixture was allowed to stir for 72 h at 90 ºC in the absence of light. The solvent was removed under reduced pressure, and the resulting residue was washed with a saturated aqueous solution of ethylenediaminetetraacetic acid (EDTA; 3 × 5 mL), water (3 × 5 mL), and methanol (3 × 5 mL). The resulting residue was dissolved in minimal THF, filtered through a 0.2 μm PTFE filter, and diluted with excess methanol. The resulting suspension was centrifuged, and the precipitated material was washed with excess methanol, dissolved in minimal THF, transferred to an 8 mL Teflon capped vial, and dried under reduced pressure. GPC: M_n = 95 kD; PDI =1.2 (**Figure 2.1A**). A Suslick cell was then charged with 5 mL of a 2 mg mL^{-1} solution of this material and subjected to the sonication conditions described above. The solvent was removed, and the resulting residue was washed with excess methanol, dissolved in minimal THF, and diluted with excess methanol. The resulting suspension was centrifuged, and the solid residue was washed with excess methanol, dissolved in minimal THF, and transferred to an 8 mL Teflon capped vial. Following concentration under reduced pressure, the iolated material was analyzed by GPC (M_n = 60 kD; PDI = 1.2; **Figure 2.1A**). Similarly, $\mathbf{2.3_{96}}$ could be subjected to ultrasonication for

2 h (M_n = 48 kD; PDI = 1.4) and the coupling procedure described above (M_n = 70 kD; PDI = 1.3; **Figure A15**).

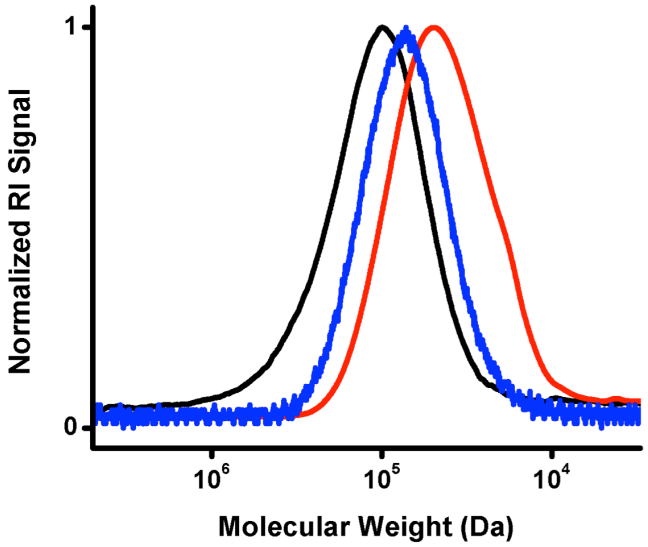

Figure A15 GPC traces of **2.3**$_{96}$ before ultrasonication, (black) after ultrasonication (red), and after recoupling (blue).

PROCEDURE FOR SONICATION AND ANALYSIS OF **2.15**$_{52}$

A Suslick cell was charged with 10 mL of a 10 mg mL^{-1} solution of **2.15**$_{52}$ and subjected to the sonication conditions described above for 7 h. The polymer was isolated by precipitation into excess methanol followed by filtration. The resulting material was divided into two equal portions. The first was dissolved in tetrahydrofuran and analyzed by GPC (**Figure A16**). The second was dissolved in $CDCl_3$ and analyzed by ^{31}P NMR spectroscopy (**Figure A17**, bottom).

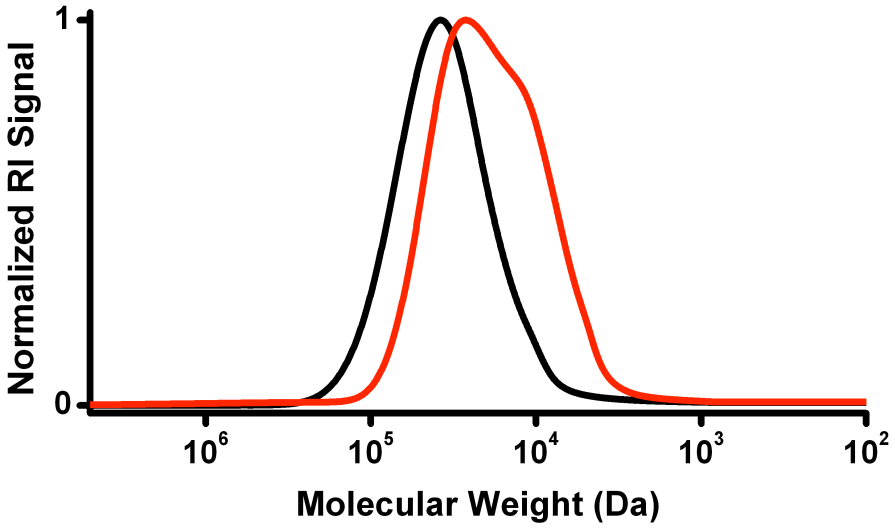

Figure A16 GPC traces of **2.15**$_{52}$ before (black) and after (red) sonication.

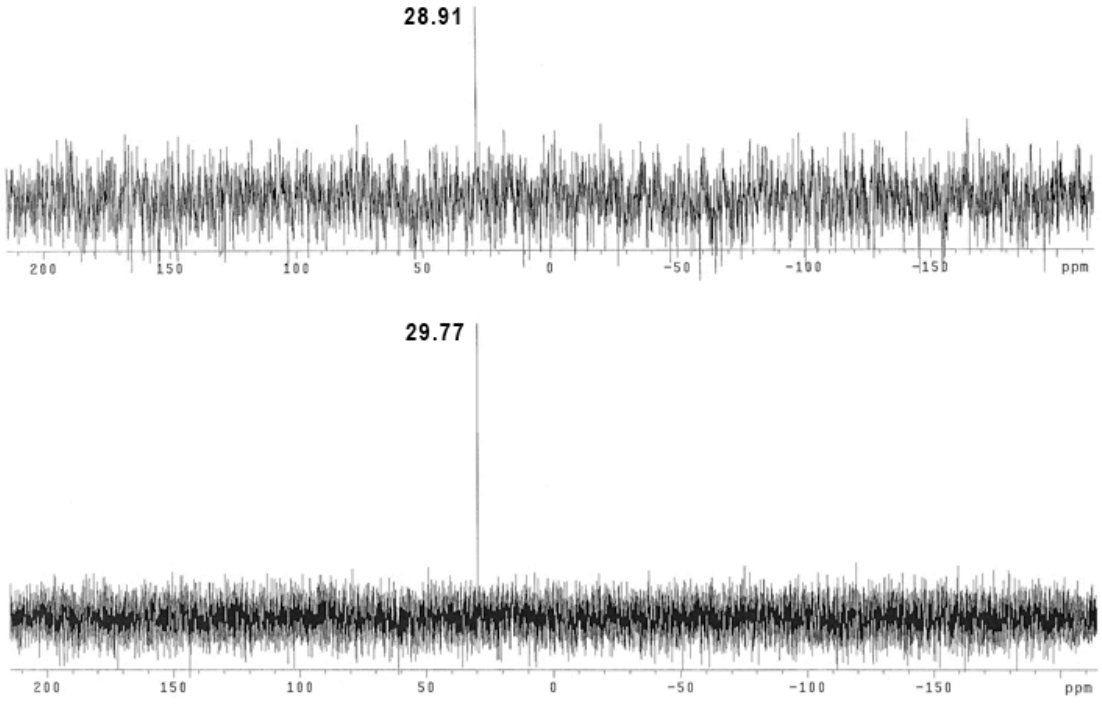

Figure A17 ^{31}P NMR spectra (CDCl3) of **2.15**$_{52}$ before (top) and after (bottom) ultrasonication. The error is ±1 ppm.

REFERENCES

1 Lu, X.; Bittmamn, R. *J. Org. Chem.* **2005**, *70*, 4746.

2 Chiba, K.; Du, H. ; Eguchi, Y.; Fujita, M.; Goto, M.; Gusovsky, F.; Harmange, J.-C.; Inoue, A.; Kawada, M.; Kawai, T.; Kawakami, Y.; Kimura, A.; Kotake, M.; Kuboi, Y.; Matsushima, T.; Mizui, Y.; Muramoto, K.; Sakurai, H.; Shen, Y.- C.; Shirota, H.; Spyvee, M.; Tanaka, I.; Wang, Y.; Wood, R.; Yamamoto, S.; Yoneda, N. *U.S. Pat. Appl. Publ.* **2004**, *20040224936*.

3 Sun, S.; Cao, Y.; Feng, J.; Wu, P. *J. Mater. Chem.* **2010**, *20*, 5605.

4 Schrock, A. K.; Schuster, G. B. *J. Am. Chem. Soc.* **1984**, *106*, 5234.

5 Sanderson, M. D.; Kamplain, J. W.; Bielawski, C. W. *J. Am. Chem. Soc.* **2006**, *128*, 16514.

6 Antonin, H. *Collect. Czech. Chem. Commun.* **1989**, *54*, 446.

7 Suslick, K. S.; Goodale, J. W.; Schubert, P. F.; Wang, H. H. *J. Am. Chem. Soc.* **1983**, *105*, 5781.

8 Nulwala, H.; Takizawa, K.; Odukale, A.; Khan, A.; Thibault, R. J.; Taft, B. R.; Lipshutz, B. H.; Hawker, C. J. *Macromolecules* **2009**, *42*, 6068.

Appendix B

General Experimental Considerations

The following compounds were prepared according to literature procedures: 2-azidoethanol,[1] 3-butynyl-2,2-dimethylpropanoate,[2] 2-azidoethyl-2-bromo-2-methylpropanoate,[3] 1-azidopyrene,[4] 1,3-dimesitylnapthoquinimidazolylidene (**NQMes**),[5] 3-azido-propane-1,2-diol,[6] 3-butynyl-2-bromo-2-methyl-propanoate,[7] and 2-azidoethyl-2,2-dmethylpropanoate.[7] All other reagents and solvents were obtained from commercial sources and used without further purification. Unless otherwise noted, solvents were dried over 3 Å molecular sieves or Al_2O_3 and deoxygenated (via a Q5 catalyst) using a Vacuum Atmospheres Company solvent purification system, and then subsequently stored over molecular sieves (3 Å). ^{1}H and ^{13}C NMR data were collected on Varian Unity INOVA 400 MHz spectrometer. Chemical shifts (δ) are reported in ppm and referenced downfield from $(CH_3)_4Si$ using the residual solvent peak as an internal standard ($CDCl_3$: 7.26 ppm for ^{1}H and 77.16 ppm for ^{13}C NMR; DMSO-d_6: 2.50 ppm for ^{1}H NMR; C_6D_6: 7.16 ppm for ^{1}H and 128.06 ppm for ^{13}C NMR). ^{31}P NMR data were acquired on Varian Oxford 600 MHz spectrometer and externally referenced to phosphoric acid (δ = 0 ppm). UV-vis spectra were recorded using a Perkin Elmer Instruments Lambda 35 spectrometer. High resolution mass spectra (HRMS) were obtained by electrospray ionization (ESI) with a VG analytical ZAB2-E instrument. IR spectra were recorded using either a Perkin-Elmer Spectrum BX FT-IR system (in KBr matrices or in solutions of tetrahydrofuran) or a Thermo Scientific Nicolet iS5 spectrometer equipped with an iD3 attenuated total reflectance (ATR; Ge crystal). Elemental analyses were performed at Midwest Microlab, LLC (Indianapolis, IN). Melting points were obtained on a Melt-temp apparatus and are uncorrected.

MACROMOLECULAR CHARACTERIZATION

Gel permeation chromatography (GPC) was performed using tetrahydrofuran as the eluent on either a Viscotek system equipped with a VE 1122 pump, a VE 7510 degasser, two fluorinated polystyrene columns (I-MBHW-3078 and I-MBLMW-3078) thermostated to 30 °C (using a ELDEX CH 150 column heater) and arranged in series, a Viscotek 270 Dual Detector (light scattering detector and differential viscometer), and a VE 3580 refractive index detector or at room temperature on a home-built gel permeation chromatograph equipped with a Waters Model 510 HPLC pump, two fluorinated polystyrene columns (IMBHW-3078 and I-MBLMW-3078) arranged in series, and a Waters 486 Tunable Absorbance Detector. Molecular weight and polydispersity data are reported relative to polystyrene standards.

GENERAL SONICATION CONSIDERATIONS

The sonication experiments were performed under an atmosphere of argon using a Sonics & Materials VC-505 Liquid Cell Ultrasonic processor operating at 20 kHz equipped with a 12.8 mm replaceable tip titanium probe. Custom Suslick cells[8] were fabricated in house. An argon line was threaded through a septum attached to a cell's side arm and placed in solution, ensuring no contact with the probe. Argon was then bubbled through the solution for 30 min prior to and continuously during each experiment performed. The cell was placed in an ice bath, which was sufficient to maintain a temperature of 6–9 °C, as determined by using a thermocouple placed directly into the solution. Pulsed ultrasound was applied (1.0 s on and 1.0 s off) at 23% power (power intensity = 9.7 W cm^{-2}) for each experiment performed.

SYNTHESES AND CHARACTERIZATION DATA

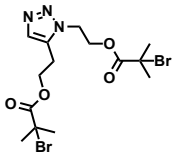

1,5-(2-((2-bromo-2-methylpropanoyl)oxy)ethyl)-1*H*-1,2,3-triazol-5-yl (4.3). A 50 mL vial with a Teflon cap was charged with a stir bar, 3-butynyl-2-bromo-2-methylpropanoate (0.045 g, 0.21 mmol), 2-azidoethyl-2-bromo-2-methylpropanoate (0.05 g, 0.21 mmol), and tetrahydrofuran (THF, 5.0 mL) in a glovebox. Pentamethylcyclopentadienylbis(triphenylphosphine) ruthenium(II) chloride (0.0034 g in 1 mL THF) was added to the resulting mixture, and the reaction was stirred at 65 °C for 2 h. The solvent was removed under reduced pressure, and the resulting residue was purified using column chromatography (eluted with hexanes followed by 1:1 hexanes/ethyl acetate) to afford the desired product as a yellow oil (0.076 g, 79%). 2D NMR spectroscopy revealed a nuclear overhauser effect (NOE) between the methylene protons in the substituents at the 1- and 5- positions (**Figure B1**). 1H NMR (CDCl3, 399.67 MHz): 7.59 (s, 1H), 4.64 – 4.60 (m, 4H), 4.45 – 4.42 (t, 3J = 6.4 Hz, 2H), 3.18 – 3.15 (t, 3J = 6.8 Hz, 2H), 1.89 (s, 6H), 1.85 (s, 6H). 13C NMR (CDCl3, 399.67 MHz): 171.43, 171.20, 133.75, 132.62, 132.02, 128.43, 64.55, 63.85, 63.17, 55.05, 49.56, 46.14, 30.60, 22.64. IR (ATR): 2929.02, 2247.60, 2105.93, 1737.74, 1557.87, 1463.27, 1390.80, 1372.16, 1272.57, 1160.58, 1110.05, 1014.47, 917.49, 833.67, 761.98. HRMS: [MH]+ calcd. for C14H22Br2N3O4: 453.9977. Found: 453.9977. Anal. Calcd. for C14H21Br2N3O4: C, 36.94; H, 4.65; N, 9.23. Found: C, 36.60; H, 4.91; N, 9.02.

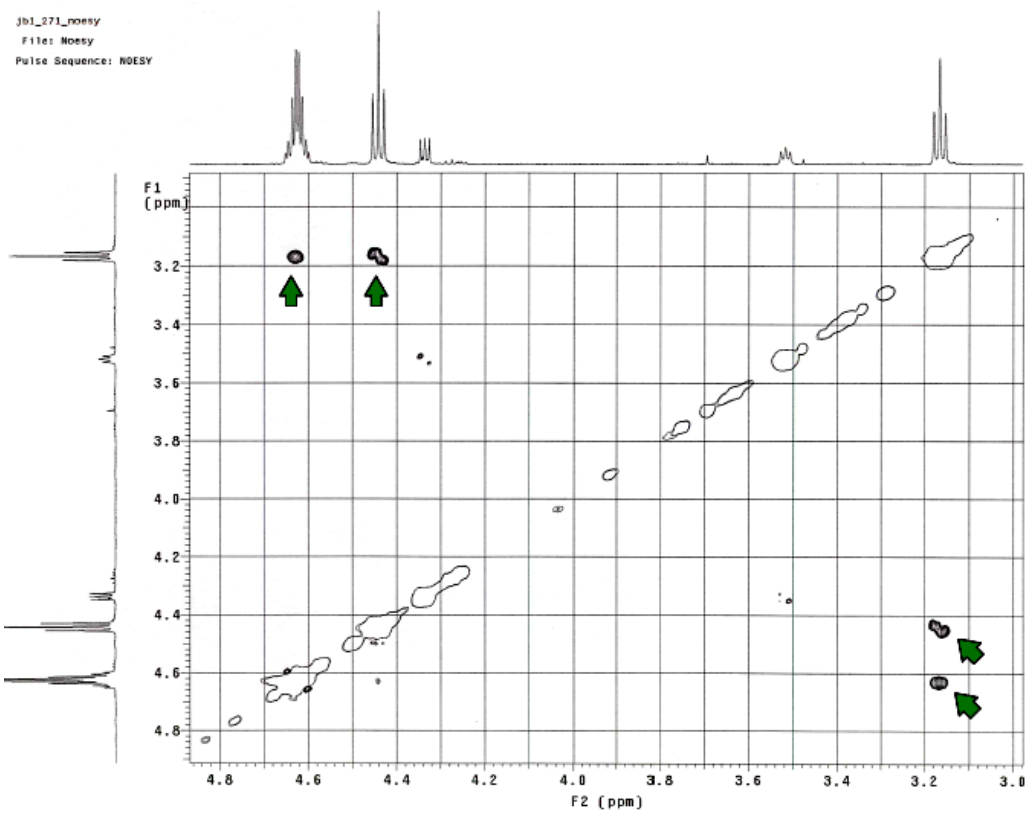

Figure B1 NOESY NMR analysis of 4.3 (green arrows indicate NOEs).

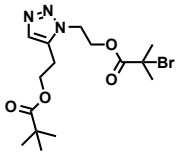

2-(1-(2-((2-bromo-2-methylpropanoyl)oxy)ethyl)-1*H*-1,2,3-triazol-5-yl)ethyl pivalate (4.5). A 50 mL vial with a Teflon cap was charged with a stir bar, 3-butynyl-2,2-dimethylpropanoate (0.035 g, 0.21 mmol), 2-azidoethyl-2-bromo-2-methylpropanoate (0.05 g, 0.21 mmol), and tetrahydrofuran (THF, 5.0 mL) in a glovebox. Pentamethylcyclopentadienylbis(triphenylphosphine) ruthenium(II) chloride (0.0034 g in 1 mL THF) was added to the resulting mixture, and the reaction was stirred at 65 °C for 2 h. The solvent was removed under reduced pressure, and the resulting residue was purified using column chromatography (eluted with hexanes followed by 1:1

hexanes/ethyl acetate) to afford the desired product as a yellow oil (0.057 g, 70%). ^{1}H NMR ($CDCl_3$, 399.67 MHz): 7.52 (s, 1H), 4.61 (bs, 4H), 4.34 – 4.31 (t, ^{3}J = 6.8 Hz, 2H), 3.11 – 3.08 (t, ^{3}J = 6.8 Hz, 2H), 1.85 (s, 6H), 1.64 (s, 9H). ^{13}C NMR ($CDCl_3$, 399.67 MHz): 178.25, 171.19, 132.57, 63.85, 61.55, 54.95, 46.02, 38.68, 30.58, 27.07, 22.93. IR (ATR): 2984.36, 2253.60, 1722.87, 1480.20, 1282.61, 1151.93, 1036.34, 905.40, 828.73, 816.79, 805.08, 795.29, 782.15, 766.93, 729.51. HRMS: $[MH]^+$ calcd. for $C_{15}H_{25}BrN_3O_4$: 390.1028. Found: 390.1032. Anal. Calcd. for $C_{15}H_{24}BrN_3O_4$: C, 46.16; H, 6.20; N, 10.77. Found: C, 46.24; H, 6.13; N, 10.73.

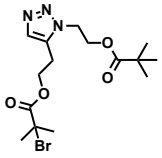

2-(5-(2-((2-bromo-2-methylpropanoyl)oxy)ethyl)-1*H*-1,2,3-triazol-1-yl)ethyl pivalate (4.6). A 50 mL vial with a Teflon cap was charged with a stir bar, 3-butynyl-2-bromo-2-methylpropanoate (0.045 g, 0.21 mmol), 2-azidoethyl-2,2-methylpropanoate (0.035 g, 0.21 mmol), and tetrahydrofuran (THF, 5.0 mL) in a glovebox. Pentamethylcyclopentadienylbis(triphenylphosphine) ruthenium(II) chloride (0.0034 g in 1 mL THF) was added to the resulting mixture, and the reaction was stirred at 65 °C for 2 h. The solvent was removed under reduced pressure, and the resulting residue was purified using column chromatography (eluted with hexanes followed by 1:1 hexanes/ethyl acetate) to afford the desired product as a yellow oil (0.059 g, 72%). ^{1}H NMR ($CDCl_3$, 399.67 MHz): 7.59 (s, 1H), 4.60 – 4.57 (t, ^{3}J = 5.6 Hz, 2H), 4.49 – 4.46 (t, ^{3}J = 5.6 Hz, 2H), 4.44 – 4.41 (t, ^{3}J = 6.8 Hz, 2H), 3.13 – 3.10 (t, ^{3}J = 6.8 Hz, 2H) 1.89 (s, 6H), 1.12 (s, 9H). ^{13}C NMR ($CDCl_3$, 399.67 MHz): 178.01, 171.42, 132.01, 128.55, 63.15, 62.32, 46.44, 38.65, 30.55, 27.05, 22.56. IR (ATR): 2979.96, 2359.98, 2340.51, 2114.31, 1734.15, 1463.55, 1369.31, 1279.09, 1158.20, 1111.18, 1014.50, 916.35,

844.84, 772.48, 746.42. HRMS: $[MH]^+$ calcd. for $C_{15}H_{25}BrN_3O_4$: 390.1028. Found: 390.1031. Anal. Calcd. for $C_{15}H_{24}BrN_3O_4$: C, 46.16; H, 6.20; N, 10.77. Found: C, 46.24; H, 6.19; N, 10.98.

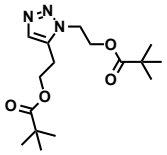

1,5-(2-((2,2-dimethylpropanoyl)oxy)ethyl)-1*H*-1,2,3-triazol-5-yl (4.7). A 50 mL vial with a Teflon cap was charged with a stir bar, 3-butynyl-2,2-dimethylpropanoate (0.045 g, 0.29 mmol), 2-azidoethyl-2,2-dimethylpropanoate (0.05 g, 0.29 mmol), and tetrahydrofuran (THF, 5.0 mL) in a glovebox. Pentamethylcyclopentadienylbis(triphenylphosphine) ruthenium(II) chloride (0.0046 g in 1 mL THF) was added to the resulting mixture, and the reaction was stirred at 65 °C for 2 h. The solvent was removed under reduced pressure, and the resulting residue was purified using column chromatography (eluted with hexanes followed by 1:1 hexanes/ethyl acetate) to afford the desired product as a yellow oil (0.072 g, 77%). ^{1}H NMR ($CDCl_3$, 399.67 MHz): 7.52 (s, 1H), 4.57 – 4.55 (t, ^3J = 6.0 Hz, 2H), 4.84 – 4.46 (t, ^3J = 5.2 Hz, 2H), 4.33 – 4.29 (t, ^3J = 6.4 Hz, 2H), 3.06 – 3.03 (t, ^3J = 6.4 Hz, 2H), 1.16 (s, 9H), 1.12 (s, 9H). ^{13}C NMR ($CDCl_3$, 399.67 MHz): 178.23, 177.99, 133.77, 132.51, 62.35, 61.55, 46.32, 38.67, 27.07, 27.04, 27.02, 26.99, 22.86. IR (ATR): 2973.23, 2253.60, 1726.80, 1480.05, 1461.13, 1399.29, 1366.91, 1282.65, 1239.72, 1152.47, 1036.26, 936.58, 905.58, 806.06, 786.58, 729.48. HRMS: $[MH]^+$ calcd. for $C_{16}H_{28}N_3O_4$: 326.2080. Found: 326.2082. Anal. Calcd. for $C_{16}H_{27}N_3O_4$: C, 59.06; H, 8.36; N, 12.91. Found: C, 58.74; H, 8.21; N, 12.46.

Representative Procedure for Preparation of $\mathbf{4.4}_{Mn}$ Polymers: Synthesis of $\mathbf{4.4}_{156}$. A Schlenk flask was charged with a stir bar wrapped with copper wire, **4.3** (0.0054 g, 0.012 mmol), methyl acrylate (2.0 mL, 22.2 mmol), Me_6TREN (1 mL, 0.1 M solution in DMSO), and DMSO (2 mL) under an atmosphere of nitrogen. The reaction mixture was stirred for 3 h at room temperature, after which time the resulting polymer was collected by precipitation from methanol with subsequent filtration (1.75 g, 92%). GPC analysis revealed the isolated polymer had a number average molecular weight (M_n) of 156 kDa and a polydispersity index (PDI) of 1.4. Additional polymers of varying molecular weights (19, 27, 42, 81, and 90 kDa) were synthesized according to this procedure by varying the initial monomer to initiator ratios; see **Table B1**.

$\mathbf{4.8}_{118}$. A Schlenk flask was charged with a stir bar wrapped with copper wire, **4.5** (0.013 g, 0.033 mmol), methyl acrylate (1.0 mL, 11.1 mmol), Me_6TREN (1 mL, 0.1 M solution in DMSO), and DMSO (2 mL) under an atmosphere of nitrogen. The reaction mixture was stirred for 3 h at room temperature, after which time the resulting polymer was collected by precipitation from methanol with subsequent filtration (2.5 g, 63%). GPC analysis revealed the isolated polymer had a number average molecular weight of 118 kDa and a polydispersity index of 1.4.

$\mathbf{4.9}_{140}$. A Schlenk flask was charged with a stir bar wrapped with copper wire, **4.6** (0.0014 g, 0.0036 mmol), methyl acrylate (0.4 mL, 4.44 mmol), Me_6TREN (1 mL, 0.1 M solution in DMSO), and DMSO (1 mL) under an atmosphere of nitrogen. The reaction mixture was stirred for 3 h at room temperature, after which time the resulting polymer was collected by precipitation from methanol with subsequent filtration (0.4 g, 95%). GPC analysis revealed the isolated polymer had a number average molecular weight of 140 kDa and a polydispersity index of 1.4.

4.10_{91}. **4.10_{91}** was prepared according to the previously reported procedure (see Appendix A).[7] GPC analysis revealed the isolated polymer had a number average molecular weight of 91 kDa and a polydispersity index of 1.4.

4.11_{90}. **4.11_{90}** was prepared according to the procedure used for **4.4_{Mn}**.[7] GPC analysis revealed the isolated polymer had a number average molecular weight of 90 kDa and a polydispersity index of 1.4.

Table B1 Selected Yield and Molecular Weight Data†

Polymer	Presonication			Postsonication		Sonication Time
	Yield	M_n (kDa)	PDI	M_n (kDa)	PDI	(h)
4.4_{156}	92%	156	1.4	80	1.5	2
4.4_{81}	93%	81	1.4	42	1.3	5
4.4_{42}	74%	42	1.3	20	1.4	5
4.4_{27}	65%	27	1.4	14	1.6	7
4.4_{19}	62%	19	1.4	19	1.3	7
4.8_{118}	63%	25	1.4	66	1.3	2
4.9_{140}	95%	140	1.4	71	1.3	2
4.10_{91}	88%	91	1.4	53	1.5	5
4.11_{90}	90%	90	1.4	50	1.5	5

†The M_n refers to the number average molecular weight. The polydispersity index (PDI) was calculated using the equation PDI = M_w/M_n, where M_w is the weight average molecular weight. M_n and M_w were determined as their polystyrene equivalents by GPC (eluent = THF).

General Procedure Used For Sonochemical Activation of $\mathbf{4.4}_{MN}$

A Suslick cell was charged with 10 mL of a 10 mg mL^{-1} solution of $\mathbf{4.4}_{Mn}$ in CH_3CN and sonicated using the general procedure described above. After sonication for the time given in **Table B1**, the solvent was removed under reduced pressure. The residual polymer was dissolved in tetrahydrofuran and the polymer was characterized by GPC (**Table B1** and **Figure B2**).

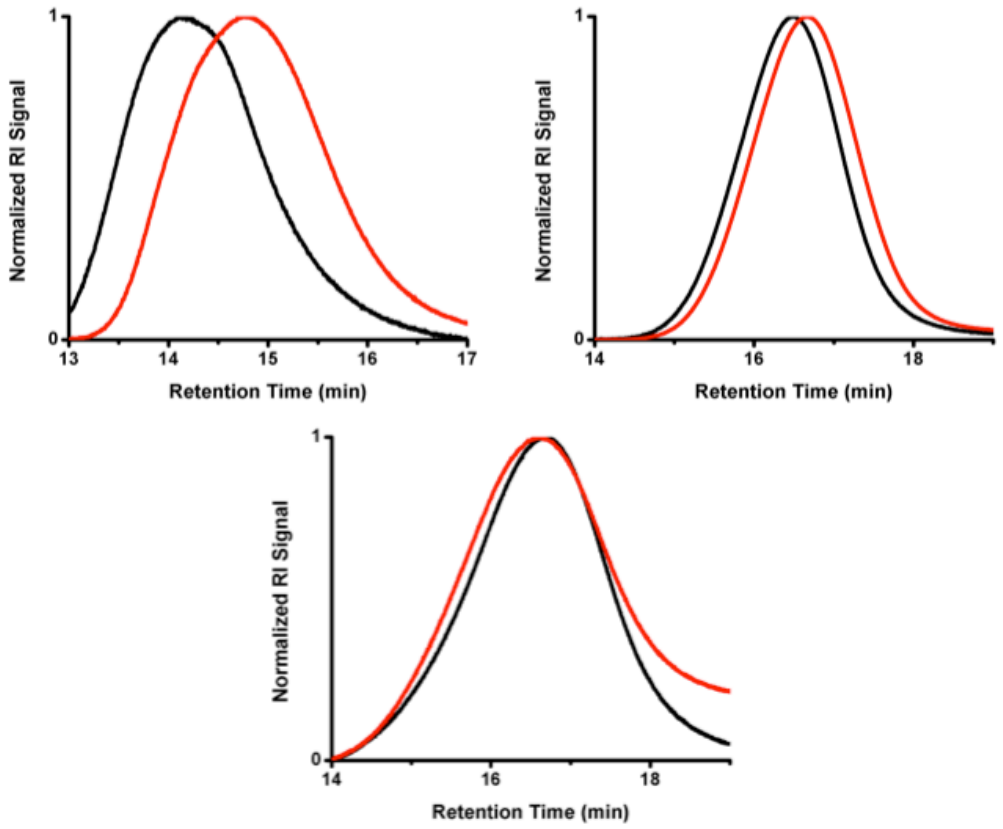

Figure B2 GPC traces of $\mathbf{4.4}_{156}$ (top, left), $\mathbf{4.4}_{27}$ (top, right), and $\mathbf{4.4}_{19}$ (bottom) before (black) and after sonochemical activation (red).

General Procedure for Ultrasonication of $\mathbf{4.8_{118}}$, $\mathbf{4.9_{140}}$, and **4.7**

A Suslick cell was charged with 10 mL of a 10 mg mL^{-1} solution of $\mathbf{4.8_{118}}$ or $\mathbf{4.9_{140}}$ in CH_3CN and sonicated according to the general procedure described above. After sonication for the time given in **Table B1**, the solvent was removed under reduced pressure, and the resulting material was washed with MeOH (3 × 10 mL). The residual polymer was then dissolved in tetrahydrofuran (10 mg mL^{-1}) and characterized by GPC (**Table B1** and **Figure B3**). Separately, a Suslick cell was charged with 10 mL of a 10 mg mL^{-1} solution of **4.7** in CH_3CN. After sonication for 7 h, the solvent was removed under reduced pressure. The corresponding residue was dried under high vacuum and then analyzed by ^1H NMR spectroscopy ($CDCl_3$, **Figure B4**).

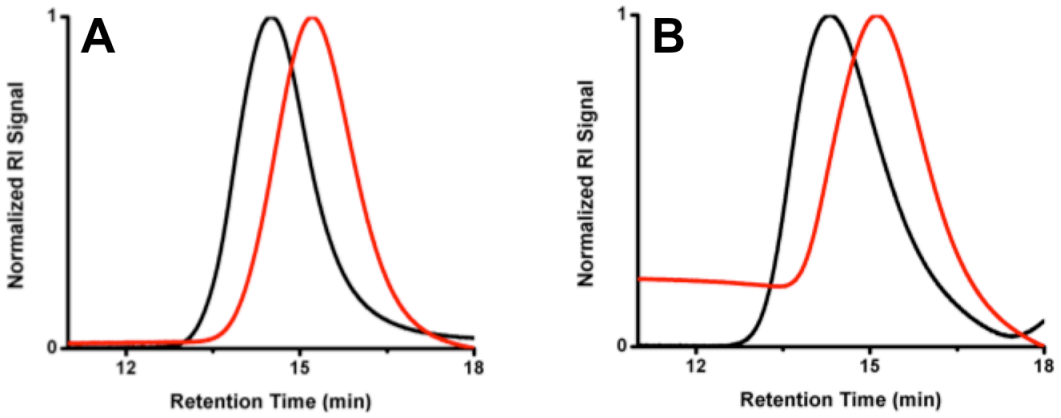

Figure B3 GPC traces of preseonicated (black) and postsonicated (red) $\mathbf{4.8_{118}}$ (A) and $\mathbf{4.9_{140}}$ (B).

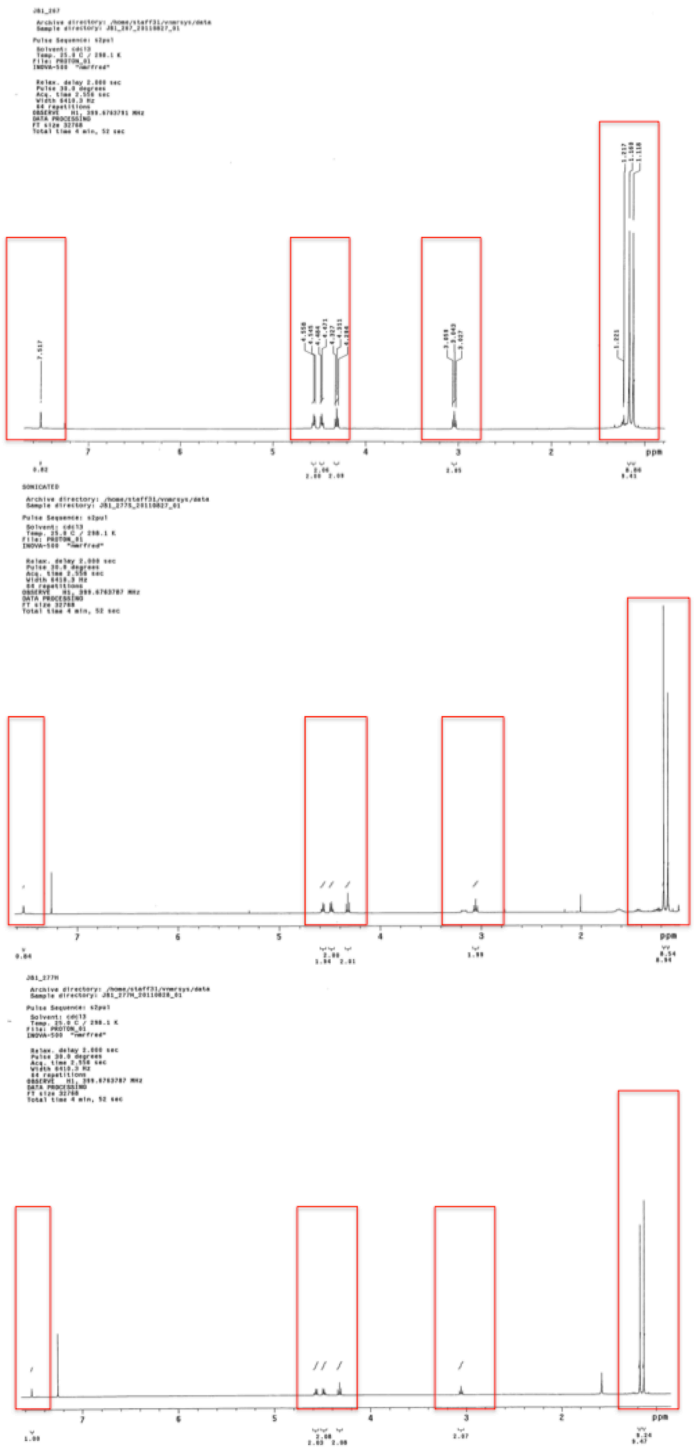

Figure B4 ^{1}H NMR spectra of **6** (top) after sonication (middle) and thermal treatment (bottom). The triazole resonances are indicated with red squares. The additional signals are from residual solvent.

General Procedure for the IR Analysis of PMATMn After Sonochemical Activation

4.4$_{Mn}$ was subjected to the ultrasonication and isolation procedures described above. The resulting material was dissolved in THF (10 mg mL^{-1}) and analyzed using infrared (IR) spectroscopy. A representative IR spectrum of **4.4$_{156}$** following ultrasonication is shown in **Figure B5**.

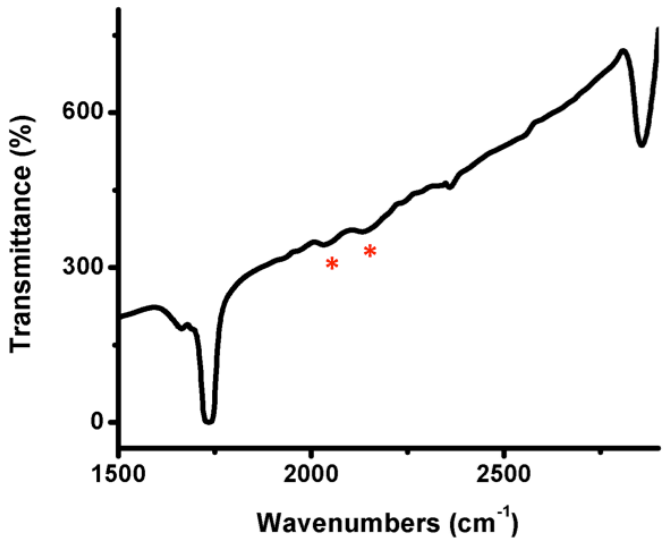

Figure B5 Infrared spectrum of **4.4$_{156}$** (THF; 10 mg mL-1) following sonication. The red asterisks indicate stretches at 2033 cm^{-1} and 2132 cm^{-1}.

General Procedure for the Thermal Activation of 4.4$_{81}$ and 4.7

A 50 mL round bottom was charged with 10 mL of a 10 mg mL^{-1} **4.4$_{81}$** in degassed diphenyl ether. The resulting solution was heated under nitrogen for 24 h at 220 °C in a sand bath. After pouring the resulting reaction mixture into excess MeOH, the precipitated material was collected by filtration, dissolved in tetrahydrofuran (10 mg mL^{-1}) and then characterized by GPC (**Figure 4.1A**).

An 8 mL vial was charged with 0.10 g of **4.7** under a cone of nitrogen and sealed. The sample was then heated in the bulk for 24 h at 220 °C in a sand bath. After cooling, the residue was analyzed by ^{1}H NMR spectroscopy ($CDCl_3$, **Figure B4**).

Representative Procedure for Alkyne Labeling Experiments Performed After the Sonication of $\mathbf{4.4_{MN}}$: Labeling of $\mathbf{4.4_{81}}$

A Suslick cell was charged with 10 mL of a 10 mg mL^{-1} solution of $\mathbf{4.4_{81}}$ in CH_3CN and subjected to the sonication conditions described above. The polymer was isolated by precipitation from excess MeOH followed by filtration. A 25 mL flask was charged with the isolated material (0.05 g, 0.001 mmol), 1-azidopyrene (3.0 mg, 0.01 mmol), and CH_3CN (5 mL). The resulting solution was degassed by sparging with nitrogen, and copper (I) iodide (10 mg, 0.05 mmol) was added under a cone of nitrogen. After sealing the reaction vessel under nitrogen, the reaction mixture was allowed to stir for 24 h at 85 °C. The reaction mixture was diluted with excess MeOH, and the precipitated polymer was collected via filtration after centrifugation. The isolated polymer was washed with MeOH (3 × 10 mL), dried under reduced pressure, dissolved in THF (10 mg mL^{-1}), and analyzed by GPC with ultraviolet-visible detection at 345 nm (**Figure 4.1C**).

Representative Procedure for the Sonication and Alkyne Labeling of $\mathbf{4.8_{118}}$ and $\mathbf{4.9_{140}}$: Labeling of $\mathbf{4.8_{118}}$

A Suslick cell was charged with 10 mL of a 10 mg mL^{-1} solution of $\mathbf{4.8_{118}}$ in CH_3CN and subjected to the sonication conditions described above. The polymer was isolated by precipitation from excess MeOH followed by filtration. A 25 mL flask was charged with the isolated material (0.05 g, 0.001 mmol), 1-azidopyrene (0.003 g, 0.01 mmol), and CH_3CN (5 mL). The resulting solution was degassed by sparging with nitrogen, and copper (I) iodide (10 mg, 0.05 mmol) was added under a cone of nitrogen.

After sealing the reaction vessel under nitrogen, the reaction mixture was allowed to stir for 24 h at 85 °C. The reaction mixture was diluted with excess MeOH, and the precipitated polymer was collected via filtration after centrifugation. The isolated polymer was washed with MeOH (3 × 10 mL), dried under reduced pressure, and analyzed by GPC visualized with ultraviolet-visible detection at 345 nm (**Figure B6**). Additionally, presonicated $\mathbf{4.8}_{118}$ was subjected to an identical procedure (**Figure B6**).

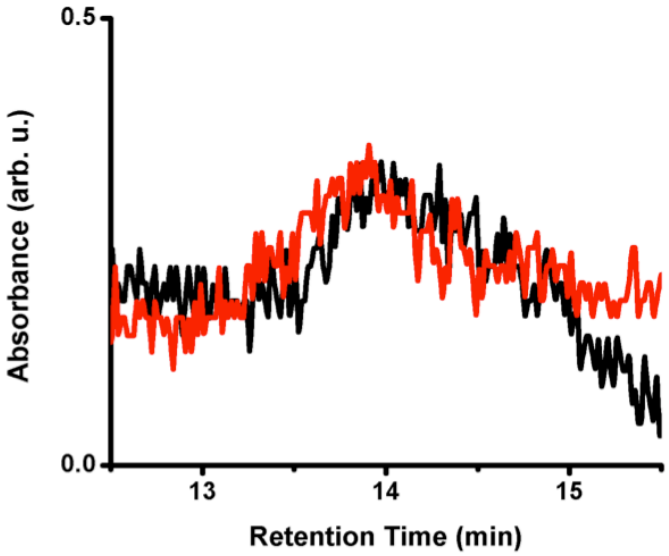

Figure B6 GPC traces visualized with ultraviolet-visible detection at 345 nm of presonicated $\mathbf{4.8}_{118}$ (red) and postsonicated $\mathbf{4.8}_{118}$ (black) after treatment with 1-azidopyrene and CuI.

Representative Procedure for Azide Labeling Experiments Performed After the Sonication of $\mathbf{4.4}_{MN}$: Labeling of $\mathbf{4.4}_{81}$

A Suslick cell was charged with 10 mL of a 10 mg mL^{-1} solution of $\mathbf{4.4}_{81}$ in CH_3CN and subjected to the sonication conditions described above. The polymer was isolated by precipitation into excess MeOH followed by filtration. In a glovebox, a 20 mL vial was charged with the isolated polymer (0.05 g, 0.001 mmol) and tetrahydrofuran (5 mL). **NQMes** (0.0043 g, 0.01 mmol) was added, the vial was sealed with a Teflon lined

cap, and the reaction mixture was stirred at room temperature. After 24 hours, the reaction mixture was diluted with excess MeOH, and the precipitated polymer was collected via filtration after centrifugation. The isolated polymer was washed with MeOH (3 × 10 mL) and dried under reduced pressure. The resulting material was dissolved in THF (10 mg mL^{-1}) and analyzed by GPC with ultraviolet-visible detection at 315 nm (**Figure 4.1B**).

Representative Procedure for the Sonication and Azide Labeling of $\mathbf{4.8_{118}}$ and $\mathbf{4.9_{140}}$: Labeling of $\mathbf{4.8_{118}}$

A Suslick cell was charged with 10 mL of a 10 mg mL^{-1} solution of $\mathbf{4.8_{118}}$ in CH_3CN and subjected to the sonication conditions described above. The polymer was isolated by precipitation into excess MeOH followed by filtration. In a glovebox, a 20 mL vial was charged with the isolated polymer (0.05 g, 0.001 mmol) and tetrahydrofuran (5 mL). **NQMes** (0.0043 g, 0.01 mmol) was added, the vial was sealed with a Teflon lined cap, and the reaction mixture was stirred at room temperature. After 24 hours, the reaction mixture was diluted with excess MeOH, and the precipitated polymer was collected via filtration after centrifugation. The isolated polymer was washed with MeOH (3 × 10 mL) and dried under reduced pressure. The resulting material was analyzed by GPC with ultraviolet-visible detection at 315 nm (**Figure B7**). Additionally, presonicated $\mathbf{4.8_{118}}$ was subjected to an identical procedure (**Figure B7**).

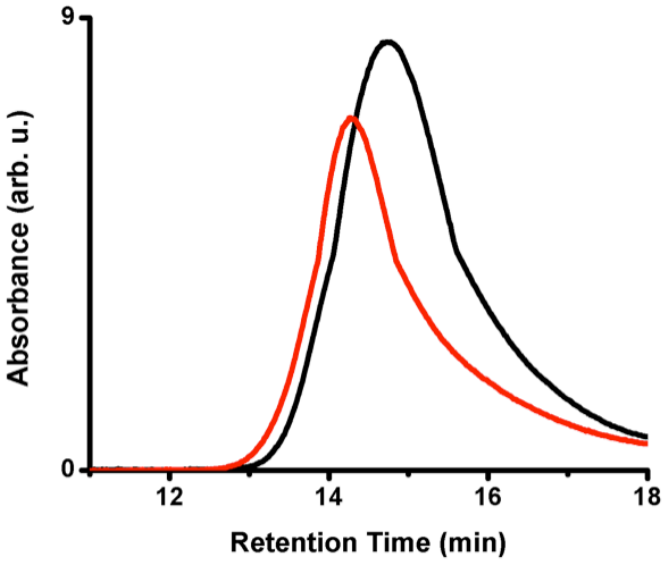

Figure B7 GPC traces visualized with ultraviolet-visible detection at 315 nm of presonicated $\mathbf{4.8_{118}}$ (red) and postsonicated $\mathbf{4.8_{118}}$ (black), both after treatment with **NQMes**.

RECOUPLING OF POLYMERIC FRAGMENTS

A Suslick cell was charged with 10 mL of a 10 mg mL^{-1} solution of $\mathbf{4.4_{81}}$ in CH_3CN and subjected to the sonication conditions described above (see **Table 4.1**). The resulting polymer product was isolated by precipitation into excess MeOH followed by filtration. A 25 mL flask was charged with the isolated material (0.10 g, 0.002 mmol) and CH_3CN (10 mL). The resulting solution was degassed by sparging with nitrogen, and copper (I) iodide (0.01 g, 0.05 mmol) was added under a cone of nitrogen. After sealing the reaction vessel under nitrogen, the reaction mixture was allowed to stir for 24 h at 85 °C. The reaction mixture was diluted with excess MeOH, and the precipitated polymer was collected via filtration after centrifugation. The isolated material was washed with MeOH (3 × 15 mL) and dried under reduced pressure. GPC: M_n = 79 kDa; PDI = 1.5 (**Table B2**, **Figure 4.1D**).

General Procedure For Determining Rate of Cycloreversion: Sonication and GPC Monitoring of $\mathbf{4.11_{91}}$

A Suslick cell was charged with 15 mL of a 10 mg mL^{-1} solution of $\mathbf{4.11_{91}}$ in CH_3CN and subjected to the sonication conditions described above. Every 30 minutes, 0.25 mL aliquots were removed and dried under reduced pressure. The residual materials were then dissolved in THF (1.0 mL) and analyzed by GPC. A representative set of GPC traces is shown in **Figure B8**. This procedure was repeated in duplicate, and the average M_n for each data point is given in **Table B2**. The reciprocal of the M_n values given in **Table B2** were calculated, and the reciprocal of the initial M_n value (0.011) was subtracted from each data point. The resulting values were then plotted vs. the corresponding time point. Linear regression analysis was then performed on the data, and the slope was taken to be the observed rate constant (**Figure 4.2**). The r^2 value (**Figure 4.2**, blue) was 0.99, and the error was $\pm$ 1.04 $\times$ 10^{-6}.

The same procedure was repeated for $\mathbf{4.10_{90}}$. The r^2 value for the linear regression of the resulting curve (**Figure 4.2**, red) was 0.99, and the error was $\pm$ 1.08 $\times$ 10^{-6}.

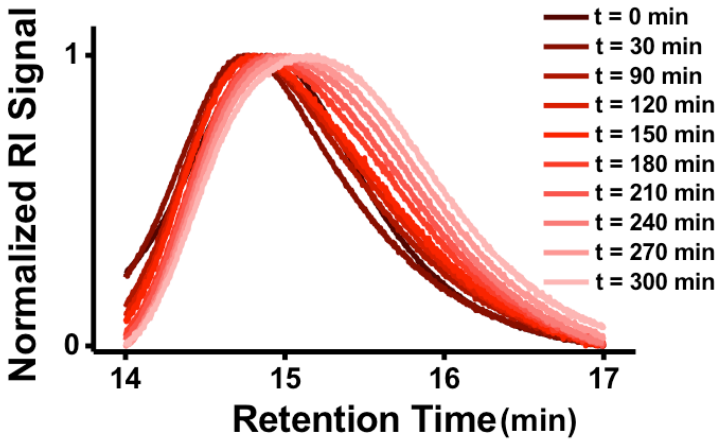

Figure B8 Time-lapsed GPC traces of sonicated $\mathbf{4.11_{91}}$.

Table B2 Representative Kinetic Data

M_n (kDa) (4.11_{90})	Time (min)	M_n (kDa) (4.10_{91})	Time (min)
90	0	91	0
81	30	87	60
73	90	78	90
69	120	73	120
62	150	69	150
58	180	65	180
55	210	60	210
54	240	59	240
53	273	55	270
50	303	53	300

COORDINATES AND ENERGIES OF TRIAZOLE ANALOGUES 4.5 – 4.11

4.5 Reactant Geometry (-320.859501519022 Hartrees)

C	0.08839139	1.10677489	0.00280770
N	-1.19853671	0.64304524	0.01493029
N	-1.19096514	-0.66172265	0.01422740
N	0.10048594	-1.06134532	0.00164520
C	0.93023290	0.01429886	-0.00579820
C	0.42247897	-2.47623668	-0.00213417
H	2.00587516	-0.07980058	-0.01616942

C	0.40716300	2.56873104	0.00047739
H	0.98782031	-2.74177882	-0.90082206
H	-0.52349981	-3.01886013	0.00664735
H	1.00490823	-2.74266318	0.88530940
H	-0.02392434	3.06324495	-0.87724443
H	1.48850149	2.73599656	-0.01024210
H	-0.00626099	3.06223279	0.88722497

4.5 Transition State Geometry (-320.714892346123 Hartrees; 1 Imaginary Frequency)

C	-0.57689457	-1.46129974	0.00000000
N	1.27219473	-0.38570083	0.00000000
N	0.88100332	0.72377926	0.00000000
N	-0.23104835	1.30745893	0.00000000
C	-1.43578628	-0.57295895	0.00000000
C	-0.32565755	2.76477633	0.00000000
H	-2.35760670	-0.03751974	0.00000000
C	-0.02395899	-2.82801431	0.00000000
H	-0.87292476	3.10121319	-0.88841656
H	0.66221277	3.23330791	0.00000000
H	-0.87292476	3.10121319	0.88841656
H	0.60634906	-2.99074727	-0.88044052
H	-0.82455516	-3.57594573	0.00000000
H	0.60634906	-2.99074727	0.88044052

4.6 Reactant Geometry (-320.856620445916 Hartrees)

C	-1.89059802	-0.79613658	0.00000000
N	-0.66474868	-0.01556910	0.00000000
C	0.64266850	-0.40800138	0.00000000
C	1.32932251	0.79176302	0.00000000
N	0.44349936	1.82256744	0.00000000
N	-0.76786337	1.33734077	0.00000000
H	-1.65169462	-1.85971638	0.00000000
H	-2.47840094	-0.55856068	0.89023503
H	-2.47840094	-0.55856068	-0.89023503
H	2.39708841	0.96070456	0.00000000
C	1.13625895	-1.82141158	0.00000000
H	1.75381276	-2.01970578	0.88320826
H	0.32168069	-2.55055521	0.00000000
H	1.75381276	-2.01970578	-0.88320826

4.6 Transition State Geometry (-320.714998000394 Hartrees; 1 Imaginary Frequency)

C	1.97165018	-1.23987881	0.00000000
N	0.64771419	-0.63047126	0.00000000
C	-0.49980645	1.36583901	0.00000000
C	-1.63935916	0.88737637	0.00000000
N	-1.54913259	-1.19260758	0.00000000
N	-0.38286266	-1.35117143	0.00000000
H	2.69255352	-0.41791411	0.00000000

H	2.15164809	-1.85069652	0.89398277
H	2.15164809	-1.85069652	-0.89398277
H	-2.70737849	0.91051556	0.00000000
C	0.60726117	2.33532985	0.00000000
H	0.54337207	2.98138803	0.88439445
H	1.59221596	1.86455847	0.00000000
H	0.54337207	2.98138803	-0.88439445

4.7 Reactant Geometry (-388.2631751397 Hartrees)

N	-0.98121994	0.41250573	0.00000000
N	0.14067895	1.16636718	0.00000000
H	-1.88231432	0.87032563	0.00000000
C	-0.69395195	-0.91300056	0.00000000
N	1.15038138	0.34068497	0.00000000
C	0.68201416	-0.94190285	0.00000000
H	-1.45188358	-1.68094095	0.00000000
H	1.35224471	-1.78869494	0.00000000

4.7 Transition State Geometry (-388.2019016952 Hartrees; 1 Imaginary Frequency)

N	1.11194869	0.74503464	0.17580722
N	-0.06955390	1.17594383	0.04744396
H	1.80871274	1.38611507	-0.21052849
C	0.57446212	-1.39037850	0.00124463
N	-1.15543624	0.74168133	0.02187840

C	-0.65700957	-1.33398563	-0.02782790
H	1.58879678	-1.71854096	0.03639008
H	-1.66657667	-1.68130169	-0.06346326

4.8 Reactant Geometry (-916.281574599116 Hartrees)

N	0.15385612	1.07813218	0.00279839
N	1.46455943	0.68788297	0.01132221
C	-0.17347828	2.48216764	0.00169512
C	-0.68022145	0.00388272	-0.00456273
N	1.47102424	-0.60394254	0.00960081
C	0.18170922	-1.06226109	-0.00001793
H	-1.75460114	0.08180163	-0.01191362
C	-0.15119801	-2.51935302	-0.00421338
F	0.31611212	3.07925869	1.08627436
F	-1.50803907	2.60357115	-0.00475447
F	0.32646941	3.08015881	-1.07772630
F	0.33235616	-3.14479462	1.08337073
F	0.34834235	-3.14217937	-1.08605514
F	-1.49490829	-2.67830995	-0.01429234

4.8 Transition State Geometry (-916.146108441572 Hartrees; 1 Imaginary Frequency)

N	0.01853187	-1.34600191	0.41338906
N	-1.07984391	-0.71863439	0.30108214
C	0.06805614	-2.70007203	-0.03671136

C	1.32477420	0.38479683	0.06916655
N	-1.43967255	0.38317845	0.22621443
C	0.51200533	1.31108258	0.02597575
H	2.20988938	-0.21286765	0.08783886
C	0.11048328	2.72437285	-0.10435470
F	-0.63974828	-3.52969821	0.74644176
F	1.35653041	-3.06254320	0.00278286
F	-0.38214628	-2.85598898	-1.29589284
F	-0.56243755	3.14073283	0.98347575
F	-0.67976157	2.90700728	-1.17729289
F	1.18780537	3.52300372	-0.24895898

4.9 Reactant Geometry (-916.255952319825 Hartrees)

N	0.56165828	0.70857666	0.04974728
N	1.79240300	1.29476988	-0.02425365
C	-0.62589033	1.53577075	0.04567836
C	0.67768158	-0.65361977	-0.03956472
N	2.66600521	0.34600075	-0.12908098
C	2.02921784	-0.86239240	-0.14284568
F	-0.33131012	2.73799101	0.51868283
F	-1.56097646	0.96668112	0.81421526
F	-1.11344812	1.65863510	-1.19280475
H	2.56653550	-1.79514872	-0.22253986
C	-0.43994355	-1.64765640	0.00955865

F	-1.41450909	-1.34026863	-0.86960586
F	-1.00015402	-1.71994680	1.23048014
F	0.03870346	-2.86603323	-0.29998218

4.9 Transition State Geometry (-916.146425329957 Hartrees; 1 Imaginary Frequency)

N	-0.39819084	-0.84465426	0.22984833
N	-1.56135975	-1.31292770	0.05778437
C	0.71848262	-1.70838371	-0.00834508
C	-1.00294453	1.27904971	-0.04003752
N	-2.64196563	-0.89034142	-0.06673925
C	-2.22603140	1.16595608	-0.14548706
F	0.68377798	-2.80486956	0.76899675
F	1.82083906	-1.01301575	0.27123511
F	0.78660047	-2.12664815	-1.28636925
H	-3.24299248	1.47659038	-0.26026225
C	0.33019928	1.90397775	0.03858926
F	1.13591507	1.47302143	-0.94933429
F	0.93384875	1.64665967	1.20998842
F	0.21352345	3.24219076	-0.08205534

4.10 Reactant Geometry (-556.747478426514 Hartrees)

C	-0.64474746	-0.00394329	0.22443966
N	0.10417660	-1.08707123	-0.11870082
N	1.25218357	-0.68867114	-0.70793855

N	1.24907668	0.61672426	-0.74648320
C	0.09706161	1.08775518	-0.18193819
C	-0.18886749	2.57198382	-0.08389177
H	-1.60300204	-0.08494277	0.70856305
C	-0.15243318	-2.54235176	0.05496585
C	0.92765240	3.24622836	0.74467580
C	-1.54998494	2.81095940	0.59346201
C	-0.20448758	3.17676122	-1.50577978
H	0.94744100	2.85601180	1.76904067
H	0.76629156	4.33009713	0.79542972
H	1.90719031	3.06070289	0.29400671
H	0.74587205	2.98947194	-2.01446477
H	-0.36831201	4.26047732	-1.45987901
H	-1.00488062	2.73619298	-2.11179761
C	-1.50905164	-2.73972427	0.74292646
C	-0.16027000	-3.19478580	-1.33874954
H	-0.96053286	-2.77622151	-1.95863709
H	-0.32418914	-4.27383620	-1.24474693
H	0.79255307	-3.02529390	-1.84591831
H	-1.53049309	-2.28036585	1.73704653
H	-1.69068742	-3.81181355	0.86715618
H	-2.33037715	-2.32924853	0.14570064
H	-1.56951208	2.40186949	1.61097468
H	-2.36788283	2.35294179	0.02395940
H	-1.75505071	3.88524199199	0.66349446

C	0.97661086	-3.12534540	0.92304216
H	0.98571276	-2.65735334	1.91338489
H	1.94790615	-2.95471621	0.45262736
H	0.82995211	-4.20334351	1.05136521

4.10 Transition State Geometry (-556.606940115397 Hartrees; 1 Imaginary Frequency)

C	-1.16492483	0.40090650	0.58458484
N	0.18235061	-1.35052901	0.38191041
N	1.11605677	-0.69866659	-0.15438672
N	1.39079825	0.41638407	-0.39153203
C	-0.48987767	1.36427408	0.19848258
C	-0.24093487	2.80787192	-0.09441387
H	-1.95493709	-0.18594092	0.99504193
C	0.02712618	-2.79935145	0.09160001
C	0.95195797	3.32316476	0.74085837
C	-1.51286060	3.60082566	0.28848984
C	0.04928514	3.00413050	-1.59857941
H	0.76215945	3.19728789	1.81253954
H	1.10818879	4.39082724	0.54466397
H	1.86906741	2.78450569	0.48966009
H	0.94546501	2.45640473	-1.90029766
H	0.20240791	4.06924492	-1.81035373
H	-0.79046908	2.65232662	-2.20815665
C	-1.24716877	-3.22426163	0.83634326

C	-0.13139014	-3.03270414	-1.42081875
H	-0.97707716	-2.45828125	-1.81337202
H	-0.30669875	-4.09406800	-1.63144957
H	0.77152939	-2.72333835	-1.95892612
H	-1.16121314	-3.01133333	1.90699669
H	-1.41414352	-4.29890702	0.71000005
H	-2.12466590	-2.69712081	0.44664142
H	-1.74357191	3.47999564	1.35225759
H	-2.37727103	3.25672186	-0.28936547
H	-1.36808291	4.66950349	0.08727430
C	1.24252468	-3.56720215	0.64166780
H	1.36476709	-3.37901241	1.71319366
H	2.16050589	-3.25618026	0.13165288
H	1.11412951	-4.64544114	0.49047751

4.11 Reactant Geometry (-556.725626511156 Hartrees)

C	-2.00135537	0.87367771	-0.03328691
N	-2.65794028	-0.30959668	0.00771929
N	-1.77681266	-1.25904353	0.06211546
N	-0.52772903	-0.70823102	0.07251919
C	-0.63052528	0.67505376	-0.00340804
C	0.58625107	-1.72057692	-0.01120682
C	0.40822684	1.80338246	0.00982893

H	-2.54676173	1.80306706	-0.08006264
C	1.51236477	1.64882143	-1.06039937
C	1.02567995	1.98052234	1.41945066
C	-0.32364489	3.12952895	-0.31963608
H	2.17569306	0.80125930	-0.88273685
H	2.13679699	2.54962992	-1.07014148
H	1.07465752	1.53457613	-2.05835375
H	-0.81768016	3.08714528	-1.29587269
H	0.40557221	3.94634659	-0.34410356
H	-1.07284566	3.38074747	0.43730165
H	1.60041778	1.11354274	1.74687962
H	0.23832131	2.15916065	2.15963006
H	1.69701412	2.84780180	1.42321690
C	1.76887463	-1.35112721	0.89646081
C	1.01457883	-1.86250858	-1.48410827
C	0.04882313	-3.08231057	0.47946787
H	2.30343604	-0.45845481	0.57400737
H	2.48627579	-2.17814444	0.88572391
H	1.43644809	-1.20920673	1.92974670
H	1.41686244	-0.93288006	-1.89195664
H	0.15702722	-2.16300133	-2.09410804
H	1.78686183	-2.63479156	-1.57258157
H	-0.33319379	-3.01314528	1.50179029
H	0.87989000	-3.79609498	0.46513504
H	-0.75303017	-3.46005191202	-0.15374325

4.11 Transition State Geometry (-556.603199842278 Hartrees; 1 Imaginary Frequency)

C	-2.14846721	1.16715831	-0.35587193
N	-2.53021754	-0.69426878	-0.44916606
N	-1.50857877	-1.26334743	-0.24501932
N	-0.32055365	-0.96840976	0.04796416
C	-0.96372098	1.45793487	-0.12150135
C	0.66169057	-2.09989769	0.05062263
C	0.26267001	2.24656615	0.11940011
H	-3.14565000	1.50640890	-0.55039740
C	1.32349417	1.95646353	-0.96317450
C	0.82722423	1.97122889	1.52871463
C	-0.15101292	3.74224634	0.02712101
H	1.60995892	0.90260466	-0.95474838
H	2.21660610	2.56711878	-0.78555265
H	0.93765317	2.19379731	-1.96036284
H	-0.56178060	3.97669600	-0.96012110
H	0.72654365	4.37802999	0.19574515
H	-0.90482620	3.98808435	0.78179078
H	1.10218496	0.92104605	1.63955334
H	0.08592980	2.21199988	2.29810863
H	1.71553382	2.59035925	1.70150687
C	1.92616279	-1.60448071	0.76351800
C	0.98665730	-2.49047319	-1.40285053
C	0.08582792	-3.30402168	0.81835183

H	2.36594170	-0.74161343	0.25482414
H	2.67664615	-2.40213921	0.78106299
H	1.70651571	-1.32123716	1.79816895
H	1.37849174	-1.63079860	-1.95700145
H	0.08648104	-2.84464042	-1.91701754
H	1.73618549	-3.29032628	-1.43313899
H	-0.18069773	-3.01750147	1.84128195
H	0.82539342	-4.11150815	0.86771389
H	-0.81242602	-3.68967275	0.32604500

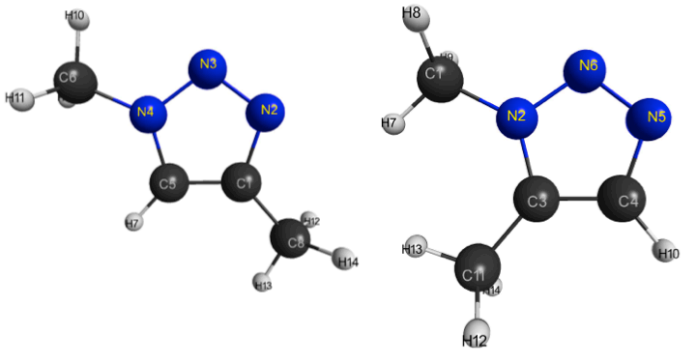

Figure B9 Reactant state geometries of **4.5** (left) and **4.6** (right) with atom labels for EBT analysis.

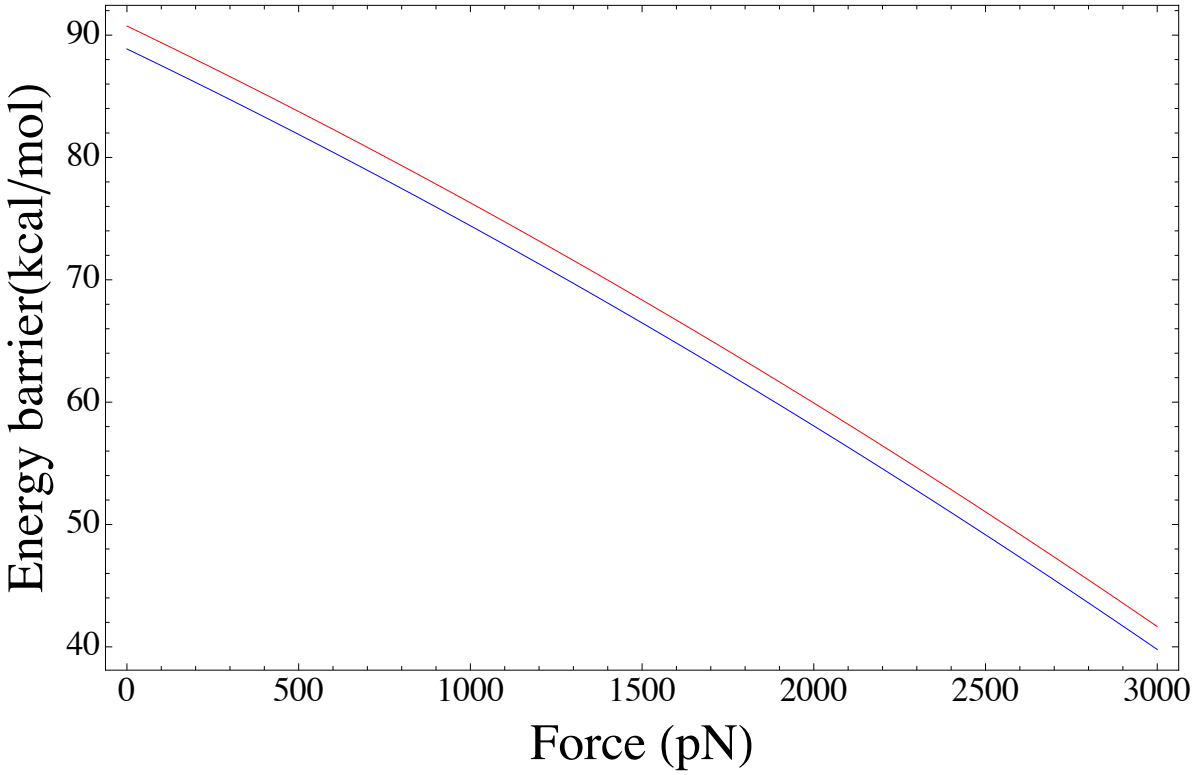

Figure B10 Force curves from EBT analysis of **4.5** (red) and **4.6** (blue) using N_4–C_1 (**4.5**; See **Figure B9**) and N_2–C_3 (**4.6**; See **Figure B9**) as the pulling points.

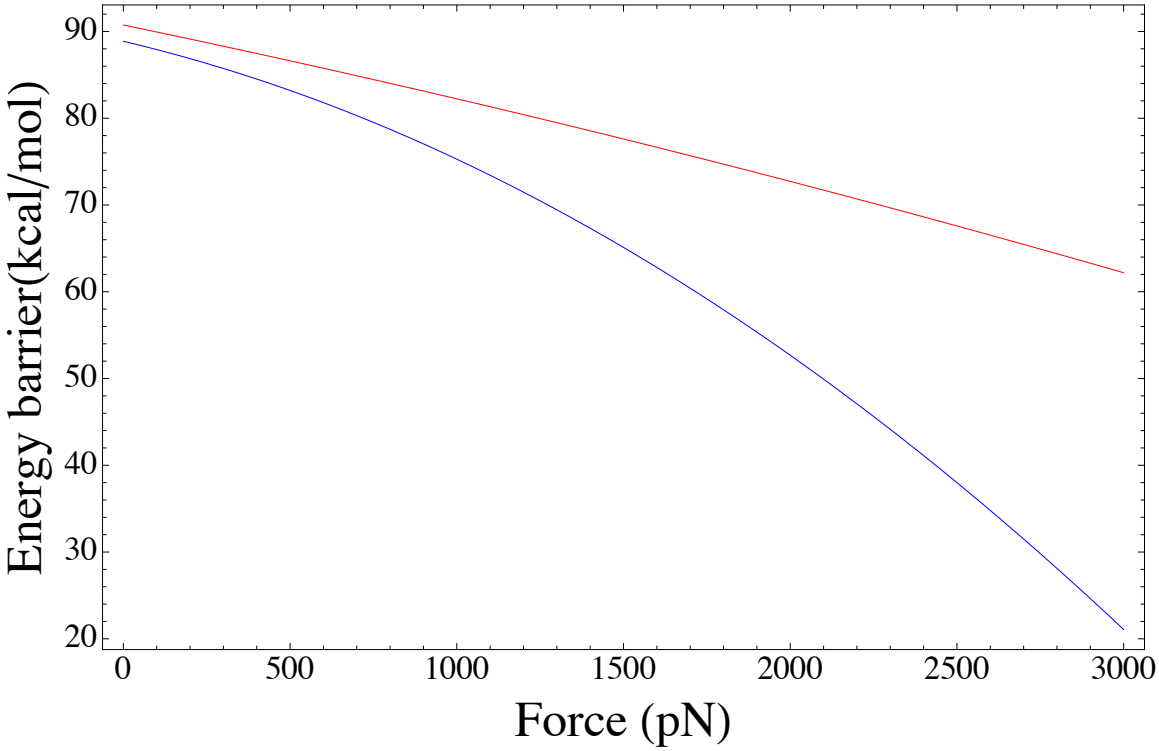

Figure B11 Force curves from EBT analysis of **4.5** (red) and **4.6** (blue) using C_6–C_8 (**4.5**; See **Figure B9**) and C_1–C_{11} (**4.6**; See **Figure B9**) as the pulling points.

REFERENCES

1 Lu, X.; Bittmamn, R. *J. Org. Chem.* **2005**, *70*, 4746.

2 Chiba, K.; Du, H. ; Eguchi, Y.; Fujita, M.; Goto, M.; Gusovsky, F.; Harmange, J.-C.; Inoue, A.; Kawada, M.; Kawai, T.; Kawakami, Y.; Kimura, A.; Kotake, M.; Kuboi, Y.; Matsushima, T.; Mizui, Y.; Muramoto, K.; Sakurai, H.; Shen, Y.- C.; Shirota, H.; Spyvee, M.; Tanaka, I.; Wang, Y.; Wood, R.; Yamamoto, S.; Yoneda, N. *U.S. Pat. Appl. Publ.* **2004**, *20040224936*.

3 Sun, S.; Cao, Y.; Feng, J.; Wu, P. *J. Mater. Chem.* **2010**, *20*, 5605.

4 Schrock, A. K.; Schuster, G. B. *J. Am. Chem. Soc.* **1984**, *106*, 5234.

5 Sanderson, M. D.; Kamplain, J. W.; Bielawski, C. W. *J. Am. Chem. Soc.* **2006**, *128*, 16514.

6 Antonin, H. *Collect. Czech. Chem. Commun.* **1989**, *54*, 446.

7 Brantley, J. N.; Wiggins, K. M.; Bielawski, C. W. *Science* **2011**, *333*, 1606.

8 Nulwala, H.; Takizawa, K.; Odukale, A.; Khan, A.; Thibault, R. J.; Taft, B. R.; Lipshutz, B. H.; Hawker, C. J. *Macromolecules* **2009**, *42*, 6068.

Appendix C

COMPUTATIONAL DETAILS

All EBT calculations were performed with the NWCHEM package[1] using density functional theory (DFT),[2] employing the 6-31G* basis set[3] and the B3LYP exchange-correlation energy functional.[4] DFT with the B3LYP functional was previously used for several mechanochemical studies involving the COGEF and EFEI methods for simulating mechanical stress.[5-7] B3LYP with the 6-31G* basis set was proven to provide excellent geometries for reactants and transition states involving pericyclic reactions.[8] However recent studies have led to the development of new functionals of which the relatively inexpensive M05-2X has shown to compare well with the more expensive and accurate electronic structure methods.[9,10]

We have chosen to compare our computational results from B3LYP/6-31G* with the M05-2X/6-31++G**/6-31G* functional for 5 distinct mechanophores: the conrotatory electrocyclic ring opening of *cis* and *trans*-disubstituted benzocyclobutene, the formal [3+2] cycloreversion of 1,2,3-triazoles, the formal [4+2] cycloreversions of a furan/maleimide Diels-Alder adduct and a maleimide/anthracene Diels-Alder adduct. Computational results from B3LYP/6-31G* were compared with M05-2X/6-31G* for the maleimide/anthracene Diels-Alder adduct owing to the size of the mechanophore. We determined $\Delta\chi$ ($\chi_{TS} - \chi_r$) and ΔR ($R_{TS} - R_r$) for each atom pair using EBT (Equation 5.1 from chapter 5), and plotted the results from M05-2X/6-31++G**/6-31G* in comparison to B3LYP/6-31G* in **Figure C1**.

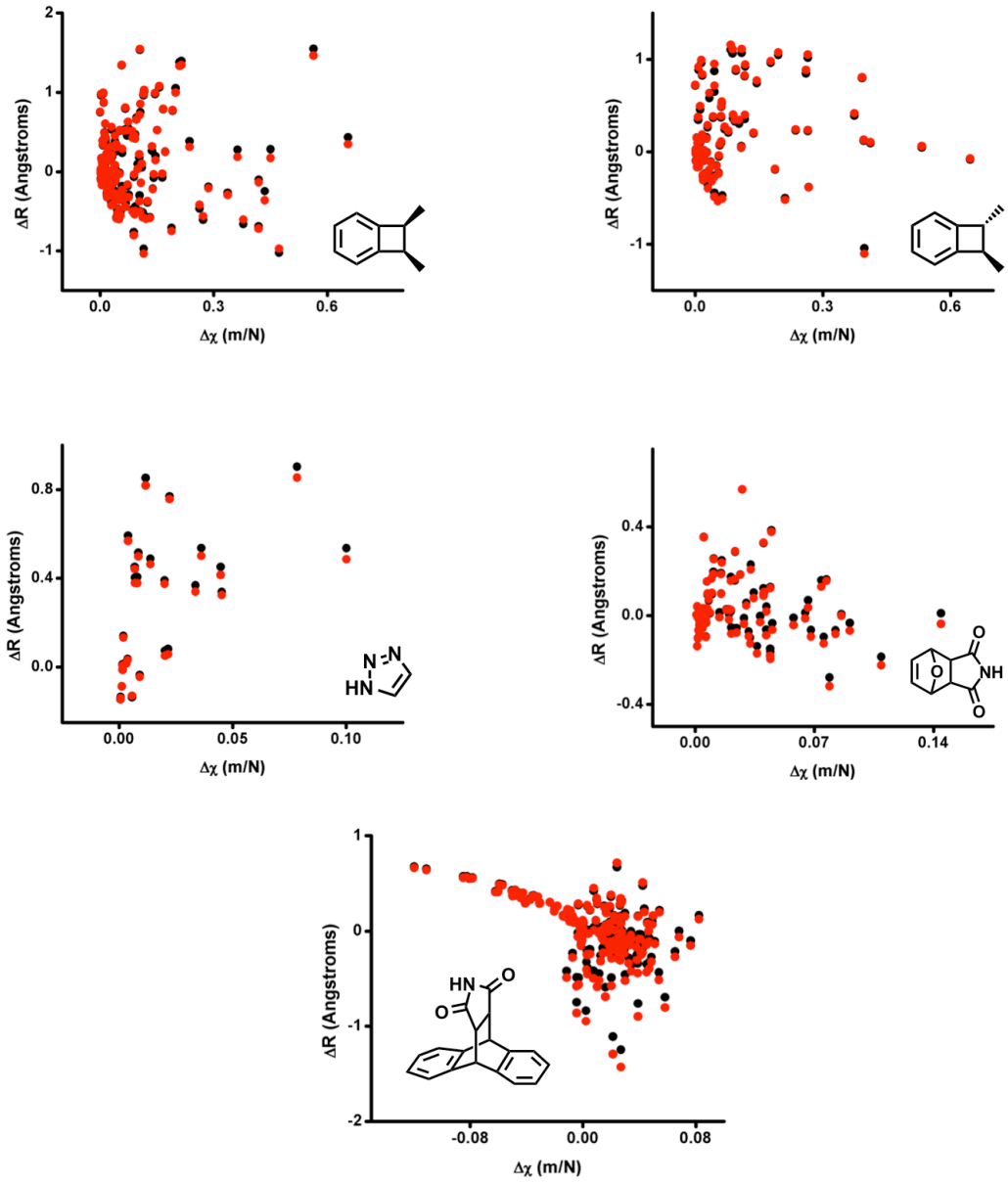

Figure C1 Comparison plots of ΔR and $\Delta\chi$ calculated using B3LYP/6-31G* (black) and M05-2X/6-31++G**/6-31G* (red) functionals.

We have also benchmarked the activation energies using different methods for the following 3 mechanophores: the conrotatory electrocyclic ring opening of *cis*- (**R1**) and *trans*- (**R2**) disubstituted benzocyclobutene and the formal [3+2] cycloreversion of 1,2,3-triazoles (**R3**). They are tabulated in **Table C1**.

Table C1 Activation energy $\Delta E^{\neq}$ (kcal/mol) and thermal correction ΔE^{TC} (kcal/mol) benchmarks.

Method	**Energies (kcal/mol)**	**R1**	**R2**	**R3**
B3LYP/6-31G*	$\Delta E^{\neq}$	42.5365	38.4494	88.7202
	ΔE^{TC}	-2.315	-2.235	-4.235
M05-2X/6-31++G**	$\Delta E^{\neq}$	45.6618	41.6523	97.6548
	ΔE^{TC}	-2.160	-2.046	-4.492
MP2/cc-pVDZ	$\Delta E^{\neq}$	43.034	39.9337	82.422
	ΔE^{TC}	-2.540	-2.409	-4.212
CASSCF(6,6)/6-31G**	$\Delta E^{\neq}$	46.6748	36.5176	97.8246
	ΔE^{TC}	-2.276	-2.728	-4.79

PROBABILITY ARGUMENT

Here we estimate the probability that "random" strain will decrease the energy of the molecule at the TS saddle resulting in $\chi_{TS} < 0$. In the vicinity of a TS saddle-point, the energy of the molecule (relative to that of the saddle) can be written in terms of appropriately chosen normal coordinates as

$$U = -k_1 u_1^2 / 2 + \sum_{i=2}^{n} k_i u_i^2 / 2 \qquad \text{(C.1)}$$

where n = 3N-6 is the total number of degrees of freedom, excluding the translations and rotations. The first term accounts for the displacement along the unstable barrier mode. For simplicity, we will further assume that all k_i's are the same. Whenever the molecule's atoms are subjected to a small displacement, this sets a directional unit vector $\mathbf{u} = (u_1,...,u_n)$ in the n-dimensional space of the molecule's internal degrees of freedom. The ends of all such vectors lie on an n-dimensional sphere of unit radius. The susceptibility χ_{TS} is negative if $-u_1^2 / 2 + \sum_{i=2}^{n} u_i^2 / 2 < 0$. Assuming random direction of the vector, the probability of this is given by

$$P_n = S_{n-1}^{-1} \int ds_{n-1} \theta(u_1^2 - \sum_{i=2}^{n} u_i^2) / \int ds_{n-1} = S_{n-1}^{-1} \int ds_{n-1} \theta(2u_1^2 - 1) \qquad \text{(C.2)}$$

where $\theta(x)$ is the Heaviside step function, $S_{n-1} \equiv \int ds_{n-1} = 2\pi^{n/2} / \Gamma(n/2)$ is the surface area of the sphere, and ds_{n-1} indicates integration over the (n-1)-dimensional surface of the sphere. Using the spherical coordinates

$$u_1 = \cos\varphi_1$$
$$u_2 = \sin\varphi_1 \cos\varphi_2$$
$$u_3 = \sin\varphi_1 \sin\varphi_2 \cos\varphi_3$$
$$...$$
$$u_{n-1} = \sin\varphi_1 \sin\varphi_2 ... \sin\varphi_{n-2} \cos\varphi_{n-1}$$
$$u_n = \sin\varphi_1 \sin\varphi_2 ... \sin\varphi_{n-2} \sin\varphi_{n-1}$$

and

$$ds_{n-1} = \sin^{n-2}\varphi_1 \sin^{n-3}\varphi_2 ... \sin\varphi_{n-2} d\varphi_1 d\varphi_2 .. d\varphi_{n-1} \ ,$$

we observe that integration over φ_1 decouples from that over the rest of the variables; therefore, the ratio of the two surface integrals in Equation C.2 can be written in terms of one-dimensional integrals:

$$P_n = \frac{\int_0^{\pi} d\varphi_1 \sin^{n-2}\varphi_1 \theta(2\cos^2\varphi_1 - 1)}{\int_0^{\pi} d\varphi_1 \sin^{n-2}\varphi_1} = 1 - \frac{\int_{\pi/4}^{3\pi/4} d\varphi_1 \sin^{n-2}\varphi_1}{\int_0^{\pi} d\varphi_1 \sin^{n-2}\varphi_1} = 1 - \frac{\int_{-1/\sqrt{2}}^{1/\sqrt{2}} dx(1-x^2)^{(n-3)/2}}{\int_{-1}^{1} dx(1-x^2)^{(n-3)/2}}$$

where $x = \cos\varphi_1$. For large n both integrals are dominated by the values of x that are close to 0; thus, their ratio is close to 1 ,and P_n becomes vanishingly small. In fact, P_n decreases exponentially with increasing n. Since the number of possible pulling directions (3*N*)(3*N*-1)/2 increases quadratically with the number of atoms, the probability that one of them will align with the unstable direction to result in a negative χ_{TS} becomes vanishingly small as *N* increases (see also **Figure C2**).

ILLUSTRATIVE EXAMPLES OF CATCH BOND BEHAVIOR

The formal [4+2] cycloreversions of a furan/maleimide and a maleimide/ anthracene Diels-Alder adduct were investigated for possible catch-bond scenarios using EBT. As shown in **Figure 5.3A** and **Figure C3**, the application of a mechanical force leads to initial reaction suppression at low forces and a rollover at high forces. The experimental pulling points correspond to atoms (bridgehead C_7 and the imide N_{17}; **Figure C3**) that are further apart in the transition state than in the reactant configuration, which leads to an acceleration of the reaction. However, EBT calculations suggest that pulling on atoms C_3 and N_{17} (which move closer together in the transition state; **Figure C3**) leads to a "jamming effect". This scenario is depicted in **Figure 5.1C** where the mechanical pulling coordinate, *R*, first decreases but eventually increases at higher forces. An alternative explanation for the "jamming effect" is that the application of a stretching force at atoms C_3 and N_{17} prevents the necessary motion/mode to access the transition state. Specifically, a stretching force exerted on these atoms could promote a "slipping" motion, as opposed to the necessary pseudo-butterfly motion, that prevents

cycloreversion. This effect can be overcome at sufficiently high forces, which results in the dissociation of the furan/maleimide fragments. A similar scenario can be seen in **Figure 5.3B** and **Figure C4**, where pulling on the mechanical coordinate leads to reaction suppression with no rollover at high forces. The experimental pulling points correspond to the atom pair (anthracene C_5 and imide N_{31}) that facilitate the reaction, whereas pulling on atoms C_8 and N_{31} leads to suppression of chemical reactivity. The absence of rollover at high forces results from a greater contribution of the first order term ($F\Delta R$) as compared to the second order term ($F^2\Delta\chi/2$) and from the overall convexity of the energy barrier plotted as a function of the force (**Figure 5.3B**), which, in turn, is a consequence of the negative sign of $\Delta\chi$.

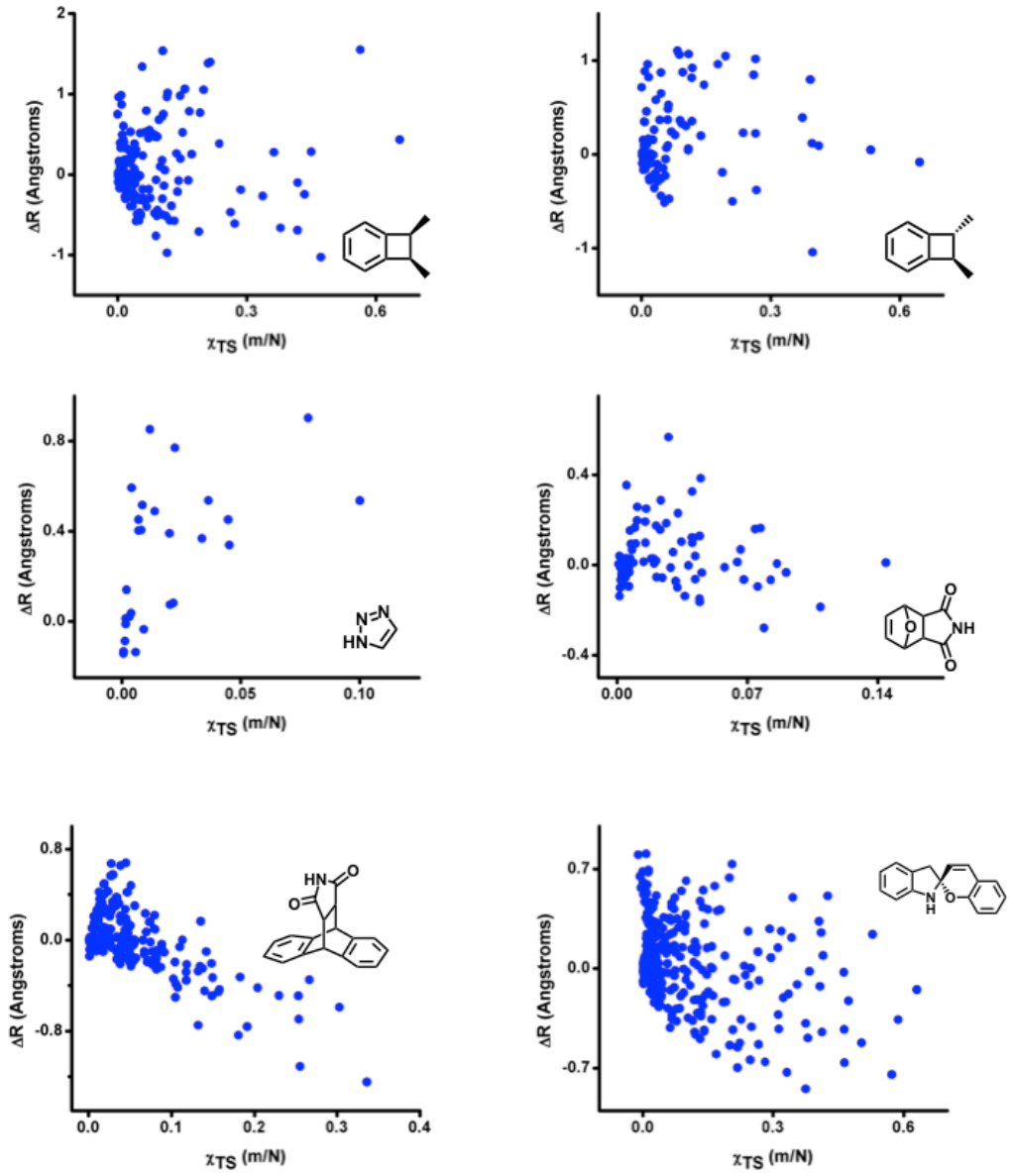

Figure C2 Computed values of ΔR and χ_{TS} (B3LYP/6-31G* level of theory) for all pulling points in the indicated mechanophores.

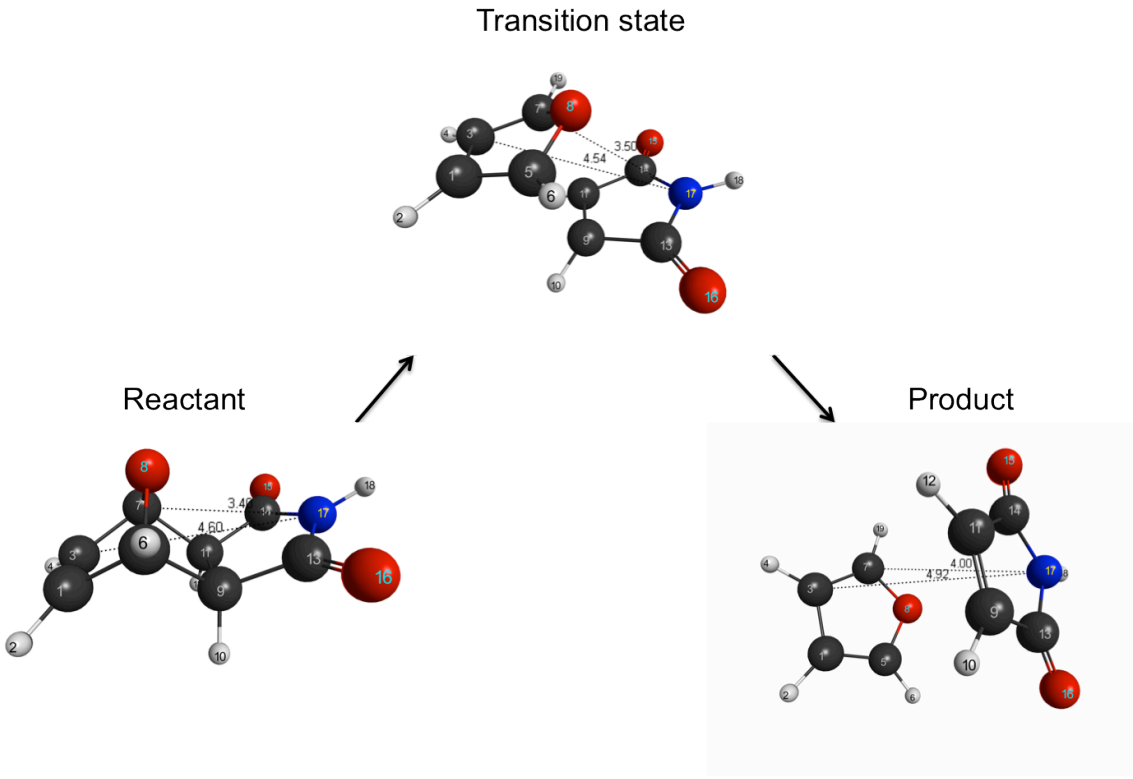

Figure C3 Computed values of ΔR at the B3LYP/6-31G* level of theory for the formal cycloreversion of a furan/maleimide Diels-Alder adduct. According to our theoretical predictions, pulling on the bridgehead C_7 and the imide N_{17} facilitates the reaction. In contrast, pulling on the methine C_3 and N_{17} suppresses the same transformation. Internuclear distances are indicated in Angstroms. Atom code: C (Black), H (White), N (Blue), O (Red).

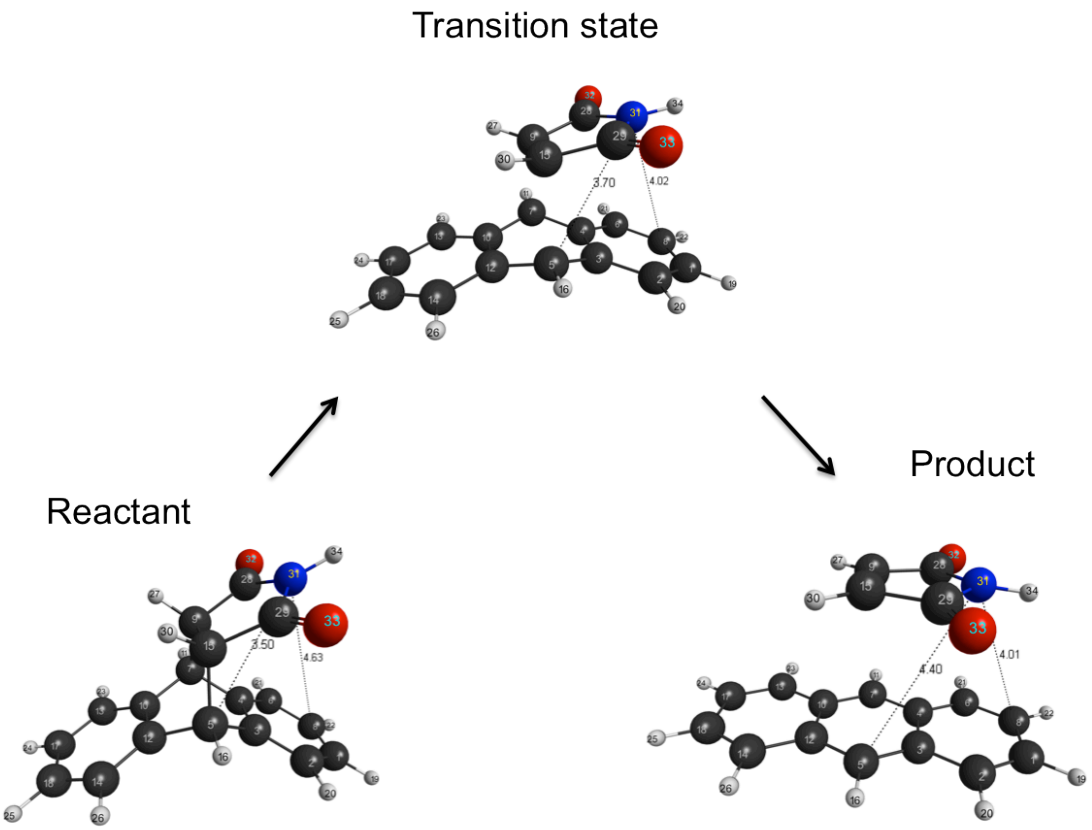

Figure C4 Computed values of ΔR at the B3LYP/6-31G* level of theory for the formal cycloreversion of a maleimide/anthracene Diels-Alder adduct. According to our theoretical predictions, pulling on the imide N_{31} and the anthracene C_5 facilitates the reaction. In contrast, pulling on the imide N_{31} and the anthracene C_8 suppresses the cycloreversion reaction. Internuclear distances are indicated in Angstroms. Atom code: C (Black), H (White), N (Blue), O (Red).

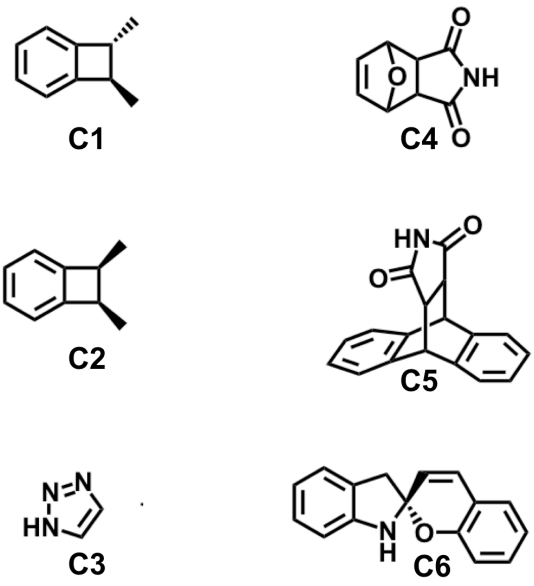

Scheme C1 Small molecule analogues of mechanophores that were evaluated computationally

C1 REACTANT GEOMETRY (-388.263169391275 HARTREES)

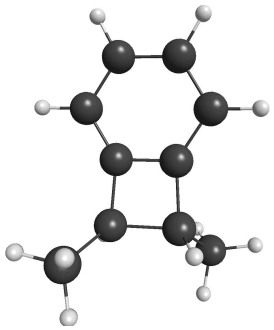

C	-0.22843003	0.66292351	-2.52592842
H	-0.39997725	1.16020496	-3.47753183
C	0.22843003	-0.66292351	-2.52592842
H	0.39997725	-1.16020496	-3.47753183
C	-0.47109269	1.35898986	-1.33052983

H	-0.82894840	2.38572990	-1.34785243
C	0.47109269	-1.35898986	-1.33052983
H	0.82894840	-2.38572990	-1.34785243
C	-0.23191256	0.65735770	-0.15675684
C	0.23191256	-0.65735770	-0.15675684
C	0.27507379	-0.74664361	1.36666460
C	-0.27507379	0.74664361	1.36666460
H	-1.29902844	0.79333718	1.76297944
C	0.59070332	1.80573186	2.04626967
H	1.62166905	1.76840241	1.67503764
H	0.20400284	2.81422234	1.85658562
H	0.61374735	1.65653208	3.13271012
H	1.29902844	-0.79333718	1.76297944
C	-0.59070332	-1.80573186	2.04626967
H	-1.62166905	-1.76840241	1.67503764
H	-0.20400284	-2.81422234	1.85658562
H	-0.61374735	-1.65653208	3.13271012

C1 TRANSITION STATE GEOMETRY (-388.201896419683 HARTREES; 1 IMAGINARY FREQUENCY)

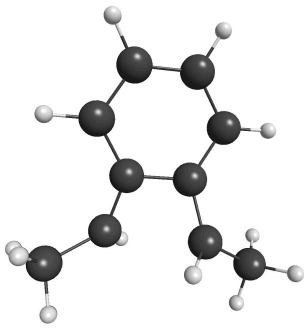

C	-0.06519415	0.70619594	2.44806756
H	-0.10889026	1.22919165	3.40017765
C	0.06519415	-0.70619594	2.44806756
H	0.10889026	-1.22919165	3.40017765
C	-0.08555267	1.43011204	1.26568955
H	-0.11689148	2.51715554	1.27773907
C	0.08555267	-1.43011204	1.26568955
H	0.11689148	-2.51715554	1.27773907
C	0.05463155	0.70670125	0.06165758
C	-0.05463155	-0.70670125	0.06165758
C	-0.35885272	-1.09559975	-1.28247800
C	0.35885272	1.09559975	-1.28247800
H	1.23861436	0.63374705	-1.71681888
C	-0.08182376	2.37904843	-1.92996291
H	-0.99292845	2.77929548	-1.47267133
H	0.69948354	3.15347331	-1.86701718
H	-0.27861563	2.22956466	-2.99925735
H	-1.23861436	-0.63374705	-1.71681888

C	0.08182376	-2.37904843	-1.92996291
H	0.99292845	-2.77929548	-1.47267133
H	-0.69948354	-3.15347331	-1.86701718
H	0.27861563	-2.22956466	-2.99925735

C2 REACTANT GEOMETRY (-388.261356494231 HARTREES)

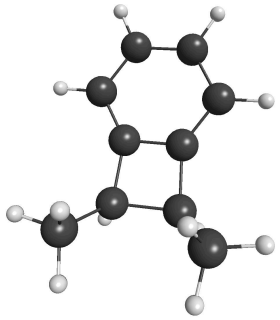

H	0.03205656	1.37452016	-2.52538455
C	0.03359020	1.35709758	-1.43807598
C	0.25347690	0.20362668	-0.69710475
C	0.54591254	-1.29005329	-0.80026670
C	0.25347690	0.20362668	0.69710475
C	0.54591254	-1.29005329	0.80026670
C	0.03359020	1.35709758	1.43807598
H	0.03205656	1.37452016	2.52538455
C	-0.19620526	2.53018945	0.70120681
H	-0.37889268	3.46405387	1.22731042
C	-0.19620526	2.53018945	-0.70120681
H	-0.37889268	3.46405387	-1.22731042

H	1.54922174	-1.50261031	1.19451381
C	-0.47173953	-2.16322134	1.53308559
C	-0.47173953	-2.16322134	-1.53308559
H	1.54922174	-1.50261031	-1.19451381
H	-1.49403468	-1.96950771	1.19175000
H	-0.25820371	-3.22895973	1.38727839
H	-0.44038577	-1.96327892	2.61079058
H	-1.49403468	-1.96950771	-1.19175000
H	-0.44038577	-1.96327892	-2.61079058
H	-0.25820371	-3.22895973	-1.38727839

C2 TRANSITION STATE GEOMETRY (-388.193570339477 HARTREES; 1 IMAGINARY FREQUENCY)

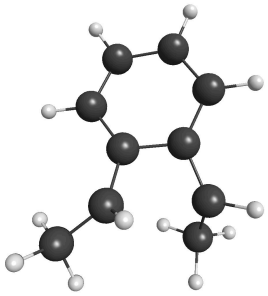

H	-2.50092493	0.71254846	-0.57141023
C	-1.46749537	0.95613323	-0.33603729
C	-0.56552082	-0.02064105	0.14486284
C	-0.75236228	-1.35109896	0.63075902
C	0.80765848	0.29276205	0.30580049
C	1.54128453	-0.94007477	0.32973065

C	1.22076754	1.63999886	0.38300320
H	2.24804715	1.90446848	0.62461141
C	0.30094474	2.61026447	0.01637889
H	0.59977414	3.65520253	-0.00707118
C	-1.01616792	2.26500316	-0.38459690
H	-1.69416415	3.05647900	-0.69415310
H	2.41290710	-1.00342204	0.99375553
C	1.65958739	-1.86253856	-0.86136294
C	-1.71907470	-2.35140510	0.07391609
H	-0.36725450	-1.55402053	1.62299074
H	0.84440496	-1.71598781	-1.57501547
H	1.67417480	-2.92107486	-0.56798503
H	2.60901883	-1.67535374	-1.39082940
H	-1.17714750	-3.22602350	-0.32032907
H	-2.29814991	-1.93580720	-0.75834260
H	-2.41361595	-2.73463967	0.83387780

C3 REACTANT GEOMETRY (-242.222324613251 HARTREES)

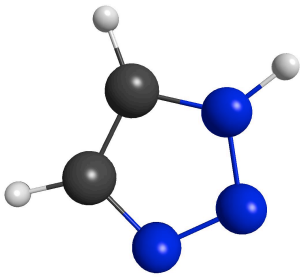

N	0.76641323	0.74735474	0.00000000
N	1.03169258	-0.57800022	0.00000000
H	1.53498012	1.40357012	0.00000000
C	-0.56789248	0.99102346	0.00000000
N	-0.11833257	-1.19329037	0.00000000
C	-1.12284537	-0.26820306	0.00000000
H	-0.98549263	1.98591066	0.00000000
H	-2.16224034	-0.56121972	0.00000000

C3 TRANSITION STATE GEOMETRY (-242.080939946128 HARTREES; 1 IMAGINARY FREQUENCY)

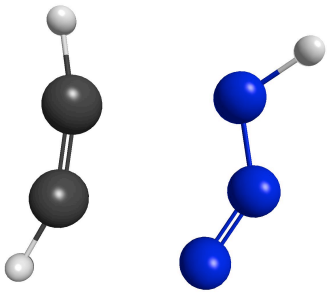

N	-1.05458399	-0.80904510	0.06669483
N	0.15639170	-1.16037631	-0.02362601

H	-1.69278966	-1.47926941	-0.36824273
C	-0.64882068	1.36031918	-0.01535740
N	1.21228287	-0.65819984	0.01210523
C	0.58384297	1.38272112	0.00914800
H	-1.68265272	1.62296074	-0.01196493
H	1.56967333	1.79365785	0.02704873

C4 REACTANT GEOMETRY (-589.463730607086 HARTREES)

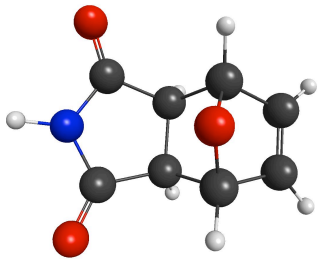

C	-0.33552903	-2.48623440	-0.66819055
H	-0.79722530	-3.19174371	-1.34878004
C	-0.33552903	-2.48623440	0.66819055
H	-0.79722530	-3.19174371	1.34878004
C	0.34247067	-1.18195474	-1.07170284
H	0.83668961	-1.12367128	-2.04064881
C	0.34247067	-1.18195474	1.07170284
O	1.27801483	-0.98102578	0.00000000
C	-0.68626373	-0.02815014	-0.77517167
H	-1.65388068	-0.18888906	-1.25546696
C	-0.68626373	-0.02815014	0.77517167
H	-1.65388068	-0.18888906223	1.25546696

C	-0.12661590	1.33583219	-1.17501407
C	-0.12661590	1.33583219	1.17501407
O	0.07382324	1.74831677	2.29624268
O	0.07382324	1.74831677	-2.29624268
N	0.13287554	2.03653260	0.00000000
H	0.56427003	2.95410763	0.00000000
H	0.83668961	-1.12367128	2.04064881

C4 TRANSITION STATE GEOMETRY (-589.419772353728 HARTREES; 1 IMAGINARY FREQUENCY)

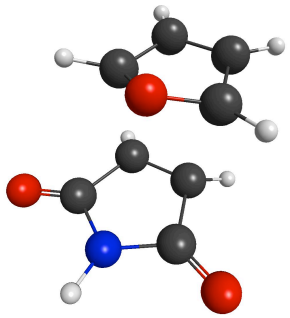

C	-0.34341884	-2.47195919	-0.68825424
H	-0.94027072	-3.07899109	-1.35593202
C	-0.34341884	-2.47195919	0.68825424
H	-0.94027072	-3.07899109	1.35593202
C	0.46557294	-1.36836061	-1.07756946
H	0.89640035	-1.14861290	-2.04559263
C	0.46557294	-1.36836061	1.07756946
O	1.22329906	-0.99122219	0.00000000

C	-0.95017133	0.19453507	-0.70613188
H	-1.76736306	-0.13584667	-1.33389101
C	-0.95017133	0.19453507	0.70613188
H	-1.76736306	-0.13584667	1.33389101
C	-0.12638819	1.35977059	-1.16565652
C	-0.12638819	1.35977059	1.16565652
O	0.10991094	1.72699823	2.29961404
O	0.10991094	1.72699823	-2.29961404
N	0.35807503	1.96193396	0.00000000
H	1.02385425	2.72336552	0.00000000
H	0.89640035	-1.14861290	2.04559263

C5 REACTANT GEOMETRY (-898.991016266601 HARTREES)

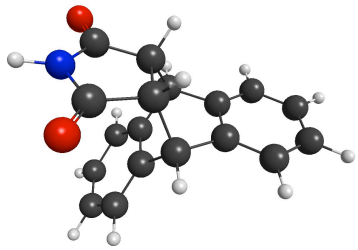

C	3.16944422	-1.51970323	-0.69790139
C	2.11897948	-0.92354062	-1.40481282
C	1.07967003	-0.31963236	-0.70303405
C	1.07967003	-0.31963236	0.70303405
C	-0.14066288	0.35885962	-1.30344764
C	2.11897948	-0.92354062	1.40481282

C	-0.14066288	0.35885962	1.30344764
C	3.16944422	-1.51970323	0.69790139
C	-1.40181983	-0.41309322	0.77523815
C	-0.23867257	1.75294437	0.70346709
H	-0.12612728	0.36104996	2.39598213
C	-0.23867257	1.75294437	-0.70346709
C	-0.33843564	2.95063418	1.40407672
C	-0.33843564	2.95063418	-1.40407672
C	-1.40181983	-0.41309322	-0.77523815
H	-0.12612728	0.36104996	-2.39598213
C	-0.43212722	4.15592911	0.69761631
C	-0.43212722	4.15592911	-0.69761631
H	3.98725284	-1.98635576	-1.24026074
H	2.11237196	-0.93222107	-2.49186656
H	2.11237196	-0.93222107	2.49186656
H	3.98725284	-1.98635576	1.24026074
H	-0.33936474	2.95073697	2.49164698
H	-0.50361777	5.09466808	1.24022405
H	-0.50361777	5.09466808	-1.24022405
H	-0.33936474	2.95073697	-2.49164698
H	-2.30002407	0.05291646	1.19218985
C	-1.39711697	-1.88880003	1.17651548
C	-1.39711697	-1.88880003	-1.17651548
H	-2.30002407	0.05291646	-1.19218985
N	-1.41933709	-2.63468523226	0.00000000

O	-1.37629402	-2.34935945	2.29704298
O	-1.37629402	-2.34935945	-2.29704298
H	-1.38871541	-3.64813818	0.00000000

C5 TRANSITION STATE GEOMETRY (-898.926505316635 HARTREES; 1 IMAGINARY FREQUENCY)

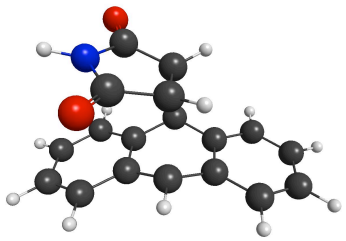

C	2.34403284	-2.60867290	-0.70611577
C	1.72277945	-1.59211634	-1.40675206
C	1.12045162	-0.51846502	-0.71161266
C	1.12045162	-0.51846502	0.71161266
C	0.40143949	0.54371730	-1.35559849
C	1.72277945	-1.59211634	1.40675206
C	0.40143949	0.54371730	1.35559849
C	2.34403284	-2.60867290	0.70611577
C	-1.65592920	-0.05907435	0.70348681
C	0.33743639	1.82841266	0.71089317
H	0.30775871	0.50738721	2.43898084
C	0.33743639	1.82841266	-0.71089317
C	0.17246958	3.04698402	1.40458734
C	0.17246958	3.04698402	-1.40458734

C	-1.65592920	-0.05907435	-0.70348681
H	0.30775871	0.50738721	-2.43898084
C	0.04710678	4.23434228	0.70541970
C	0.04710678	4.23434228	-0.70541970
H	2.82978024	-3.41835762	-1.24362557
H	1.70108791	-1.60070128	-2.49297292
H	1.70108791	-1.60070128	2.49297292
H	2.82978024	-3.41835762	1.24362557
H	0.16197816	3.04362017	2.49188745
H	-0.05438352	5.17263539	1.24365314
H	-0.05438352	5.17263539	-1.24365314
H	0.16197816	3.04362017	-2.49188745
H	-2.10203385	0.70309578	1.32775319
C	-1.66369888	-1.48040741	1.16666576
C	-1.66369888	-1.48040741	-1.16666576
H	-2.10203385	0.70309578	-1.32775319
N	-1.60148118	-2.25077200	0.00000000
O	-1.69996515	-1.91722619	2.30018045
O	-1.69996515	-1.91722619	-2.30018045
H	-1.50647360	-3.25759625	0.00000000

C6 REACTANT GEOMETRY (-747.497776633712 HARTREES)

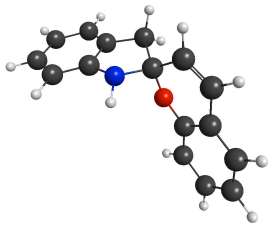

H	-1.08626680	-5.49419332	0.88777205
C	-0.78722642	-4.54739647	0.44746226
C	-1.21211446	-4.21045786	-0.83888717
H	-1.84281869	-4.89922442	-1.39507965
C	-0.84478341	-2.99483469	-1.42990495
H	-1.18157285	-2.73753920	-2.43064134
C	-0.04172635	-2.12772933	-0.69363954
N	0.49457340	-0.88753367	-1.07145250
C	0.39182901	-2.45621837	0.60101135
C	1.25952780	-1.32560186	1.10550681
C	0.02379949	-3.66301937	1.17492998
H	0.35270362	-3.92100039	2.17894309
C	0.94674966	-0.17025154	0.11538298
H	2.32491202	-1.58422420	1.04620513
H	1.04533240	-1.00535734	2.12824392
C	2.09178783	0.74705746	-0.21682785
O	-0.15751810	0.56234115	0.72803766
H	0.01913014	-0.33480304	-1.77523743
C	1.91023381	2.06468181	-0.38897343

H	3.05487660	0.27411227	-0.38273493
C	0.60336131	2.66905241	-0.18123509
H	2.73715156	2.70637500	-0.68517784
C	-0.40575614	1.85591683	0.37141466
C	0.30255833	4.00688177	-0.47560277
C	-1.67800839	2.37042561	0.62718579
H	1.07996194	4.63755717	-0.90136665
C	-0.96553031	4.52632284	-0.22825385
C	-1.95225011	3.70431270	0.32718596
H	-1.18501340	5.56392276	-0.46197019
H	-2.94347237	4.10278753	0.52601987
H	-2.42932106	1.71776557	1.06059471

C6 TRANSITION STATE GEOMETRY (-747.461918836480 HARTREES; 1 IMAGINARY FREQUENCY)

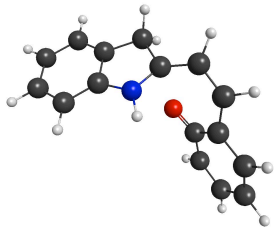

H	1.23787206	5.49738556	0.64026500
C	0.93097746	4.51788356	0.28569526
C	1.60035979	3.92938193	-0.79000051
H	2.42330593	4.45614319	-1.26471623
C	1.23098218	2.66718132	-1.26977653
H	1.75221803	2.20820766	-2.10468642

C	0.17861084	2.02745068	-0.62741911
N	-0.41837743	0.79250069	-0.92421839
C	-0.50548612	2.60081362	0.45417119
C	-1.57769656	1.63010067	0.89128710
C	-0.13202437	3.85355952	0.91538654
H	-0.64785129	4.31448241	1.75371684
C	-1.36064844	0.43945522	-0.02288321
H	-2.59628924	2.02676070	0.77759981
H	-1.46609737	1.30184552	1.92899778
C	-2.23793824	-0.66779167	-0.17112169
O	0.25366886	-0.68292476	1.09127530
H	-0.05591767	0.13020803	-1.59786343
C	-1.82702345	-1.94006124	-0.49947384
H	-3.29154337	-0.47723161	0.02372389
C	-0.52510854	-2.48797601	-0.31423992
H	-2.60488760	-2.64352276	-0.80034872
C	0.40649373	-1.85706711	0.62535798
C	-0.23284062	-3.78717690	-0.81827333
C	1.53380814	-2.65786575	1.03206564
H	-0.94560146	-4.23833352	-1.50726108
C	0.90750285	-4.47050900	-0.46738913
C	1.79237464	-3.88756658	0.47623765
H	1.11757169	-5.45175449	-0.88253092
H	2.68811513	-4.43035796	0.77226357
H	2.20599912	-2.21145855	1.75902248

EXPERIMENTAL MATERIALS AND METHODS

2-(2,5-dioxo-2,5-dihydro-1*H*-pyrrol-1-yl)ethyl-2-bromo-2-methylpropanoate (**5.2**)[11] and ((9*S*,10*S*,11*S*)-13-(2-((2-bromo-2-methylpropanoyl)oxy)ethyl)-12,14-dioxo-9,10-[3,4]epipyrroloanthracen-10(9*H*)-yl)methyl 2-bromo-2-methylpropanoate (**5.5**)[12] were prepared according to literature procedures. All other reagents were commercially available and used without further purification. All synthetic manipulations involved standard Schlenk techniques unless otherwise noted. Unless otherwise noted, solvents were dried over 3 Å molecular sieves or using a Vacuum Atmospheres Company solvent purification system and then subsequently stored over 3 Å molecular sieves. ^{1}H and ^{13}C NMR data were collected on Varian DirectDrive 400 MHz spectrometer. Chemical shifts (δ) are reported in ppm and referenced downfield from $(CH_3)_4Si$ using the residual solvent peak as an internal standard (^{1}H: $CDCl_3$, 7.26 ppm; DMSO-d_6, 2.49 ppm; ^{13}C: $CDCl_3$, 77.0 ppm). High resolution mass spectra (HRMS) were obtained by chemical ionization (CI) using a VG analytical ZAB2-E instrument. IR spectra were recorded using a Thermo Scientific Nicolet iS5 system equipped with an iD3 attenuated total reflectance (ATR) attachment (germanium crystal). UV-visible spectra were recorded using a Perkin Elmer Instruments Lambda 35 spectrometer. Melting points were obtained using a Stanford Research Systems automated melting point system and are uncorrected. Elemental analyses were performed on a Thermo Scientific Flash2000 elemental analyzer.

MACROMOLECULAR CHARACTERIZATION

Gel permeation chromatography (GPC) was performed on a Viscotek GPCmax Solvent/Sample Module. Two fluorinated polystyrene columns (IMBHW-3078 and I-MBLMW-3078) were used in series and maintained at 24 °C. THF was used as the eluent at a flow rate of 1.0 mL min^{-1}. Detection was performed using a Viscotek VE 3580

Refractive Index Detector or a Viscotek 2600 Photodiode Array Detector (tuned at 370 nm). Molecular weight and dispersity data are reported relative to polystyrene standards.

GENERAL SONICATION CONDITIONS

All sonication experiments were performed under an atmosphere of argon using a Sonics & Materials VC-505 Liquid Cell Ultrasonic processor operating at 20 kHz and equipped with a 12.8 mm replaceable tip titanium probe. Custom Suslick cells[13] were fabricated in house. An argon line was threaded through a septum attached to one of the cell's side arms and placed in solution, ensuring no contact with the probe. Argon was bubbled through the solution for 30 min prior to each experiment and continuously during each experiment conducted. The entire system was placed in an ice bath, which was sufficient to maintain a temperature of 6–9 °C, as determined using a thermocouple placed directly into the solution within the reaction vessel. Pulsed ultrasound was applied (1.0 s on and 1.0 s off) at 20% power (power intensity = 7.9 W cm^{-2}).

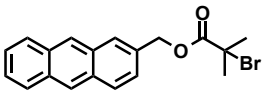

Synthesis and Characterization of anthracen-2-ylmethyl 2-bromo-2-methylpropanoate (5.1). A flame dried 150 mL Schlenk flask was charged with ethyl acetate (EtOAc; 50 mL), 2-anthrachenyl methanol (100 mg; 0.48 mmol), and a magnetic stir bar. The resulting solution was cooled in an ice bath, and triethylamine (0.1 mL; 0.71 mmol) was added via syringe. Upon stirring for 10 min, 2-bromo-2-methylpropionyl bromide (0.1 mL; 0.80 mmol) was added dropwise via syringe. The resulting mixture was stirred at 0 °C for 10 min, and then allowed to slowly warm to room temperature over 12 h. The reaction mixture was then filtered over a plug of neutral alumina, and the filtrate was concentrated under reduced pressure. The resulting residue was purified via column chromatography (eluted with 1:1 EtOAc/Hexanes) to afford a

pale yellow solid (116 mg; 68% yield). Decomp.: 150 °C. 1H NMR (CDCl3; 400.08 MHz): 8.39 (s, 2H), 8.00 – 7.98 (m, 4H), 7.48 – 7.42 (m, 3H), 5.39 (s, 2H), 1.99 (s, 6H). 13C NMR (CDCl3; 399.67 MHz): 171.67, 132.30, 132.06, 131.28, 131.24, 128.95, 128.28, 128.27, 127.33, 126.64, 126.29, 125.71, 125.13, 67.96, 55.88, 30.93. IR (ATR): 1734.12, 1461.00, 1272.76, 1154.93, 1107.47, 1008.82, 971.19, 959.03, 948.29, 899.78, 891.44, 873.04, 868.81, 755.28, 743.03, 671.78, 667.91, 647.43, 630.31, 617.59. HRMS: [MNa]+ calcd. for C19H17BrNaO2: 379.03051. Found: 379.03041. Anal. calcd. for C19H17BrO2: C, 63.88; H, 4.80. Found: C, 64.18; H, 4.62.

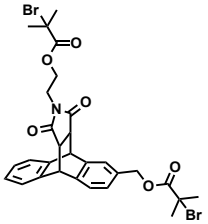

Synthesis and Characterization of ((9*S*,10*R*,11*S*)-13-(2-((2-bromo-2-methylpropanoyl)oxy)ethyl)-12,14-dioxo-9,10-dihydro-9,10-[3,4]epipyrroloanthracen-3-yl)methyl 2-bromo-2-methylpropanoate (5.3). A 250 mL round bottom flask was charged with toluene (100 mL), **5.1** (100 mg; 0.28 mmol), **5.2** (82.0 mg; 0.28 mmol), and a magnetic stir bar. The reaction mixture was refluxed at 130 °C for 19 h without taking special precaution to exclude air or moisture. Upon cooling to room temperature, the solvent was removed under reduced pressure, and the resulting residue was purified *via* column chromatography (eluted with 1:1 Et_2O/Petroleum Ether) to afford a foamy white solid (130 mg; 72% yield). m.p.: 79-82 °C. ^{1}H NMR ($CDCl_3$; 400.08 MHz): 7.37 – 7,37 (m, 2H), 7.26 – 7.24 (m, 2H), 7.18 – 7.13 (m, 3H), 5.15 – 5.11 (d, ^2J = 12.4 Hz, 2H), 4.78 (s, 2H), 3.71 – 3.56 (m, 2H), 3.55 – 3.32 (t, ^3J = 5.6 Hz, 2H), 3.21 (s, 2H), 1.93 (s, 3H), 1.89 (s, 3H), 1.86 (s, 3H), 1.85 (s, 3H). ^{13}C NMR ($CDCl_3$; 399.67 MHz): 176.45, 171.47, 171.32, 141.15, 139.13, 138.90, 134.70, 134.41, 127.38,

127.07, 126.91, 125.35, 124.66, 124.61, 124.52, 124.48, 67.31, 62.00, 55.72, 55.62, 46.99, 46.97, 45.63, 45.44, 36.77, 30.87, 30.81, 30.74. IR (ATR): 1777.36, 1733.38, 1461.59, 1435.55, 1390.79, 1371.42, 1336.97, 1270.89, 1158.73, 1108.26, 992.09, 913.67, 839.97, 760.30, 734.53. HRMS: $[MNa]^+$ calcd. for $C_{29}H_{29}Br_2NNaO_6$: 670.02359. Found: 670.02464. Anal. calcd. for $C_{29}H_{29}Br_2NO_2$: C, 53.81; H, 4.52; N, 2.16. Found: C, 54.05; H, 4.62; N, 2.43.

Representative Procedure for Preparation of $\mathbf{5.4}_{Mn}$ Polymers (M_n = 16, 56, 88, 137): Synthesis of $\mathbf{5.4}_{88}$. An oven dried 25 mL Schlenk flask was charged a 0.01 M solution of tris(2-[*N*,*N*-dimethyl]-aminoethyl)amine (2.0 mL, 20 μmol) in dimethyl sulfoxide (DMSO), **5.3** (13 mg, 20 μmol), and a magnetic stirbar wrapped with copper wire. The solution was stirred for several minutes to ensure homogeneity, and then subjected to three freeze-pump-thaw cycles. The resulting solution was frozen in liquid nitrogen, and methyl acrylate (2.2 mL; 22 mmol) was added *via* syringe ([methyl acrylate]$_0$/[**5.3**]$_0$ = 1023). The reaction mixture was warmed to room temperature and then allowed to stir for 5 h. The resulting viscous solution was added dropwise to excess methanol (300 mL), which caused a polymeric material to precipitate as a gummy solid. After decanting the supernatant, the residual material was washed with methanol (3 × 50 mL), collected via filtration, and then dried under vacuum to afford the desired product in 95% yield (1.67 g). GPC: M_n = 88 kDa, PDI = 1.3. See **Table C2** for additional molecular weight data.

Synthesis of $\mathbf{5.6}_{79}$. An oven dried 10 mL Schlenk flask was charged with methyl acrylate (3.16 mL, 35 mmol), a magnetic stirbar wrapped with copper wire, and a 0.01 M solution of tris(2-[*N*,*N*-dimethyl]-aminoethyl)amine (3.0 mL, 30 μmol) in dimethyl sulfoxide (DMSO). The solution was stirred for several minutes to ensure homogeneity, and then equimolar amounts of **5.3** (12 mg, 19 μmol) and **5.5** (12 mg, 19 μmol) were

added ([methyl acrylate]$_0$/[**5.3** + **5.5**]$_0$ = 930). The flask was sealed, removed from the drybox, and then stirred at room temperature for 4 h. The resulting viscous solution was then added slowly to excess methanol (200 mL), which caused a polymeric material to precipitate as a gummy solid. After decanting the supernatant, the residual material was washed with methanol (5 × 20 mL), collected via filtration, and then dried under vacuum to afford the desired product in 93% yield (2.8 g). GPC: M_n = 79 kDa, PDI = 1.3.

Synthesis of $\mathbf{5.7_{120}}$. $\mathbf{5.7_{120}}$ was prepared according to a previously reported procedure.[12] GPC: M_n = 120 kDa, PDI = 1.3.

Table C2 Selected Yield and Molecular Weight Data†

Polymer	Yield	Presonication		Postsonication	
		M_n (kDa)	PDI	M_n (kDa)	PDI
$\mathbf{5.4_{17}}$	70%	16	1.4	17	1.4
$\mathbf{5.4_{56}}$	83%	56	1.3	51	1.3
$\mathbf{5.4_{88}}$	95%	88	1.3	85	1.3
$\mathbf{5.4_{130}}$	92%	130	1.4	88	1.4

† The M_n refers to the number average molecular weight of the polymer. The polydispersity index (PDI) was calculated using the equation PDI = M_w/M_n, where M_w is the weight average molecular weight and M_n is the number average molecular weight. The M_n and M_w values were determined by GPC (eluent = tetrahydrofuran). Molecular weights are reported as their polystyrene equivalents.

ULTRASONICATION OF $\mathbf{5.4_{\mathit{Mn}}}$

A Suslick cell was charged with 10 mL of a 10 mg mL^{-1} solution of $\mathbf{5.4_{\mathit{Mn}}}$ in CH_3CN and sonicated using the general procedure described above. After sonication for 6 h, the solvent was removed under reduced pressure. The residual polymer was washed with methanol and dried. The resulting polymer was then dissolved in tetrahydrofuran

(30 mg mL^{-1}) and characterized by GPC visualized with ultraviolet-visible detection at 370 nm (see **Figure C5** and **Figure C6**)

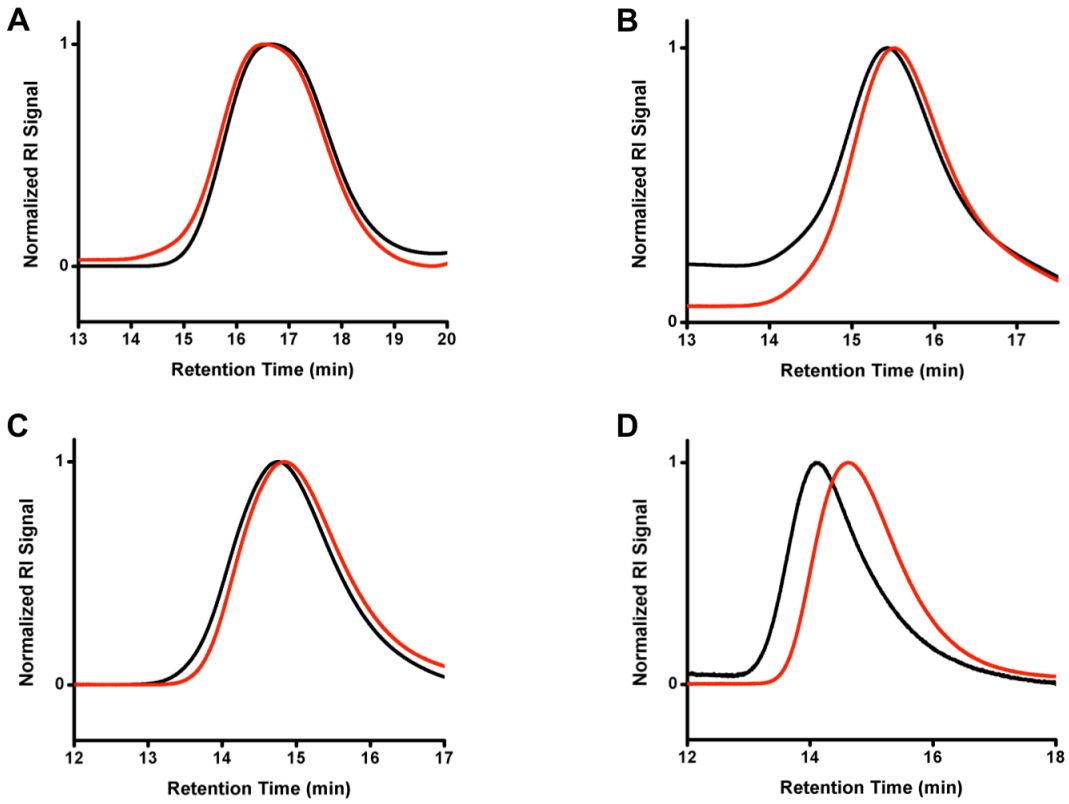

Figure C5 GPC chromatograms of presonicated (black) and postsonicated (red) $\mathbf{5.4_{17}}$ (A), $\mathbf{5.4_{56}}$ (B), $\mathbf{5.4_{88}}$ (C), and $\mathbf{5.4_{130}}$ (D) materials.

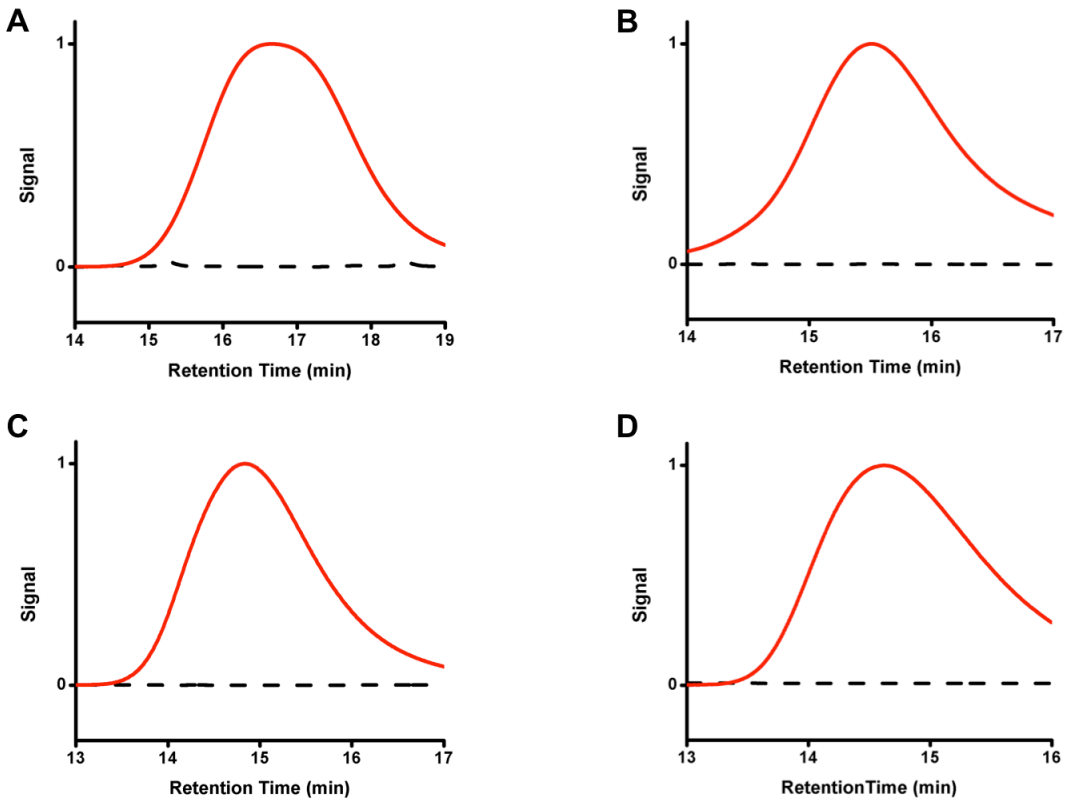

Figure C6 GPC chromatograms visualized with ultraviolet-visible detection at 370 nm (dashed black) of $\mathbf{5.4}_{17}$ (A), $\mathbf{5.4}_{56}$ (B), $\mathbf{5.4}_{88}$ (C), and $\mathbf{5.4}_{130}$ (D) materials following ultrasonication. For reference, the normalized refractive index signals of the materials isolated following ultrasonication (red) are included in each chromatogram.

ULTRASONICATION OF $\mathbf{5.6}_{79}$

A Suslick cell was charged with 10 mL of a 10 mg mL^{-1} solution of $\mathbf{5.6}_{79}$ in CH_3CN and sonicated using the general procedure described above. After sonication for 6 h, the solvent was removed under reduced pressure. The residual polymer was washed with methanol and dried. The resulting polymer was then dissolved in tetrahydrofuran (30 mg mL^{-1}) and characterized by GPC (see **Figure 5.4**). GPC: M_n = 50 kDa, PDI = 1.8.

Two distinct peak molecular weight, M_p, values were observed at M_p = 83 and M_p = 46, compared to the pre-sonicated polymer at the same concentration, where M_p = 101.

THERMAL ACTIVATION OF $\mathbf{5.4}_{MN}$: REPRESENTATIVE PROCEDURE FOR $\mathbf{5.4}_{88}$

A 50 mL pressure tube was charged with $\mathbf{5.4}_{88}$ (50 mg) and toluene (5 mL). The tube was sealed and agitated to effect the dissolution of $\mathbf{5.4}_{88}$. The resulting mixture was heated at 130° C for 19 h. Upon cooling to room temperature, the solvent was removed, and the resulting material was dissolved in THF (10 mg mL^{-1}). GPC analysis with ultraviolet-visible detection at 370 nm did not reveal the generation of anthracenylated polymer fragments (see **Figure C7**). M_n = 80 kDa, PDI = 1.4.

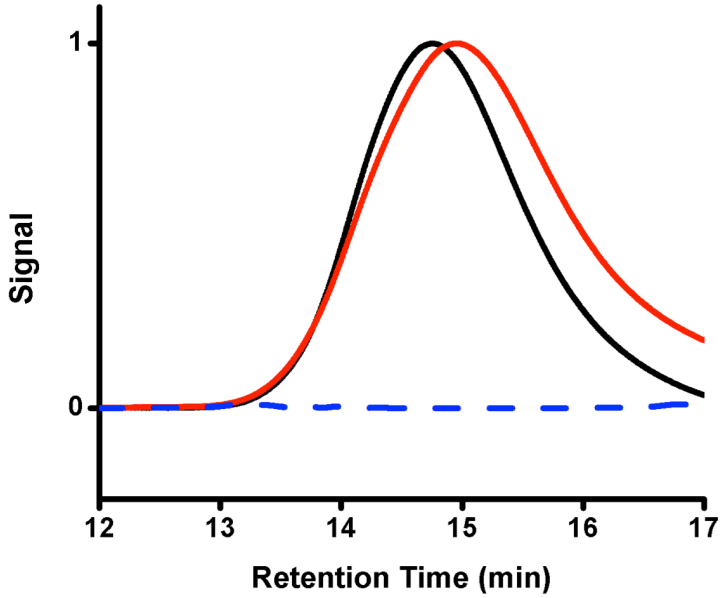

Figure C7 GPC chromatograms showing the normalized refractive index signal for $\mathbf{5.4}_{88}$ (black) following thermal treatment (red). The GPC chromatogram visualized with ultraviolet-visible detection at 370 nm (dashed blue) of the material isolated following thermal treatment is included for reference.

DETERMINATION OF K_{OBS} FOR CHAIN SCISSION DURING ULTRASONICATION

The rate of ultrasound-induced chain scission within the **5.4**$_{Mn}$ materials was determined based on the work of Malhotra.[14,15] Briefly, the rate of chain scission could be estimated using the relationship:

$$\frac{1}{M_t} = \frac{1}{M_i} + k't$$

where M_t is the number average molecular weight (M_n) of the polymer at time t, M_i is the initial M_n, and k' is proportional to the observed rate constant for chain scission (k_{obs}) by the following relationship:

$$k' = \frac{k_{obs}}{M_0}$$

Each of the **5.4**$_{Mn}$ materials were subjected to pulsed ultrasound as previously detailed (vide supra). Aliquots of 300 μL were removed every 30 minutes, concentrated under reduced pressure, diluted with tetrahydrofuran (THF), and analyzed using GPC. **Figure C8** shows plots of reciprocal molecular weights versus time for each of the **5.4**$_{Mn}$ materials, as well as plots of k_{obs} versus M_n. **Table C3** tabulates the corresponding values of *k'* and k_{obs} that were extrapolated from the plots shown in **Figure C8**. All data points represent averages from duplicate experiments.

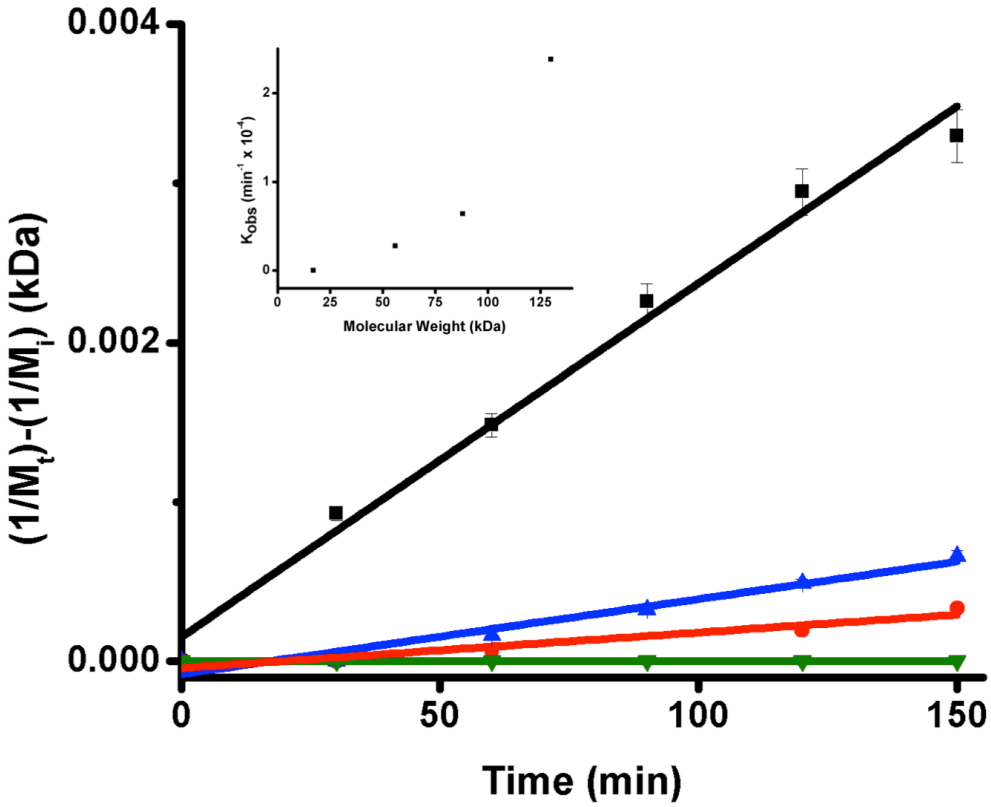

Figure C8 Plots of $\frac{1}{M_t} - \frac{1}{M_i}$ versus time for **5.4**$_{17}$ (green), **5.4**$_{56}$ (red), **5.4**$_{88}$ (blue), and **5.4**$_{130}$ (black). The inset plot shows the values of k_{obs} that were calculated as discussed above.

Table C3 Rate Constants for Scission of **5.4**$_{Mn}$ Materials.

Polymer	k_{obs} (min^{-1})
5.4$_{17}$	0
5.4$_{56}$	$2.76 \times 10^{-5} \pm 2.51 \times 10^{-7}$
5.4$_{88}$	$6.39 \times 10^{-5} \pm 3.42 \times 10^{-8}$
5.4$_{130}$	$2.38 \times 10^{-4} \pm 1.32 \times 10^{-6}$

REFERENCES

1 Valiev, M.; Bylaska, E. J.; Govind, N.; Kowalski, K.; Straatsma, T. P.; Van Dam, H. J. J.; Wang, D.; Nieplocha, J.; Apra, E.; Windus, T. L.; de Jong, W. A. *Comput. Phys. Commun.* **2010**, *181*, 1477.

2 Parr, R. G. and Yang, W. *Density-Functional Theory of Atoms and Molecules*; Oxford University Press: New York, 1989.

3 Gordon, M. S.; Binkley, J. S.; Pople, J. A.; Pietro, I. W. J.; Hehre, W. J. *J. Am. Chem. Soc.* **1982**, *104*, 2797.

4 Becke, A. D. *J. Chem. Phys.* **1993**, *98*, 1372.

5 Ribas-Arino, J.; Shiga, M.; Marx, D. *Angew. Chem. Int. Ed.* **2009**, *48*, 4190.

6 Hickenboth, C. R.; Moore, J. S.; White, S. R.; Sottos, N. R.; Baudry, J.; Wilson, S. R. *Nature* **2007**, *446*, 423.

7 Kryger, M. J.; Munaretto, A. M.; Moore, J. S. *J. Am. Chem. Soc.* **2011**, *133*, 18992.

8 Guner, V.; *et al. J. Phys. Chem.* **2003**, *107*, 11445.

9 Johnson, E. R.; *et al. J. Chem. Phys.* **2008**, *129,* 204112.

10 Zhao, Y.; Truhlar, D. G.; *J. Chem. Theory Comput.* **2011**, *7,* 669.

11 Mantovani, G.; Lecolley, F.; Tao, L.; Haddleton, D. M.; Clerx, J.; Cornelissen, J. J. L. M.; Velonia, K. *J. Am. Chem. Soc.* **2004**, *127*, 2966.

12 Wiggins, K. M.; Syrett, J. A.; Haddleton, D. M.; Bielawski, C. W. *J. Am. Chem. Soc.* **2011**, *133*, 7180.

13 K. S. Suslick, J. W. Goodale, P. F. Schubert, H. H. Wang. *J. Am. Chem. Soc.* **1983,** *105*, 5781.

14 Malhotra, S. *J. Macromol. Sci., Part A* **1986**, 37.

15 Malhotra, S. *J. Macromol. Sci., Part A* **1982**, *18*, 1055.

Appendix D

EXPERIMENTAL CONSIDERATIONS

1-Butyl-3-methylimidazolium hexafluorophosphtae (BMIM-PF_6) was prepared according to literature procedures.[1] All other reagents and materials were commercially available. Methyl methacrylate (MMA) was passed over a plug of basic alumina to remove any stabilizer prior to use. Azobisisobutyronitrile (AIBN) was recrystallized from acetone prior to use. Isopropyl β-D-1-thiogalactopyranoside (IPTG) and nickel-nitrilotriacetic acid agarose (Ni-NTA) were used without further purification. GFPuv (*A. victoria* green fluorescent protein exhibiting the following mutations: Q24H, A76S, L79V, A83S, Q91R, F99S, Y100F, M141L, M153T, P105Q, V163A, K173E, and I219V) was expressed from plasmid pNGFP-BC[2] (generous gift of Prof. Eric Gouaux, Oregon Health Science University). eYFP (*A. victoria* green fluorescent protein with the following mutations: S61G, S68A, R86Q, S98F, T154M, A164V, T204Y, and K207A)[3] was expressed from plasmid pET21a (generous gift of Prof. Andrew Ellington, University of Texas at Austin). Mechanical tests were performed using a standard benchtop Carver hydraulic press. Dynamic mechanical analysis (DMA) was performed using a TA Instruments Q800 series DMA outfitted with a compression clamp. Differential scanning calorimetry (DSC) was performed using a Metler Toledo 823^e DSC. Fluorescence spectra were acquired using a QuantaMaster Photon Technology International fluorometer. Gel permeation chromatography (GPC) was performed on a Viscotek GPCmax Solvent/Sample Module. Two fluorinated polystyrene columns (IMBHW-3078 and I-MBLMW-3078) were used in series and maintained at 24 °C. THF was used as the eluent at a flow rate of 1.0 mL min^{-1}. Detection was performed using a Viscotek VE 3580 Refractive Index Detector or a Viscotek 2600 Photodiode Array

Detector (tuned at 370 nm). Molecular weight and dispersity data are reported relative to polystyrene standards.

Site Directed Mutagenesis

Site directed mutagenesis of GFPuv was performed using pNGFP-BC as a template according to the quickchange method. To prepare GFPuv(D103C), the following primers were used (altered sequences are bold and red):

1) 5'-CGCACTATATCTTTCAAA**TG**TGACGGGAACTACAAGACG-3'

2) 5'-CGTCTTGTAGTTCCCGTCACATTT**GA**AAGATATAGTGCG-3'.

The following primers were used to prepare GFPuv(Y39C):

1) 5'-GAAGGTGATGCAACAT**G**CGGAAAACTTACCCTT-3'

2) 5'-AAGGGTAAGTTTTCCG**C**ATGTTGCATCACCTTC-3'

The GFPuv(Y39C/D103C) double mutant was generated using the GFPuv(Y39C) plasmid as a template and the above primers for GFPuv(D103C). All mutations were confirmed by DNA sequencing, and the mutants were expressed and purified using the same procedure as that described for the isolation of GFPuv (*vide infra*).

Protein Expression and Purification

Both GFPuv and eYFP were transformed into *E. coli* BL21 (DE3). Starter cultures (50 mL) were grown to inoculate pre-warmed Luria Broth supplemented with 50 μg/mL ampicillin. When OD_{600} = 0.4, the media was cooled to 15 °C and induced with 0.5 mM IPTG. After 16 h, the cells were harvested by centrifugation (3,000 relative centrifugal force for 20 minutes) and re-suspended in lysis buffer (10% glycerol v/v, 0.5 M NaCl, 100 mM HEPES pH 7.5), sonicated, and centrifuged (30,000 relative centrifugal force for 45 minutes) to remove cellular debris. The lysate was passed over a Ni-NTA agarose column equilibrated with lysis buffer. The column was washed with lysis buffer

containing 15 mM imidazole and protein was eluted with lysis buffer containing 150 mM imidazole. GFPuv was further purified using a Superdex 200 column equilibrated in 10 mM HEPES, pH 7.5, 150 mM NaCl. Final protein concentrations were determined using a Thermo Scientific Nanodrop 100 (absorbance at 280 nm).

PROCEDURE FOR THE PREPARATION OF EYFP COMPOSITES

An 8 mL Teflon capped vial was charged with a stir bar, eYFP (64 μL 9.4 mg mL^{-1} solution in lysis buffer; 1.8×10^{-8} mmol), MMA (0.5 mL; 4.7 mmol), BMIM-PF_6 (160 mg; 0.56 mmol) and AIBN (4.0 mg; 2.4×10^{-2} mmol). The vial was purged with nitrogen, sealed, and heated at 40 °C for 19 h with vigorous stirring. The resulting polymeric material was removed from the vial, washed with acetone (5 mL) and dried under reduced pressure. Cuboidal specimens for mechanical testing were prepared by cutting approximately 50 mg samples from the bulk material and polishing with ultrafine sanding paper.

REPRESENTATIVE PROCEDURE FOR THE PREPARATION OF GFP COMPOSITES: PREPARATION OF GFPUV(Y39C/D103C) COMPOSITES

An 8 mL Teflon capped vial was charged with a stir bar, GFPuv(Y39C/D103C) (0.35 mL 1.7 mg mL^{-1} solution in lysis buffer; 1.8×10^{-8} mmol), MMA (0.5 mL; 4.7 mmol), and AIBN (4.0 mg; 2.4×10^{-2} mmol). The vial was purged with nitrogen, sealed, and heated at 40 °C for 19 h with vigorous stirring. The resulting polymeric material was removed from the vial, washed with acetone (5 mL) and dried under reduce pressure. The resulting material was dissolved in tetrahydofuran (THF; 10 mg mL^{-1}) and analyzed with gel-permeation chromatography (**Figure D1**). Cuboidal specimens for mechanical testing were prepared by cutting approximately 50 mg samples from the bulk material and

polishing with ultrafine sanding paper. GFPuv, GFPuv(Y39C), and GFPuv(D103C) composites were prepared using an analogous procedure.

PREPARATION OF POLY(METHYL METHACRYLATE)

An 8 mL Teflon capped vial was charged with a stir bar, methyl methacrylate (MMA) (0.5 mL; 4.7 mmol), ethylene glycol dimethyacrylate (44 μL; 2.3×10^{-1} mmol) and AIBN (4.0 mg; 2.4×10^{-2} mmol). The vial was purged with nitrogen, sealed, and heated at 40 °C for 19 h with vigorous stirring. The resulting polymeric material was removed from the vial, washed with acetone (5 mL) and dried under reduced pressure. The resulting material was dissolved in tetrahydofuran (THF; 10 mg mL^{-1}) and analyzed with gel-permeation chromatography (**Figure D1**).

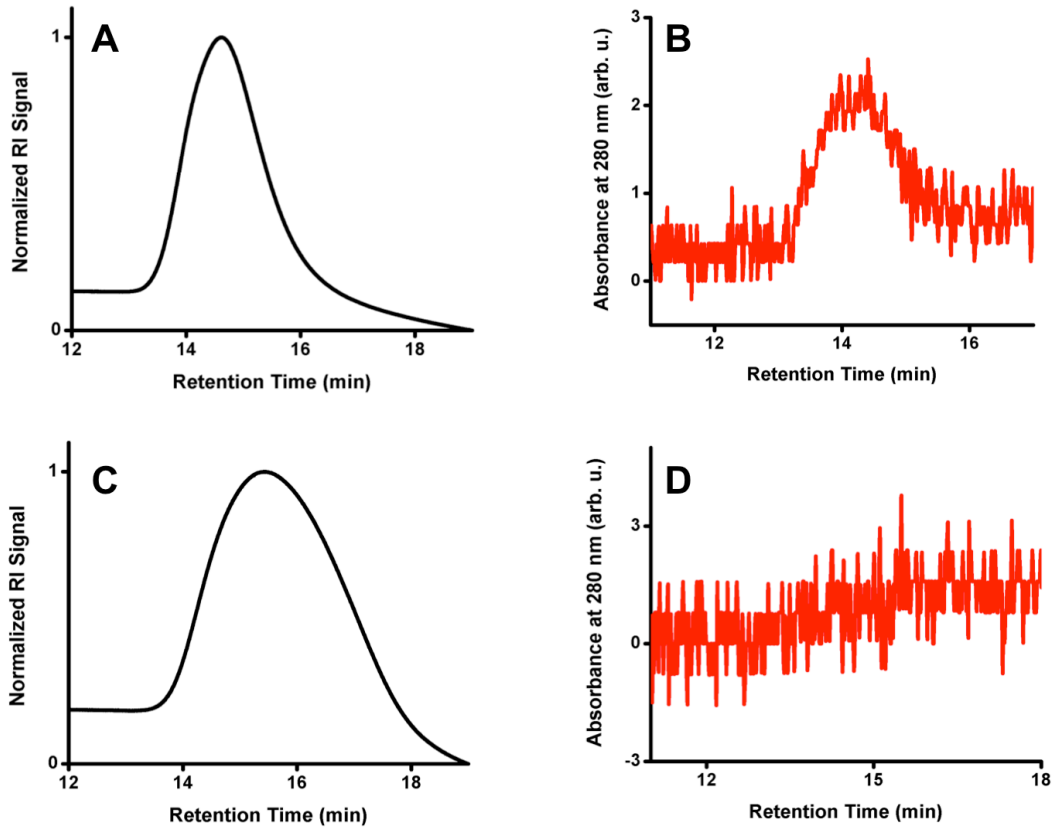

Figure D1 (A) Gel-permeation chromatograph of the GFPuv(Y39C/D103C) composite material (see section 1.5 for additional details). (B) Gel-permeation chromatograph of the GFPuv(Y39C/D103C) composite material visualized with ultraviolet-visible detection at 280 nm. (C) Gel-permeation chromatograph of poly(methyl methacrylate) (see section 1.6 for additional details). (D) Gel-permeation chromatograph of poly(methyl methacrylate) visualized with ultraviolet-visible detection at 280 nm.

General Procedure for Mechanical Activation of eYFP Composites

A 50 mg sample of the eYFP composite was cut from the bulk material (*vide supra*), and the fluorescence of the material was recorded. The sample was then compressed (30, 110, 180, or 360 MPa) in a Carver hydraulic benchtop press for 45 s. The pressure exerted on the sample was determined using the relationship $P = FA^{-1}$, where F is the applied load, A is the cross-sectional area of the sample, and P is the applied pressure. As the Carver press employed two disk-shaped plates, the samples were

found to compress into disks during the experimental studies. As such, *A* was approximated as the area of the disk following compression (DMA studies involving GFPuv composites validated this approximation; *vide infra*). **Figure 6.1** in Chapter 6 shows representative fluorescence spectra (normalized) of the material compressed at 0, 30, 110, 180, and 360 MPa. Increasing the compression time to 1 h did not cause the λ_{em} of the material to shift beyond what was measured after compression for 45 s (see **Figure D2**). A decrease in fluorescence intensity, which was attributed to frictional denaturing (*vide infra*), was also observed (**Figure D3** and **Figure D4**).

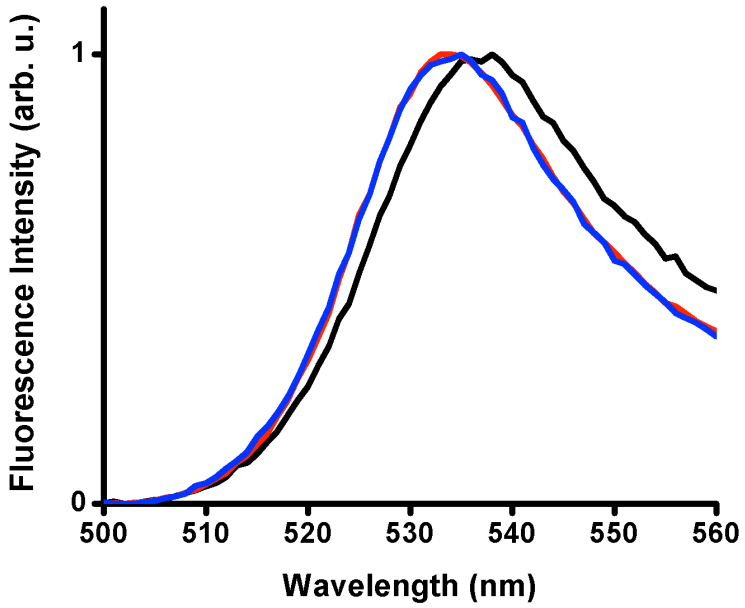

Figure D2 Normalized fluorescence spectra of eYFP composite (black) following compression (110 MPa) for 45 s (red) and 1 h (blue).

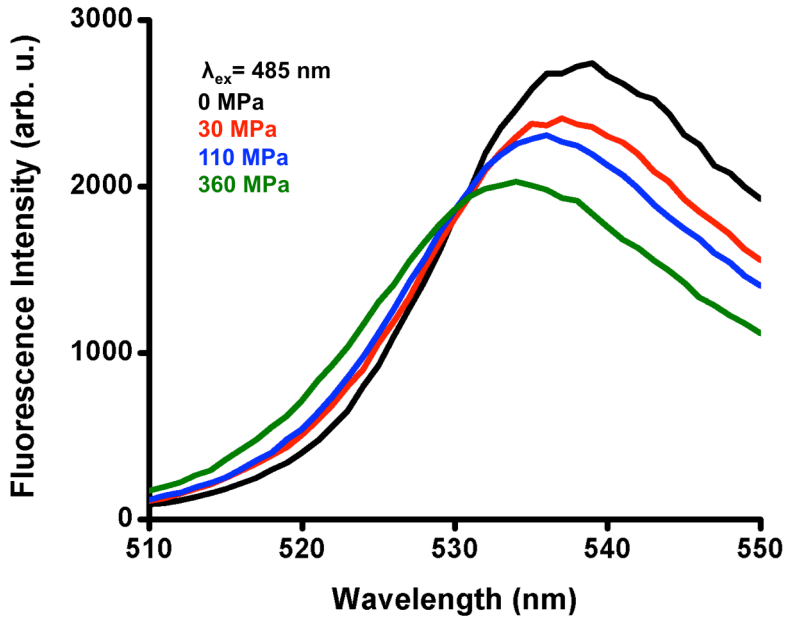

Figure D3 Fluorescence spectra of an eYFP composite (black) after compression at 30 MPa (red), 110 MPa (blue), and 360 MPa (green).

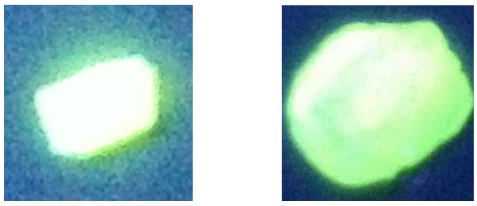

Figure D4 An eYFP-containing composite before (left) and after (right) compression at 110 MPa.

COMPRESSION OF LYOPHILIZED EYFP

Lyophilized eYFP (0.6 mg; 1.8×10^{-8} mmol) was loaded onto a Carver benchtop press and subjected to compression (external load of 3000 psi) for 45 s. The solid-state fluorescence of the sample was recorded (**Figure D5**), and the reduction in fluorescence intensity was attributed to thermal denaturation through frictional heating (a phenomenon previously observed[4] by Bruns *et al.*)

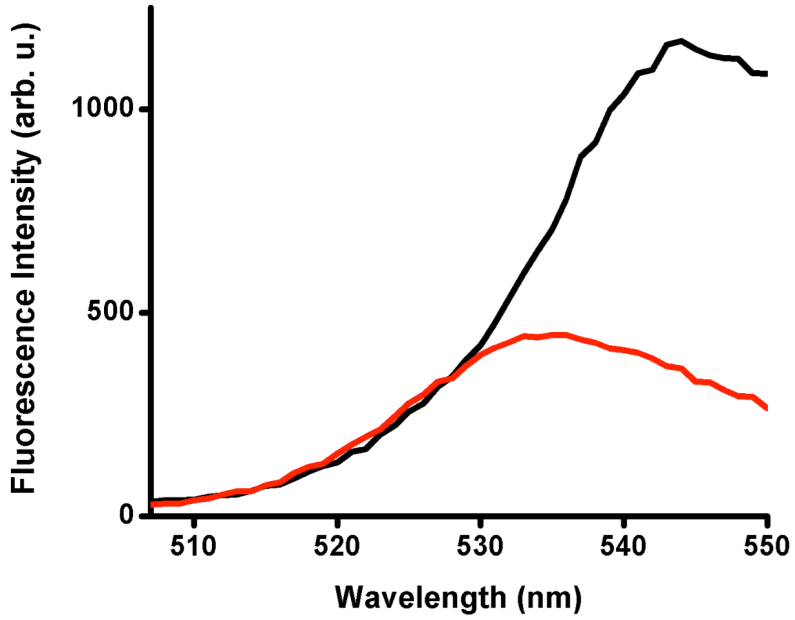

Figure D5 Fluorescence spectra of lyophilized eYFP (black) following compression (external load of 3000 psi; red).

PREPARATION AND MECHANICAL ACTIVATION OF MIXED eYFP/GFPUV(Y39C/D103C) COMPOSITES

A Teflon capped 8 mL vial was charged with eYFP (64 μL 9.4 mg mL^{-1} solution in lysis buffer; 1.8×10^{-5} mmol), GFPuv(Y39C/D103C) (0.24 mL 1.7 mg mL^{-1} solution in lysis buffer; 1.2×10^{-8} mmol), MMA (0.5 mL; 4.7 mmol), BMIM-PF_6 (160 mg; 0.56 mmol) and AIBN (4.0 mg; 2.4×10^{-2} mmol). The vial was purged with nitrogen, sealed, and heated at 40 °C for 19 h with vigorous stirring. The resulting polymeric material was removed from the vial, washed with acetone (5 mL) and dried under reduced pressure. A cuboidal specimen for mechanical testing was prepared by cutting an approximately 50 mg sample from the bulk material and polishing with ultrafine sanding paper. The sample was then compressed at 30 MPa for 45 s. **Figure D6** shows that the λ_{em} of eYFP was hypsochromically shifted following compression, whereas the λ_{em} of

GFPuv(Y39C/D103C) did not shift following compression (the fluorescence intensity did, however, decrease).

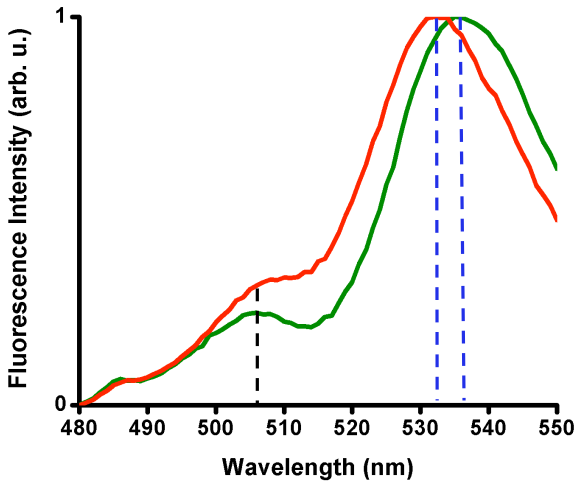

Figure D6 Normalized fluorescence spectra of mixed eYFP/GFPuv(Y39C/D103C) composite (green) following compression (30 MPa; 45 s). Dashed blue lines are drawn from the λ_{em} associated with eYFP. A dashed black line is drawn from the λ_{em} associated with GFPuv(Y39C/D103C).

General Procedure for Compression of GFP Composites

A 50 mg sample of the GFP composite was cut from the bulk material (*vide supra*), and the fluorescence of the material was recorded. The sample was then compressed (21, 31, or 41 MPa) in a Carver hydraulic benchtop press for 45 s. The pressure exerted on the sample was determined using the relationship $P = FA^{-1}$, where F is the applied load, A is the cross-sectional area of the sample, and P is the applied pressure. As the Carver press employed two disk-shaped plates, the samples were found to compress into disks during the experimental studies. As such, A was approximated as the area of the disk following compression. **Figure 6.2** in Chapter 6 shows representative fluorescence spectra of the GFP materials following compression at various pressures (see also **Figure D9**). Increasing the compression time to 1 h did not cause the

fluorescence intensity of the GFPuv(Y39C/D103C) material to decrease beyond what was measured after compression for 45 s at the same pressure (see **Figure D7**). Moreover, increasing the compression time to 1 h did not cause the fluorescence intensity of the control materials (*e.g.*, the GFPuv composite) to alter significantly from that measured following compression for 45 s at the same pressure (**Figure D8**).

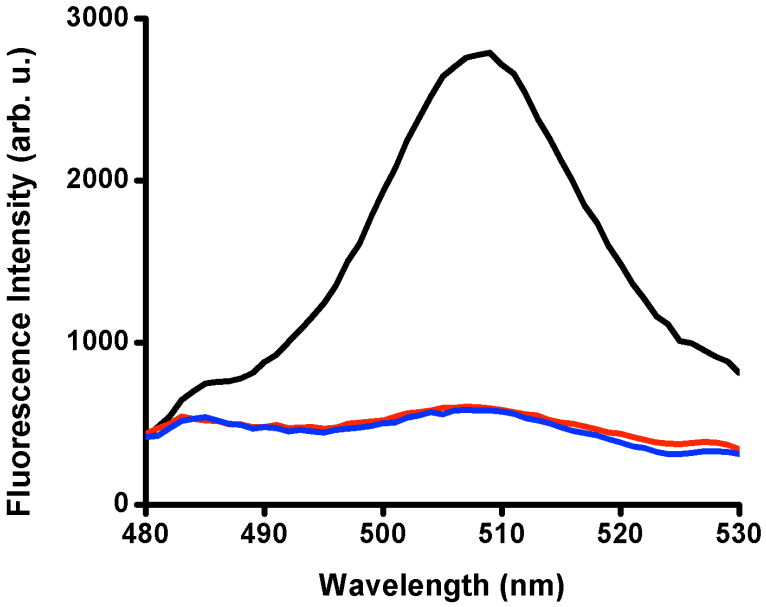

Figure D7 Fluorescence spectra of GFPuv(Y39C/D103C) composite (black) following compression (31 MPa) for 45 s (red) and 1 h (blue).

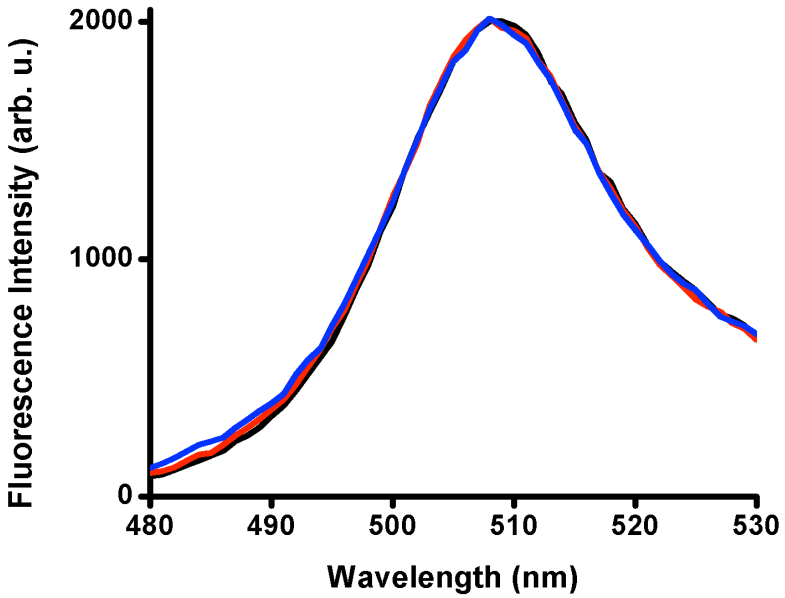

Figure D8 Fluorescence spectra of GFPuv composite (black) following compression (31 MPa) for 45 s (red) and 1 h (blue).

Figure D9 A GFPuv(Y39C/D103C)-containing composite before (left) and after (right) compression (external load of 7000 psi).

REPRESENTATIVE PROCEDURE FOR DMA ANALYSIS OF GFPUV(Y39C/D103C) COMPOSITE

A cuboidal specimen of the GFPuv(Y39C/D103C) composite (1.14 mm × 1.14 mm × 0.72 mm) was mounted in a TA Instruments Q800 series DMA outfitted with a compression clamp and subjected to controlled force compression (pre-load force of 0.001 N; force ramp rate of 1 N min^{-1}). The applied stress and resultant material strain

were recorded until a maximal stress of approximately 10.4 MPa was exerted on the sample (**Figure D10**). The fluorescence intensity of the material following DMA analysis was found to decrease relative to the fluorescence intensity of the material prior to DMA analysis (**Figure D10**).

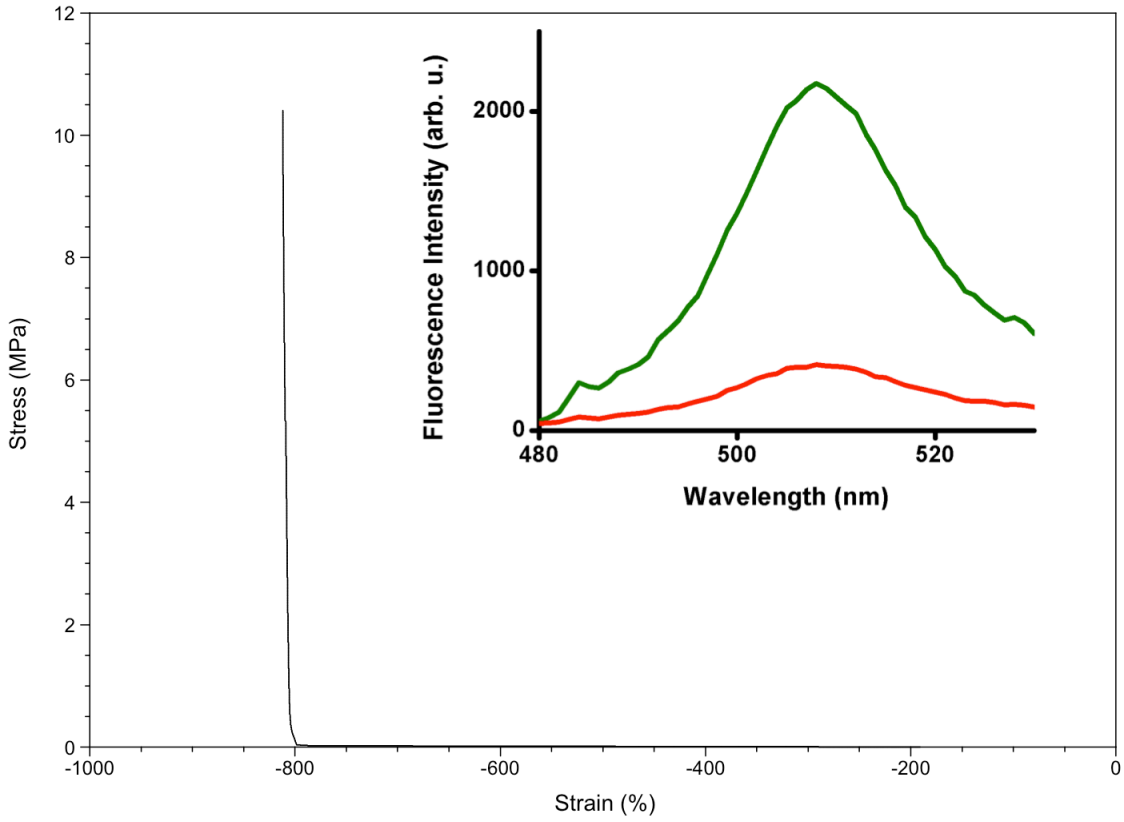

Figure D10 Stress/strain curve for DMA analysis of GFPuv(Y39C/D103C) composite. Inset shows the fluorescence of the composite prior to (green) and following (red) DMA analysis.

REPRESENTATIVE PROCEDURE FOR DMA ANALYSIS OF GFP CONTROL MATERIALS: DMA ANALYSIS OF GFPUV COMPOSITE.

A cuboidal specimen of GFPuv composite (1.18 mm × 1.18 mm × 0.71 mm) was mounted in a TA Instruments Q800 series DMA outfitted with a compression clamp and

subjected to controlled force compression (pre-load force of 0.001 N; force ramp rate of 1 N min^{-1}). The applied stress and resultant material strain were recorded until a maximal stress of approximately 10.4 MPa was exerted on the sample (**Figure D11**). The fluorescence intensities of the material prior to and following DMA analysis are shown in **Figure D11**.

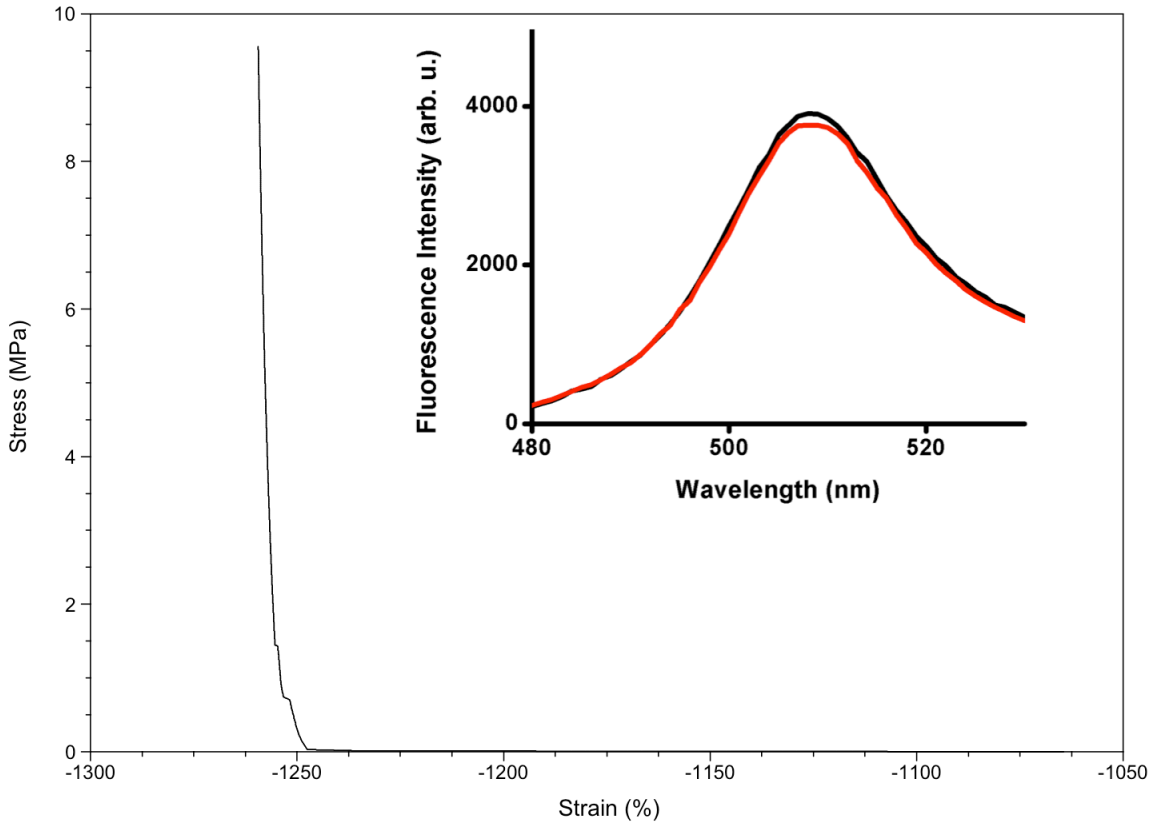

Figure D11 Stress/strain curve for DMA analysis of GFPuv composite. Inset shows the fluorescence of the composite prior to (black) and following (red) DMA analysis.

GFPuv Mass Spectrometry Studies: General Considerations

Proteins were infused into an Orbitrap Elite mass spectrometer (ThermoFisher, San Jose, CA) at 5 μL/min. Intact protein spectra were collected in positive mode and were a composite of 50 averaged scans acquired at maximum resolution (240,000 at m/z 400). Neutral masses were then extrapolated using the Xtract algorithm (ThermoFisher, San Jose, CA) with a signal to noise ratio of 5:1.

Procedure for Evaluating the Reactivity of GFPuv(Y39C/D103C) with Methyl Methacrylate under Polymerization Conditions

An 8 mL Teflon capped vial was charged with a stir bar, GFPuv(Y39C/D103C) (0.35 mL 1.7 mg mL^{-1} solution in lysis buffer; 1.8×10^{-8} mmol), MMA (0.5 mL; 4.7 mmol), and AIBN (4.0 mg; 2.4×10^{-2} mmol). The vial was purged with nitrogen, sealed, and heated at 40 °C for 10 minutes with vigorous stirring. The vial was exposed to the ambient atmosphere, and the reaction mixture was subsequently desalted and buffer exchanged via 5 sequential exchanges using a 10 kDa molecular weight cutoff filter into LC-MS grade water. The resulting protein solution was diluted to 10 μM in 49/50/1 water/acetonitrile/formic acid, and infused into an Orbitrap Elite mass spectrometer. As shown in **Figure D12**, both cysteine mutations were reactive with methyl methacrylate under these conditions.

Procedure for Evaluating the Reactivity of GFPuv(Y39C/D103C) with Methyl Methacrylate in the Absence of Radical Initiators

An 8 mL Teflon capped vial was charged with a stir bar, GFPuv(Y39C/D103C) (0.35 mL 1.7 mg mL^{-1} solution in lysis buffer; 1.8×10^{-8} mmol), and MMA (0.5 mL; 4.7 mmol). The vial was purged with nitrogen, sealed, and heated at 40 °C for 10 minutes with vigorous stirring. The vial was exposed to the ambient atmosphere, and the reaction mixture was subsequently desalted and buffer exchanged via 5 sequential exchanges

using a 10 kDa molecular weight cutoff filter into LC-MS grade water. The resulting protein solution was diluted to 10 μM in 49/50/1 water/acetonitrile/formic acid, and infused into an Orbitrap Elite mass spectrometer. As shown in **Figure D12**, both cysteine mutations were not reactive with methyl methacrylate under these conditions.

Procedure for Evaluating the Reactivity of GFPuv with Methyl Methacrylate under Polymerization Conditions

An 8 mL Teflon capped vial was charged with a stir bar, GFPuv (0.14 mL 4.2 mg mL^{-1} solution in lysis buffer; 1.8×10^{-8} mmol), MMA (0.5 mL; 4.7 mmol), and AIBN (4.0 mg; 2.4×10^{-2} mmol). The vial was purged with nitrogen, sealed, and heated at 40 °C for 10 minutes with vigorous stirring. The vial was exposed to the ambient atmosphere, and the reaction mixture was subsequently desalted and buffer exchanged via 5 sequential exchanges using a 10 kDa molecular weight cutoff filter into LC-MS grade water. The resulting protein solution was diluted to 10μM in 49/50/1 water/acetonitrile/formic acid, and infused into an Orbitrap Elite mass spectrometer. **Figure D12** shows that no change in the mass of the protein was observed under these conditions.

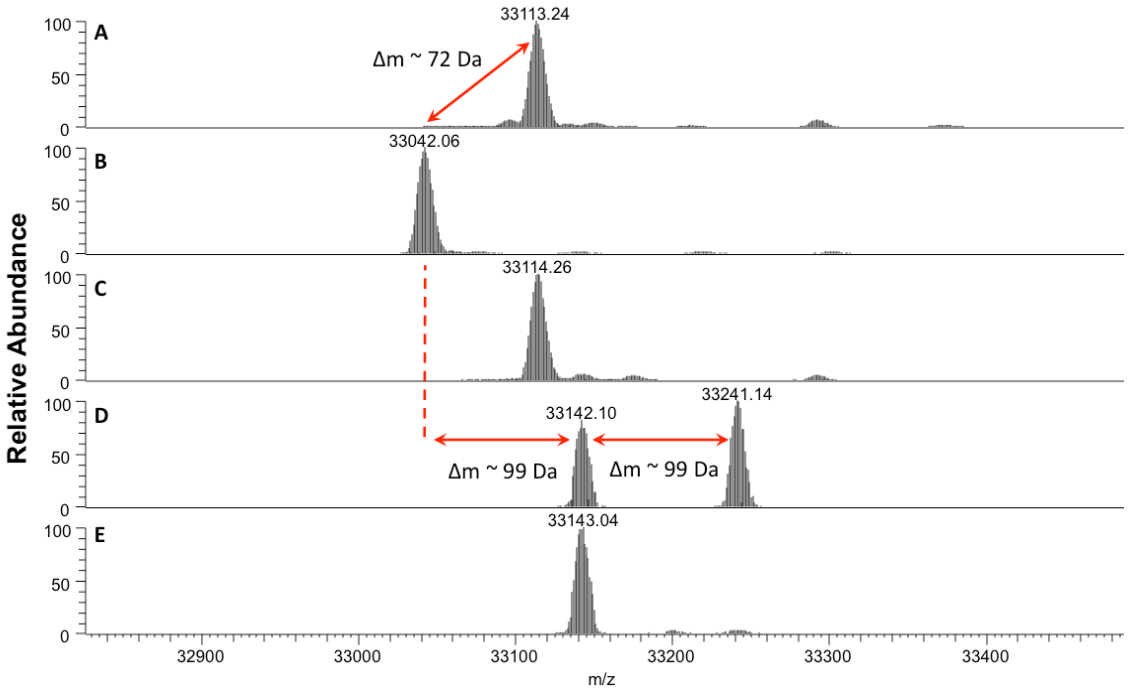

Figure D12 (A, B) Deconvoluted intact mass spectra of GFPuv (A) and GFPuv(Y39C/D103C) (B). The expected 72 Da mass shift associated with both mutations is observed. (C) Deconvoluted intact mass spectrum of GFPuv following reaction with methyl methacrylate in the presence of AIBN. (D) Deconvoluted intact mass spectrum of GFPuv(Y39C/D103C) following reaction with methyl methacrylate in the presence of AIBN. (E) Deconvoluted intact mass spectrum of GFPuv(Y39C/D103C) following reaction with methyl methacrylate in the absence of AIBN.

WIDE FIELD FLUORESCENCE MICROSCOPY GENERAL CONSIDERATIONS

Fluorescence images were collected at room temperature using an upright microscope (Olympus BX60) with high-pressure mercury lamp excitation and a dichroic mirror (Olympus WB filter cube) combined with a digital camera (SPOT). The microscope objective lens used was a 5 X, 0.12 N.A., dry, CP-Achromat (Zeiss, 440920). All fluorescence images are false-colored (ImageJ thallium filter).

PREPARATION OF GFPUV(Y39C/D103C) COMPOSITE FOR WIDE FIELD FLUORESCENCE MICROSCOPY ANALYSIS

An 8 mL Teflon capped vial was charged with a stir bar, GFPuv(Y39C/D103C) (0.35 mL 1.7 mg mL^{-1} solution in lysis buffer; 1.8×10^{-8} mmol), MMA (0.5 mL; 4.7 mmol), and AIBN (4.0 mg; 2.4×10^{-2} mmol). The vial was purged with nitrogen, sealed, and heated at 40 °C for 19 h with vigorous stirring. The resulting polymeric material was removed from the vial, washed with acetone (5 mL) and dried under reduced pressure. A cuboidal specimen was prepared by cutting an approximately 50 mg sample from the bulk material and polishing with ultrafine sanding paper. The specimen was mounted into a Carver benchtop hydraulic press, and a square plate (2.41 mm × 2.41 mm) was compressed into the material. The area of the plate and the applied load were used to calculate the pressure exerted on the sample (approximately 10.3 MPa). The sample was then analyzed using a wide field fluorescence microscope, which revealed decreased fluorescence intensity in the compressed area relative to the uncompressed material (**Figure D13**).

PREPARATION OF GFPUV COMPOSITE FOR WIDE FIELD FLUORESCENCE MICROSCOPY ANALYSIS

An 8 mL Teflon capped vial was charged with a stir bar, GFPuv (0.14 mL 4.2 mg mL^{-1} solution in lysis buffer; 1.8×10^{-8} mmol), MMA (0.5 mL; 4.7 mmol), and AIBN (4.0 mg; 2.4×10^{-2} mmol). The vial was purged with nitrogen, sealed, and heated at 40 °C for 19 h with vigorous stirring. The resulting polymeric material was removed from the vial, washed with acetone (5 mL) and dried under reduced pressure. A cuboidal specimen was prepared by cutting an approximately 50 mg sample from the bulk material and polishing with ultrafine sanding paper. The specimen was mounted into a Carver benchtop hydraulic press, and a square plate (2.41 mm × 2.41 mm) was compressed into

the material. The area of the plate and the applied load were used to calculate the pressure exerted on the sample (approximately 10.3 MPa). The sample was then analyzed using a wide field fluorescence microscope, which revealed negligible changes in the fluorescence intensity in the compressed area relative to the uncompressed material (**Figure D14**).

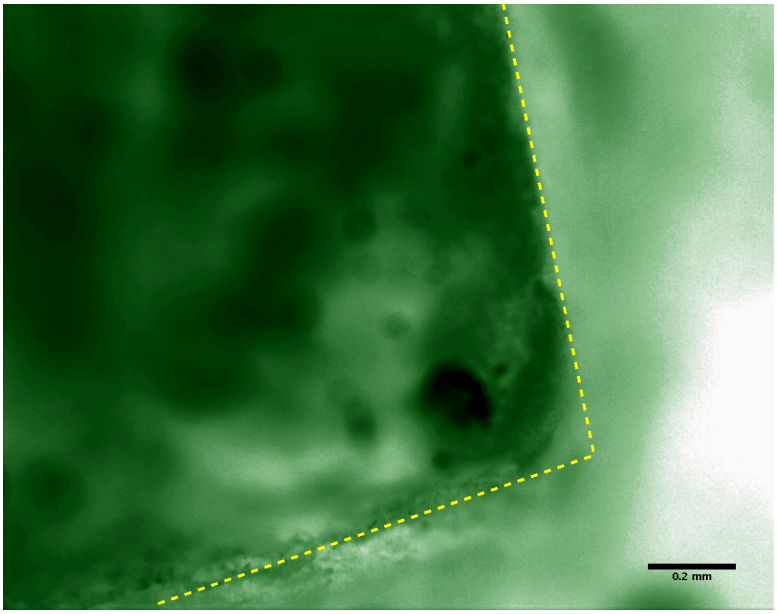

Figure D13 Wide field fluorescence micrograph of GFPuv(Y39C/D103C) composite following compression. The yellow dashed line outlines the edge of the square compression site (see text for additional details).

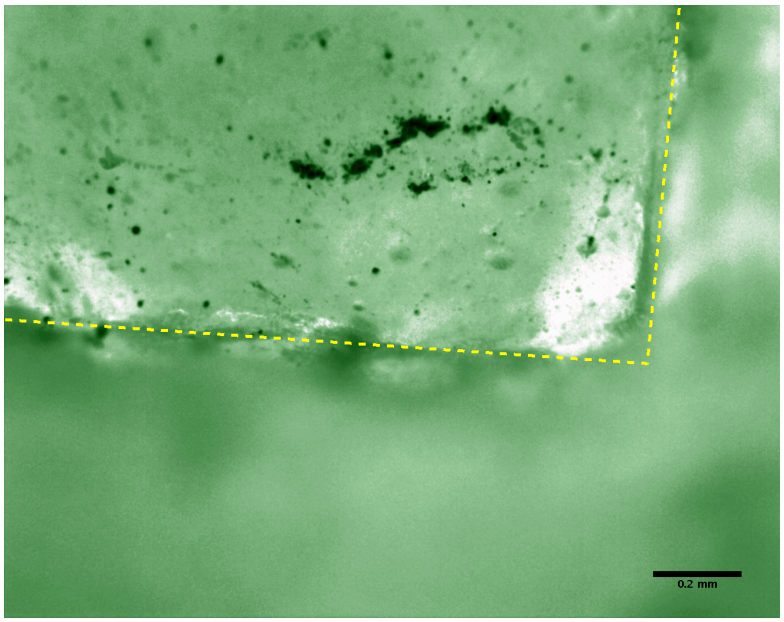

Figure D14 Wide field fluorescence micrograph of GFPuv composite following compression. The yellow dashed line outlines the edge of the square compression site (see text for additional details).

REFERENCES

1 Dupont, J.; Consorti, C.; Suarez, P.; de Souza, R. *Org. Synth.* **2004**, *10*, 184.

2 Kawate, T.; Gouaux, E. *Structure* **2006**, *14*, 673.

3 Nagai, T.; Ibata, K.; Park, E. S.; Kubota, M.; Mikoshiba, K.; Miyawaki, A. *Nature Biotech.* **2002**, *20*, 87.

4 Makyła, K.; Müller, C.; Lörcher, S.; Winkler, T.; Nussbaumer, M. G.; Eder, M; Bruns, N. *Adv. Mater.* **2013**, *25*, 2701.

References

Agnew, H. D.; Rhode, R. D.; Millward, S. W.; Nag, A.; Yeo, W. S.; Hein, J. E.; Pitram, S. M.; Tariq, A. A.; Burns, V. M.; Krom, R. J.; Fokin, V. V.; Sharpless, K. B.; Heath, J. R. *Angew. Chem. Int. Ed.* **2009**, *48*, 4944.

Akbulatov; S.Tian, Y.; Kapustin, E.; Boulatov, R. *Angew. Chem. Intl. Ed.* **2013**, *52*, 6992.

Antoni, P.; Robb, M. J.; Campos, L.; Montanez, M.; Hult, A.; Malmström, E.; Malkoch, M.; Hawker, C. J. *Macromolecules* **2010**, *43*, 6625.

Antonin, H. *Collect. Czech. Chem. Commun.* **1989**, *54*, 446.

Azzaroni, O.; Trappmann, B.; van Rijn, P.; Zhou, F.; Kong, B.; Huck, W. T. S. *Angew. Chem. Int. Ed.* **2006**, *45*, 7440.

Bailey, A.; Mosey, N. J. *J. Chem. Phys.* **2012**, *136*, 044102.

Barsegov, V.; Thirumalai, D. *Proc. Natl Acad. Sci. USA* **2005**, *102*, 1835.

Barstow, B.; Ando, N.; Kim, C. U.; Gruner, S. M. *Proc. Natl. Acad. Sci. USA* **2008**, *105*, 13362.

Barstow, B.; Ando, N.; Kim, C. U.; Gruner, S. M. *Biophys. J.* **2009**, *97*, 1719.

Baytekin, H. T.; Baytekin, B.; Grzybowski, B. A. *Angew. Chem. Int. Ed.* **2012**, *124*, 3656.

Becke, A. D. *J. Chem. Phys.***1993**, *98*, 1372.

Beiermann, B. A.; Davis, D. A.; Kramer, S. L. B.; Moore, J. S.; Sottos, N. R.; White, S. R. *J. Mater. Chem.* **2011**, *21*, 8443.

Bell, G. *Science* **1978**, *200*, 618.

Berezin, I. V.; Klibanov, A. M.; Martinek, K. **1974**, *364*, 193.

Berkowski, K. L.; Potisek, S. L.; Hickenboth, C. R.; Moore, J. S. *Macromolecules* **2005**, *38*, 8975.

Beyer, M. K. *J. Chem. Phys.* **2000**, *112*, 7307.

Beyer, M. K.; Clausen-Schaumann, H. *Chem. Rev.* **2005**, *105*, 2921.

Black, A. L.; Lenhardt, J. M.; Craig, S. L. *J. Mater. Chem.* **2011**, *21*,1655.

Black, A. L.; Orlicki, J. A.; Craig, S. L. *J. Mater. Chem.* **2011**, *21*, 8460.

Bode, B. M.; Gordon, M. S. *J. Mol. Graphics Modell.* **1998**, *16*, 133.

Boltzmann, L. *Lectures on Gas Theory*, Translated by Stephen G. Brush. Univ. of California Press, Berkeley. **1964**.

Boren, B. C.; Narayan, S.; Rasmussen, L. K.; Zhang, L.; Zhao, H.; Lin, Z.; Jia, G.; Fokin, V. V. *J. Am. Chem. Soc.* **2008**, *130*, 8923.

Boul, P. J.; Reutenaur, P.; Lehn, J. M.; *Org. Lett.* **2005**, *7*, 15.

Boulatov, R.; Kucharski, T. J. *J. Mater. Chem.* **2011**, *21*, 8237.

Brantley, J. N.; Bailey, C. B.; Wiggins, K. M.; Keatinge-Clay, A. T.; Bielawski, C. W. *Polym. Chem.* **2013**, *4*, 3916.

Brantley, J. N.; Konda, S. S. M.; Makarov, D. E.; Bielawski, C. W. *J. Am. Chem. Soc.* **2012**, *134*, 9882.

Brantley, J. N.; Wiggins, K. M.; Bielawski, C. W. *Science* **2011**, *333*, 1606.

Brockwell, D. J.; Paci, E.; Zinober, R. C.; Beddard, G. S.; Olmsted, P. D.; Smith, D. A.; Perham, R. N.; Radford, S. E. *Nat. Struct. Biol.* **2003**, *10*, 731.

Browne, W. R.; Feringa, B. L. *Nat. Nano.* **2006**, *1*, 1748.

Bruns, N.; Clark, D. *Chimia.* **2010**, *65*, 245.

Bruns, N.; Pustelny, K.; Bergeron, L. M.; Whitehead, T. A.; Clark, D. S. *Angew. Chem. Int. Ed.* **2009**, *48*, 5666.

Buchholz, B. A.; Zahn, J. M.; Kenward, M.; Slater, G. W.; Barron, A. E. *Polymer* **2004**, *45*, 1223.

Bustamante, C.; Chemla, Y.R.; Forde, N. R.; Izhaky, D. *Annu. Rev. Biochem.* **2004**, *73*, 705.

Carrington, S. P.; Odell, J. A. *J. Non-Newtonian Fluid Mech.* **1996**, *67*, 269 and references cited therein.

Caruso, M. M.; Davis, D. A.; Shen, Q.; Odom, S. A.; Sottos, N. R.; White, S. R.; Moore, J. S. *Chem. Rev.* **2009**, *109*, 5755.

Casale, A.; Porter, R. S. *Polymer Stress Reactions,* Academic Press, New York, **1978**.

Chen, X.; Dam, M.; Ono, K.; Mal, A.; Shen, H.; Nutt, S. R.; Sheran, K.; Wudl, F. *Science* **2002**, *295*, 1698.

Chen, Y.; Spiering, A. J. H.; Karthikeyan, S.; Peters, G. W. M.; Meijer, E. W.; Sijbesma, R. P. *Nat. Chem.* **2012**, *4*, 559.

Chiba, K.; Du, H. ; Eguchi, Y.; Fujita, M.; Goto, M.; Gusovsky, F.; Harmange, J.- C.; Inoue, A.; Kawada, M.; Kawai, T.; Kawakami, Y.; Kimura, A.; Kotake, M.; Kuboi, Y.; Matsushima, T.; Mizui, Y.; Muramoto, K.; Sakurai, H.; Shen, Y.- C.; Shirota, H.; Spyvee, M.; Tanaka, I.; Wang, Y.; Wood, R.; Yamamoto, S.; Yoneda, N. *U.S. Pat. Appl. Publ.* **2004**, *20040224936*.

Cho, S.- Y.; Kim, J.- G.; Chung, C.- M. *Sens. Actuators B* **2008**, *134*, 822.

Choi, B.; Zocchi, G.; Wu, Y.; Chan, S.; Jeanne Perry, L. *Phys. Rev. Lett.* **2005**, *95*, 078102.

Coady, D. J.; Bielawski, C. W. *Macromolecules* **2006**, *39*, 8895.

Coady, D. J.; Khramov, D. M.; Norris, B. C.; Tennyson, A. G.; Bielawski, C. W. *Angew. Chem. Int. Ed.* **2009**, *48*, 5187.

Corbett, P. T.; Leclaire, J.; Vial, L.; West, K. R.; Wietor, J. L.; Sanders, J. K. M.; Otto, S. *Chem. Rev.* **2006**, *106*, 3652.

Cramer, N. B.; Bowman, C. N. *J. Polym. Sci. Part A Polym. Chem.* **2001**, *39*, 3311.

Crameri, A.; Whitehorn, E. A.; Tate, E.; Stemmer, W. P. *Nat. Biotechnol.* **1996**, *14*, 315.

Crenshaw, B. R.; Weder, C. *Chem. Mater.* **2003**, *15,* 4717 and references cited therein.

Davis, D. A.; Hamilton, A.; Yang, J.; Cremar, L. D.; Van Gough, D.; Potisek, S. L.; Ong, M. T.; Braun, P. V.; Martínez, T. J.; White, S. R.; Moore, J. S.; Sottos, N. R. *Nature* **2009**, *459*, 68.

Davis, J. R. *Tensile Testing*, ASM International, Ohio, 2nd ed., **2004**, ch. 1, pp 1–12.

Diesendruck, C. E.; Steinberg, B. D.; Sugai, N.; Silberstein, M. N.; Sottos, N. R.; White, S. R.; Braun, P. V.; Moore, J. S. *J. Am. Chem. Soc.* **2012**, *134*, 12446.

Dietz, H.; Rief, M.; Lorimer, G. H. **2004**, *101*, 16192.

Dimroth, O. *Liebigs Ann.* **1909**, *364*, 183.

Dimroth, O.; Michaelis, W. *Liebigs Ann.* **1927**, *459*, 39.

Dopieralski, P.; Anjukandi, P.; Ruckert, M.; Shiga, M.; Ribas-Arino, J.; Marx, D. *J. Mater. Chem.* **2011**, *21*, 8309.

Dopieralski, P.; Ribas-Arino, J.; Anjukandi, P.; Krupicka, M.; Kiss, J.; Marx, D. *Nat. Chem.* **2013**, *5*, 685.

Dudko, O. K.; Filippov, A. E.; Klafter, J.; Urbakh, M. *Proc. Natl. Acad. Sci. U.S.A.* **2003**, *100*, 11378.

Dudko, O. K.; Graham, T. G.; Best, R, B. *Phys. Rev. Lett.* **2011**, *107*, 208301.

Dudko, O. K.; Hummer, G.; Szabo, A. *Phys. Rev. Lett.* **2006**, *96*, 108101.

Dudko, O. K.; Hummer, G.; Szabo, A. *Proc. Natl. Acad. Sci. U.S.A.* **2008**, *105*, 15755.

Dudko, O. K.; Mathe, J.; Szabo, A.; Meller, A.; Hummer, G. *Biophys. J.* **2007**, *92*, 4188.

Dupont, J.; Consorti, C.; Suarez, P.; de Souza, R. *Org. Synth.* **2004**, *10*, 184.

Encina, M. V.; Lissi, E.; Sarasúa, M.; Gargallo, L.; Radic, D. *J. Poly. Sci.: Poly. Lett. Ed.* **1980**, *18*, 757.

Eom, K.; Baek, S. C.; Ahn, J. H.; Na, S. *J. Comput. Chem.* **2007**, *28*, 1400.

Evans, E.; Ritchie, K. *Biophys. J.* **1997**, *72*, 1541.

Evans, E.; Ritchie, K. *Biophys. J.* **1999**, *76*, 2439.

Florea, M. *J. Appl. Polym. Sci.* **1993**, *50*, 2039 and references cited therein.

Flosdorf, E. W.; Chambers, L. A. *J. Am. Chem. Soc.* **1933**, *55*, 3051.

Franco, I.; George, C. B.; Solomon, G. C.; Schatz, G. C.; Ratner, M. A. *J. Am. Chem. Soc.* **2011**, *133*, 2242.

Franco, I.; Schatz, G. C.; Ratner, M. A. *J. Chem. Phys.* **2009**, *131*, 124902.

Glynn, P. A. R.; van der Hoff, B. M. E. *J. Macromol. Sci., Part A* **1973**, *A7*, 1695.

Gonzalez, C.; Schlegel, H. B. *J. Chem. Phys.* **1989**, *90*, 2154.

Gonzalez, C.; Schlegel, H. B. *J. Phys. Chem.* **1990**, *94*, 5523.

Gordon, M. S.; Binkley, J. S.; Pople, J. A.; Pietro, W. J.; Hehre, W. J. *J. Am. Chem. Soc.* **1982**, *104*, 2797.

Groote, R.; van Haandel, L.; Sijbesma, R. P. *J. Polym. Sci. Part A Polym. Chem.* **2012**, *50*, 4929.

Guyan, R. J. *AIAA J.* **1965**, *3*, 380.

Hanggi, P.; Talkner, P.; Borkovec, M. *Rev. Mod. Phys.* **1990**, *62*, 251.

Hein, J. E.; Tripp, J. C.; Krasnova, L. B.; Sharpless, K. B.; Fokin, V. V. *Angew. Chem. Int. Ed.* **2009**, *48*, 8018.

Helms, V.; Straatsma, T. P.; McCammon, J. A. *J. Phys. Chem. B* **1999**, *103*, 3263.

Herndon, W.; Grayson, C. *J. Org. Chem.* **1967**, *32*, 526.

Hickenboth, C. R.; Moore, J. S.; White, S. R.; Sottos, N. R.; Baudry, J.; Wilson, S. R. *Nature* **2007**, *446*, 423.

Hickenboth, C. R.; Rule, J.; Moore, J. S. *Tetrahedron* **2008**, *64*, 8435.

Horn, A. F.; Merrill, E. W. *Nature* **1984**, *312*, 140.

Horneff, T.; Chuprakov, S.; Chernyak, N.; Gevorgyan, V.; Fokin, V. V. *J. Am. Chem. Soc.* **2008**, *130*, 14972.

Huang, Z.; Boulatov, R. *Chem. Soc. Rev.* **2011**, *40*, 2359.

Huang, Z.; Boulatov, R. *Pure App. Chem.* **2010**, *82*, 931.

Hummer, G.; Szabo, A. *Biophys. J.* **2003**, *85*, 5.

Hyeon, C.; Thirumalai, D. *Biophys. J.* **2006**, *90*, 3410.

Iha, R. K.; Wooley, K. L.; Nyström, A. M.; Burke, D. J.; Kade, M. J.; Hawker, C. J. *Chem Rev.* **2009**, *109*, 5620.

Ikawa, T.; Shiga, T.; Okada, A. *J. Appl. Polym. Sci.* **1997**, *66*,1569.

Ikawa, T.; Shiga, T.; Okada, A. *J. Appl. Polym. Sci.* **2002**, *83*, 2600 and references cited therein.

Jagannathan, B.; Elms, P. J.; Bustamante, C.; Marqusee, S. *Proc. Natl Acad. Sci. USA* **2012**, *109*, 17820.

Karthikeyan, S.; Potisek, S. L.; Piermattei, A.; Sijbesma, R. P. *J. Am. Chem. Soc.* **2008**, *130*, 14968.

Kauzmann, W.; Eyring, H. *J. Am. Chem. Soc.* **1940**, *62*, 3113.

Kawate, T.; Gouaux, E. *Structure* **2006**, *14*, 673.

Kean, Z. S.; Black Ramirez A. L.; Craig, S. L. *J. Polym. Sci. B. Polym. Phys.* **2012**, *50*, 3481.

Khramov, D. M.; Bielawski, C. W. *Chem. Commun.* **2005**, 4958.

Khramov, D. M.; Bielawski, C. W. *J. Org. Chem.* **2007**, *72*, 9407.

Kim, S.- J.; Reneker, D. H. *Polym. Bull.* **1993**, *31*, 367.

Kingsbury, C. M.; May, P. A.; Davis, D. A.; White S. R.; Moore, J. S.; Sottos, N. R.; *J. Mater. Chem.* **2011**, *21*, 8381.

Kirmizialtin, S.; Huang, L.; Makarov, D. E. *J. Chem. Phys.* **2005**, *122*, 234915.

Klibanov, A.; Samokhin, G.; Martinek, K.; Berezin, I. V. *Biochim. Biophys. Acta* **1976**, *438*, 1.

Klukovich, H. M.; Kean, Z. S.; Iacono, S. T.; Craig, S. L. *J. Am. Chem. Soc.* **2011**, *133*, 17882.

Klukovich, H. M.; Kean, Z. S.; Ramirez, A. L. B.; Lenhardt, J. M.; Lin, J.; Hu, X.; Craig, S. L. *J. Am. Chem. Soc.* **2012**, *134*, 9577.

Kochhar, G. S.; Bailey, A.; Mosey, N. J. *Angew. Chem. Int. Ed.* **2010**, *49*, 7452.

Konda, S. S. M.; Brantley, J. N.; Bielawski, C. W.; Makarov, D. E. *J. Chem. Phys.* **2011**, *135*, 164103.

Kryger, M. J.; Munaretto, A. M.; Moore, J. S. *J. Am. Chem. Soc.* **2011**, *133*, 18992.

Kryger, M. J.; Ong, M. T.; Odom, S. A.; Sottos, N. R.; White, S. R.; Martinez, T. J.; Moore, J. S. *J. Am. Chem. Soc.* **2010**, *132*, 4558.

Kucharski, T. J.; Boulatov, R. *J. Mater. Chem.* **2011**, *21*, 8237.

Kwart, H.; King, K. *Chem. Rev.* **1968**, *68*, 415.

Lacks, D. J.; Willis, J.; Robinson, M.-P. *J. Phys. Chem. B* **2010**, *114*, 10821.

Laland, S. G.; Overend, W. G.; Stacey, *M. J. Chem. Soc.* **1952**, 303.

Lee, C. K.; Davis, D. A.; White, S. R.; Moore, J. S.; Sottos, N. R.; Braun, P. V. *J. Am. Chem. Soc.* **2010**, *132*, 16107.

Lehn, J. M. *Chem. Soc. Rev.* **2007**, *36*, 151.

Lenhardt, J. M.; Black, A. L.; Beirmann, B. A.; Steinberg, B. D.; Rahman, F.; Somaborski, T.; Elsakr, J.; Moore, J. S.; Sottos, N. R.; Craig, S. L. *J. Mater. Chem.* **2011**, *21*, 8454.

Lenhardt, J. M.; Black, A. L.; Craig, S. L. *J. Am. Chem. Soc.* **2009**, *131*, 10818.

Lenhardt, J. M.; Ong, M. T.; Choe, R.; Evenhuis, C. R.; Martinez, T. J.; Craig, S. L. *Science* **2010**, *329*, 1057.

Li, H.; Cao, Y. *Acc. Chem. Res.* **2010**, *43*, 1331.

Li, P.-C.; Makarov, D. E. *J. Chem. Phys.* **2003**, *119*, 9260.

Li, P.-C.; Makarov, D. E. *J. Chem. Phys.* **2004**, *121*, 4826.

Lietard, J.; Meyer, A.; Vasseur, J.; Morvan, F. *J. Org. Chem.* **2008**, *73*, 191.

Lu, X.; Bittmamn, R. *J. Org. Chem.* **2005**, *70*, 4746.

Lumley, J. L. *Ann. Rev. Fluid Mech.* **1969**, *1*, 367.

Makarov, D. E. *Biophys. J.* **2007**, *92*, 4135.

Makarov, D. E. In *Single-molecule Studies of Proteins*; Oberhauser, A. F. Ed.; Springer, New York, 2013.

Makyła, K.; Müller, C.; Lörcher, S.; Winkler, T.; Nussbaumer, M. G.; Eder, M; Bruns, N. *Adv. Mater.* **2013**, *25*, 2701.

Malhotra, S. *J. Macromol. Sci., Part A* **1982**, *18*, 1055.

Malhotra, S. *J. Macromol. Sci., Part A* **1986**, 37.

Maloney, C. E.; Lacks, D. J. *Phys. Rev. E Stat. Nonlinear Soft Matter Phys.* **2006**, *73*, 061106.

Mantovani, G.; Lecolley, F.; Tao, L.; Haddleton, D. M.; Clerx, J.; Cornelissen, J. J. L. M.; Velonia, K. *J. Am. Chem. Soc.* **2004**, *127*, 2966.

Marshall, B. T.; Long, M.; Piper, J. W.; Yago, T.; McEver, R. P.; Zhu, C. *Nature* **2003**, *423*, 190.

Masci, B.; Pasquales, S.; Thuery, P. *Org. Lett.* **2008**, *10*, 4835.

Mason, T. J.; Lorimer, J. P. in *Applied Sonochemistry: Uses of Power Ultrasound in Chemistry and Processing*, Wiley-VCH Verlag, Weinheim, **2002**.

McCullagh, M.; Franco, I.; Ratner, M. A.; Schatz, G. C. *J. Am. Chem. Soc.* **2011**, *133*, 3452.

Merrill, E. W.; Leopairat, P. *Polym. Eng. Sci.* **1980**, *20*, 505.

Moses, D.; Feldblum, A.; Ehrenfreund, E.; Heeger, A. J.; Chung, T.- C.; MacDiarmid, A. G. *Phys. Rev. B.* **1982**, *26*, 3361 and references cited therein.

Muramatsu, Y.; Yamamoto, T.; Hasegawa, M.; Yagi, T.; Koinuma, H. *Polymer* **2001**, *42*, 6673.

Nagai, T.; Ibata, K.; Park, E. S.; Kubota, M.; Mikoshiba, K.; Miyawaki, A. *Nature Biotech.* **2002**, *20*, 87.

Nguyen, T. Q. *Chimia*, **2001**, *55*, 147.

Niwa, H.; Inouye, S. *Proc. Natl. Acad. Sci. USA* **1996**, *93*, 13617.

Nulwala, H.; Takizawa, K.; Odukale, A.; Khan, A.; Thibault, R. J.; Taft, B. R.; Lipshutz, B. H.; Hawker, C. J. *Macromolecules* **2009**, *42*, 6068.

Parr, R. G.; Yang, W. *Density-Functional Theory of Atoms and Molecules*. Oxford Univ. Press, New York, **1989**.

Paulusse, J. M. J.; Sijbesma, R. P. *Chem. Commun.* **2008**, 4416.

Percec, V.; Guliashvili, T.; Ladislaw, J. S.; Wistrand, A.; Stjerndahl, A.; Sienkowska, M. J.; Monteiro, M. J.; Sahoo, S. *J. Am. Chem. Soc.* **2006**, *128*, 14156-14165.

Perez-Jimenez, R.; Garcia-Manyes, S.; Ainavarapu, S. R. K.; Fernandez, J. M. *J. Biol. Chem.* **2006**, *281*, 40010.

Piermattei, A.; Karthikeyan, S.; Sijbesma R. P. *Nat. Chem.* **2009**, *1*, 133.

Pool, B.; White, J. *Org. Lett.* **2000**, *2*, 3505.

Potisek, S. L.; Davis, D. A.; Sottos, N. R.; White, S. R.; Moore, J. S. *J. Am. Chem. Soc.* **2007**, *129*, 13808.

Pourceau, G.; Meyer, A.; Vasseur, J.; Morvan, F. *J. Org. Chem.* **2009**, *74*, 6837.

Prezhdo, O. V.; Pereverzev, Y. V. *Acc. Chem. Res.* **2009**, *42*, 693.

Pucci, A.; Riggeri, G. *J. Mater. Chem.* **2011**, *21*, 8282 and references cited therein.

Ramirez, A. L. B.; Ogle, J. W.; Schmitt, A. L.; Lenhardt, J. M.; Cashion, M. P.; Mahanthappa, M. K.; Craig, S. L. *ACS Macro Letters* **2012**, *1*, 23.

Ribas-Arino, J.; Marx, D. *Chem. Rev.* **2012**, *112*, 5412.

Ribas-Arino, J.; Shiga, M.; Marx, D. *Angew. Chem. Int. Ed.* **2009**, *48*, 4190.

Rostovtsev, V. V.; Green, L. G.; Fokin, V. V.; Sharpless, K. B. *Angew. Chem. Int. Ed.* **2002**, *41*, 2596.

Saghatelian, A.; Guckian, K. M.; Thayer, D. A.; Ghadiri, M. R. *J. Am. Chem. Soc.* **2003**, *125*, 344.

Sanderson, M. D.; Kamplain, J. W.; Bielawski, C. W. *J. Am. Chem. Soc.* **2006**, *128*, 16514.

Sawano, A. *Nucleic Acids Res.* **2000**, *28*, 78e.

Schrock, A. K.; Schuster, G. B. *J. Am. Chem. Soc.* **1984**, *106*, 5234.

Seela, F.; Ingale, S. A. *J. Org. Chem.* **2010**, *75*, 284.

Seo, T.; Li, Z.; Ruparel, H.; Ju, J. *J. Org. Chem.* **2003**, *68*, 609.

Soheilifard, R.; Makarov, D. E.; Rodin, G. J. *J. Chem. Phys.* **2011**, *135*, 054107.

Song, Y. K.; Lee, K. H.; Hong, W. S.; Cho, S. Y.; Yu, H. C.; Chung, C. M. *J. Mater. Chem.* **2012**, *22*, 1380.

Spain, I. L.; Dunstan, D. J. *J. Phys. E: Sci. Instrum.* **1989**, *22*, 923.

Staudinger, H.; Schweitzer, O. *Ber. Dtsch. Chem. Ges.* **1930**, *63*, 3132.

Sun, S.; Cao, Y.; Feng, J.; Wu, P. *J. Mater. Chem.* **2010**, *20*, 5605.

Suslick, K. S.; Goodale, J. W.; Schubert, P. F.; Wang, H. H. *J. Am. Chem. Soc.* **1983**, *105*, 5781.

Suzuki, Y.; Dudko, O. K. *J. Chem. Phys.* **2011**, *134*, 065102.

Suzuki, Y.; Dudko, O. K. *Phys. Rev. Lett.* **2010**, *104*, 048101.

Tennyson, A. G.; Wiggins, K. M.; Bielawski, C. W. *J. Am. Chem. Soc.* **2010**, *132*, 16631.

Tian, Y.; Boulatov, R. *ChemPhysChem* **2012,** *13*, 2277.

Toms, B. A. *Proc. 1st Int. Congress on Rhelogy*; North Holland, **1948**, pp 135–141.

Tornøe, C. W.; Christensen, C.; Meldal, M. *J. Org. Chem.* **2002**, *67*, 3057.

Tsien, R. Y. *Annu. Rev. Biochem.* **1998**, *67*, 509.

Valiev, M.; Bylaska, E. J.; Govind, N.; Kowalski, K.; Straatsma, T. P.; Van Dam, H. J. J.; Wang, D.; Nieplocha, J.; Apra, E.; Windus, T. L.; de Jong, W. A. *Comput. Phys. Commun.* **2010**, *181*, 1477.

Voth, G. A.; Hochstrasser, R. M. *J. Phys. Chem.* **1996**, *100*, 13034.

Ward, W. W.; Cody, C. W.; Hart, R. C.; Cormier, M. J. *Photochem. Photobiol.* **1980**, *31*, 611.

West, D. K.; Paci, E.; Olmsted, P. D. *Phys. Rev. E Stat. Nonlinear Soft Matter Phys.* **2006**, *74*, 061912.

White, S. R.; Caruso, M. M.; Moore, J. S. *MRS Bull.* **2008**, *33*, 766 and references cited therein.

Wiggins, K. M.; Bielawski, C. W. *Angew. Chem. Int. Ed.* **2012**, *51*, 1640.

Wiggins, K. M.; Hudnall, T. W.; Shen, Q.; Kryger, M. J.; Moore, J. S.; Bielawski, C. W. *J. Am. Chem. Soc.* **2010**, *132*, 3256.

Wiggins, K. M.; Hudnall, T. W.; Tennyson, A. G.; Bielawski, C. W. *J. Mater. Chem.* **2011**, *21*, 8355.

Wiggins, K. M.; Syrett, J. A.; Haddleton, D. M.; Bielawski, C. W. *J. Am. Chem. Soc.* **2011**, *133*, 7180.

Woodward, R. B.; Hoffmann, R. *Angew. Chem. Int. Ed.* **1969**, *8*, 781.

Yamada, T.; Peng, C. G.; Matsuda, S.; Addepalli, H.; Jayaprakash, K. N.; Alam, M. R.; Mills, K.; Maier, M. A.; Charisse, K.; Sekine, M.; Manoharan, M.; Rajeev, K. G. *J. Org. Chem.* **2011**, *76*, 1198.

Yew, Z. T.; Schlierf, M.; Rief, M.; Paci, E. *Phys. Rev. E Stat. Nonlinear Soft Matter Phys.* **2010**, *81*, 031923.

Zhao, L.; Li, Y.; Cao, X.; You, J.; Dong, W. *Nanotechnology* **2012**, *23*, 255702.

Zhao, Y.; Schultz, N.; Truhlar, D. G. *J. Chem. Theory Comput.* **2006**, *2*, 364.

Zhurkov, S. N. *Int. J. Frac. Mec.* **1965**, *1*, 311.

Zill, L.; Vanwagtendonk, W. *Biochim. Biophys. Acta* **1950**, *6*, 524.